Synthesis of novel conjugates based on a functionalized *cyclo*[DKP-*iso*DGR] integrin ligand and potent cytotoxic agents

Lizeth Alicia Bodero Padilla

This work is dedicated to my dear family: David, Alicia, Maybe, Davicho and Yeshi.

TABLE OF CONTENTS

Abbreviations

5-FU: 5-Fluoracil

6-MP: 6-Mercaptopurine

A549: Human lung carcinoma cell line

ACN: Acetonitrile

ACPP: Active cell penetrating peptide

ADC: Antibody-drug conjugate

ADCC: Antibody-dependent cellular cytotoxicity

AKt/PKB: Protein kinase B

Ala: Alanine

ALL: Acute lymphoblastic leukemia

AMAS: N-(α-maleimidoacetoxy) succinimide ester

AML: Acute myeloid leukemia

APN: Aminopeptidase N

aq.: Aqueous solution

Bn: Benzyl

Boc: *tert*-Butyloxycarbonyl

CAIX: Carbonic anhydrase IX

CCRF-CEM: human leukemic lymphoblasts

CDC: Complement dependent cytotoxicity

Cit: Citrulline

CPT: Camptothecin

CuAAC: Copper (I) catalyzed alkyne-azide cycloaddition

DAR: Drug-antibody ratio

DAVBH: Desacetyl vinblastine hydrazide

DCC: *N,N'*-Dicyclohexylcarbodiimide

DCM: Dichloromethane

DIC: *N,N'*-Diisopropylcarbodiimide

DIPEA: *N,N*-Diisopropylethylamine

DKP Diketopiperazine

DM1: N_2'-deacetyl-N_2'-(3-mercapto-1-oxopropyl)-maytansine

DMAP: 4-Dimethylaminopyridine

DMF: *N,N*-Dimethylformamide

DMSO: Dimethyl sulfoxide

DNA: Deoxyribonucleic acid

DOX: Doxorubicin

DOXSF: Doxsaliform

DUPA: 2-[3-(1,3-dicarboxypropyl)ureido] pentanedioic acid

ECM: Extracellular matrix

EDC: *N*-(3-Dimethylaminopropyl)-*N'*-ethylcarbodiimide hydrochloride

EDT: ethanedithiol

EEDQ: *N*-Ethoxycarbonyl-2-ethoxy-1,2-dihydroquinoline

EGFR: Epithelial growth factor receptor

Ep-CAM: Epithelial cell adhesion molecule

eq.: equivalents

ESI Electrospray ionization

EtOAc: Ethyl acetate

FACS: Fluorescence-activated cell sorting

FAK: Focal adhesion kinases

FDA: US Food and Drug Administration

FL: Follicular lymphoma

Fmoc: 9-Fluorenylmethoxycarbonyl

FN: Fibronectin

FR: Folate receptor

GI: Gastrointestinal

GM: Glioblastoma multiforme

HAMA: Human anti-mouse antibodies

HATU: O-(7-azabenzotriazol-1-yl)-tetramethyl-uronium hexafluorophosphate

HOAt 1-Hydroxy-7-azabenzotriazole

HPLC: High performance liquid chromatography

HT29: Human colon cancer

HUVEC: Human umbilical endothelial cells

IC$_{50}$: Maximum half inhibitory concentration

ICAM 1: (Intercellular Adhesion Molecule 1

IgG: Immunoglobulin G

IL-8: Interleukin 8

*i*Pr: Isopropyl

*iso*DGR: isoAspartic-Glycine-Arginine

LNCaP: androgen-sensitive human prostate adenocarcinoma cell line

LRP1: Low-density lipoprotein

LTT: Ligand-targeted therapeutics

mAb: Monoclonal antibody

MS: Mass spectroscopy

mCRC: metastatic colorectal cancer

MCRPC: Metastatic castration-resistant prostate cancer

MDA-MB-468: Human breast cancer cell line

MED: Minimum effective dose

MeOH: Methanol

MIDAS: Metal ion-dependent adhesion site

MMAE: Monomethyl auristatin E

MMAF: Monomethyl auristatin F

MMP: Matrix metalloproteinase

MTD: Maximum tolerated dose

Mtr: 4-methoxy-2,3,6-trimethyl benzene sulphonyl

MTT: 3-(4,5-dimethylthiazol-2-yl)-2,5-diphenyltetrazolium bromide

MW Molecular weight

NaHCO$_3$: Sodium bicarbonate

NGR: Asparagine-Glycine-Arginine

NHL: Non-Hodgkin's lymphoma

NHS: *N*-Hydroxysuccinimide

NMR: Nuclear Magnetic Resonance

NSCLC: Non-small-cell lung cancer

OATP: organic anion transporting polypeptide

PABA: *p*-aminobenzyl alcohol

PABC: *p*-aminobenzyl carbamate

PaCa2: human pancreatic duct adenocarcinoma

PBS Phosphate-buffered saline

PEG: Polyethylene glycol

pHLIP: pH low insertion peptides

PNP: *p*-nitrophenyl chloroformate

PSMA: Prostate specific membrane antigen

PTX: Paclitaxel

RGD: Arginine-Glycine-Aspartic

rt.: room temperature

SCLC: Small-cell lung cancer

SIP: Small immune proteins

SMDC: Small molecule-drug conjugate

SPDP: N-Succinimidyl 3-(2-pyridyldithio) propionate

SSTR: Somatostatin receptor

sulfo-Lc-SMPT : sulfosuccinimidyl 6-[α-methyl-α-(2-pyridyldithio)toluamido] hexanoate

TFA: Trifluoroacetic acid

THF: Tetrahydrofuran

TK: Tyrosine kinase

TMS Tetramethylsilane

TNF: Tumor necrosis factor

*t*R: Retention time

U87-MG: Human glioblastoma cell line

Val: Valine

VEGF: Vascular endothelial growth factor receptor

Project overview

The lack of selectivity is one of the main limitations of traditional chemotherapy because of the severe side effects associated to high drug dosages. Targeted drug delivery is therefore a growing-interest field in cancer therapy as a strategy for overcoming the systemic cytotoxicity. This approach is inspired by the "magic-bullet" concept of Paul Ehrlich, awarded with the Medicine Nobel Prize in 1908 for his work in immunotherapy, concept applied to cancer therapy nowadays to propose the use of drug-delivery vehicles (monoclonal antibodies, peptides, nanoparticles, polymers) targeting a specific antigen or receptor to liberate the payload at the tumor site without affecting the healthy tissue.

The antibody-drug conjugates (ADCs) and the small molecule-drug conjugates (SMDC) belong to this new generation of therapeutics. In ADCs, the targeting agent is a monoclonal antibody (mAb) while in SMDCs the targeting is performed by a low molecular weight ligand (peptide, vitamin or peptidomimetic). In both cases the targeting moiety is connected to a potent warhead by means of a stable linker and they are expected to efficiently deliver the cytotoxic agent to the tumor cells preferentially *via* receptor-mediated endocytosis. Currently, four ADCs: Mylotarg, Kadcyla, Adcetris and Besponsa, have been approved by the US FDA for the treatment of different cancers. Despite this success, ACDs present some drawbacks related to the use of mAbs such as high manufacturing costs, unfavorable pharmacokinetics (low tissue diffusion and low accumulation rate) and possible immune response, for this reason smaller formats like SMDCs have become an interesting alternative for the selective delivery of drugs into tumors.

Our research group has developed during the last decade a number of cyclic peptidomimetic ligands containing the tripeptide RGD or *iso*DGR sequences and the bifunctional diketopiperazine (DKP) scaffold. These ligands are recognized by the integrin receptor $\alpha_V\beta_3$, which is widely expressed on the blood vessels of several human

cancers (e.g. breast cancer, glioblastoma, pancreatic tumor, prostate carcinoma) but not on the vasculature of healthy tissues, constituting a suitable therapeutic target. In particular, the *cyclo*[DKP-*iso*DGR] integrin ligand has shown not only a high binding affinity and selectivity for the purified receptor $\alpha_V\beta_3$ but also an integrin antagonist activity, becoming a promising ligand for the preparation of SMDCs.

This PhD thesis describes the synthesis and biological evaluation of SMDCs containing the functionalized *cyclo*[DKP-*iso*DGR] integrin ligand and potent cytotoxic drugs (α-amanitin, MMAE and MMAF) combined *via* different linkers and spacers. The purpose of this project is to study the efficacy of the *cyclo*[DKP-*iso*DGR] integrin ligand developed by our research group as a vector for targeted drug delivery. The work is divided in three chapters: the Chapter 1 introduces the definition of SMDC as part of the new targeted therapies strategies; the Chapter 2 presents the characteristics of the integrin receptors family, previous work on targeted drug-delivery *via* integrin ligands and the synthesis of the functionalized *cyclo*[DKP-*iso*DGR] integrin ligand; and the Chapter 3 presents the synthesis of the SMDCs containing the *cyclo*[DKP-*iso*DGR] integrin ligand and different cytotoxic agents, along with the discussion of the *in vitro* results, including binding affinity tests towards the isolated $\alpha_V\beta_3$ integrin receptor and antiproliferative activity assays in cancer cell lines with different levels of $\alpha_V\beta_3$ expression.

Finally, the experimental procedures and *in vitro* test protocols are detailed in the Experimental Section, together with the spectroscopic and analytical data of the new products.

Chapter 1. Targeted drug delivery for tumor therapy

1.1. Targeted cancer therapies

Cancer has a major impact on society as it represents one of the main causes of death worldwide. Statistics from the World Health Organization indicate that 8.8 million people died of cancer in 2015 and, approximately 1 in 6 deaths globally is related to this desease.[1]

Among the anticancer therapies developed during the last decades, chemotherapy remains the most employed together with radiation therapy and surgery. Traditional chemotherapy uses low-molecular weight drugs (Figure 1) that modify or interrupt the cell cycle at different stages.[2,3] These cytotoxic drugs can be classified by their mechanism of action in:

- Antimetabolites

  These drugs can alter essential biological pathways by mimic nitrogenous bases or inhibiting enzymes involved in the synthesis of nucleic acids. 5-Fluoracil (5-FU) and 6-mercaptopurine (6-MP), analogues of pyrimidine and purine respectively, are examples of antimetabolite drugs. The incorporation of these analogues during the phase S of cell cycle interrupts the replication of DNA and leads to apoptosis. Another example of this group is methotrexate, an antifolate that blocks the synthesis of nucleotides by inhibition of the dihydrofolate reductase.[4]

- DNA damaging agents

  - Alkylating agents: They act by alkylating DNA on purine bases blocking replication. Nitrogen mustards derivatives (e.g. cyclophosphamide, chlorambucil, melphalan); nitrosoureas (e.g. carmustine, lomustine, semustine); triazenes (e.g. dacarbazine,

temozolomide) and natural products like mitomycin C and streptozotocin belong to this group.[4,5]

- Cross-linking agents: Some alkylating agents can also bind DNA causing inter-strand crosslink (DNA crosslink on opposite strands of the double helix), with subsequent double toxic effect in cells. Platinum complexes and derivates (e.g. cisplatin, carboplatin, oxaliplatin) can form intra-strand crosslinks when forming adducts with adjacent bases on the same DNA strand. Both inter-strand and intra-strand crosslinks lead to apoptosis by interruption of DNA replication.[5]

- Intercalating agents: Bind between base pairs of nucleic acids preventing replication. Examples of this group of drugs are the anthracyclines doxorubicin, daunorubicin, epirubicin, mitoxantrone and antinomycin-D.[4,5]

- Toposisomerase poisons: Topoisomerases are enzymes responsible for the cleavage, annealing and topological state of DNA double helix. Toposisomerase I inhibitors (e.g. camptothecin, irinotecan, topotecan) and toposisomerase II inhibitors (etoposide, anthracyclines) trap the DNA-enzyme complex inhibiting replication fork progression.[6]

- Antitubulin agents

Tubulin is a globular protein that plays an essential role in cellular replication. Antitubulin agents, also known as mitotic inhibitors, alter the microtubule polymerization dynamics (coexistence of tubulin assembly and disassembly) blocking the division of the nucleus and leading cell to apoptosis. There exist two groups of antitubulin agents: microtubules stabilizers (e.g. Paclitaxel, docetaxel, epothilones) and microtubule inhibitors (e.g. vincristine, vinblastine, dolastatin 10, colchicine).[7]
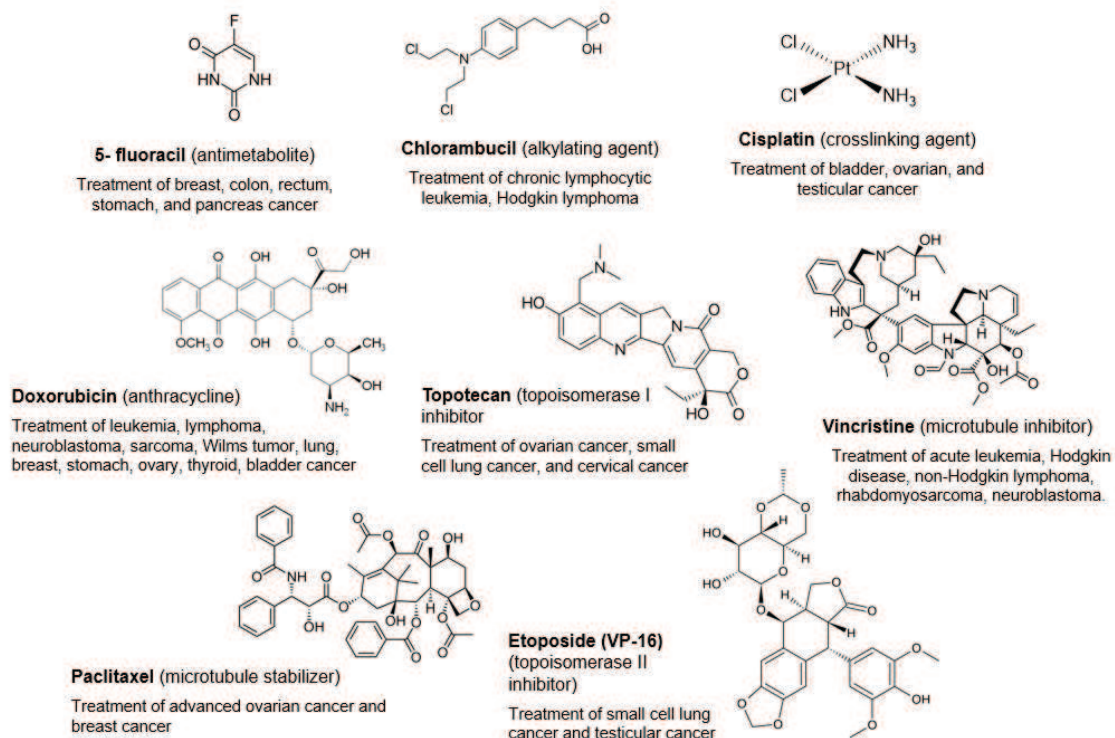
Figure 1. Molecular structures and use of common anticancer drugs[8]

The cytotoxic agents described above are expected to attack preferentially the tumor cells, as these undergo much more rapid proliferation than normal cells. Unfortunately, these drugs can also kill normal dividing cells in the body (e.g. hair, bone marrow, gastrointestinal track) and accumulate in other organs rather than tumor area (Figure 2), displaying severe side effects. Due to the systemic cytotoxicity, the administrated dose is often reduced to suboptimal level with poor benefit for the patient.[3,9,10]
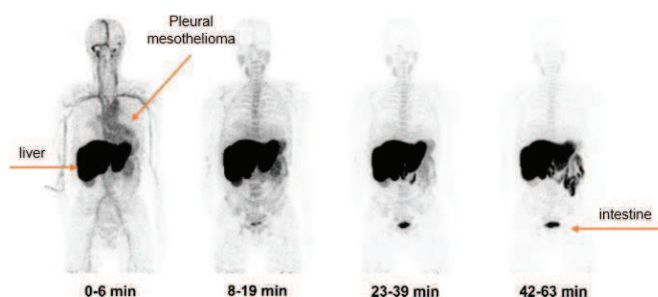
Figure 2. Biodistribution of ^{11}C-docetaxel in male patient with metastatic malignant pleural mesothelioma. PET scans at different time points (0–6, 8–19, 23–39 and 42–63 min) display low drug uptake in the affected region (pleural mesothelium) but high accumulation in the liver and intestine. Adapted with permission from A.A.M. van der Veldt, N.H. Hendrikse, E.F. Smit et al. *Eur. J. Nucl. Med. Mol. Imaging* 2010, *37*, 1950–1958. Copyright © 2010.[11]

With the purpose of improving the therapeutic index (maximum tolerated dose/minimum effective dose) of anticancer drugs, modern strategies are oriented towards targeted therapies. These are based on the concept of "magic-bullet", envisaged by Paul Ehrlich (Medicine Nobel Prize, 1908) who coined the term referring to a therapeutic agent that could attack the bacteria responsible of diseases without hurting the host.[12]
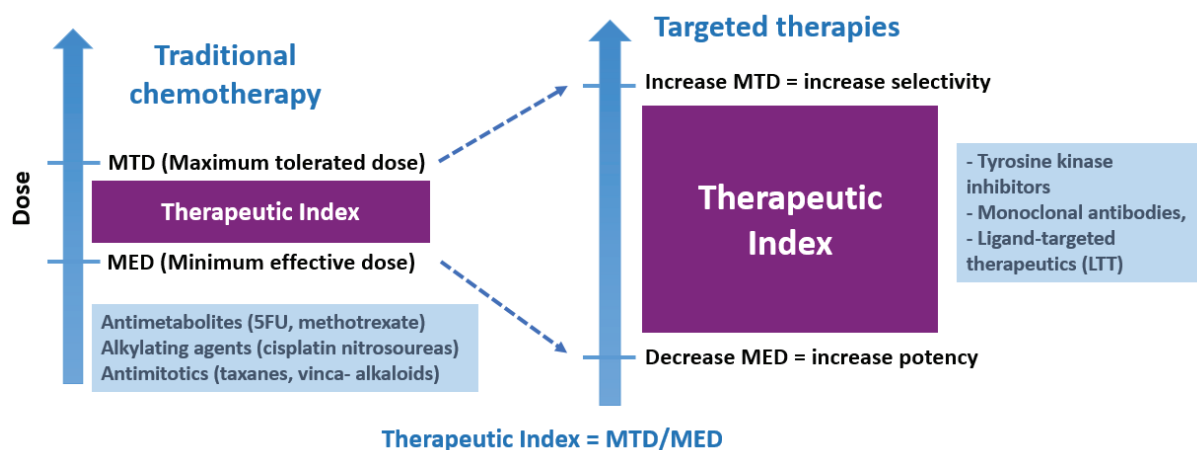
Figure 3. Targeted chemotherapy approach. Adapted with permission from Siler Panowski, Sunil Bhakta, Helga Raab, Paul Polakis and Jagath R. Junutula; mAbs, 2014, 6 (1), 34-45. Copyright © 2014 Landes Bioscience

Nowadays, targeted cancer therapies aim at selectively killing cancer cells by interfering with essential pathways involved in tumor growth (e.g. signal-transduction pathways) or by efficiently delivering the cytotoxic agents to the tumor without compromising the healthy cells. Most common targets are molecular markers or antigens that play an important role in cell proliferation (e.g. cell surface proteins, glycoproteins, or carbohydrates) and that are over-expressed in tumor cells compared with normal tissues.[3,13]

Three main approaches can be identified in this field: small molecules tyrosine kinase inhibitors designed to prevent the activation of signaling pathways dysregulated in tumor cells (e.g. imatinib – Gleevec®, sunitinib)[14–16]; monoclonal antibodies (mAbs) targeting specific antigens displayed in tumor cells; and ligand-targeted therapeutics (LTT) where a drug-delivery vehicle (e.g. monoclonal antibody, small ligand, peptide, nanoparticle, polymer) is used to target specific antigens or receptors and liberate the payload at the tumor site.[17,18] Antibody-drug conjugates (ADCs) and small molecule-

drug conjugates (SMDCs) belong to this last category and will be described in the next sections.

1.2.   Monoclonal antibodies

Antibodies, also known as immunoglobulins (Ig), are a group of glycoproteins produced by the immune system that detect and selectively bind antigens displayed in abnormal cells, prompting an immune attack that destroys the cell expressing the antigen.[19] In 1975, Köhler and Milstein developed the hybridoma technology,[20] where antibodies produced by B lymphocytes of mice were isolated and fused with immortal myeloma cell lines to obtain clonal cells known as hybridomas. Hybridomas can be cultured to produce large amounts of identical antibodies specific for an antigen, these are called monoclonal antibodies (mAbs).
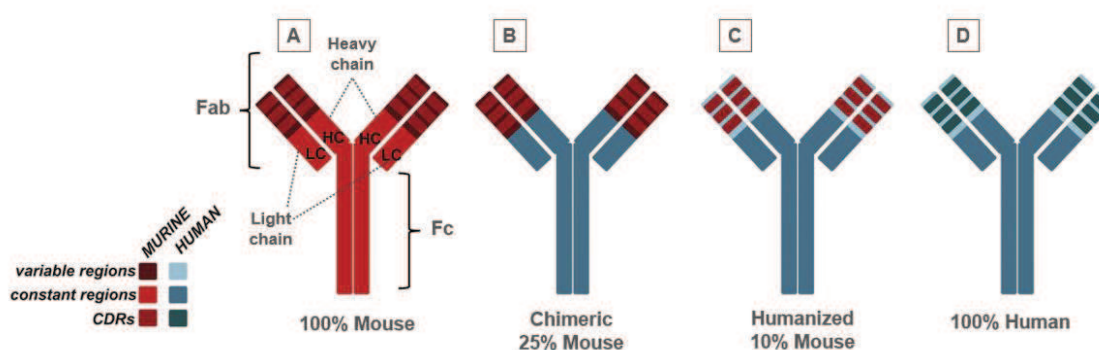
Figure 4. Structure and classification of monoclonal antibodies (mAbs).[21] Fab: fragment antigen-binding; Fc: fragment crystallizable; CDR: complementary determining region; A) murine antibody; B) Chimeric antibody: murine variable regions and human constant regions; C) Humanized antibody: human variable and constant region, murine CDRs; D) Fully human antibody. Adapted with permission from K. R. Rodgers and R. C. Chou. *Biotechnol. Adv.* 2016, *34* (6), 1149–1158. Copyright © 2016 Elsevier Inc.

The therapeutic potential of mouse mAbs (Figure 4A) was restricted by the response of patients' immune system, which recognized the antibodies as foreign entities and generated human anti-mouse antibodies (HAMA), resulting in rapid clearance of the mAb from circulation. Further advances in recombinant DNA technology led to the production of chimeric mAbs (Figure 4B) where the constant regions of the murine antibody were replaced by human constant regions sequences, retaining the murine variable domains responsible for antigen binding. Later, it was also possible to replace the variable sequences of mouse mAbs with human sequences to obtain humanized mAbs with less than 10% mouse protein. More recently, the phage display technology

and the use of transgenic mice have made possible the generation of fully human mAbs, significantly reducing the immune response reported for the first mAbs.[3,21,22]

The antitumoral activity of monoclonal antibodies can be attributed to different cell-killing mechanisms.[23] Among them we can summarize:

- Direct action of the antibody: by binding the targeted receptor and displaying an antagonist activity, blocking the dimerization, kinase activation and downstream signaling, inhibiting proliferation and inducing apoptosis.

- Immune-mediated cell killing: induction of phagocytosis, complement dependent cytotoxicity (CDC), antibody-dependent cellular cytotoxicity (ADCC) or regulation of T-cell function.

- Effect of the antibody on tumor vasculature and stroma: vasculature receptor antagonism, stromal cell inhibition.

These mechanisms have been validated in the clinic, leading to the approval of more than 24 mAbs targeting 16 different antigens, that are currently available in the market for the treatment of an increasing number of cancers.[24] Some examples include the chimeric mAb Rituximab (the first mAb approved by the FDA for cancer treatment in 1997), that binds the CD20 antigen expressed on the surface of B cells, indicated for the treatment of follicular lymphoma (FL) and low-grade non-Hodgkin's lymphoma (NHL);[25] Alemtuzumab, a humanized mAb that targets CD52 antigen overexpressed on malignant lymphocytes, approved for therapy of resistant lymphocytic leukemia;[26] Bevacizumab, another humanized mAb that binds to the vascular endothelial growth factor receptor (VEGF) on cancer cells, inhibiting the formation and growth of tumor blood vessels, used in the treatment of metastatic colon and kidney cancer, non-small cell lung cancer and glioblastoma;[27] the human mAb panitumumab, indicated for the treatment of metastatic colorectal cancer (mCRC) expressing the epithelial growth factor receptor (EGFR);[28] and the humanized mAb trastuzumab (Herceptin®), that targets the human epidermal growth factor receptor 2 (HER2) overexpressed in 20-30% of breast cancers and some metastatic gastrointestinal (GI) cancers.[29,30]

1.3. Antibody-drug conjugates (ADC)

The high specificity of monoclonal antibodies and the positive results obtained from the combination of mAbs with chemotherapy led to the idea of developing new conjugated entities where the mAbs were covalently bound to cytotoxic drugs. The so-called antibody-drug conjugates (ADCs) consist of a monoclonal antibody connected to a potent cytotoxic drug *via* a chemically stable linker to prevent the premature release of the payload in the blood circulation. Ideally, an ADC should liberate the cytotoxic agent at the tumor site after selectively binding its target, expressed on tumor cells surface, leaving the healthy cells unharmed.[13,31]

The first generation of ADCs, based on chimeric or humanized mAbs and regular-potency cytotoxic payloads (e.g. doxorubicin, methotrexate), faced several problems in clinical trials because of immunogenicity, limited potency and insufficient selectivity.[32] Learning from the early results, scientists optimized the ADCs design by selecting more specific targets, replacing chimeric mAbs by humanized or fully human mAbs to prevent immunogenicity, and using ultra-potent cytotoxic drugs (100-1000 times more potent). The drug-antibody ratio (DAR) in the second-generation ADCs is around 4:1, resulting in more efficient cytotoxicity.[33,34] Currently, a new generation of ADCs is being developed with the incorporation of bispecific antibodies and site-specific conjugation of the drug that allows a better control of the DAR.[35]

At present, four ADCs have received FDA approval and more than 60 are being evaluated at different stages of clinical trials (Figure 5). The first ADC commercialized was gemtuzumab ozogamicin (Mylotarg®, Wyeth-Pfizer), a first-generation ADC approved in 2000 for the treatment of CD33-positive acute myeloid leukemia (AML). It was voluntarily withdrawn from the US market in June 2010 and reintroduced in September 2017. The other three are second-generation ADCs: brentuximab vedotin (Adcetris®, Seattle Genetics) approved in 2011 for the treatment of anaplastic large cell lymphoma and Hodgkin lymphoma; ado-trastuzumab emtansine (Kadcyla®, Genentech), approved in 2013 for the treatment of HER2-positive breast cancer and inotuzumab ozogamicin (Besponsa®, Pfizer) approved in 2017 for the treatment of adults with relapsed or refractory B-cell precursor acute lymphoblastic leukemia (ALL).[31,36]
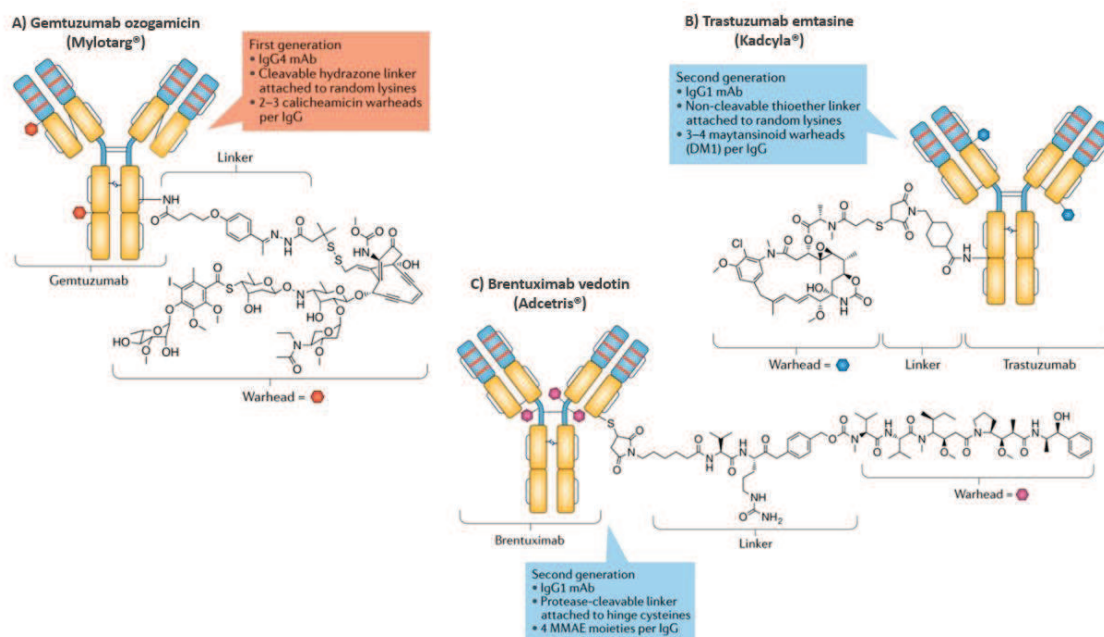
Figure 5. Structure and classification of three ADCs approved by FDA.[35] A) The first-generation ADC gemtuzumab ozogamicin (Mylotarg®) contains a humanized mAb (IgG4) specific for CD33 antigen conjugated to 2–3 calicheamicin moieties which are attached *via* cleavable hydrazone linkers to random lysine residues; B) The second-generation ADC trastuzumab emtansine (Kadcyla ®) contains a humanized mAb (IgG1) specific for human epidermal growth factor receptor 2 (HER2) and 3–4 DM1 moieties attached *via* non-cleavable thioether linkers to random lysine residues; C) The second-generation ADC brentuximab vedotin (Adcetris®) contains a chimeric mAb (IgG1) specific for CD30 antigen and 4 monomethyl auristatin E (MMAE) moieties attached to the hinge region through a protease-cleavable Val-Cit linker. Adapted with permission from A. Beck; L. Goetsch; C. Dumontet; N. Corvaïa. *Nat. Rev. Drug Discov.* 2017, *16* (5), 315–337. Copyright © 2016 Elsevier Inc.

1.3.1. Design and mechanism of action of ADCs

Among the factors to consider for the development of efficient ADCs, the most determinant are the choice of the target, the binding affinity and immunogenicity of the antibody, the nature of the linker and the potency of the cytotoxic drug.[31] Most ADCs are designed to kill cancer cells in a target-dependent mechanism that involves the internalization of the ADC *via* a receptor-mediated endocytosis pathway (Figure 6).[37,38] The first step in this process is the binding of the antibody to its antigen, localized preferentially on the cell surface of tumor cells. Once the ADC-antigen complex is formed, it is internalized into endosomes that subsequently mature and fuse with lysosomes. In the lysosomes, the drug is released *via* cleavage of the linker by specific proteases such as cathepsin B or by degradation of the ADC, then the free drug reaches its target in cytoplasm leading to cell death. The cell-killing mechanism depends of the class of cytotoxic drug used (e.g. tubulin polymerization inhibition by maytansines and auristatins, DNA damage by calcheamicins and duocarmycins).[34,38] Neighboring cancer

cells can also be killed when the free drug crosses the plasma membrane and access the extracellular environment in a process known as the bystander killing effect.[39,40]
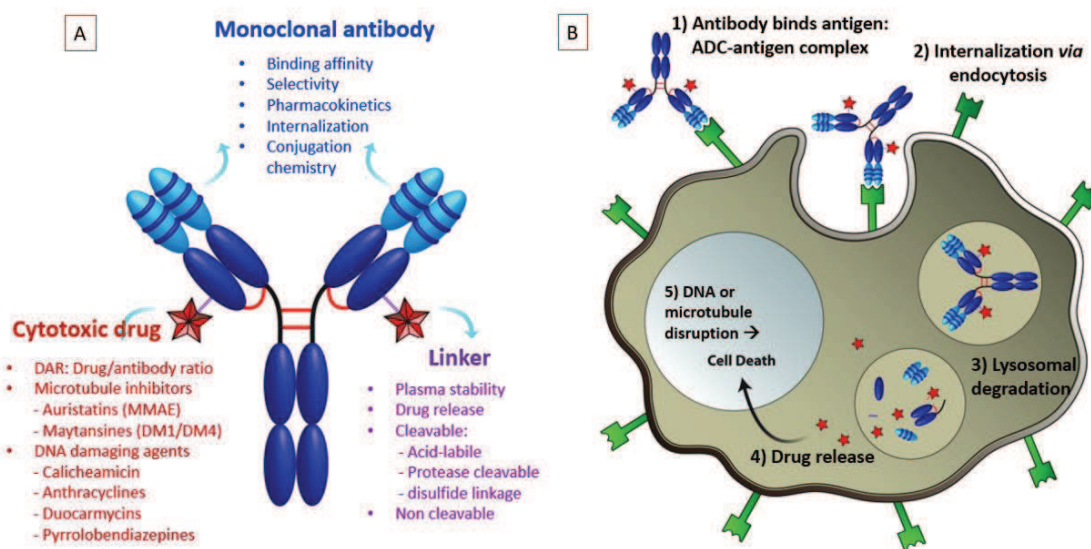
Figure 6. Design of ADCs and cell-killing mechanism. A) General structure of ADCs and factors to be consider for the design. B) Receptor-mediated endocytosis pathway: 1) the antibody moiety binds to its cell-surface antigen receptor target and form an ADC-antigen complex; 2) the complex is internalized into endosome that fuse with lysosomes; 3) the internalized complex undergoes lysosomal processing; 4) the cytotoxic payload is released inside the cytosol; 5) the payload reaches its target leading to cell death. Adapted with permission from Siler Panowski, Sunil Bhakta, Helga Raab, Paul Polakis and Jagath R. Junutula; mAbs, 2014, 6 (1), 34-45. Copyright © 2014 Landes Bioscience

Recent approaches in the design of ADCs have questioned the internalization requirement for ADC efficiency. In effect, potent activity in tumor preclinical models has been reported for non-internalizing ADCs directed against splice isoforms of fibronectin and tenascin-C, both expressed on the extracellular matrix of tumor blood vessels.[41–43] In this case, the release of the cytotoxic drug is triggered by the glutathione or proteases present in the extracellular space upon tumor cell death, followed by the passive diffusion of the drug, which should be lipophilic enough to guarantee a homogeneous drug delivery to the tumor.

1.3.2. Limitations of ADCs

Despite the successful approval of four ADCs and the remarkable progress achieved in this field, there remain some limitations concerning the immunogenicity of the antibody, the stability of the linker, the antigen targeting and the heterogeneity of the antigen expression in the tumor.[44,45] Specifically, in the case of solid tumors, the number of targeted receptors that ensure the internalization is relatively limited, and

contrary to hematologic tumors, the targets are overexpressed in a small portion of the patient populations (e.g. only 20% of breast cancer express HER2 and is eligible for the treatment with Kadcyla). Also, due to its large size antibodies do not extravasate and diffuse efficiently into tissue, once they reach the blood vessels they are trapped by the antigens located on perivascular tumor cells, preventing the targeting on the integrity of the tumor area. This is known as the "antigen-barrier" effect.[9,46]
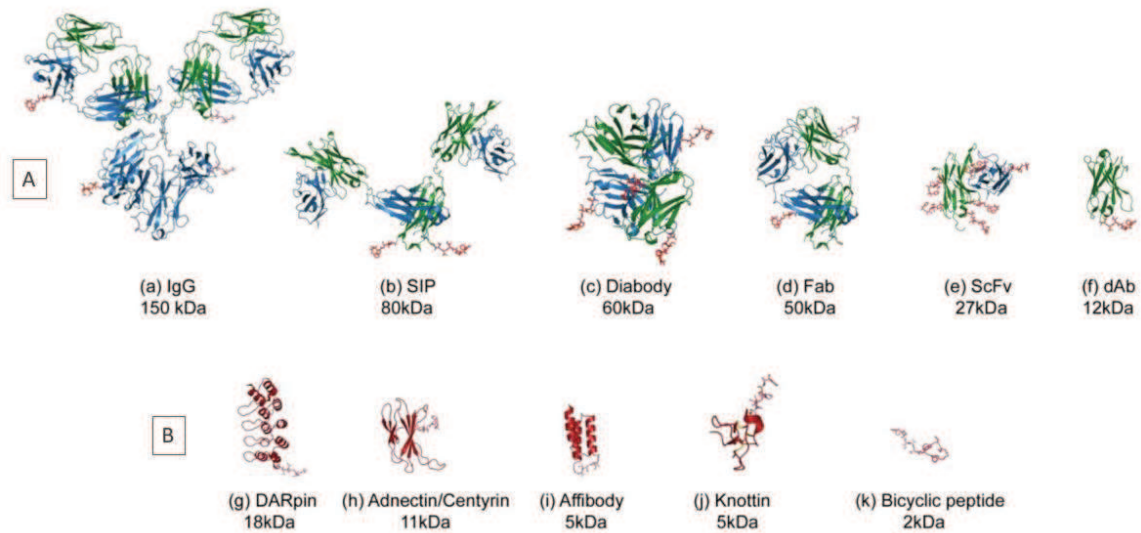
Figure 7. Various sizes antibody formats and alternative scaffolds for drug delivery.[47] A) Engineered antibody formats: (a) Immunoglobulin-G, (b) Small immune protein SIP, (c) diabody, (d) Fab fragment, (e) single chain Fv (scFv), (f) domain antibody (dAb); B) Protein scaffolds: (g) Designed ankyrin repeat protein (DARPin), (h) Adnectin,(monobody) (i) affibody, (j) knottin peptide, (k) bicyclic peptide. Adapted with permission from M. Deonarain; G. Yahioglu; I. Stamati et al. *Antibodies* **2018**, *7* (2), 16.

Current strategies in ADC technology seek to overcome the pharmacokinetic limitations by using smaller formats such as antibody fragments, diabodies, mini-antibodies or small immune proteins (SIP) (Figure 7). Even though immunoglobulins (IgG) have a longer circulation half-life that allows maximal accumulation at the tumor site, recent studies support the concept that smaller formats have higher diffusion and extravasation coefficients, hence they can penetrate better the solid tumors.[48,49] Lower plasma exposure also reduces the risk of premature release of the payload and the lack of a Fc domain in mAb fragments can minimize cross-reactivity with Fc-receptors on various normal cells, reducing off-target cytotoxicity.[35,47]

1.4.   Small molecule-drug conjugates (SMDCs)

The search for smaller vehicles for targeted drug delivery generated a new class of ligand-targeted cytotoxic agents where the targeting moiety is a low-molecular weight ligand (e.g. peptide, vitamin, peptidomimetic) with potentially favorable pharmacokinetic properties and that can be easily accessed by chemical synthesis. The so called small-molecule drug conjugates (SMDC) are similar to ADCs in structure and mechanism of action. They contain a linker system that connects the ligand to the cytotoxic drug and are expected to deliver the payload at its intracellular target in the tumor by receptor-mediated endocytosis (Figure 8). The considerations for the design of efficient ADCs are also valid for the SMDCs, being most determinant the choice of the target, the ligand, the nature of the linker and the potency of the payload.[9,18,50]
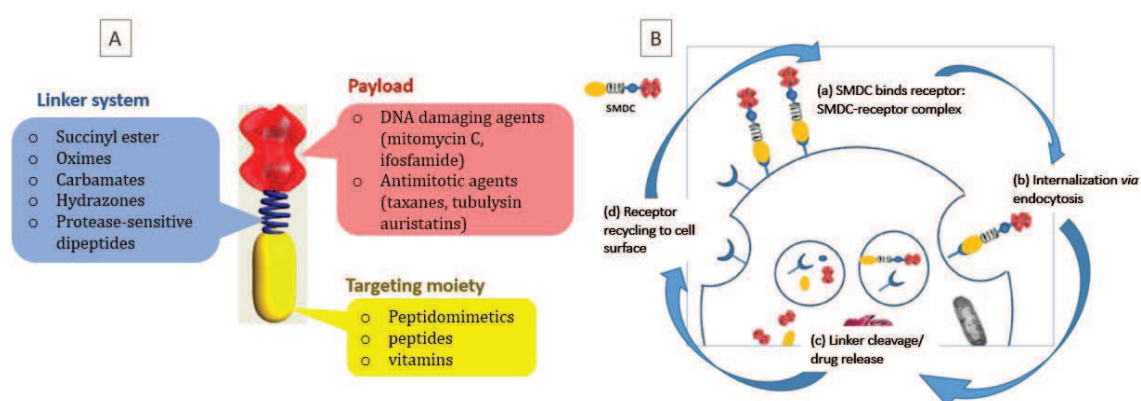
Figure 8. General structure and mechanism of action of SMDCs. A) General structure of SMDCs. B) Receptor-mediated endocytosis pathway: (a) the targeting moiety binds to its cell-surface receptor target and form a SMDC-receptor complex; (b) the complex is internalized into endosomes that fuse with lysosomes; (c) the internalized complex undergoes lysosomal processing; the linker is cleaved and the cytotoxic drug is released to reaches its intracellular target; (d) the receptor is recycled to cell surface. Adapted from https://endocyte.com/.

1.4.1. Target selection

One of the most important aspects for the choice of a suitable target is the receptor expression profile. This includes the expression of the targeted receptor in tumor cells vs normal tissues and the absolute level of receptor's isoforms expression in tumor cells. Ideally, the targeted receptor must be sufficiently overexpressed in tumor cells compared to normal to avoid off-target cytotoxicity; some studies have stablished as acceptable a 3-fold or higher magnitude of receptor overexpression in cancer cells.[51,52] For example, the expression of the folate receptor type α (FRα) is about 2.8 million

receptors per cancer cell[53] and the prostate-specific membrane antigen (PSMA) is expressed in 1 million excess by LNCaP prostate cancer cell line[54]. Other receptors overexpressed in a variety of cancer cells are the somatostatin receptor 2 (SSTR2), the sigma non-opioid intracellular receptor (SIGMAR1 and 2), cell-adhesion proteins ICAM1, LFA1 and CD24 and certain integrins.[9,13]

Most targeted receptors are expressed on the surface of cancer cells, allowing a better accessibility for the targeting ligand. In general, once the ligand binds the cell-surface receptor, forms the SMDC-receptor complex that is internalized *via* endocytosis to an intracellular compartment (recycling endosome or a lysosome) where the complex is dissociated, allowing the receptor to be either degraded or recycled to the cell surface (Figure 8B). As the availability of empty receptors on the targeted tumor cell depends on the rate of return of unoccupied receptors, an ideal receptor will be frequently recycled or resynthesized following degradation.[9,50]

1.4.2. Choice of the ligand

The binding affinity and specificity of the small ligand for the targeted receptor are basic for the optimal performance of SMDCs. A high binding affinity allowing the access to the targeted receptor and rapid extravasation, can increase the accumulation ratio tumor:blood, tumor:organ of the drug, avoiding the fast clearance often associated to the use of small molecules.[13,18] The specificity is also very important, especially when there are other members of the receptor family that can be recognized by the ligand, compromising the tumor targeting. Some of the ligands currently used in SMDCs include PSMA ligands,[50,55] folic acid analogues[56] and carbonic anhydrase IX (CAIX) ligands (Figure 9).[57,58]
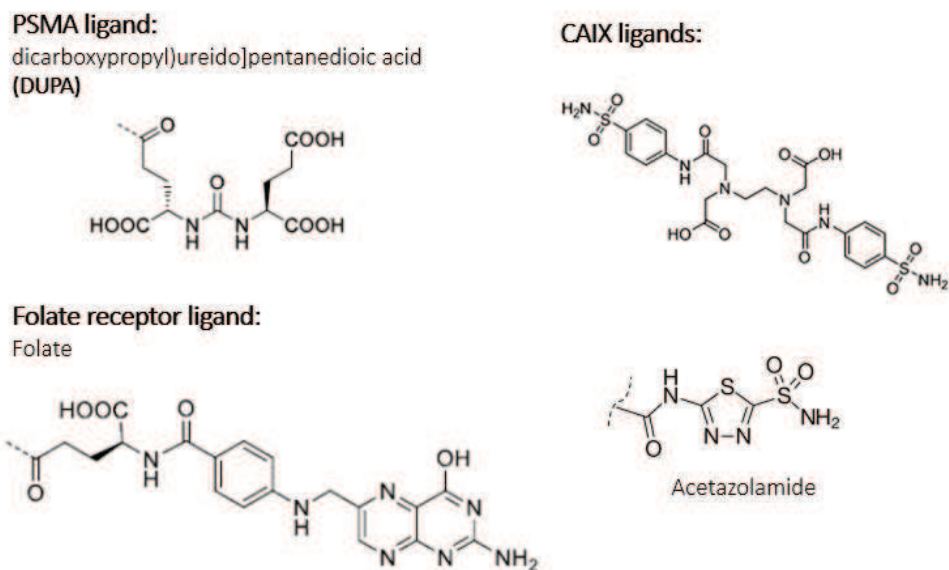
Figure 9. Small ligands targeting PSMA, folate receptor and CAIX

Another important aspect is the derivatizability of the ligand. In order to be conjugated to the linker (or to the connecting spacer) the targeting ligand should preferably have a derivatizable functional group (e.g. carboxylic acid, amine, alcohol, thiol) that enable the coupling to further entities via simple chemistry (e.g. formation of amides, carbamates, oximes, esters, carbonates or disulphides). One advantage of the use of small molecule ligands is that they can be prepared by chemical synthesis and optimized through structure-activity relationship (SAR) studies to identify the sites where modification will not interfere with receptor binding.[50,59]

1.4.3. Linker design

The design of the linker system is a key factor in the optimization of the SMDCs because it has direct influence in the pharmacokinetic profile. As most SMDCs are designed to be cleaved or degraded intracellularly, the linker should be stable at physiological conditions but assure an efficient release of the payload after receptor-mediated internalization. In general, linkers can be divided in:

- Acid-sensitive linkers: functional groups (e.g. esters or hydrazone) that remain stable in blood circulation (pH 7.5) and get hydrolyzed in acidic tumor micro-environment (lysosomal pH 4.8 and endosomal pH 5–6). The hydrazone linker has been used in conjugates containing doxorubicin,[60–62] paclitaxel[63] and Pt agents.[64,65]

This linker is applicable for conjugating drugs or their derivatives containing a chemical moiety (e.g. ketone or aldehyde) that can be coupled to a hydrazine-terminated linker (Figure 10).[66]
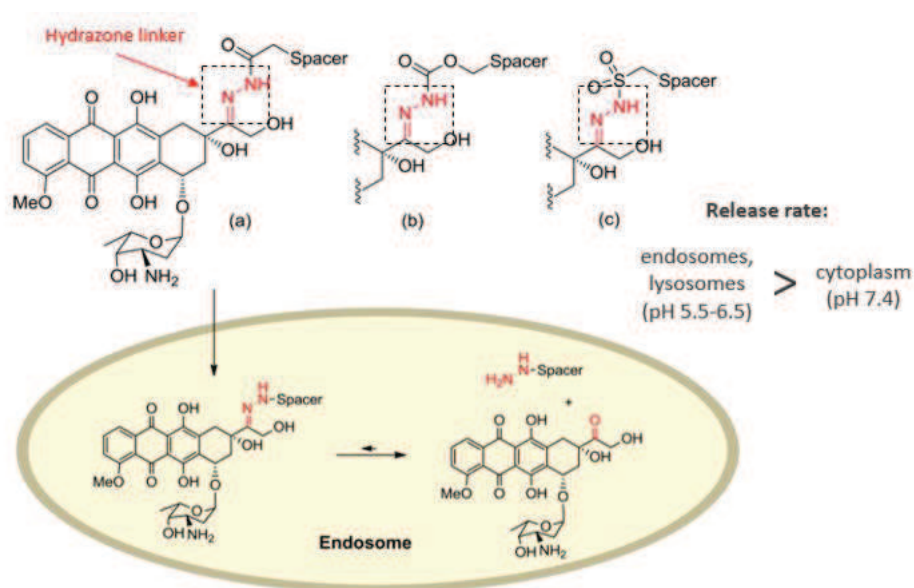
Figure 10. Structures of hydrazone-based linker types as applied for doxorubicin conjugation: (a) acyl hydrazone, (b) alkoxycarbonyl hydrazone, (c) sulfonyl hydrazone. Doxorubicin release occurs primarily in acidic compartments such as endosomes and lysosomes as a result of acid-catalyzed hydrolysis of the hydrazone linker. Adapted with permission from P. T. Wong and S. K. Choi; *Chem. Rev.* 2015, 115, 3388-3432. Copyright © 2015 American Chemical Society.

- Disulfide linkers: disulfide bonds can be reduced inside cytoplasm by endogenous thiol molecules (e.g. cysteine, glutathione). Glutathione is a low molecular weight thiol present in the cytoplasm (0.5–10 mM) and the extracellular environment in minor scale (2–20 µM in plasma). Tumor cells present elevated levels of glutathione (10-20 mM) due to stress conditions such as hypoxia.[67,68] This higher expression serves as a mechanism for the controlled release of the drug into the targeted cells (Figure 11).
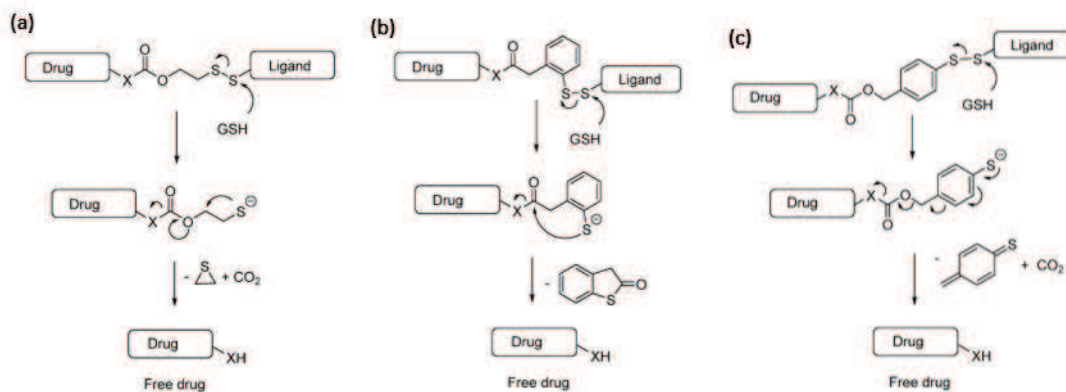
Figure 11. Mechanism of drug release of self-immolative disulfide linkers. (a) when reduced by glutathione, a self-immolative cleavage of the disulfide bond leads to release of a free drug with the formation of stable byproducts (a) CO_2 + a thiirane, (b) CO_2 + thiolactone, (c) CO_2 + thioquinone methide. GSH = glutathione; X = O or NH. Adapted with permission from: M. Srinivasarao and P. S. Low; *Chem. Rev.* 2017, 117, 12133-12164. Copyright © 2017 American Chemical Society

- Enzymatically-cleavable linkers: these linkers are generally constituted by short peptide sequences (e.g. Val-Ala, Val-Cit) designed to be cleaved by enzymes upregulated or activated inside the tumor cells, such as the lysosomal protease cathepsin B. In serum conditions (pH 7.5) these proteases are inactivated due to the presence of different protease inhibitors, for this reason the peptide linker is stable in systemic circulation and it is only cleaved upon internalization in tumors. In 2011, the FDA approved the ADC Adcetris® containing a Val-Cit linker connected to the self-immolative p-aminobenzylcarbamate-monomethyl auristatin E and an anti-CD30-mAb.[34,69]
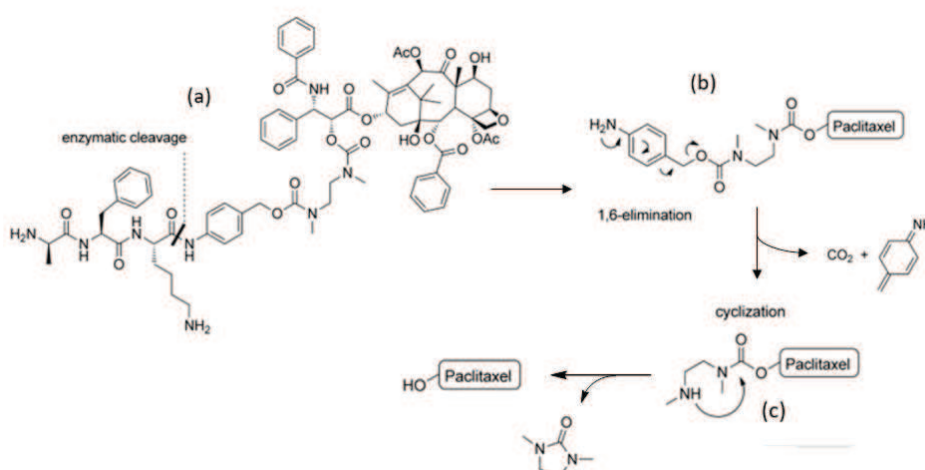
Figure 12. Enzymatic cleavage and drug release of paclitaxel prodrug containing the peptide linker [D]-Ala–Phe–Lys. Prodrug [D]-Ala-Phe-Lys-PABC-PTX **a** undergoes enzymatic cleavage giving **b**, 1,6-elimination of self-immolative p-aminobenzylcarbamate moiety gives the metabolite **c**. Finally, intramolecular cyclization allows the release of the paclitaxel.[70] Adapted with permission from A. dal

- Non-cleavable linkers: alkyl or polymeric moieties that liberate the payload only after lysosomal degradation of the conjugate inside the cell. Their main advantage is the increased plasma stability compared to cleavable linkers[71] and the specificity of the drug release mechanism. This type of linker has been successfully used in ADCs, notably in trastuzumab emtansine (Kadcyla®), that contains a non-reducible thioether, N-succinimidyl-4-(N-maleimidomethyl) cyclohexane-1-carboxylate (SMCC or MC after conjugation), that connects the antibody with the maytansinoid DM1.[72]

1.4.4. Payload selection

The choice of the cytotoxic drug depends on the molecular target and the chemical structure of the conjugate. The drug is expected to exert a potent cytotoxic activity after internalization *via* receptor-mediated endocytosis, which means that a good membrane permeability is needed to diffuse across the endosomal membranes and some organelles (e.g. mitochondrion or nucleus). In addition, its chemical properties must afford an easy conjugation to the linker or self immolative moiety, for example through functional groups like hydroxyl, carboxyl, amines, carbonyls or thiols. In some cases it is also necessary to regulate the hydrophobicity of the payload to improve the conjugate's pharmacokinetics, this can be achieved by introducing hydrophilic PEG spacers.[18,50]

Among the cytotoxic drugs used in SMDC currently in clinical trials there are antimitotic agents such as paclitaxel, docetaxel, tubulysin B and desacetyl vinblastine hydrazide; and DNA damaging agents like ifosfamide and mitomycin C (Figure 13).[50] However, promising cytotoxic agents with higher potency ($IC_{50} < 10^{-9}$ M) are also being evaluated as payloads for SMDCs. This is the case of the tubulin polymerization inhibitors monomethyl auristatin E (MMAE),[58,73] cryptophycins[74] and maytansinoids (e.g. DM1),[57,75] and the intercalating agent PNU-159682.[73]
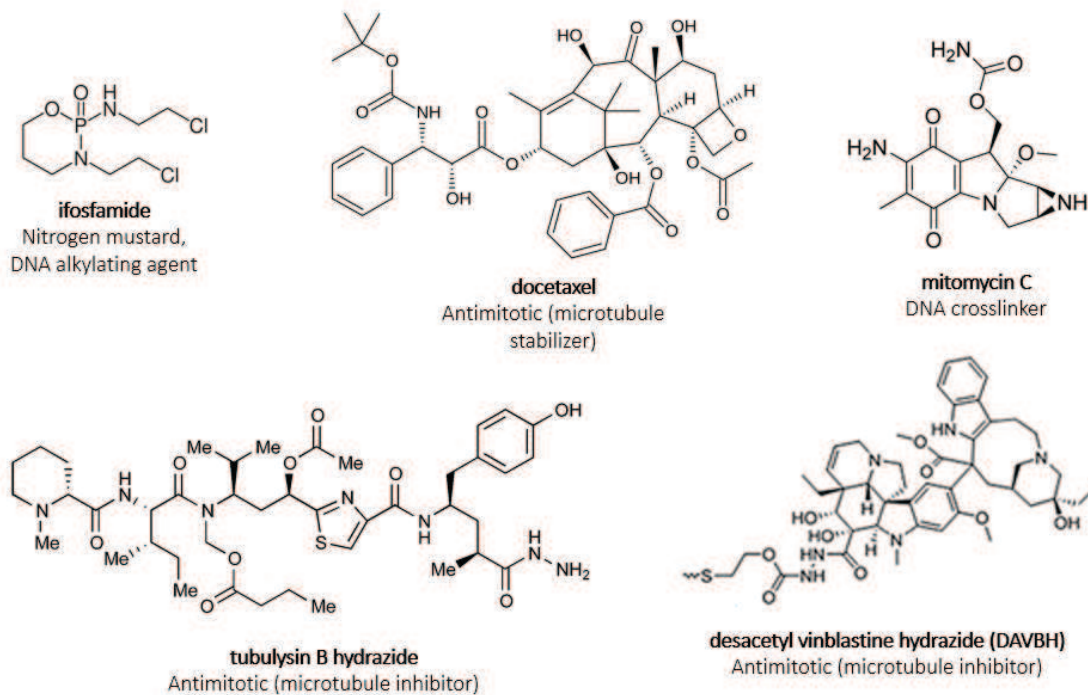
Figure 13. Cytotoxic drugs used in SMDCs

1.4.5. SMDCs in clinical trials

At present there are nine SMDCs in different stages of clinical trials (Table 1).[47,50] Most of these conjugates target the vitamin folate receptor alpha (FRα) overexpressed in a variety of human tumors (e.g. ovary, lung, kidney, endometrium, colon and breast) and have been developed by Endocyte. Their lead candidate EC145, also known as vintafolide, contains the vitamin folic acid conjugated to desacetyl vinblastine monohydrazide (DAVBH) *via* a dithiol cleavable linker. It is currently in Phase II testing against non-small-cell lung carcinoma and solid tumors.[76]

Table 1. Small molecule-drug conjugates in clinical trials[50,77]

Conjugate	Target	Ligand	Cytotoxic agent	State
Glufosfamide	Glut1	β-D-glucose	Ifosfamide	Phase 3: metastatic pancreatic cancer Phase 2: GM, pancreatic cancer and soft tissue sarcoma Phase 1: pancreatic neoplasm

NGR-TNF	APN	NGR	TNF-α	Phase 2: metastatic ovarian cancer, metastatic SCLC, adult soft tissue carcinoma, metastatic HCC, colorectal cancer Phase 1: advanced solid tumors
GRN1005	LRP1	Angiopep2	Paclitaxel	Phase 2: brain cancer, glioma, metastatic breast cancer
BIND 014	PSMA	DUPA	Liposomal docetaxel	Phase 2: prostate cancer, NSCLC
EC1169	PSMA	DUPA	Tubulysin	Phase 1: recurrent MCRPC
EC145	FR	Folic acid	Desacetyl vinblastine hydrazide (DAVBH)	Phase 2: solid tumors, ovarian and endometrial cancer, NSCLC, lung adenocarcinoma Phase 1: recurrent or refractory solid tumors
EC0225	FR	Folic acid	DAVBH and mitomycin C	Phase 1: refractory or metastatic solid tumors
EC0489	FR	Folic acid	DAVBH	Phase 1: refractory or metastatic solid tumors
EC1456	FR	Folic acid	tubulysin	Phase 1: solid tumors, NSCLC, ovarian cancer

Glut1 = glucose transporter 1, TNF = tumor necrosis factor, APN = aminopeptidase N, LRP1 = low-density lipoprotein receptor-related protein 1, PSMA = prostate-specific membrane antigen, DUPA = 2-[3-(1,3-dicarboxypropyl)ureido]pentanedioic acid, DAVBH = desacetylvinblastine hydrazide, GM = glioblastoma multiforme, SCLC = small-cell lung cancer, NSCLC = nonsmall-cell lung cancer, HCC = hepatocellular carcinoma, FR = folate receptor, MCRPC = metastatic castration-resistant prostate cancer.

Endocyte has also developed a SMDC targeting the prostate specific membrane antigen (PSMA). EC1169 is constituted by the ligand DUPA and tubulysin B hydrazide as a payload, and it is currently in Phase I clinical trials for recurrent metastatic castration-resistance prostate cancer (MCRPC) patients.[78,79] Another SMDC targeting the PSMA is BIND 014, developed by Bind Therapeutics. This conjugate containing DUPA and a docetaxel-based nanoparticle payload, has recently shown acceptable safety in phase II with MCRPC patients.[80]

NGR-TNFα is a SMDC developed by Corti and coworkers[81] that targets the aminopeptidase-N (APN), overexpressed on the vasculature of several human cancers. It contains a small peptide ligand formed by the sequence Asn-Gly-Arg, conjugated to the tumor necrosis factor α (TNFα), a multifunctional cytokine that plays a key role in apoptosis and cell survival, as well as in inflammation and immunity.[82] This compound has shown promising activity in Phase I clinical trials in combination with doxorubicin for treatments of solid tumors.[81] Other peptide-drug conjugate in clinical evaluation is GRN 1005 (or ANG 1005), developed by Angiochem and containing three molecules of paclitaxel bound to the 19-aminocid sequence angiopep2 that targets the low-density lipoprotein receptor-related protein 1 (LRP-1).[83] This conjugate has been recently tested in non-small cell lung cancer patients with brain metastasis (GRABM-L).

The progress of SMDCs in the pipeline of new therapeutics reassures the validity of this approach. Furthermore, the increasing diversity of ligands, spacers, linkers and payloads now available makes possible the design of novel and more efficient conjugates with improved affinity for their specific targets and better control of drug delivery and release.[9,50]

Chapter 2. Tumor targeting with integrin ligands

2.1. Role of integrins in cancer

Integrins are cell surface receptors constituted by α and β subunits associated in a non-covalent manner. Both subunits are type I transmembrane glycoproteins that contain an extracellular domain, a single transmembrane domain and a short intracellular tail. In vertebrates, 18 α subunits and eight β subunits form 24 integrin αβ heterodimers expressed in different tissues.[84,85] Each integrin exhibits a distinct binding affinity to particular ligands determined mostly by the α subunit (Figure 14), defining integrin subfamilies with specificity for Arg-Gly-Asp (RGD) motifs (α_{IIb}, α_V, α_5, α_8), intercellular adhesion molecules and inflammatory ligands (α_4, α_L, α_M, α_X, and α_D), collagens (α_1, α_2, α_{10}, α_{11}) and laminins (α_3, α_6, α_7).[86]
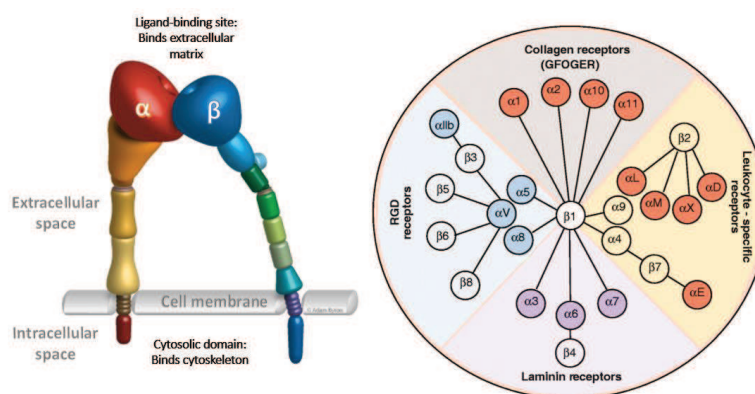
Figure 14. Schematic representation of two integrins subunits and the 24 members of integrin family[86]

Integrins play an important role in cell adhesion (cell-cell, cell-ECM), migration, survival and growth. After binding to ECM proteins (e.g. fibronectin and vitronectin) or cell surface immunoglobulin proteins (e.g. ICAM-1 and VCAM-1), integrins initiate a signaling cascade that can include tyrosine phosphorylation of focal adhesion kinases (FAK) and interaction with growth factors receptors (GFRs).[87,88] They mediate a bidirectional "outside-in" and "inside-out" signaling across the cell membrane,

exchanging information between the ECM and intracellular molecules.[89,90] These complex signaling pathways allow the control of cell polarity, mobility, ECM remodeling and assembly that results in cell survival and proliferation.[91] During the last two decades, integrins have gained increasing attention in pharmacological research since some integrins, notably $\alpha_V\beta_3$, $\alpha_5\beta_1$ and $\alpha_V\beta_6$, are overexpressed in a variety of cancers contributing to progression and metastasis (Table 2).[92,93]

Table 2. Integrins in cancer progression[92]

Tumor Type	Integrin expressed
Melanoma	$\alpha_V\beta_3$, $\alpha_5\beta_1$
Breast	$\alpha_V\beta_3$, $\alpha_6\beta_4$
Prostate	$\alpha_V\beta_3$
Pancreatic	$\alpha_V\beta_3$
Ovarian	$\alpha_V\beta_3$, $\alpha_4\beta_1$
Cervical	$\alpha_V\beta_3$, $\alpha_V\beta_6$
Glioblastoma	$\alpha_V\beta_3$, $\alpha_V\beta_5$
Non-small-cell lung carcinoma	$\alpha_5\beta_1$
Colon	$\alpha_V\beta_6$

The integrin receptor $\alpha_V\beta_3$, first identified by Ruoslahti and coworkers,[94] is widely expressed on blood vessels of tumor cells (e.g. breast, glioblastoma, ovarian, prostate cancer) but not on vessels of normal tissue.[95] Integrin $\alpha_V\beta_3$ is upregulated during tumor angiogenesis due to the stimuli of angiogenic growth factors such as fibroblast growth factor-2 (FGF-2), tumor necrosis factor α (TNF-α) and interleukin 8 (IL-8) present at wounds and inflammation sites. This is a critical step in tumor progression and metastasis because it provides oxygen and nutrients to the cells.[96,97] Moreover, the activation of $\alpha_V\beta_3$ also facilitates tumor cell migration by regulation of the matrix-degrading protease MMP2 on the surface of angiogenic blood vessels, resulting in collagen degradation and ECM modification.[87,98]

Because its implication in biological functions determinant for cancer progression and its high expression in tumor tissues, $\alpha_V\beta_3$ has been largely studied and validated as a therapeutic target.

2.2. Integrin ligands targeting the αᵥβ₃ receptor

2.2.1. RGD integrin ligands

2.2.1.1. RGD recognition motif

In 1987, Ruoslahti reported the tripeptide sequence RGD (Figure 15) as the basic motif present in many natural ligands of the $\alpha_V\beta_3$ receptor such as fibronectin and other cell adhesion proteins (e.g. vitronectin, osteopontin, collagen).[99]

Figure 15. RGD sequence

The complete understanding of the interactions between RGD and $\alpha_V\beta_3$, however, was only possible in 2002 when Xiong and coworkers[100] reported the crystal structure of the extracellular segment of the $\alpha_V\beta_3$ integrin receptor complexed with the $\alpha_V\beta_3$ integrin binder Cilengitide (Figure 16).

Figure 16. Cilengitide–integrin $\alpha_V\beta_3$ interaction. A) Surface representation of the RGD ligand-binding site; (B) Crystal structure of the $\alpha_V\beta_3$ -Cilengitide complex. (ADMIDAS and MIDAS regions are shown in violet and cyan respectively; Cilengitide is represented in yellow; α_V and β_3 residues are labelled in blue and red, respectively; O and N atoms are represented in red and blue respectively. Hydrogen bonds and salt bridges are represented with dotted lines). Adapted with permission from Jian-Ping Xiong, Thilo Stehle et al.; *Science*. 2002, 296 (5565), 151–155. Copyright © 2002 The American Association for the Advancement of Science.

The crystal structure showed an extended conformation of the RGD sequence in the binding pocket, with a distance of 9 Å between the C_β atoms of the Arg and Asp residues. This folding allows the guanidine group of Arg to interact with two anionic aspartic acid residues in the α-subunit (Asp 218 and Asp150), whereas the aspartic acid binds to Mn^{2+} divalent cation in the metal ion-dependent adhesion site (MIDAS) region of the β-subunit. The glycine residue, at the interface between both subunits, presents weak hydrophobic interactions with the carbonyl group of Arg216, same than the aromatic group of the ligand with Tyr122.[100,101] All these integrin-ligand interactions, also known as "electrostatic clamp", suggested structural requirements that constituted the starting point for the development of high affinity synthetic $\alpha_v\beta_3$ integrin ligands.

2.2.1.2. Cyclic RGD integrin ligands

Several small molecules, peptides and peptidomimetics containing the RGD sequence have been designed to target the integrin $\alpha_v\beta_3$ either as antagonists or as vehicles for selective delivery of drugs and imaging probes to tumors.[102,103]

First synthetic RGD ligands were linear peptides that included the RGD-motif and other amino acids added to the sequence (e.g. RGD, RGDS, GRGD, GRGDS, GRGDSP, GRGDSPK). Whereas linear ligands showed good binding affinity for the $\alpha_v\beta_3$ receptor, also presented low stability regarding enzymatic degradation, resulting in limited applicability for *in vivo* studies.[104,105] This led to the use of different strategies including cyclization, modification of the stereochemical configuration of the constituent amino acids and N-methylation to improve the biological activity of RGD ligands.[106,107]

In 1991, Kessler and coworkers developed the cyclic pentapeptide *cyclo*(RGDfV) (Figure 17a) which displayed high binding affinity towards $\alpha_v\beta_3$ (IC_{50} $\alpha_v\beta_3$ = 1.54 ± 0.12 nM) while retaining selectivity against other integrins (e.g. $\alpha_{IIb}\beta_3$, $\alpha_v\beta_5$, $\alpha_v\beta_8$).[108,109] This base structure was later modified to produce new ligands with improved activity and selectivity profiles.[110] Among them, *cyclo*[RGDf-(*N*Me)V] (Cilengitide, Figure 17b) showed outstanding binding affinity for $\alpha_v\beta_3$ (IC_{50} $\alpha_v\beta_3$ = 0.61 ± 0.06 nM) and $\alpha_v\beta_5$ (IC_{50} $\alpha_v\beta_5$ = 8.4 ± 2.1 nM) as well as subnanomolar antagonistic activity for the $\alpha_v\beta_3$ receptor.[111,112] Cilengitide became the first integrin antagonist to be tested in clinical trials and it is currently undergoing phase II studies for the treatment of different

tumors[113–115] despite its failure in phase III trial for the treatment of patients with newly diagnosed glioblastoma.[116]

a) c(RGDfV)
IC_{50} $\alpha_v\beta_3$ = 3.2 ± 1.3 nM

b) Cilengitide - *c*(RGDf-(NMe)V)
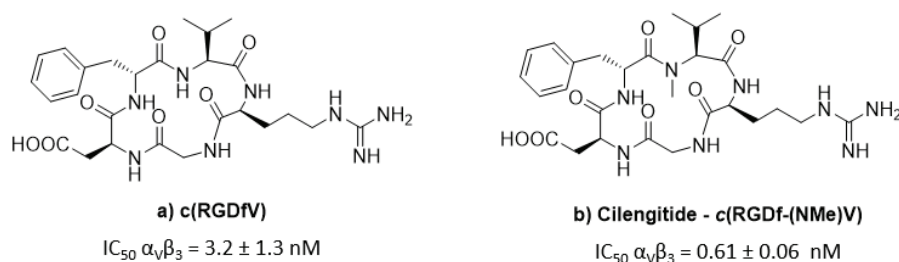IC_{50} $\alpha_v\beta_3$ = 0.61 ± 0.06 nM

Figure 17. Structure of cyclic RGD ligands c(RGDfV) and c[RGDf-(NMe)V]

Other RGD ligands reported by the same group are *cyclo*(RGDfK), *cyclo*(RGDyK), *cyclo*(RGDfC) (Figure 18, a-c) and RGD4C (Figure 18, d).[95,103] The amino group of the lysine residue of *cyclo*(RGDfK) and *cyclo*(RGDyK) allows further chemical conjugation, similarly in the case of *cyclo*(RGDfC), the thiol group of the cysteine residue is often used in the conjugation to maleimide-functionalized linkers *via* Michael addition. For these reason, the mentioned ligands are commonly used as vectors for the delivery of therapeutic agents.[95,117,118] In 1995, Ruoslahti and coworkers reported the discovery by phage display technology of the undecapeptide RGD4C (ACDCRGDCFCG)[119], which is structurally constrained by two disulfide bonds. RGD4C has been used delivery systems by conjugation at its N- or C-terminals.[120–123] Furthermore, it can be expressed by recombinant methods into proteins and viruses, as in the case of the RGD4C-TNF fusion protein,[124] used for the targeted delivery of TNF to $\alpha_v\beta_3$ expressing tumors.
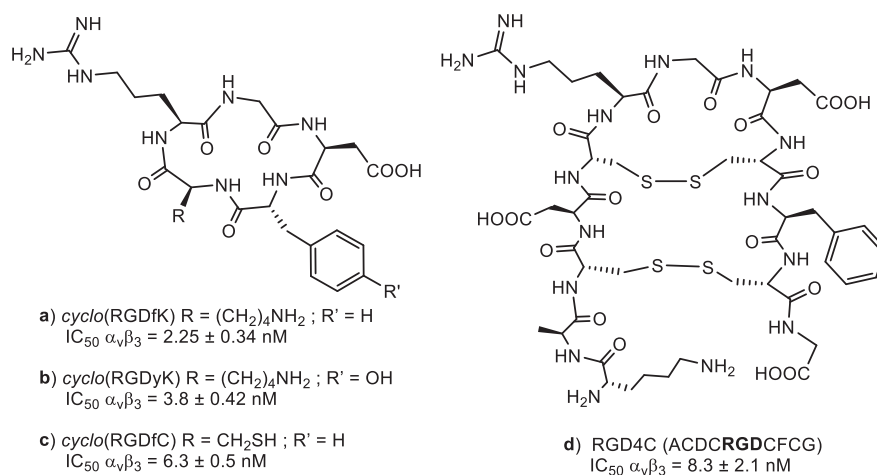

a) *cyclo*(RGDfK) R = $(CH_2)_4NH_2$; R' = H
   IC_{50} $\alpha_v\beta_3$ = 2.25 ± 0.34 nM

b) *cyclo*(RGDyK) R = $(CH_2)_4NH_2$; R' = OH
   IC_{50} $\alpha_v\beta_3$ = 3.8 ± 0.42 nM

c) *cyclo*(RGDfC) R = CH_2SH ; R' = H
   IC_{50} $\alpha_v\beta_3$ = 6.3 ± 0.5 nM

d) RGD4C (ACDC**RGD**CFCG)
   IC_{50} $\alpha_v\beta_3$ = 8.3 ± 2.1 nM

Figure 18. RGD ligands used in delivery systems[95]

2.2.1.3.   Cyclo[DKP-RGD] integrin ligands

In 2009 our research group reported the synthesis of low-nanomolar peptidomimetics where the RGD sequence was cyclized by means of a bifunctional diketopiperazine (DKP) scaffold containing a carboxylic and an amino function.[125,126]   In 2012, a small library of different cyclo[DKP-RGD] ligands was reported, differing in the configuration at the two DKP stereocenters (position 3 and 6) and in the substituents at the DKP nitrogen atoms (Figure 19). The introduction of the DKP scaffold confers metabolic stability and conformational rigidity to the ligand, facilitating the interactions needed to fit into the RGD pocket of $\alpha_V\beta_3$ receptor.[127,128] In particular, the RGD peptidomimetics **2-7** derived from *trans*-DKP scaffolds (DKP2-DKP7) showed a preferential binding affinity towards integrin $\alpha_V\beta_3$, inhibiting the binding of biotinylated vitronectin, a natural integrin ligand, to the purified $\alpha_V\beta_3$ at low-nanomolar IC_{50} values in a competition binding assay (Table 3).[127]
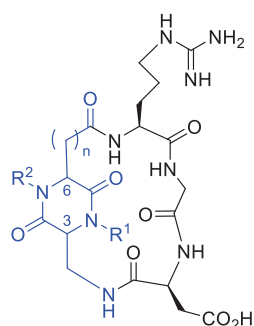
1. *cyclo*[**DKP1**-RGD]: 3*S*, 6*S*, R^1 = Bn, R^2 = H, n = 1
2. *cyclo*[**DKP2**-RGD]: 3*R*, 6*S*, R^1 = Bn, R^2 = H, n = 1
3. *cyclo*[**DKP3**-RGD]: 3*S*, 6*R*, R^1 = Bn, R^2 = H, n = 1
4. *cyclo*[**DKP4**-RGD]: 3*R*, 6*S*, R^1 = H, R^2 = Bn, n = 1
5. *cyclo*[**DKP5**-RGD]: 3*R*, 6*S*, R^1 = Bn, R^2 = Bn, n = 1
6. *cyclo*[**DKP6**-RGD]: 3*S*, 6*R*, R^1 = H, R^2 = Bn, n = 1
7. *cyclo*[**DKP7**-RGD]: 3*S*, 6*R*, R^1 = Bn, R^2 = Bn, n = 1
8. *cyclo*[**DKP8**-RGD]: 3*S*, 6*R*, R^1 = Bn, R^2 = H, n = 2

Figure 19. Library of cyclo[DKP-RGD] integrin ligands

Table 3. Inhibition of biotinylated vitronectin binding to $\alpha_V\beta_3$ and $\alpha_V\beta_5$ receptors[126,127]

Compound N°	Structure	$\alpha_V\beta_3$ IC_{50} [nM]	$\alpha_V\beta_5$ IC_{50} [nM]
1	*c*yclo[DKP1-RGD]	3898 ± 418	>10^4
2	*cyclo*[DKP2-RGD]	3.2 ± 2.7	114 ± 99
3	*cyclo*[DKP3-RGD]	4.5 ± 1.1	149 ± 25
4	*cyclo*[DKP4-RGD]	7.6 ± 4.3	216 ± 5
5	*cyclo*[DKP5-RGD]	12.2 ± 5.0	131 ± 29
6	*cyclo*[DKP6-RGD]	2.1 ± 0.6	79 ± 3
7*	*cyclo*[DKP7-RGD]	a) 220.2 ± 82.3 b) 0.2 ± 0.09	a) >10^4 b) 109 ± 15
8	*cyclo*[DKP8-RGD]	7.5 ± 0.0	>10^3

| - | cyclo(RGDfV) | 3.2 ± 1.3 | 7.5 ± 4.8 |

[a]IC$_{50}$ values are calculated as the concentration of compound required for 50% inhibition of biotinylated vitronectin binding. * Two diastereoisomers detected.

NMR characterization and conformational studies performed on the cyclo[DKP-RGD] ligands **1-8** revealed that the ligands with highest affinity values (trans configuration) displayed well-defined preferential conformations with an average distance of 8.8Å between C$_\beta$(Arg) and C$_\beta$(Asp) consistent with an extended arrangement of the RGD sequence (Figure 20).[127]
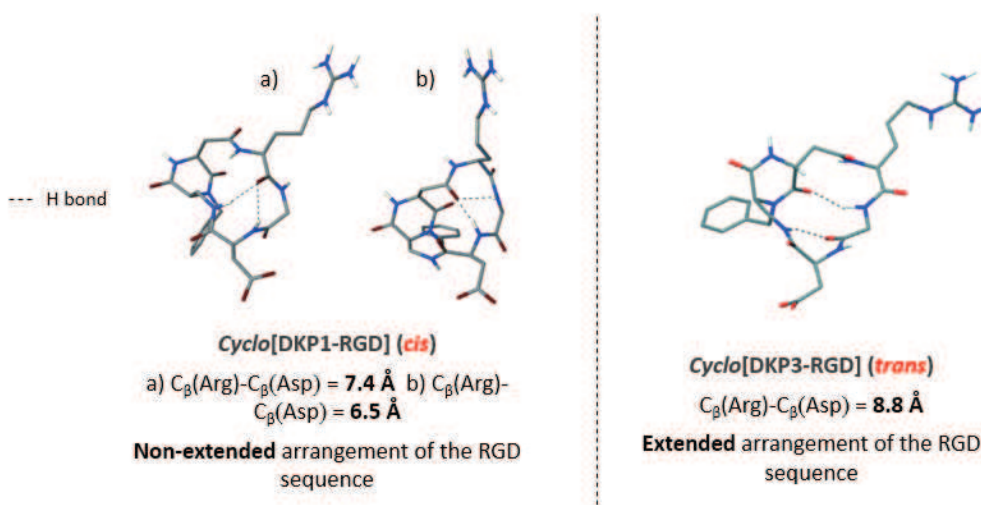

Figure 20. Structures obtained by restrained MC/SD simulations based on NOESY spectra distance information[127]

Docking studies were performed based on the representative conformations obtained from the MC/SD simulations. During these studies the ligand cyclo[DKP3-RGD] **3**, produced top-ranked poses displaying all the important interactions RGD- α$_V$β$_3$ integrin, taking as a reference the crystal structure of the extracellular segment of the α$_V$β$_3$ integrin receptor complexed with the peptide binder Cilengitide.[127]
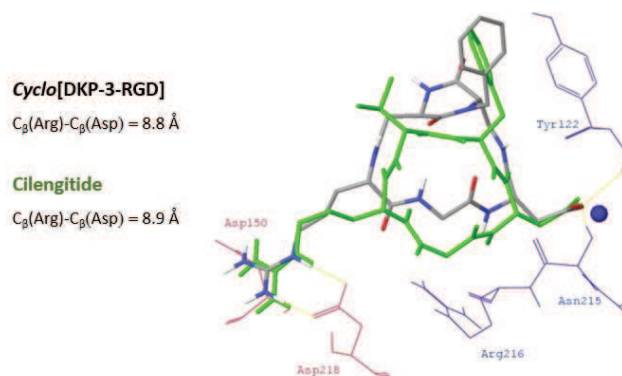
Figure 21. Best pose of compound *cyclo*[DKP3-RGD] into the crystal structure of $\alpha_v b_3$ integrin overlaid on Cilengitide (green tube representation).

In further biological evaluation, the *c*[DKP3-RGD] ligand **3** was tested for its effect on cell viability, proliferation, migration and capillary network formation; mRNA expression of α_V, β_3 and β_5 subunits and Akt phosphorylation in human umbilical vein endothelial cells (HUVEC). Results showed that *cyclo*[DKP3-RGD] significantly inhibit the cell adhesion and angiogenesis induced by growth factors (VEGF, EGF, IGF-I, FGF2 and IL-8) as well as the phosphorylation of Akt, a protein kinase important in the regulation of vascular homeostasis and angiogenesis.[129] Recent studies demonstrated that *c*[DKP3-RGD] was able to inhibit also the FAK/Akt integrin-activated transduction signaling pathway and integrin-mediated cell infiltration process in U373 human glioblastoma cell line, reinforcing its condition of true integrin $\alpha_v\beta_3$ antagonist.[130]

The former results increased the interest in *cyclo*[DKP3-RGD] **3** as a potential vehicle for the delivery of cytotoxic agents. For this purpose the DKP3 scaffold was modified by substituting one amine proton with a benzylamine moiety, obtaining the functionalized *c*[DKP-*f3*-RGD] ligand (**9**, Figure 22)[131] that has been used in the preparation of SMDCs targeting the $\alpha_v\beta_3$ receptor.[70,132,133]
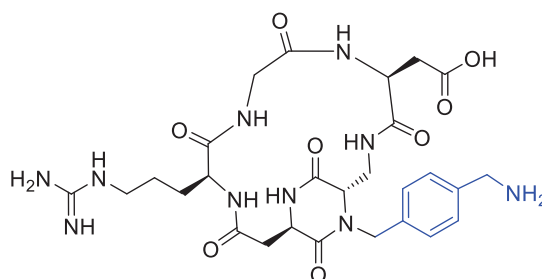

Figure 22. *Cyclo*[DKP-*f3*-RGD] (*c*[DKP-RGD]-CH_2NH_2) integrin ligand (**9**)

2.2.1.4. RGD integrin ligands in SMDCs

The recognition of integrins as potential targets for cancer treatment has led to the development of drug delivery systems based on RGD integrin ligands that can selectively target the tumor cells overexpressing the $\alpha_v\beta_3$ receptor and release the cytotoxic agent into the cell after internalization *via* receptor-mediated endocytosis.[134] Some examples of RGD-drug conjugates are presented in this section, including the work developed by our research group in the field. (An extended review about RGD conjugates used in drug delivery and theranostics can be found in references 95,102,117,135–137.

- RGD-Doxorubicin conjugates

Two conjugates containing the doxorubicin prodrug doxsaliform (DOXSF) and RGD ligands were reported by Burhart and co-workers in 2004.[138] The linker in this case was the *N*-Mannich base of doxsaliform that released DOX upon hydrolysis. The conjugates, DOXSF-acyclicRGD4C and DOXSF-*c*[RGDf(N-Me)V] (Figure 23, a-b), displayed good binding affinity values in a vitronectin cell adhesion assay (IC_{50} = 5 nM and 10 nM respectively) and resulted slightly more toxic compared than the free DOX in a cell viability assay carried out in MDA MB-435 cell line. Later, Ryppa and co-workers[139] reported the synthesis of two DOX-E[*c*(RGDfK)]$_2$ conjugates. In one of them DOX was attached to the ligand through an amide bond (Figure 23, c) while in the second one the linker used was a MMP2/MMP9 cleavable octapeptide (Figure 23, d). The conjugate bearing the protease cleavable linker demonstrated to be more efficient in the HUVEC antiproliferative, however, it displayed a moderate antitumor activity compared to free DOX in vivo.
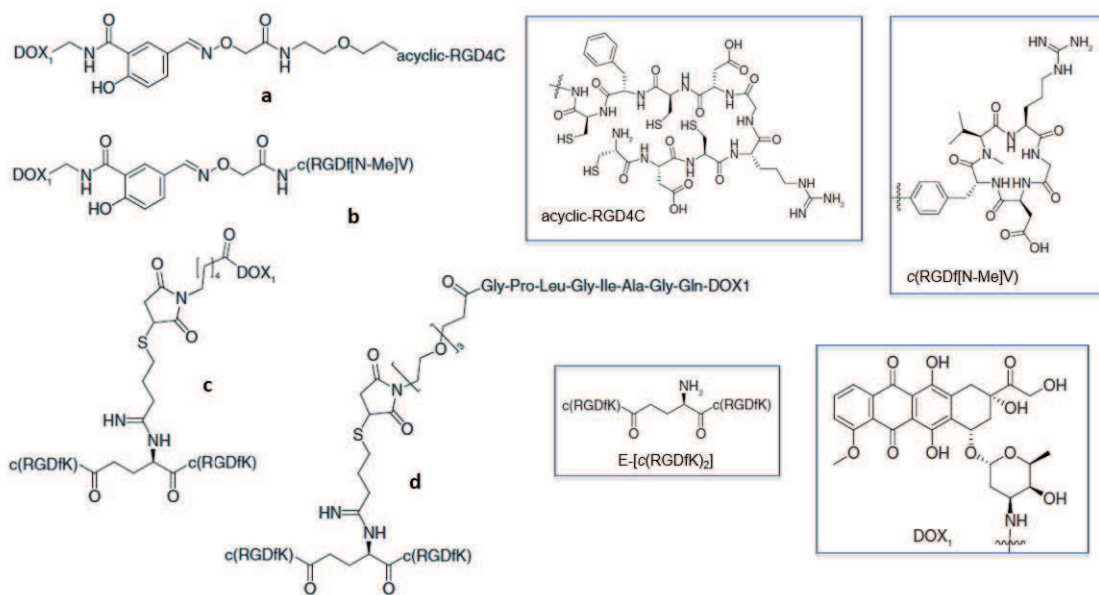
Figure 23. RGD-DOX conjugates

- ### RGD-MMAE conjugates

In 2014, Tsien's group developed the cyclic RGD conjugate RGD-PLGC(Me)AGMMAE-ACPP (Figure 24),[140] a dual targeting conjugate containing the potent tubulin polymerization inhibitor MMAE, an activable cell penetrating peptide (ACPP) targeting the MMP2, a far-red fluorescent dye (Cy5) and the *cyclic*(RGDfC) integrin ligand, for theranostic applications. The drug is connected to the ACPP *via* a maleimide-Val-Cit-PAB cleavable linker, whereas the cyclic RGD and Cy5 are connected to ACPP through PEG and maleimide linkers. The conjugate showed better cellular uptake compared with cyclic-RAD-PLGC(Me)AG-MMAE-ACPP, the negative control for $\alpha_v\beta_3$ targeting, in U87MG cell line. During *in vivo* experiments, the conjugate reduced tumor volume in 40% compared to the control group in MDA-MB-231 orthotopic human breast tumor and inhibit tumor growth in syngeneic Py230 murine breast tumors.
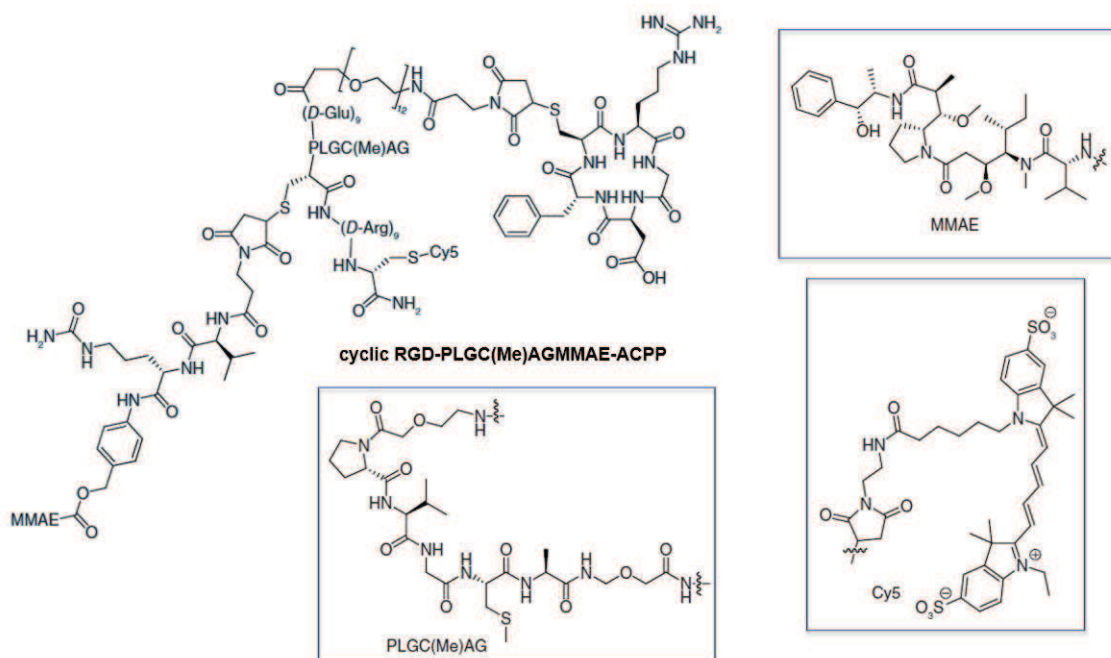
Figure 24. Cyclic RGD-PLGC(Me)AG-MMAE-ACPP conjugate

- RGD-camptothecin conjugates

In 2010 Dal Pozzo and co-workers presented the synthesis of five camptothecin (CPT) conjugates with c(RGDfV) analogues, bearing an uncleavable amide (Figure 25, a-c) or an hydrazone linker (Figure 25, d-e). All the conjugates showed good binding affinity for the $\alpha_v\beta_3$ receptor, but only the conjugates containing the hydrazone acid labile linker displayed a cytotoxicity superior to free CPT in A2780 ovarian carcinoma, A498 renal carcinoma and PC3 prostate carcinoma cell lines. However, the acid labile conjugates showed poor solubility and stability even at pH 7.4, which suggests the high cytotoxicity was due to the premature release of CPT in the medium.[141]
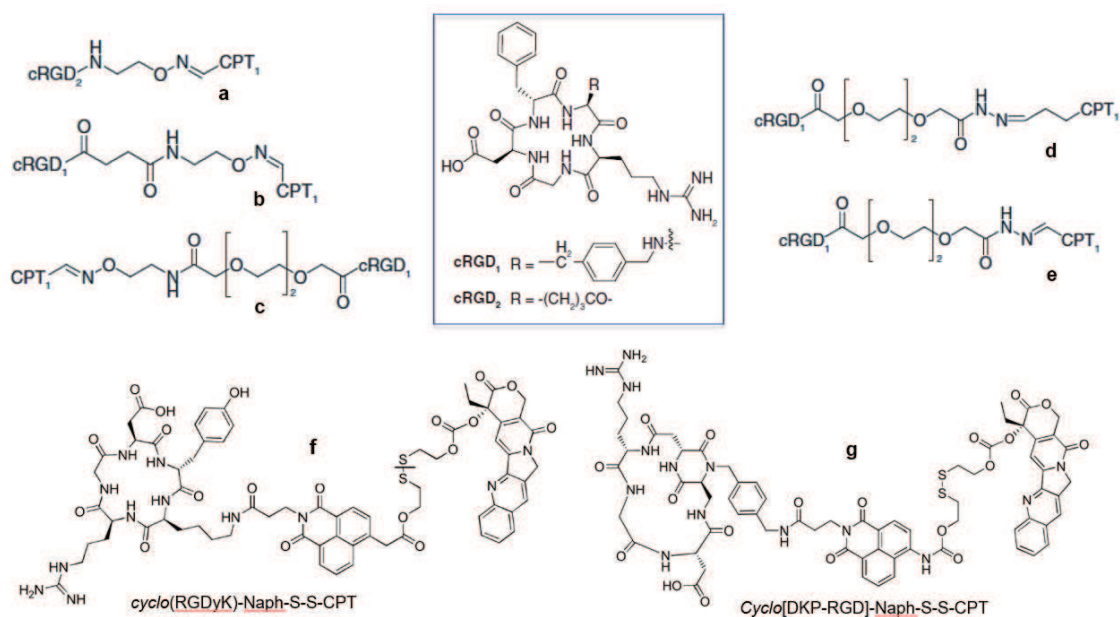
Figure 25. RGD-CPT conjugates

Recently, Gennari's group reported the synthesis and *in vitro* evaluation of two theranostic RGD-camptothecin conjugates (Figure 25, f-g), conformed by cyclo(RGDfK) or *c*[DKP-RGD]-CH$_2$NH$_2$ **9** and a fluorescent naphthalimide moiety bound to CPT via a disulfide linker. Both conjugates exhibited a good binding affinity for integrin α$_v$β$_3$, inhibiting the binding of biotinylated vitronectin to the purified receptor at nanomolar concentrations (IC$_{50}$ 5-21 nM). Nevertheless, in cell viability assays carried out in U87 (α$_v$β$_3$+) cell line and α$_v$β$_3$ non- expressing clone U87 β$_3$-KO the conjugates showed an antiproliferative activity similar to the free CPT and not dependent on the α$_v$β$_3$ expression. These results were consistent with confocal microscopy and immunofluorescence internalization studies where it was not observed a correlation between the internalization and the expression of α$_v$β$_3$.[132]

- RGD-Paclitaxel conjugates

In 2012, the synthesis and biological evaluation of SMDC based on the *c*[DKP-RGD]-CH$_2$NH$_2$ **9** and paclitaxel connected by an acid-labile ester linker was reported by the groups of Gennari and Piarulli. The conjugate *c*[DKP-RGD]-CH$_2$NH$_2$-PTX (Figure 26, a) displayed a binding affinity for the α$_v$β$_3$ receptor comparable to the ligand non-functionalized *c*[DKP3-RGD] **3** (IC$_{50}$ α$_v$β$_3$: 5.2 and 4.5 nM respectively) and a selectivity towards integrin α$_v$β$_3$ compared to α$_v$β$_5$ (IC$_{50}$ α$_v$β$_5$: 219 nM). Cell viability tests performed on a panel of human tumor cell lines (i.e. IGROV-1, IGROV-1/Pt1, U2-OS,

SKOV3, PANC-1 and MIA-PaCa2) showed that the conjugate exert a cytotoxicity similar to the free PTX. However, in vivo studies carried out on IGROV-1/Pt1 carcinoma xenotransplanted in nude mice showed that the conjugate c[DKP-RGD]-CH$_2$NH$_2$-PTX was more effective than PTX, inhibiting tumor growth at 15 mg/kg-mouse doses. Moreover, the histopathological analysis of tumors from treated mice revealed the existence of aberrant mitotic cells, which is consistent with PTX mechanism of action.[131]
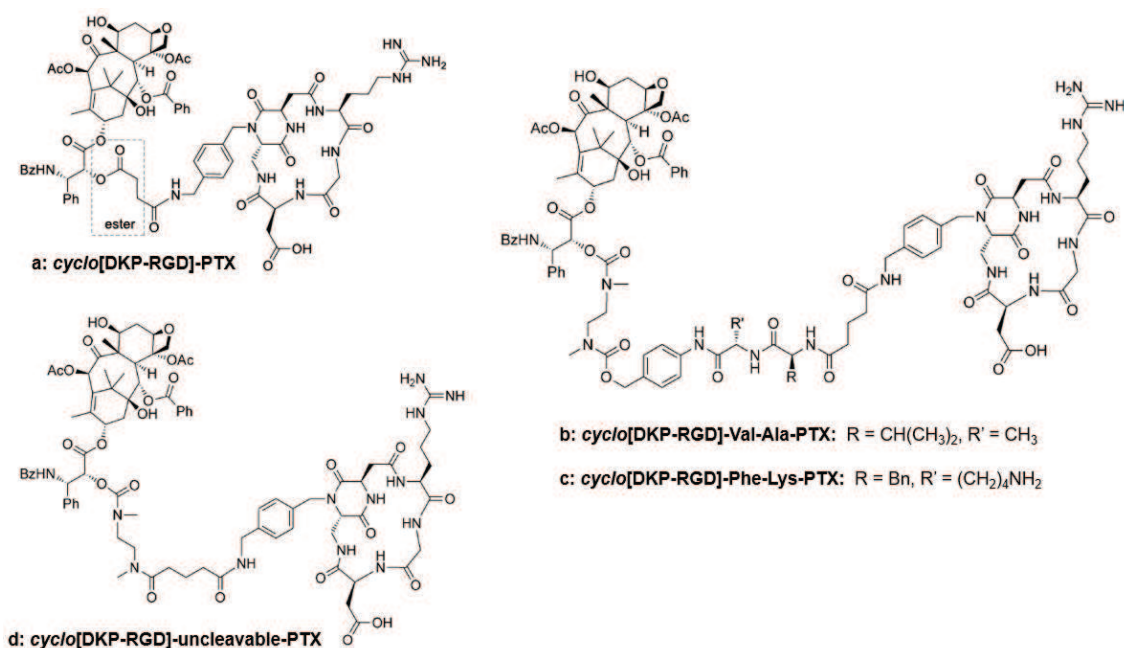

Figure 26. cyclo[DKP-RGD]-PTX conjugates

The same groups developed in 2015 two c[DKP-RGD]-PTX conjugates containing the ligand **9** bound to PTX through lysosomally cleavable dipeptide linkers: Val-Ala and Phe-Lys (Figure 26, b-c). Additionally, a c[DKP-RGD]-PTX conjugate containing an 'uncleavable' nonpeptide linker was synthetized as a negative control of the linker efficacy (Figure 26, d). In the competitive binding assay, the three conjugates displayed slightly lower binding affinity than the unconjugated ligand **9**, remaining in the low nanomolar range and conserving the selectivity towards $\alpha_v\beta_3$ compared to $\alpha_v\beta_5$. The conjugates bearing the dipeptide linkers were stable at different pH conditions and showed an efficient linker cleavage and release of the drug after treatment with lysosomal extract. The antiproliferative activity of the conjugates was evaluated on two isogenic cell lines expressing different levels of $\alpha_v\beta_3$: acute lymphoblastic leukemia cell line CCRF-CEM ($\alpha_v\beta_3$-) and its sub-clone CCRF-CEM ($\alpha_v\beta_3$+). The conjugate bearing the uncleavable linker showed no cytotoxicity, whereas the conjugates bearing the

dipeptide cleavable linkers displayed an antiproliferative activity similar to free PTX with an increased potency in CCRF-CEM ($\alpha_V\beta_3$+) compared to the negative cell line. These results suggested an integrin-targeting effect presented by the conjugates.[70]

2.2.2. *iso*DGR integrin ligands

2.2.2.1. *Iso*DGR sequence: a new $\alpha_V\beta_3$ recognition motif

In 2006 Corti and co-workers identified the *iso*Asp-Gly-Arg sequence (Figure 27) resulting from the spontaneous transformation of the NGR (Asn-Gly-Arg) portion of fibronectin, as a new binding motif recognized by the $\alpha_V\beta_3$ receptor.[142]
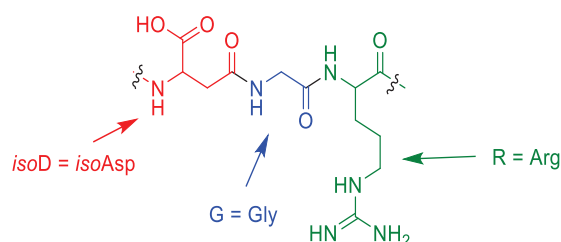

Figure 27. *iso*DGR sequence

In effect, the asparagine residue of NGR can undergo a non-enzymatic deamidation at physiological pH, passing through the formation of a succinimide intermediate that generates *iso*DGR and DGR tripeptides mostly in L-configuration after hydrolysis (Figure 28). In the fifth type I fibronectin (FN-I5), the NGR deamidation of Asn263 was associated to the increase of cell-adhesion after an accelerated aging process (heat-induced treatment). The gain of function in cell adhesion indicated $\alpha_V\beta_3$ integrin binding that could be attributed to *iso*DGR or DGR motif, however, competitive binding tests performed on synthetic peptides containing the *iso*DGR, DGR and *iso*-dGR (D-*iso*DGR) sequences showed a superior binding affinity of *iso*DGR for the $\alpha_V\beta_3$ receptor (in the sub-micromolar range). These results led to the conclusion that *iso*DGR is a $\alpha_V\beta_3$ binding motif.[142,143]
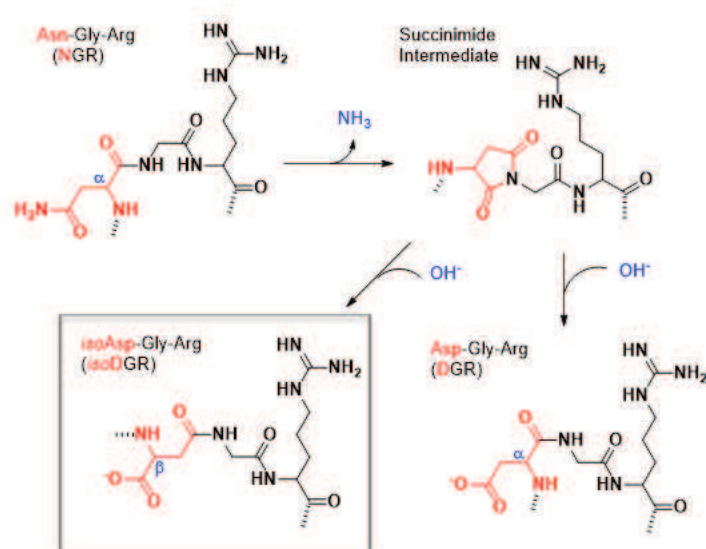
Figure 28. Schematic representation of the NGR deamidation reaction

In order to determine if the interaction of the *iso*DGR motif with the $\alpha_V\beta_3$ integrin receptor occurred at the binding site of the RGD sequence, a competitive binding test was carried out with the cyclopeptides RGD-2C (CRGDCGVRY) and *iso*DGR-2C (C*iso*DGRCGVRY), in presence of a known $\alpha_V\beta_3$ integrin binder: ACDCRGDCFC-TNF. Results showed that both ligands, RGD-2C and *iso*DGR-2C, were able to inhibit the binding of ACDCRGDCFC-TNF to $\alpha_V\beta_3$, displaying similar binding affinity values (K_d RGD = 0.41 µM, K_d *iso*DGR = 0.57 µM) suggesting that the *iso*DGR motif binds to $\alpha_V\beta_3$ at the site of RGD. The same study demonstrated that *iso*DGR can also bind the integrin $\alpha_V\beta_5$ at the binding site of RGD but with less affinity than in the case of $\alpha_V\beta_3$.[142]

In addition to biological evaluation, structural NMR analysis and docking studies performed on RGD-2C and *iso*DGR-2C confirmed that *iso*DGR binds the integrin $\alpha_V\beta_3$ fitting into the RGD pocket.[144] The model of the ligands in complex with $\alpha_V\beta_3$ (Figure 29) showed that *iso*DGR-2C displays a reversed orientation compared to RGD-2C, preserving all the interactions previously described for RGD: *iso*Asp residue coordinates with the metal ion of the MIDAS region of the β domain through its carboxylate and forms hydrogen bonds with Asn215, Tyr122 and Arg214, whereas Arg residue forms a bidentate salt bridge with Asp218 and an hydrogen bond with Asp150 and Gln180 at the α subunit. Interestingly, the *iso*DGR motif established additional interactions such as an hydrogen bond between the amide proton of the glycine residue and the carbonyl group of Arg216 that contributes to the ligand recognition.[144,145]
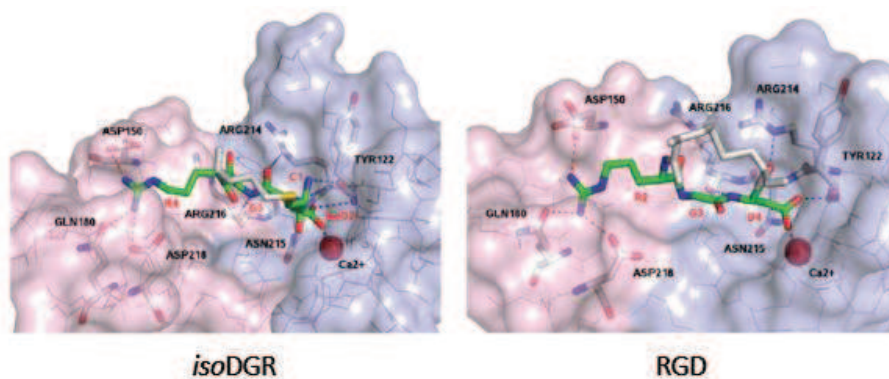
Figure 29. Model for the interaction for *iso*DGR and RGD at integrin $\alpha_v\beta_3$ binding site. Representation of the $\alpha_v\beta_3$-binding pocket in complex with C*iso*DGRC (left) or CRGDC (right). α_v and β_3 subunits are represented in pink and pale cyan respectively; RGD and *iso*DGR motifs are shown in green; cystine in gray; N, O and S atoms in blue, red and yellow respectively; Ca^{2+} of MIDAS region is represented by a red sphere; hydrogen bonds are represented by dotted lines. Adapted with permission from A. Spitaleri; S. Mari; F. Curnis et al. *J. Biol. Chem.* 2008, *283*, 19757–19768 Copyright © 2008 The American Society for Biochemistry and Molecular Biology, Inc.

The finding of isoDGR as an alternative motif for integrin recognition encouraged the research for new $\alpha_v\beta_3$ ligands based on this motif. The group of Corti developed in 2010 a small library of *iso*DGR ligands conformed by: $_{ac}iso$DGR-2C, a derivate of the *iso*DGR-2C with an acetyl group linked to the α-amino group of the cysteine residue (Figure 30); *iso*DGR-2G and the respective $_{ac}iso$DGR-2G. Competitive binding tests performed on the four compounds showed that *iso*DGR-2C presented 10–100-fold higher binding affinity values for $\alpha_v\beta_3$ than for other integrins (i.e. $\alpha_v\beta_5$, $\alpha_v\beta_6$, $\alpha_v\beta_8$, $\alpha_5\beta_1$) while *iso*DGR-2G displayed a weak binding affinity for $\alpha_v\beta_6$ and no binding affinity for $\alpha_v\beta_3$. The acetylated compounds presented an increased binding affinity for all integrins with loss of selectivity. These results suggested that flanking residues had an influence on the binding affinity and selectivity of the ligands.[146]
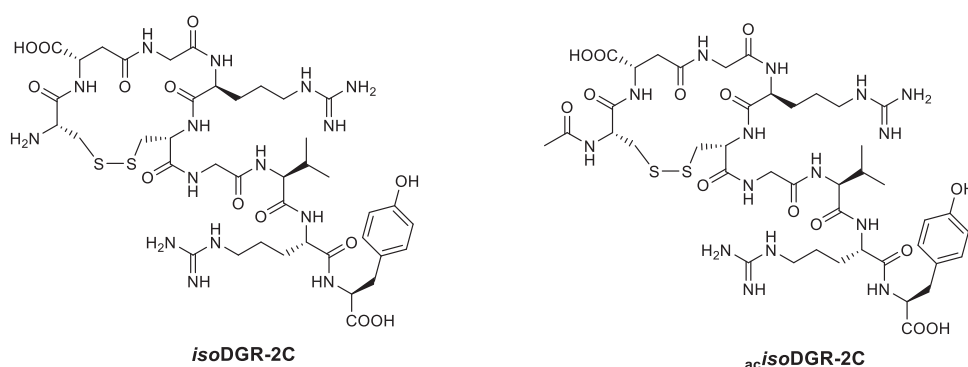

Figure 30. Integrin ligand *iso*DGR-2C (C*iso*DGRCGVRY) and its derivate $_{ac}iso$DGR-2C ($_{ac}$C*iso*DGRCGVRY)

Further computational and biochemical studies performed on *iso*DGR-2C and $_{ac}iso$DGR-2C showed they could block the ligand binding site inhibiting receptor allosteric

activation, acting as true $\alpha_v\beta_3$ antagonists.[147] In 2013 the same group reported the synthesis of a cyclic hexapeptide containing the *iso*DGR sequence, *cyclo*(CG*iso*DGRG),[148] that showed preferential binding affinity for $\alpha_v\beta_3$ compared to $\alpha_v\beta_5$ and $\alpha_5\beta_1$, and was used for the preparation of peptide-HSA (human serum albumin) conjugates with potential application in drug delivery. Moreover, recent studies have demonstrated that the antagonist condition is an inherent property of the *iso*DGR ligands, independent of the scaffold or chemical entities accompanying the tripeptide sequence.[149] This characteristic constitutes a main advantage of *iso*DGR integrin ligands over their RGD pairs, considering adverse effects (e.g. angiogenesis, tumor growth) associated to a partial agonist-like activity detected for some RGD-based peptidomimetics.[150]

2.2.2.2. *Cyclo*[DKP-*iso*DGR] integrin ligands

Based on the cyclo[DKP-RGD] library previously reported, our research group produced a small library of four cyclo[DKP-*iso*DGR] integrin ligands (Figure 31).[130,151]

10. *c*[**DKP2**-*iso*DGR]: (3*R*,6*S*), R = Ph, R^1= H
11. *c*[**DKP3**-*iso*DGR]: (3*S*,6*R*), R = Ph, R^1= H
12. *c*[**DKP5**-*iso*DGR]: (3*R*,6*S*), R = R^1 = Ph
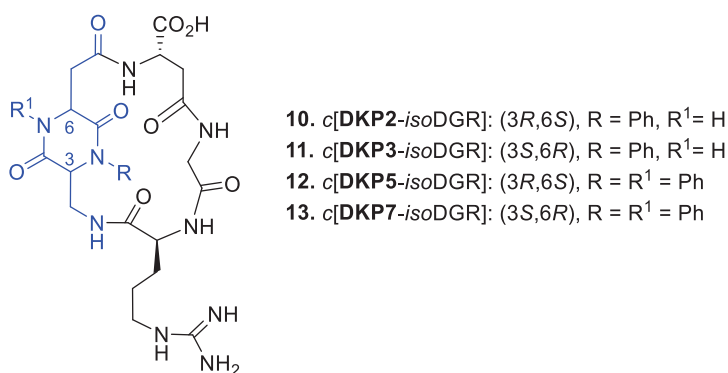**13.** *c*[**DKP7**-*iso*DGR]: (3*S*,6*R*), R = R^1 = Ph

Figure 31. *Cyclo*[DKP-*iso*DGR] integrin ligands

The ligands 10-13 were evaluated for their ability to inhibit the binding of biotinylated vitronectin to isolated $\alpha_v\beta_3$ and $\alpha_v\beta_5$ receptors in a competitive binding assay (Table 4). The compound **11**, structural analogue of *c*[DKP3-RGD] (**3**), displayed a preferential binding affinity for $\alpha_v\beta_3$ than for the $\alpha_v\beta_5$ receptor. Also, it showed better affinity values (low-nanomolar IC_{50}) than the other *c*[DKP-*iso*DGR] ligands and the cyclopentapeptide *c*[GisoDGRphg],[152] resulting comparable to *c*[DKP3-RGD] and Cilengitide.

Compound	Structure	$\alpha_v\beta_3$ IC$_{50}$ [a] [nM]	$\alpha_v\beta_5$ IC$_{50}$ [a] [nM]
10	c[DKP2-isoDGR]	46.7±18.2	220±84
11	c[DKP3-isoDGR]	9.2±1.1	312±21
12	c[DKP5-isoDGR]	490±77	9100±800
13	c[DKP7-isoDGR]	255±140	5100±400
3	c[DKP3-RGD]	4.5±1.1	149±25
	c[RGDfV]	3.2±1.3	7.5±4.8
	c[GisoDGRphg]	89 ± 19*	n.d.
	Cilengitide	0.6±0.1	11.7±1.5

[a]IC$_{50}$ values are calculated as the concentration of compound required for 50% inhibition of biotinylated vitronectin binding. *determined by a solid phase binding assay by using supported vitronectin, soluble $\alpha_v\beta_3$ integrin, specific primary and secondary antibodies.[152] n.d. = non determined

To get a better understanding of the interactions responsible for integrin binding affinity of c[DKP3-isoDGR] (**11**), conformational NMR spectroscopy and docking experiments were performed.[151] NMR data and MC/SD simulations indicated the existence of two preferred conformations for **11**: a distorted β-turn at Gly-Arg and a pseudo-β-turn at DKP-isoAsp (Figure 32). About 80% of the simulations adopted an extended arrangement of the isoDGR sequence (pseudo-β-turn), with an average distance C$_\beta$(Arg)-C$_\beta$(Asp) of 10.8 Å.
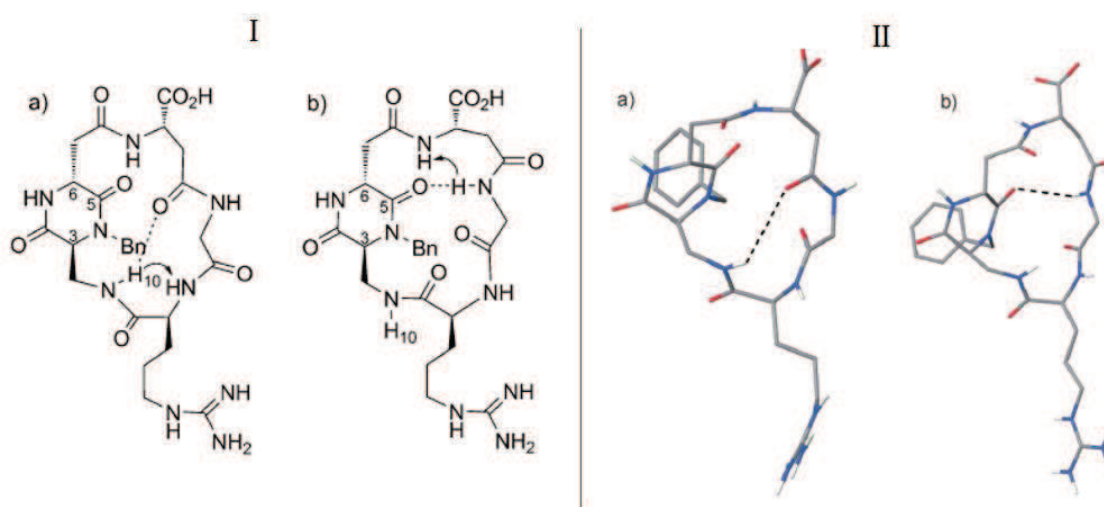

Figure 32. NMR conformational studies on **11**. I) Preferred intramolecular hydrogen-bonded pattern proposed from NMR data, NOE contacts are indicated by an arrow: a) β-turn at Gly-Arg; b) pseudo-β-

turn at DKP-*iso*Asp; II) MC/SD simulations based on experimental distance information after energy minimization: a) Distorted β-turn (10% of the simulations), distance C_β(Arg)-C_β(Asp) = 10.7 Å; b) pseudo-β-turn, (80% of the simulations), distance C_β(Arg)-C_β(Asp) = 10.8 Å.[151] Adapted with permission from M. Mingozzi; A. Dal Corso; M. Marchini et al. *Chem. - A Eur. J.* 2013, *19*, 3563–3567. Copyright © 2013 WILEY-VCH Verlag GmbH & Co.

Docking studies were performed based on the conformations of **11** obtained from the MC/SD simulations and taking as a reference the crystal structure of the extracellular segment of the $\alpha_V\beta_3$ integrin receptor complexed with the peptide binder Cilengitide for the ligand-protein interactions. In the case of the distorted β-turn Gly-Arg conformation, it conserved main electrostatic interactions corresponding to RGD binding model, but it lacked the hydrogen bond interactions with the β_3 subunit. Instead, the pseudo-β-turn DKP-*iso*Asp conformation presented all the interactions described for the X-ray complex of integrin-Cilengitide (Figure 33) including the interaction of the guanidium group with the carboxylates of Asp218 and Asp150 in the α unit, the coordination of a carboxylate oxygen of the ligand to the metal cation of the MIDAS region of the β subunit, the hydrophobic interactions with Asn215 and Tyr122 of the β unit, and additional hydrogen bond between the amide proton of the Gly residue and the carbonyl group of Arg216 of the β subunit.[151]
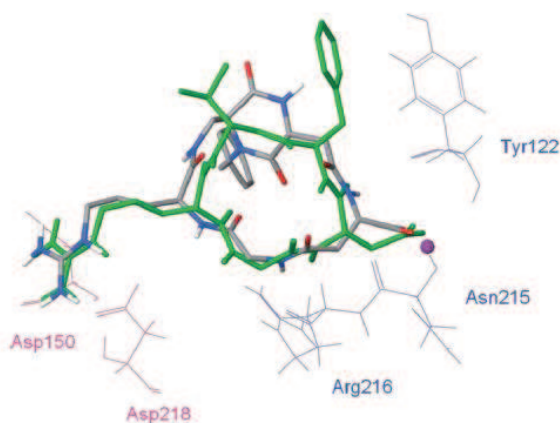

Figure 33. Best pose of *c*[DKP3-*iso*DGR] (**11**) pseudo-β-turn conformation into the crystal structure of the extracellular domain of $\alpha_v\beta_3$ integrin (α unit in pink and β unit in blue), overlaid on the bound conformation of Cilengitide (green tube representation). The metal ion in the MIDAS region is represented by a magenta sphere. Adapted with permission from M. Mingozzi; A. Dal Corso; M. Marchini et al. *Chem. - A Eur. J.* 2013, *19*, 3563–3567. Copyright © 2013 WILEY-VCH Verlag GmbH & Co.

Recently, our research group carried out a series of biological studies to evaluate the antiangiogenic and integrin antagonist activity of the ligands *c*[DKP3-*iso*DGR] (**11**) and *c*[DKP3-RGD] (**3**), similar in terms of structure and binding affinity for integrin $\alpha_V\beta_3$.[130]

MTS cell viability tests performed in U373 glioblastoma cell line indicated no cytotoxicity of the compounds **3** and **11**, as expected for integrin antagonists.[129,153] In fact, ELISA nucleosome assays showed a significant increase of nucleosome content after 72 hours treatment, suggesting that both ligands could induce cell apoptosis (Figure 34).
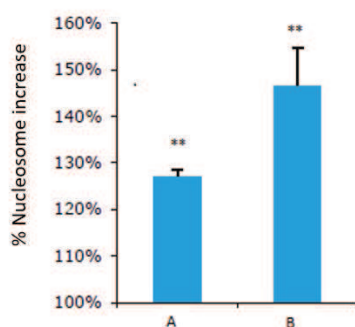

Figure 34. ELISA nucleosome assay. Nucleosome content after 72h treatment with A: *c*[DKP3-RGD] (**3**) and B: *c*[DKP3-*iso*DGR] (**11**). ** calculated probability value P>0.005.[130] Adapted with permission from S. Panzeri; S. Zanella; D. Arosio et al. *Chem. - A Eur. J.* 2015, *21*, 6265–6271. © 2015 WILEY-VCH Verlag GmbH & Co.

Infiltration assays conducted on U373 cell line showed a marked inhibitory effect on cell migration and cell infiltration processes for ligand **3** and **11** at 10 µM concentration, remaining basically unchanged at 25 µM (Figure 35).
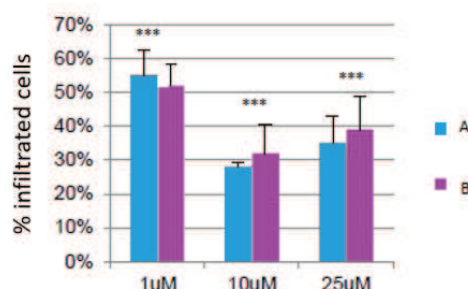

Figure 35. Infiltration assay. A: *c*[DKP3-RGD] (3); B: *c*[DKP3-*iso*DGR] (**11**); *** calculated probability value P>0.001.[130] Adapted with permission from S. Panzeri; S. Zanella; D. Arosio et al. *Chem. - A Eur. J.* 2015, *21*, 6265–6271. © 2015 WILEY-VCH Verlag GmbH & Co.

Compounds **3** and **11** were also tested for their ability to inhibit FAK and Akt phosphorylation in U373 cell lines. FAK is a cytoplasmic tyrosine kinase involved in cell motility, survival and proliferation. The activation of FAK signaling cascade is regulated by integrin-ECM interactions and it plays a key role in tumor cell growth, progression, and metastasis.[154] Integrin activation of FAK derives in the activation of Akt signaling cascade which is involved in the regulation of vascular homeostasis and angiogenesis. For this reason, the inhibition of the Akt cascade becomes a suitable control of the

ligand mediated integrin activation[129]. In the case of the tested compounds, both ligands demonstrated to inhibit the FAK and Akt phosphorylation after 24h treatment (Figure 36).
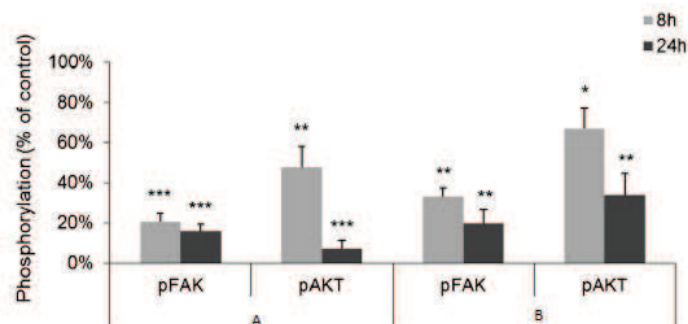

Figure 36. FAK and Akt phosphorylation inhibition. A: *c*[DKP3-RGD] (**3**); B: *c*[DKP3-*iso*DGR] (**11**); *calculated probability value P>0.5, **calculated probability value P>0.005, ***calculated probability value P>0.001. Adapted with permission from S. Panzeri; S. Zanella; D. Arosio et al. *Chem. - A Eur. J.* 2015, *21*, 6265–6271. © 2015 WILEY-VCH Verlag GmbH & Co.

These results indicate that *c*[DKP3-*iso*DGR] (**11**), same as its analog *c*[DKP3-RGD] (**3**), displays an integrin antagonist activity which is consistent with previous studies reporting that cyclic *iso*DGR peptide ligands are true $\alpha_V\beta_3$ antagonists.[147]

This feature together with the high binding affinity and selectivity of *c*[DKP3-*iso*DGR] towards integrin $\alpha_V\beta_3$ makes this ligand a suitable candidate for its use in targeted drug delivery via SMDCs.

2.3. Synthesis of a functionalized *cyclo*[DKP-*iso*DGR] integrin ligand

Based on the biological results of *cyclo*[DKP3-*iso*DGR] **11** and the work realized with the functionalized integrin ligand *cyclo*[DKP-*f3*-RGD] **9** (see Section 2.2.1.4), our research group reported in 2017 the synthesis of a SMDC bearing a functionalized *cyclo*[DKP-*iso*DGR] integrin ligand (**14**, Figure 37), a cleavable Val-Ala linker and Paclitaxel as a payload.[155] The antiproliferative activity of this conjugate was evaluated *in vitro* on isogenic $\alpha_V\beta_3$-expressing and $\alpha_V\beta_3$-non expressing cell lines. The cyclo[DKP-isoDGR]-Val-Ala-PTX conjugate showed higher selectivity towards the $\alpha_V\beta_3$-expressing cell line (targeting index = 9.9) compared to the related cyclo[DKP-RGD]-Val-Ala-PTX conjugate (targeting index = 2.4).[155]
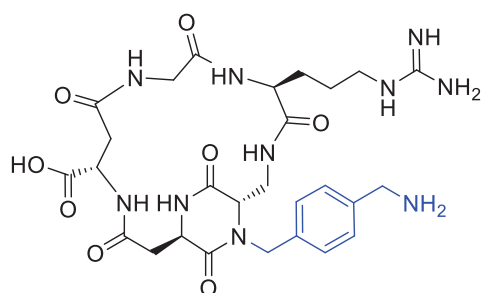
Figure 37. *Cyclo*[DKP-*f3-iso*DGR] (*c*[DKP-*iso*DGR]-CH$_2$NH$_2$) integrin ligand (**14**)

Prompted by these promising results we decided to investigate the efficacy of the *cyclo*[DKP-*iso*DGR] integrin ligand as a vector in the preparation of SMDCs bearing different cytotoxic agents. The first part of my PhD project consisted then in scaling up the synthesis of the *iso*DGR ligand **14** containing the benzylamine handle that allows its conjugation to other chemical entities.

2.3.1. Synthesis of DKP-*f3* scaffold

The synthesis of the functionalized DKP-*f3* scaffold was achieved as presented in Scheme 1, starting from commercially available D-aspartic acid and L-serine methyl ester[131].
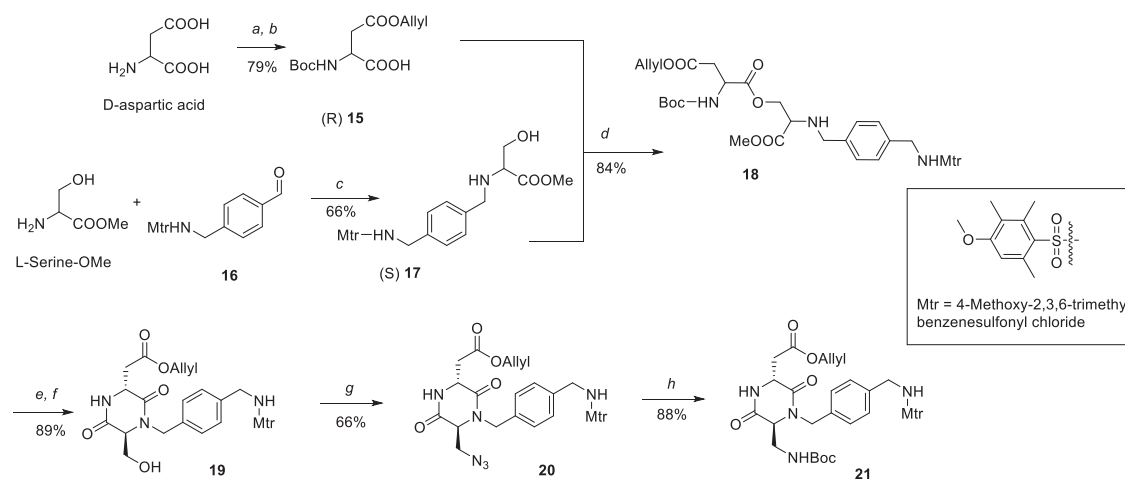

Scheme 1. Synthesis of DKP-*f3* scaffold: (a) Allyl alcohol, acetyl chloride; (b) Boc$_2$O, TEA, dioxane, water, 79% over two steps; (c) NaBH(OAc)$_3$, THF, 3 h, rt.; (d) HATU, HOAT, DIPEA, DMF, 3 h, 0 °C to rt.; (e) TFA/DCM 1:2, 3 h, 0 °C to rt.; (f) DIPEA, *iPr*OH, overnight, rt., 89% over two steps; (g) HN$_3$·Tol, DIAD, Ph$_3$P, DCM/Toluene 1:2, 4 h, −20 °C; (h) Me$_3$P, BOC-ON, THF, 3 h, −20 °C to rt.

The side chain of the aspartic acid was protected with an allyl group before N-Boc protection to give the compound **15**. On the other hand, the aldehyde **16** undergoes a reductive amination with L-serine methyl ester using sodium triacetoxyborohydride to obtain the functionalized serine **17**. The intermediates **15** and **17** reacted under direct

coupling conditions (HATU, HOAt, DIPEA) to afford the isopeptide **18** in high yield (84%). The selective acylation of the unprotected β-hydroxy group of the functionalized serine occurs instead of the expected peptide bond formation, this was reported also in the synthesis of DKP1-3.[127,156] Next, the Boc protecting group of **18** was cleaved, then O,N-acyl migration and subsequent ring closure were prompted by treatment with DIPEA in isopropyl alcohol[156], giving the DKP-*f3*-OH **19** (89% over two steps). The hydroxyl group of **19** was substituted by an azide group *via* a Mitsunobu reaction using HN_3 as nucleophile, affording the DKP-*f3*-N_3 **20** in satisfactory yield (66%). The reaction was carried out at low temperature (-20°C) to avoid the formation of the elimination product. The final step was a one-pot Staudinger reduction–Boc protection, allowing to reduce the azide under mild conditions and directly react with the 2-(t-butoxy-carbonyl-oxyimino)-2-phenylacetonitrile (Boc-ON) present in the medium, affording the DKP-*f3*-NHBoc **21** in good yield (88%).

2.3.2. Synthesis of *cyclo*[DKP-*iso*DGR] integrin ligand 14

Once the compound **21** was obtained in gram scale, the synthesis of *cyclo*[DKP-*iso*DGR]-CH_2-NH_2 (**14**) continued as indicated in the Scheme 2. Differently from the synthesis of *cyclo*[DKP-*iso*DGR] **10-13** carried out in solid phase,[151] this strategy was entirely performed in solution allowing to synthesize the *iso*DGR ligand in a larger scale.
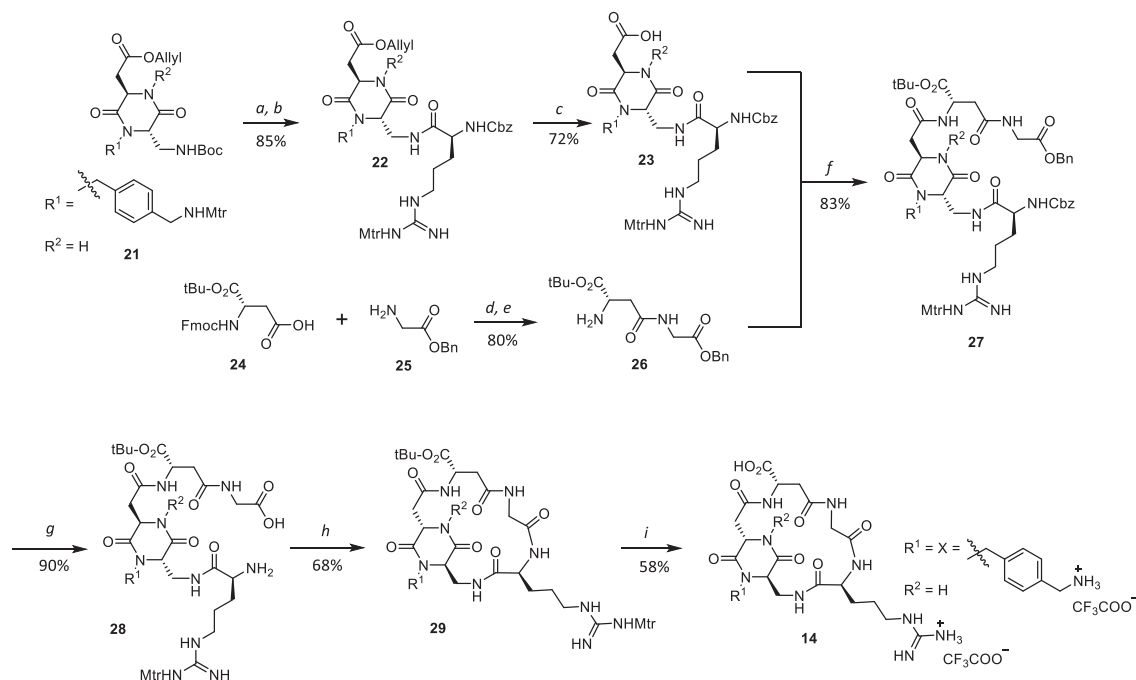
Scheme 2. Synthesis of *c*[DKP-*f3-iso*DGR] (**14**): (a) TFA, DCM, r.t., 2h; (b) Cbz-Arg(Mtr)-OH; HATU, HOAt, DIPEA, DMF, 0 °C to rt., overnight; (c) [Pd(PPh₃)₄], N-methylaniline, DCM, 0 °C, 1 h; (d) HATU, HOAt, DIPEA, DMF, 0 °C to rt., overnight; e) piperidine, DMF, 3 h, rt.; (f) HATU, HOAt, DIPEA, DMF, 0 °C to rt., overnight; (g) H₂, 10% Pd/C, THF/water 1:1, rt., overnight; (h) HATU, HOAt, DIPEA, DMF (1.4 mM), 0 °C to rt., overnight; (i) TFA/TMSBr/thioanisole/EDT/phenol 70:14:10:5:1.

The DKP-*f3*-NHBoc **21** was Boc-deprotected and reacted with Cbz-Arg(Mtr)-OH under coupling conditions (HATU, HOAt, DIPEA) to give the compound **22** in high yield (85% over two steps), then the allyl protecting group was cleaved in presence of N-methylaniline and [Pd(PPh₃)₄] to obtain the Arg-DKP fragment **23** (72%). The dipeptide, *iso*Asp-Gly **26**, was achieved by regular coupling of Fmoc-L-Asp(OH)-O*t*Bu with glycine benzyl ester, followed by cleavage of Fmoc group to afford **26** (80% yield over 2 steps).

Intermediates **23** and **26** were attached under coupling conditions (HATU, HOAt and DIPEA) to give the linear protected compound **27** (83%). Afterwards, the benzyl and Cbz protecting groups were removed by palladium catalyzed hydrogenation in water/THF 1:1 giving the compound **28** in good yield (90%). The linear peptidomimetic was then treated with coupling agents (HATU, HOAt, DIPEA) under high dilution conditions (1.4 mM in 1:1 DCM/DMF) to promote an intramolecular cyclization, giving the cyclic intermediate **29** in reasonable yield (68%). Finally, the 4-methoxy-2,3,6-trimethylbenzenesulphonyl (Mtr) and *tert*-butyl protecting groups were removed by using TFA in presence of scavengers thioanisol, phenol, EDT and trimethylsilyl bromide

to afford *cyclo*[DKP-*iso*DGR]-CH$_2$-NH$_2$ **14** as a TFA salt with a yield of 58% after purification by reversed-phase HPLC and freeze-drying from water.

The preparation of the new SMDCs containing the integrin ligand *cyclo*[DKP-*iso*DGR]-CH$_2$-NH$_2$ **14** as the targeting moiety is described in the Chapter 3.

Chapter 3. Synthesis of SMDCs based on the functionalized *cyclo*[DKP-*iso*DGR] integrin ligand

Part of the work described in this Chapter has been published in the following article:[157]

- Bodero, L.; López Rivas, P.; Korsak, B.; Hechler, T.; Pahl, A.; Müller, C.; Arosio, D.; Pignataro, L.; Gennari, C.; Piarulli, U. Synthesis and Biological Evaluation of RGD and IsoDGR Peptidomimetic-α-Amanitin Conjugates for Tumor-Targeting. *Beilstein J. Org. Chem.* **2018**, *14* (1), 407–415.

3.1. Synthesis and biological evaluation of *iso*DGR-α-amanitin conjugates

3.1.1. α-Amanitin in targeted therapy

α-Amanitin is the main amatoxin found in the death cap mushroom, *Amanita Phalloides* (Figure 38). Amatoxins are bicyclic octapeptides that present a high thermostability and water solubility, besides a resistance to enzyme and acid degradation. For these reasons, they can traverse the gastrointestinal tract without suffering any alteration, reaching and accumulating in the liver where they display a lethal toxicity, leading to hepatic failure after 6-8 days.[158,159] In the case of α-amanitin, the LD_{50} value is 0.1 mg/kg of bodyweight in humans.[160]
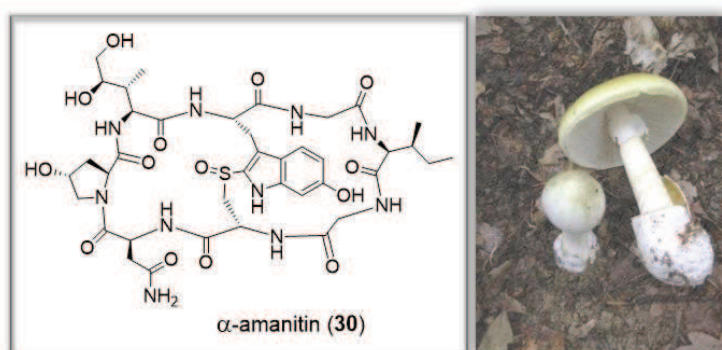

Figure 38. α-amanitin structure and *Amanita Phalloides* (Death cap)

The mechanism of action of α-amanitin consists in the inhibition of the RNA polymerase II, an enzyme present in the nuclei of eukaryotic cells and responsible for the transcription of DNA to mRNA.[158,161] In effect, α-amanitin binds the RNA polymerase II forming a tight complex (Figure 39), causing the inhibition of the elongation step and subsequent blocking of the DNA transcription process, resulting finally in cell death.[159,162,163] However, due to its hydrophilicity and poor membrane permeability, cellular uptake of α-amanitin takes place only when it is mediated by a transport system, such as the transporting protein OATP1B3 present on the surface of human hepatocytes. For other mammalian cells α-amanitin displays a micromolar cytotoxicity associated to poor cellular uptake.[161,164]
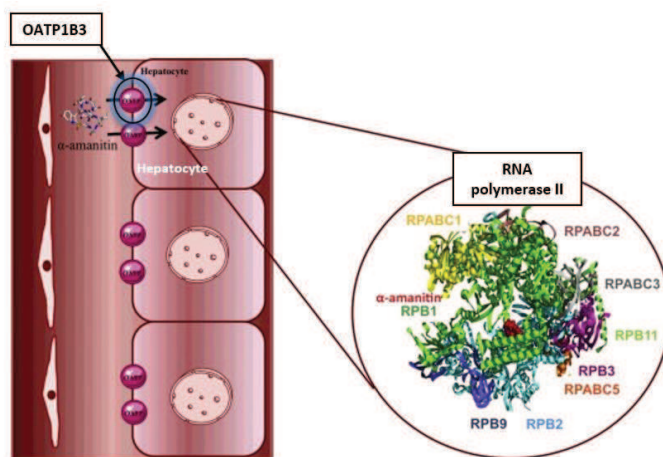

Figure 39. Transport and main toxic mechanism of α-amanitin in hepatocytes. Accumulation of α-amanitin occurs in the liver upon uptake *via* the organic anion transporting polypeptide OATP1B3 located in the sinusoidal membrane of hepatocytes. Once inside the hepatocyte, α-amanitin binds to RNA polymerase II causing inhibition of its activity. Adapted with permission from Juliana Garcia, Vera M. Costa et al.; *Food and Chemical Toxicology*, 2015, 86, 41–55. DOI: 10.1016/j.fct.2015.09. Copyright © 2015 Elsevier Ltd.[165]

Because of the strong and specific cytotoxicity achieved upon internalization by endocytosis mediators, α-amanitin has become a promising payload for targeted drug delivery systems such as ADCs or SMDCs where the monoclonal antibody or the small ligand facilitate a receptor-mediated endocytosis and intracellular release of the drug.

In 1981, Davis and Preston reported the synthesis of an ADC containing an azo-functionalized α-amanitin (α-amanitinyl-azobenzoyl-N-glycyl-glycine) conjugated to the anti-Thy 1.2 immunoglobulin (anti-Thy 1.2 IgG). The conjugate displayed 277-fold and 47-fold greater toxicity than the unconjugated α-amanitin in the murine T lymphoma S49.1 cell line after 1 and 48 hours incubation respectively.[166] In 2012, the ADC α-

amanitin-glutarate-chiHEA125 (chiHEA125-Ama), containing a chimeric anti-EpCAM (epithelial cell-adhesion molecule) monoclonal antibody, was reported by Moldenhauer and coworkers.[167] The cytotoxic activity of this conjugate was tested in different cancer cell lines overexpressing EpCAM (i.e. human pancreatic BxPc-3 and Capan-1, colorectal Colo205, breast MCF-7 and bile duct OZ) obtaining IC_{50} values from 2.5×10^{-10} to 5.4×10^{-12} M, which represented in all cases; an increase of the cytotoxicity compared to unconjugated α-amanitin (IC_{50} 2.0×10^{-7} to 5.8×10^{-8} M). Further *in vivo* studies performed in mice bearing BxPc-3 pancreatic xenograft tumors showed complete tumor regression in 90% of the mice treated with two injections of chiHEA125-Ama at dose of 100 μg/kg. The treatment also proved to stop the development of recurrent tumors for a 3-4 weeks period without induce systemic toxicity. These two examples of α-amanitin-based ADCs confirmed the validity of the targeted approach in terms of potency and selectivity in comparison to the unconjugated drug.

Regarding the SMDCs containing α-amanitin as a payload, Reshetnyak and coworkers investigated in 2013 three α-amanitin-pHLIP (pH low insertion peptide) conjugates bearing different cross-linkers (i.e. cleavable: SPDP, sulfo-Lc-SMPT and non-cleavable AMAS).[168] In this case, the drug delivery mechanism is the pHLIP mediated direct translocation across the cell membrane. The results of antiproliferative tests in human cervix adenocarcinoma HeLa-GFP cell line showed an increased cytotoxicity for the pHLIP-SPDP-amanitin conjugate at pH 6 compared to pH 7, inducing apoptosis in 48 hours. On the other hand, the conjugate bearing the uncleavable linker, pHLIP-AMAS-amanitin, did not display cellular toxicity, which suggested that the activity of the conjugates is conditioned to the release of the free amanitin after linker cleavage.

More recently, Perrin and co-workers reported the synthesis of an amanitin analog functionalized with a *N*-propargyl-asparagine and its conjugation to *cyclo*(RGDfK) through azide-linkers, using a copper-catalyzed azide-alkyne cycloaddition (CuAAC).[169] The antiproliferative activity of the conjugates was evaluated in U87 ($\alpha_v\beta_3^+$) glioblastoma cell line, showing only a modest enhancement in the cytotoxicity of the conjugates over α-amanitin.

3.1.2. Synthesis of *cyclo*[DKP-*iso*DGR]-α-amanitin conjugates

Three *cyclo*[DKP-*iso*DGR]-α-amanitin conjugates were prepared in collaboration with Heidelberg Pharma AG, by joining the functionalized ligand *c*[DKP-*iso*DGR]-CH$_2$-NH$_2$ (**14**) to α-amanitin *via* an ether group at the 6'-hydroxyindole, using two different linkers: an "uncleavable" six carbon aliphatic chain (Figure 40, compound **31**) and a lysosomally cleavable Val-Ala linker connected to a self-immolative spacer (Figure 40, compounds **32** and **33**).[157]
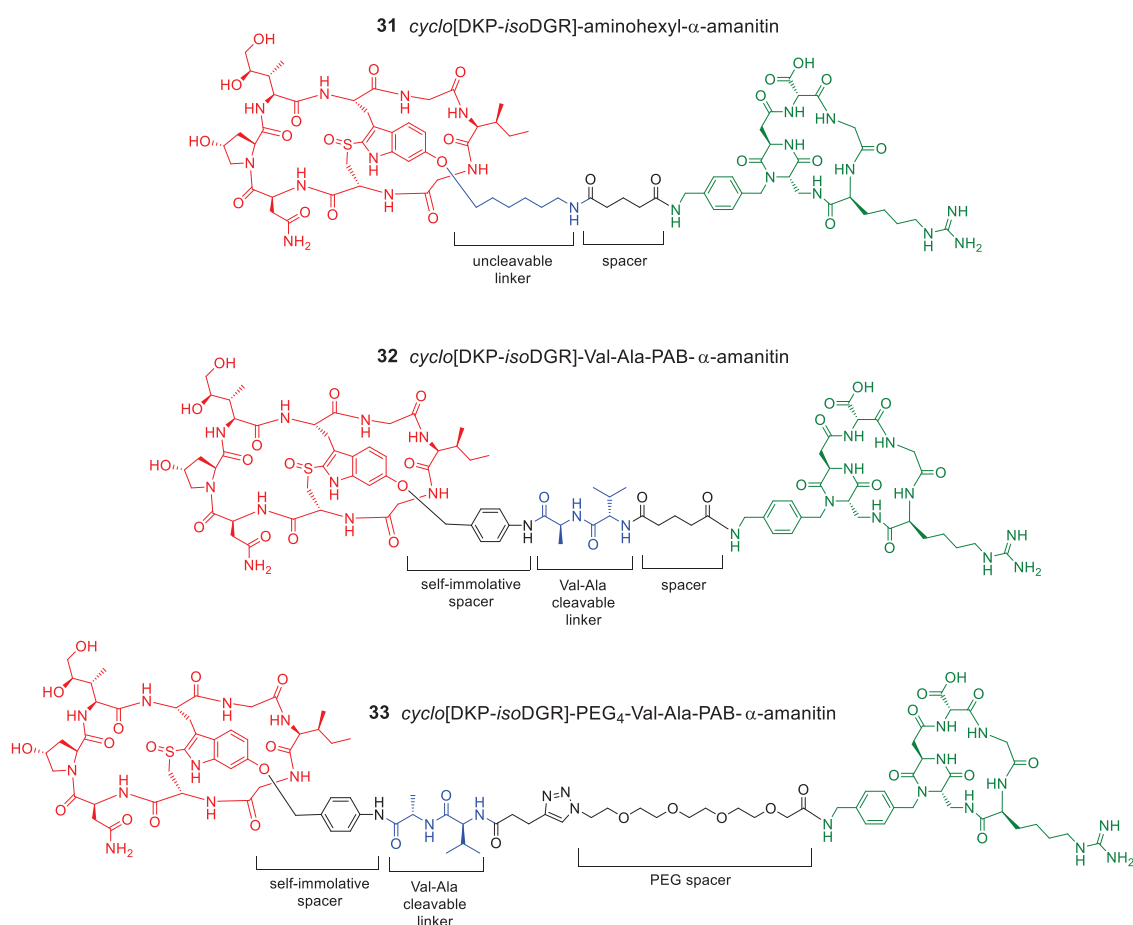

Figure 40. Structure of *cyclo*[DKP-*iso*DGR]-α-amanitin conjugates

Compound **31** bearing the uncleavable aminohexyl linker was synthetized as described in the Scheme 3. The α-Amanitin 6'-aminohexyl ether (**34**) provided by Heidelberg Pharma AG[170,171] reacted with the commercial di-*N*-succinimidyl glutarate in presence of DIPEA to give the pre-activated hemiglutarate-aminohexyl-α-amanitin (**35**) in high yield (90%). For this reaction the activated di-*N*-succinimidyl glutarate was used in 1.2 equivalents in order to avoid an undesired substitution of the other hydroxy groups present in α-amanitin. In addition, this procedure allowed us to introduce the glutarate

spacer already activated as NHS ester in one step, differently from the 2-step procedure used in the synthesis of the RGD analogs.[157] The resulting intermediate **35** was then conjugated to the ligand *cyclo*[DKP-*iso*DGR]-CH₂NH₂ (**14**) *via* pH-controlled coupling where the pH was maintained in a range of 7.3-7.6 with the addition of small aliquots of NaOH 0.2 M to prevent the hydrolysis of the NHS ester that can compete with the formation of the amide bond at pH > 7.6, and also because at this pH range the guanidinium group of the arginine residue is still largely protonated and does not compete with the primary benzylic amine of compound **14**. The resulting conjugate **31** was obtained with 45% yield after HPLC purification and freeze-drying from ACN:H₂O 1/1.
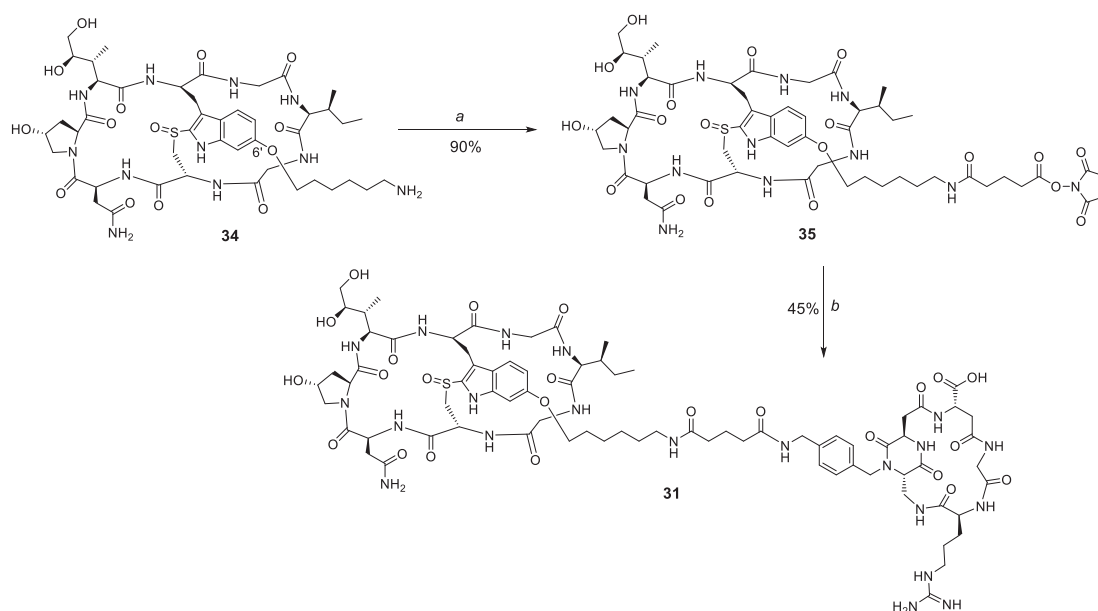
Scheme 3. Synthesis of *cyclo*[DKP-*iso*DGR]-uncleavable-α-amanitin (**31**). Reagents and conditions: a) di-*N*-succinimidyl glutarate, DIPEA, DMF, 6 hours, Y: 90%; b) *cyclo*[DKP-*iso*DGR]-CH₂-NH₂ (**14**), PBS (pH 7.5), overnight, Y: 45%.

The synthesis of the compound **32**, containing the lysosomally cleavable Val-Ala linker was carried out with the strategy used for conjugate **31** as described in the Scheme 4. NH₂-Val-Ala-PAB-α-amanitin (**36**) provided by Heidelberg Pharma AG,[170,171] reacted with di-*N*-succinimidyl glutarate in presence of DIPEA to give the hemiglutarate-Val-Ala-PAB-α-amanitin activated as an NHS ester (**37**) with 71% yield. Then **37** was conjugated to the ligand *cyclo*[DKP-*iso*DGR]-CH₂NH₂ (**14**) by pH-controlled coupling at pH range of 7.3-7.6, affording the conjugate **32** in good yield (62%) after HPLC purification and freeze-drying from water: acetonitrile 1/1. Differently from the "uncleavable" conjugate **31**,

cyclo[DKP-*iso*DGR]-Val-Ala-PAB-α-amanitin (**32**) is expected to release the unchanged α-amanitin after intracellular cleavage of the dipeptide linker (mediated by cathepsin B or other enzymes) and 1,6-elimination of the PAB self immolative spacer.
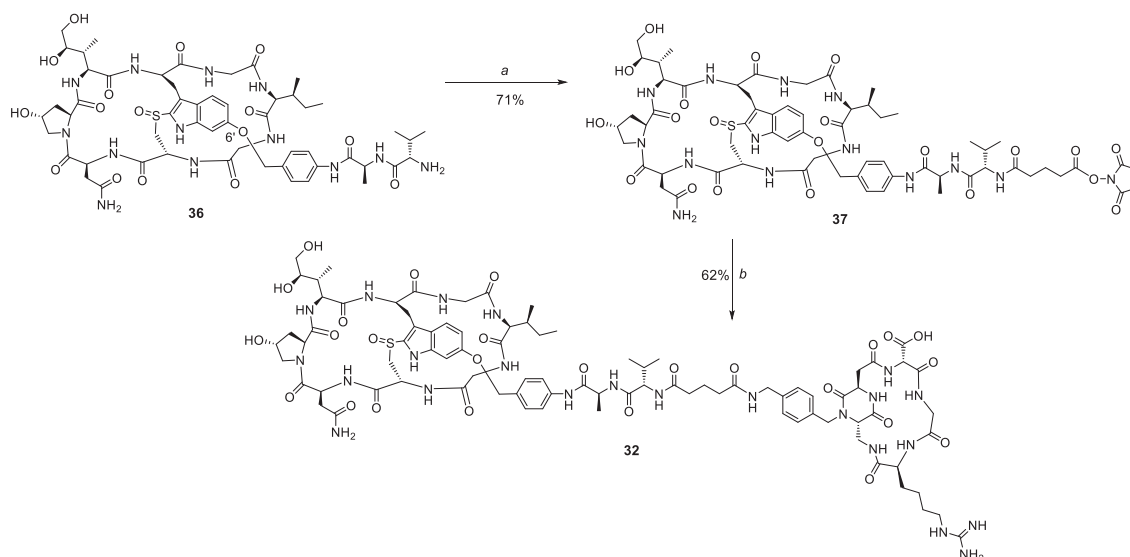
Scheme 4. Synthesis of *cyclo*[DKP-*iso*DGR]-Val-Ala-PAB-α-amanitin (**32**). Reagents and conditions: a) di-*N*-succinimidyl glutarate, DIPEA, DMF, 6 hours, Y: 71%; b) *cyclo*[DKP-*iso*DGR]-CH₂-NH₂ (**14**), PBS (pH 7.5), overnight, Y: 62%.

For the synthesis of conjugate **33** containing the cleavable Val-Ala linker and the PEG spacer, two intermediates were prepared as indicated in the Scheme 5. Val-Ala-PAB-α-amanitin (**36**) reacted with 4-pentynoic acid-NHS-ester (**39**) to give 4-pentynoic acid-Val-Ala-PAB-α-amanitin (**38**) with 88% yield. On the other hand, *cyclo*[DKP-*iso*DGR]-CH₂NH-PEG-4-N₃ (**41**) was prepared by pH-controlled coupling between the isoDGR ligand **14** and commercial COOH-PEG-4-azido pre-activated as NHS ester (**40**). The final step was a click reaction, the copper catalyzed alkyne-azide cycloaddition (CuAAC) between the azido group of **41** and the alkyne moiety of **38** under inert atmosphere, that gave conjugate **33** with 62% yield after HPLC purification and freeze-drying from water/acetonitrile 1/1. In this case, the introduction of the PEG chain between the linker and the ligand is expected to increase the stability of the conjugate at physiological conditions and to give more flexibility to the ligand, facilitating the targeting at the α$_v$β$_3$ surface receptor.
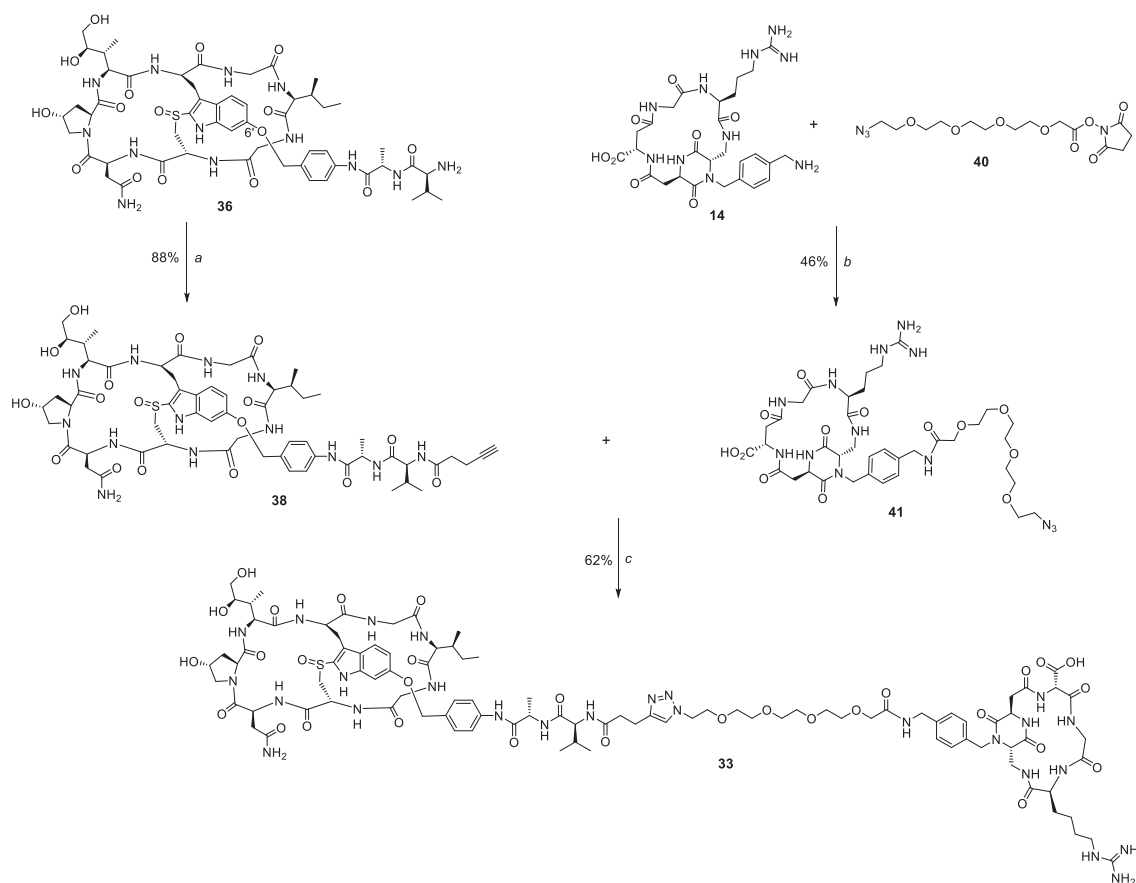
Scheme 5. Synthesis of *cyclo*[DKP-*iso*DGR]-PEG-4-Val-Ala-α-amanitin (**33**). Reagents and conditions: a) 4-pentynoic acid-NHS ester (**39**), DIPEA, DMF, overnight, Y: 88 %; b) PBS (pH 7.5), overnight, Y: 46 %. c) Sodium ascorbate, $CuSO_4.5H_2O$, DMF/H_2O 1:1, overnight, Y: 62%.

3.1.3. *In vitro* studies

3.1.3.1. Binding affinity assays

The *iso*DGR-α-amanitin conjugates **31-33**, as well as the RGD analogs of **31** and **32** (Figure **41**) synthesized by Paula Lopez Rivas (University of Milano), containing the *cyclo*[DKP-RGD]-CH_2NH_2 integrin ligand **9**, were tested in collaboration with the Institute of Molecular Science and Technology of the Italian National Research Council in Milano, for their binding affinity towards the integrin $\alpha_v\beta_3$ in a competitive binding assay that measured their ability to inhibit the binding of biotinylated vitronectin to the purified $\alpha_v\beta_3$ receptor.
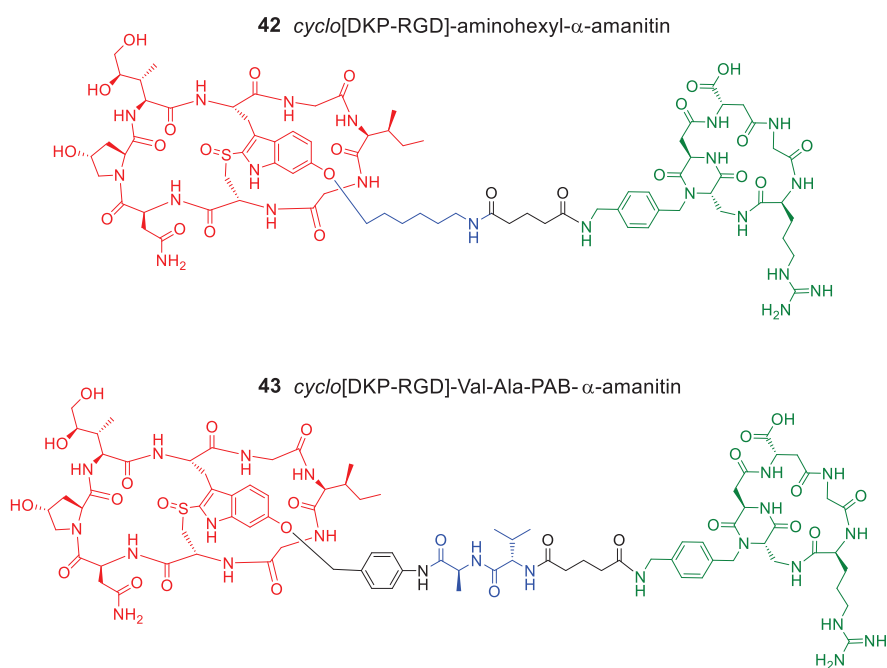
42 *cyclo*[DKP-RGD]-aminohexyl-α-amanitin

43 *cyclo*[DKP-RGD]-Val-Ala-PAB- α-amanitin

Figure 41. Structure of *cyclo*[DKP-RGD]-α-amanitin conjugates

The assays were performed by incubating the immobilized $\alpha_v\beta_3$ integrin receptor with solutions of the conjugates *cyclo*[DKP-RGD]-α-amanitin (**42-43**) and *cyclo*[DKP-*isoDGR*]-α-amanitin conjugates (**31-33**) at increasing concentrations (10^{-12}-10^{-5} M) in the presence of biotinylated vitronectin (1 µg mL^{-1}) and measuring bound vitronectin. The calculated half-maximal inhibitory concentrations (IC_{50}) are listed in Table 5.

Table 5. Inhibition of biotinylated vitronectin binding to $\alpha_v\beta_3$ receptor

Compound	Structure	IC_{50} (nM) [a] $\alpha_v\beta_3$
42	*cyclo*[DKP-RGD]-uncleavable-α-amanitin	11.6 ± 2.4
31	*cyclo*[DKP-*iso*DGR]-uncleavable-α-amanitin	6.8 ± 4.3
43	*cyclo*[DKP-RGD]-Val-Ala-α-amanitin	14.7 ± 6.6
32	*cyclo*[DKP-*iso*DGR]-Val-Ala-α-amanitin	6.4 ± 1.9
33	*cyclo*[DKP-*iso*DGR]-PEG-4-Val-Ala-α-amanitin	3.8 ± 0.3

[a] IC_{50} values were calculated as the concentration of compound required for 50% inhibition of biotinylated vitronectin binding as estimated by GraphPad Prism software. All values are the arithmetic mean ± the standard deviation (SD) of triplicate determinations.

These results indicate that the *cyclo*[DKP-RGD]-α-amanitin conjugates (**42-43**) and the *cyclo*[DKP-*iso*DGR]-α-amanitin conjugates (**31-33**) retain good binding affinity for the integrin $\alpha_v\beta_3$, notwithstanding the conjugation of the integrin ligand to the linker system and the α-amanitin. The binding affinity values displayed by the conjugates were in the

low-nanomolar range, similar to the original integrin ligands *cyclo*[DKP-3-RGD] **3** and *cyclo*[DKP-3-*iso*DGR] **11** (IC$_{50}$ $\alpha_v\beta_3$ = 4.5 and 9.2 nM respectively, cf. Table 4).

3.1.3.2.   Cell viability assays

In order to study the selectivity of the integrin ligand-α-amanitin conjugates targeting the $\alpha_v\beta_3$ receptor, as well as their activity with respect to free α-amanitin, cell viability assays were performed in three cell lines expressing different levels of integrin $\alpha_v\beta_3$: human glioblastoma U87 cells line ($\alpha_v\beta_3$+), human lung carcinoma A549 cell line ($\alpha_v\beta_3$-) and breast adenocarcinoma MDA-MB-468 ($\alpha_v\beta_3$-). The expression of $\alpha_v\beta_3$ integrin on the cell membrane of the three cell lines was assessed by flow cytometry (Figure 42), confirming the information found in the literature for U87 ($\alpha_v\beta_3$ expressing) and A549 ($\alpha_v\beta_3$ non-expressing).[172–174] In the case of MDA-MB-468, FACS analyse did not detect $\alpha_v\beta_3$ expression, although the presence of the β_3 integrin subunit in this cell line is a matter of discussion[175,176] and a positive interaction with RGD ligands has been reported in the literature.[177]
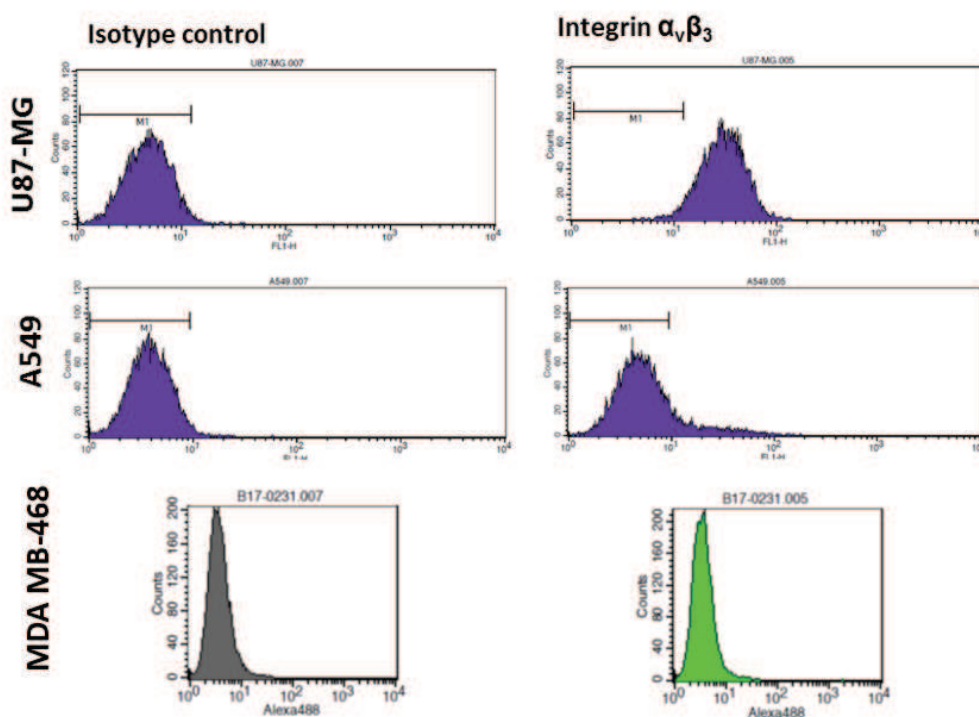

Figure 42. Flow cytometry analysis of integrin $\alpha_v\beta_3$ expression in cancer cell lines. U87-MG: integrin $\alpha_v\beta_3$ overexpressed; A549 and MDA-MB 468: integrin $\alpha_v\beta_3$ negative.

The cells were treated with different concentrations of the free α-amanitin and the conjugates **42-43**, **31-33** for 96 hours. Cell viability was measured in a CellTiterGlo 2.0

assay with triplicated samples. IC$_{50}$ values representing the concentration of compound required for 50% inhibition of cell viability were calculated from the viability curves using GraphPad Prism and are shown in Table 6.

Table 6. Evaluation of anti-proliferative activity of integrin ligand-α-amanitin conjugates **42-43, 31-33** in U-87, MDA-MB-468 and A549

Entry	Structure	IC$_{50}$ (nM)[a]		
		U87 ($\alpha_v\beta_3$ +)	MDA-MB-468 ($\alpha_v\beta_3$ -)	A549 ($\alpha_v\beta_3$ -)
1	α-amanitin (30)	347 ± 132.5[b]	185 ± 49.6[b]	518 ± 305[b]
2	cyclo[DKP-RGD]-uncleavable-α-amanitin (42)	2552 ± 37.6	1111 ± 228.4	n.d.[c]
3	cyclo[DKP-isoDGR]-uncleavable-α-amanitin (31)	3355 ± 19.1	2200 ± 96.2	n.d.[c]
4	cyclo[DKP-RGD]-Val-Ala-α-amanitin (43)	1446 ± 83.9	202 ± 10.3	2160 ± 23.3
5	cyclo[DKP-isoDGR]-Val-Ala-α-amanitin (32)	143 ± 33.8	59 ± 23.4	217 ± 98.3
6	cyclo[DKP-isoDGR]-PEG-4-Val-Ala-α-amanitin (33)	165 ± 4.0	66 ± 24.1	720 ± 98.1

[a] IC$_{50}$ values were calculated as the concentration of compound required for 50% inhibition of cell viability. All cell lines were treated with different concentrations of α-amanitin and compounds **42-43, 31-33** for 96 hours. The samples were measured in triplicates. [b] Average values from three replicates. [c] n.d.: The IC$_{50}$ could not be determined.

The cyclo[DKP-isoDGR]-α-amanitin conjugate bearing the lysosomally cleavable Val-Ala linker **32** showed an enhanced cytotoxicity compared to the free α-amanitin in the $\alpha_V\beta_3$ expressing U87 cell line, as well as in the $\alpha_V\beta_3$ non-expressing A549 and MDA-MB-468 cell lines (2.4-3.1 times more potent cf. entry 5 and 1 in Table 6). Conversely, cyclo[DKP-RGD]-Val-Ala-α-amanitin (**43**) the RGD analog of **32**, resulted less toxic than α-amanitin in the three cell lines, which indicates an influence of the isoDGR sequence in the efficacy of the conjugates. In the case of the cyclo[DKP-isoDGR]-PEG-4-Val-Ala-PAB-α-amanitin **33**, the cytotoxic activity was slightly higher compared to free α-amanitin in U87 ($\alpha_V\beta_3$+) and MDA-MB-468 ($\alpha_V\beta_3$-) cell lines (2.1-2.8 times more, cf. entry 6 and 1 in Table 6) but it turned out to be less potent than the free drug in A549 ($\alpha_V\beta_3$-) cell line (1.4 times less).

The uncleavable conjugates c*yclo*[DKP-RGD]-uncleavable-α-amanitin (**42**) and *cyclo*[DKP-*iso*DGR]-uncleavable-α-amanitin (**31**) were less cytotoxic than α-amanitin and the conjugates bearing the cleavable linker Val-Ala (**43**, **32**, **33**) in the three cell lines. This can be attributed to a more efficient drug release mechanism displayed by the dipeptide cleavable linker and the self immolative moiety.

In summary, the results of the antiproliferative assays revealed that the use of dipeptide cleavable linkers can improve the activity of the α-amanitin conjugates in comparison to the "uncleavable" systems, as in the case of conjugates **43**, **32** and **33**. It was also observed that the cleavable conjugates **32** and **33**, containing the *iso*DGR motif, afforded better cytotoxic activity than the cleavable RGD conjugate **43**, showing also a modest improvement compared to the activity the free α-amanitin. Nevertheless, a selective cytotoxicity of the integrin ligand-α-amanitin conjugates towards the $\alpha_v\beta_3$-expressing cell line U87 was not observed.

With the aim of determining if the cytotoxicity of the *cyclo*[DKP-*iso*DGR]-α-amanitin conjugates **32** and **33** was associated to an integrin-mediated binding and internalization process, a competition experiment[178] was performed on U87 ($\alpha_v\beta_3$+, $\alpha_v\beta_5$+, $\alpha_v\beta_6$-, $\alpha_5\beta_1$+) and MDA-MB-468 ($\alpha_v\beta_3$-, $\alpha_v\beta_5$+, $\alpha_v\beta_6$+, $\alpha_5\beta_1$-)[173,174] cell lines, testing the antiproliferative activity of the conjugates in the presence of a 50-fold excess of the integrin ligand Cilengitide (*cyclo*[RGDf-(*N*Me)V], see also Chapter 2). Indeed, if the release of α-amanitin occurs upon integrin-mediated endocytosis, a drop in the activity of the conjugates would be expected when blocking the cell surface integrins with the competitor Cilengitide. The results of this experiment are shown in the Table 7.

Table 7. Competition experiment of conjugates 10 and 11 in the presence of a 50-fold excess of Cilengitide in U-87 and MDA-MB-468.

Entry	Compound	IC$_{50}$ (nM)[a]	
		U87 ($\alpha_v\beta_3$ +, $\alpha_v\beta_5$ +, $\alpha_v\beta_6$ -, $\alpha_5\beta_1$ +)	MDA-MB-468 ($\alpha_v\beta_3$ -, $\alpha_v\beta_5$ +, $\alpha_v\beta_6$ +, $\alpha_5\beta_1$ -)
1	*Cyclo*[DKP-*iso*DGR]-Val-Ala-α-amanitin **32**	107 ± 26.8	47 ± 21.1
	Compound **32** + 50-fold excess of Cilengitide	106 ± 11.6	259 ± 55.2
2	*Cyclo*[DKP-*iso*DGR]-PEG-4-Val-Ala-α-amanitin **33**	91 ± 30.6	65 ± 17.6

	Compound **33** + 50-fold excess of Cilengitide	143 ± 59.3	340 ± 210.3

[a] IC_{50} values were calculated as the concentration of compound required for 50% inhibition of cell viability. Both cell lines were treated with different concentrations compounds **10** and **11** in the presence of a 50-fold excess of Cilengitide for 96 hours. The samples were measured in triplicates.

In the case of U87 cell line, the activity of the conjugate **32** was not altered with the excess of Cilengitide (Table 7, entry 1), whereas the conjugate **33** registered a modest decrease of its cytotoxic activity: IC_{50} value increased from 91 nM to 143 nM with excess of Cilengitide (Table 7, entry 2). In the MDA-MB-468 cell line, the loss of activity was more pronounced for both conjugates: in presence of Cilengitide the IC_{50} of conjugate **32** increased from 47 nM to 259 nM and the IC_{50} of conjugate **33** increased from 65 nM to 340 nM (Table 7, entry 2).

The results from the competition experiment showed no correlation between the expression of integrin $\alpha_V\beta_3$ and the cytotoxicity of the *iso*DGR- α-amanitin conjugates **32** and **33**. Nevertheless, since the cell lines used overexpress different integrins ($\alpha_5\beta_1$ in U87, $\alpha_V\beta_6$ in MDA-MB-468, and $\alpha_V\beta_5$ in both), the increase of the IC_{50} values of conjugates **32** and **33** (up to 5.5 times) may be caused by the blocking of other integrins with excess of Cilengitide, which binds efficiently integrin $\alpha_V\beta_3$ (IC_{50} = 0.6 nM) but also $\alpha_V\beta_5$ (IC_{50} = 8.4 nM), $\alpha_5\beta_1$ (IC_{50} = 14.9 nM)[103] and $\alpha_V\beta_6$ (IC_{50} = 82.8 nM).[179]

3.1.4. Conclusions

Three cyclo[DKP-*iso*DGR]-α-amanitin conjugates **31-33** were synthesized by joining the functionalized *cyclo*[DKP-*iso*DGR]-CH_2NH_2 integrin ligand **14** to α-amanitin *via* cleavable and uncleavable linkers and different spacers. The conjugates were tested in a competitive binding assay, retaining good binding affinity for the purified $\alpha_V\beta_3$ receptor in the low nanomolar range as the free ligand *cyclo*[DKP-3-*iso*DGR] **11** and the RGD-α-amanitin conjugates **42** and **43**.

The cell viability assays performed on U87 ($\alpha_V\beta_3$+), A549 ($\alpha_V\beta_3$-) and MDA-MB-468 ($\alpha_V\beta_3$-) cancer cell lines showed that the conjugates bearing the lysosomally cleavable linker Val-Ala were more potent than the "uncleavable" conjugates on the three cell lines. Furthermore, *cyclo*[DKP-*isoDGR*]-α-amanitin conjugates **32** and **33** displayed a better cytotoxic activity than the RGD cleavable conjugate **43** and were found slightly more potent than free α-amanitin in U87, MDA-MB-468 and partly in A549 cell lines.

However, contrary to what expected from the binding affinity tests, it was not observed a correlation between the cytotoxicity of the conjugates and the expression of integrin $\alpha_V\beta_3$.

The competition experiments carried out with the *iso*DGR conjugates **32** and **33** in U87 ($\alpha_V\beta_3$+, $\alpha_V\beta_5$+, $\alpha_V\beta_6$-, $\alpha_5\beta_1$+) and MDA-MB-468 ($\alpha_V\beta_3$-, $\alpha_V\beta_5$+, $\alpha_V\beta_6$+, $\alpha_5\beta_1$-) in presence of 50-fold excess of the integrin binder Cilengitide, showed a more pronounced effect of the integrin blocking when using the $\alpha_V\beta_3$-non expressing MDA-MB-468 cell line (IC_{50} of conjugates increased up to 5.5-fold). Since Cilengitide is known to strongly bind not only $\alpha_V\beta_3$, but also $\alpha_V\beta_5$, $\alpha_V\beta_6$, and $\alpha_5\beta_1$, these results suggest that the internalization of the *cyclo*[DKP-*isoDGR*]-α-amanitin conjugates **32** and **33** is possibly mediated by other integrins different from $\alpha_V\beta_3$.

3.2. Synthesis and biological evaluation of *iso*DGR-MMAE and *iso*DGR-MMAF conjugates

3.2.1. Monomethyl auristatin E and F

Monomethyl auristatin E and monomethyl auristatin F (Figure 43) are synthetic analogs of dolastatin 10, a natural pseudopeptide isolated from the sea hare *Dolabella auricularia*.[180] Dolastatin 10 is highly cytotoxic at very low concentrations (average $IC_{50} <$ 1 nM), acting as a potent inhibitor of tubulin polymerization leading to the arrest of cell cycle at G2/M phase and cell death.[181,182]
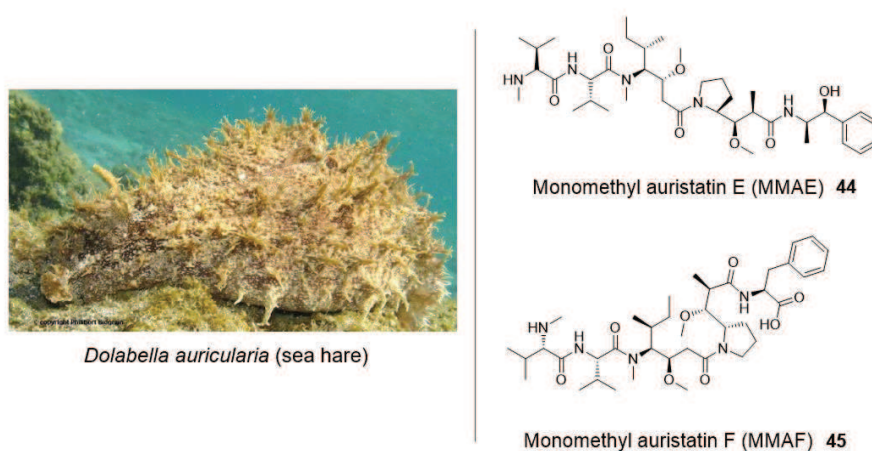
Figure 43. *Dolabella auricularia* and chemical structures of dolastatin 10 derivatives monomethyl auristatin E and monomethyl auristatin F

MMAE and MMAF were developed by Seattle Genetics for its use as payloads in ADCs.[183,184] MMAE is the cytotoxic agent of the FDA approved Adcetris®, where it is linked to an anti-CD30 mAb via the protease cleavable Val-Cit dipeptide linker with average DAR of 4.[185] Due to its high cytotoxicity ($IC_{50} \approx 1$ nM in pancreatic cell lines)[186] MMAE has been used in conjugation with several targeting agents besides monoclonal antibodies, for example: aptamers,[187] HLIPS,[188] and small ligands.[140,189,190]

Differently from MMAE, free MMAF possesses a carboxylic acid at the C- terminus that is charged at physiological pH, thus increasing the hydrophilicity and limiting the cell permeability of the drug. Nevertheless, MMAF is designed to display a high cytotoxicity when delivered inside the tumor cells in conjugation to a monoclonal antibody. This feature was demonstrated by Doronina and co-workers, who studied the cytotoxic activity of ADCs based on MMAF and the anti-CD30 mAb cAC10, reporting a significant
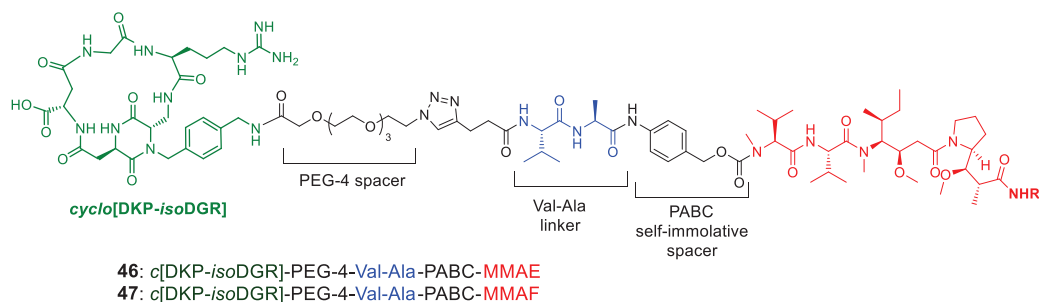
increase of the cytotoxicity of the conjugates (2200-fold more potent) compared to the free drug *in vitro* and *in vivo*.[184] Further studies carried out by the same group, compared the activity of cAC10vc-MMAF conjugate with its MMAE analogs in CD30 lymphoma cell lines. While free MMAE displayed 50-200-fold higher activity than MMAF, the cAC10vc-MMAF conjugate was up to 3-fold times more potent that cAC10vc-MMAE in CD30 positive cell lines, confirming the efficacy of MMAF as a payload for targeted therapy.[191]

These studies also proved the importance of the protease cleavable dipeptide linker Val-Cit for the effective intracellular delivery, lysosomal cleavage and drug release since both MMAE and MMAF, execute their mechanism of action in the cytosol.[191,192] In addition, their physicochemical properties have an influence in the killing efficacy: cell-permeable MMAE is able to diffuse through neighbor cells, extending its toxic activity (bystander-killing effect)[39,40] while MMAF is retained inside the cell due to its poor membrane permeability, resulting in increased drug accumulation.[193]

3.2.2. Synthesis of *cyclo*[DKP-*iso*DGR]-MMAE and *cyclo*[DKP-*iso*DGR]-MMAF conjugates

The properties of MMAE and MMAF, and the results from the investigations previously cited, raised our interest and we decided to evaluate the efficacy of SMDCs containing MMAE or MMAF and the integrin ligand *cyclo*[DKP-*iso*DGR]-CH$_2$NH$_2$ **14**. For this, we planned to synthesize two *cyclo*[DKP-*iso*DGR]-MMAE and two *cyclo*[DKP-*iso*DGR]-MMAF conjugates (Figure 43), in collaboration with the University of Milan, by connecting the *iso*DGR ligand **14** containing a PEG-4 spacer to MMAE or MMAF *via* the lysosomally cleavable Val-Ala linker (**46-47**) or by direct peptidic conjugation (**48-49**).

Lysosomally cleavable linker system

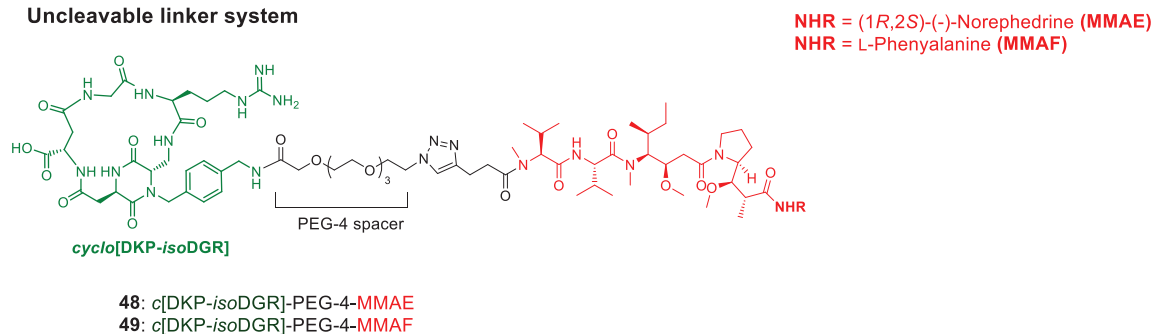cyclo[DKP-*iso*DGR]   PEG-4 spacer   Val-Ala linker   PABC self-immolative spacer

46: c[DKP-*iso*DGR]-PEG-4-Val-Ala-PABC-MMAE
47: c[DKP-*iso*DGR]-PEG-4-Val-Ala-PABC-MMAF

Uncleavable linker system

NHR = (1*R*,2*S*)-(-)-Norephedrine **(MMAE)**
NHR = L-Phenyalanine **(MMAF)**

cyclo[DKP-*iso*DGR]   PEG-4 spacer

48: c[DKP-*iso*DGR]-PEG-4-MMAE
49: c[DKP-*iso*DGR]-PEG-4-MMAF

Figure 44. Structure of cyclo[DKP-*iso*DGR]-MMAE and cyclo[DKP-*iso*DGR]-MMAF conjugates

The preparation of the *iso*DGR ligand (**41**) containing the PEG spacer, was carried out as indicated in Scheme 6.[194,195] Commercial tetraethylenglycol was activated with 0.2 equivalents of *p*-toluenesulfonyl chloride (to avoid a double substitution) and NaOH in THF to obtain PEG-4-OTs **50-a** (96% yield). The tosyl group was then substituted using sodium azide as a nucleophilic agent, giving the PEG-4-N$_3$ **50-b** (70% yield). The next step was the alkylation of **50-b** with bromoacetic acid and excess of NaH to give the 14-azido-3,6,9,12-tetraoxatetradecanoic acid **51** (73% yield), which was activated with EDC.HCl and NHS to obtain intermediate **40** (99% yield) that was coupled to the ligand cyclo[DKP-*iso*DGR]-CH$_2$NH$_2$ **14**, *via* pH-controlled reaction (pH 7.3-7.6) in PBS pH 7/MeCN 1:1 to afford **41** in good yield (65%).
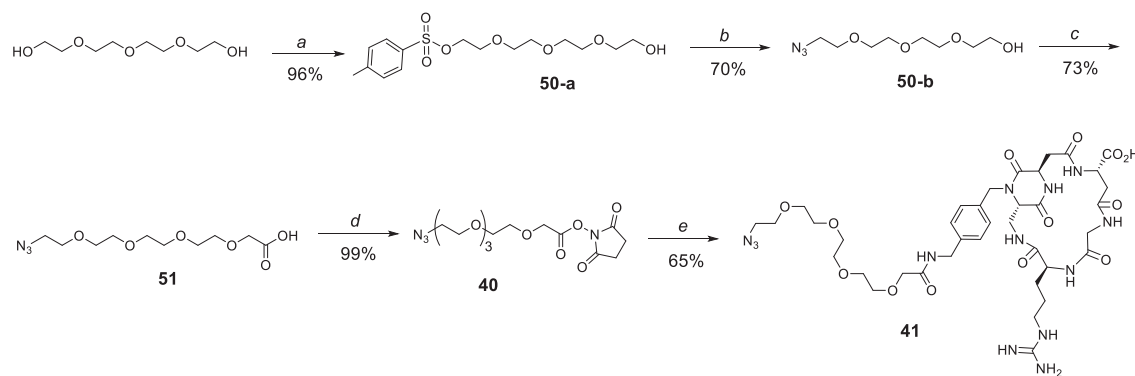
Scheme 6. Synthesis of *cyclo*[DKP-*iso*DGR]-CH$_2$NH-PEG-4-N$_3$ (**41**). a) TosCl, NaOH, THF, 0° C, 2 h, Y: 96%; b) NaN$_3$, MeCN, reflux, overnight, Y: 70%; c) NaH, THF, 0°C to rt. 4 h, Y: 73%; d) EDC.HCl., NHS, DCM, rt. overnight, Y: 99%; e) *cyclo*[DKP-*iso*DGR]-CH$_2$-NH$_2$ (**14**), PBS/MeCN 1:1, pH 7.3-7.6, rt. overnight, Y: 65%.
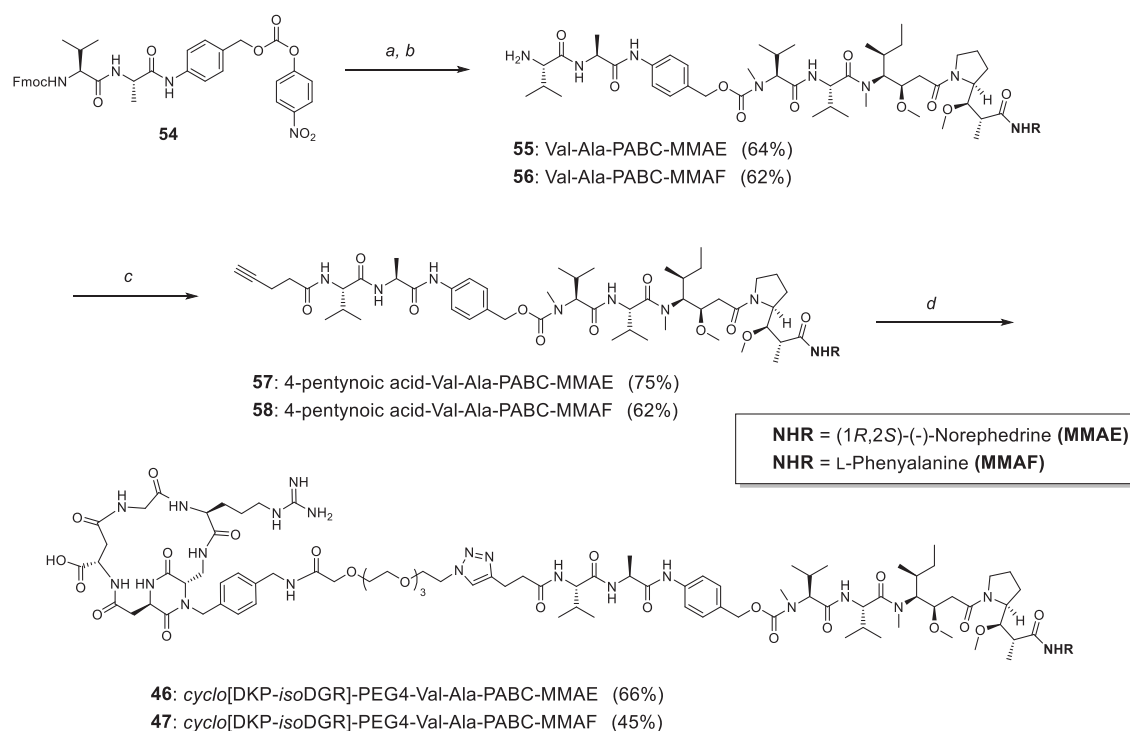
The protease cleavable linker Val-Ala containing the *p*-aminobenzyl alcohol (PABA) self-immolative spacer was prepared following the procedure of Kratz and coworkers,[196] as described in Scheme 7. The peptidic synthesis was carried out in solution, allowing to obtain the linker in grams scale. Commercial Fmoc-Val was activated with NHS and DCC (1:1) in THF and then coupled to alanine (free amino acid) using NaHCO$_3$ as a base in a mixture water/THF/diethyl to obtain Fmoc-Val-Ala-OH (**52**) with 74% yield. *P*-aminobenzyl alcohol reacted with the dipeptide **52** in a mixture of DCM/MeOH 2:1, using EEDQ as coupling agent to avoid racemization, giving Fmoc-Val-Ala-PABOH **53** (58%). Finally, the hydroxy group of **53** was activated with *p*-nitrophenyl chloroformate in THF, using pyridine as HCl scavenger, to afford the activated linker Fmoc-Val-PAB-PNP **54** with 62% yield.
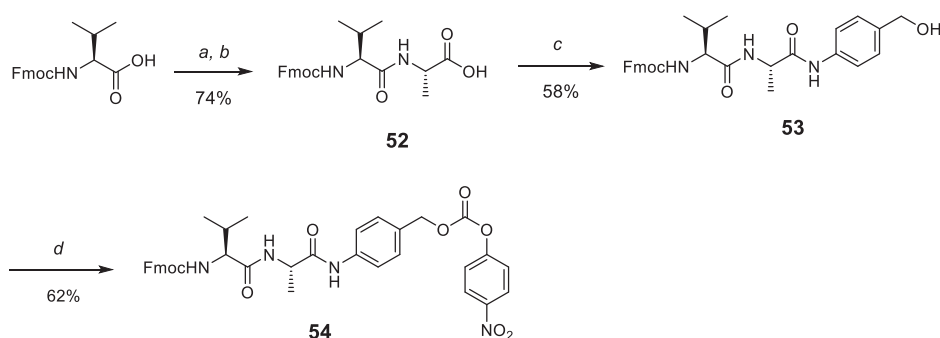
Scheme 7. Synthesis of Val-Ala-PAB-PNP **54**. a) DCC, NHS, THF, 0°C to rt. overnight; b) Alanine, NaHCO$_3$, THF/diethyl ether/water 1:1:1, rt., 4 days; c) *p*-aminobenzyl alcohol, EEDQ, DCM/MeOH 2:1, rt. 48 h; d) *p*-nitrophenyl chloroformate, pyridine, THF, 0°C to rt., 4h.

The conjugates bearing the lysosomally cleavable linker Val-Ala were prepared as described in the Scheme 6. The Fmoc-protected Val-Ala-PAB-PNP linker (**54**) was coupled to the secondary amine of commercial MMAE or MMAF in presence of DIPEA

and a catalytic amount of HATU, giving Val-Ala-PABC-MMAE/MMAF (**55** or **56**) after removal of the Fmoc group (62-65% yield over 2 steps). The intermediates were reacted with 4-pentynoic acid activated as NHS ester (**39**) to obtain 4-pentynoic acid-Val-Ala-PABC-MMAE/MMAF (**57** or **58**). Finally, a copper catalyzed alkyne-azide cycloaddition (CuAAC) between these intermediates and *cyclo*[DKP-*iso*DGR]-CH$_2$NH-PEG-4-N$_3$ (**41**), followed by HPLC purification and freeze-drying form H$_2$O/ACN afforded the cleavable conjugates *cyclo*[DKP-*iso*DGR]-PEG-4-Val-Ala-PABC-MMAE/MMAF **46** and **47** (yield: 66 and 42% respectively).

54

55: Val-Ala-PABC-MMAE (64%)
56: Val-Ala-PABC-MMAF (62%)

57: 4-pentynoic acid-Val-Ala-PABC-MMAE (75%)
58: 4-pentynoic acid-Val-Ala-PABC-MMAF (62%)

NHR = (1*R*,2*S*)-(-)-Norephedrine (**MMAE**)
NHR = L-Phenylalanine (**MMAF**)

46: *cyclo*[DKP-*iso*DGR]-PEG4-Val-Ala-PABC-MMAE (66%)
47: *cyclo*[DKP-*iso*DGR]-PEG4-Val-Ala-PABC-MMAF (45%)

Scheme 8. Synthesis of lysosomally cleavable *cyclo*[DKP-*iso*DGR]-MMAE and *cyclo*[DKP-*iso*DGR]-MMAF conjugates. a) MMAE or MMAF, DIPEA, HOAt, DMF, rt., overnight; b) piperidine, DMF, rt., 2h; c) 4-pentynoic acid-NHS activated (**39**), DIPEA, DMF, rt., overnight; d) *cyclo*[DKP-*iso*DGR]-CH$_2$NH$_2$-PEG-4-N$_3$ (**41**), sodium ascorbate, CuSO$_4$·5H$_2$O, H$_2$O:DMF 1/1, rt., overnight.

The "uncleavable" conjugates **48** and **49** were synthetized as described in the Scheme 7. The commercial MMAE or MMAF reacted directly with 4-pentynoic acid-NHS ester (**39**) to give 4-pentynoic acid-MMAE/MMAF (**59** or **60**) in good yields (69-73%). These intermediates underwent a copper catalyzed alkyne-azide cycloaddition (CuAAC) with the azide functionalized ligand **41** to obtain the conjugates *cyclo*[DKP-*iso*DGR]-PEG-4-MMAE/MMAF **48** and **49** (yield: 67 and 40% respectively).
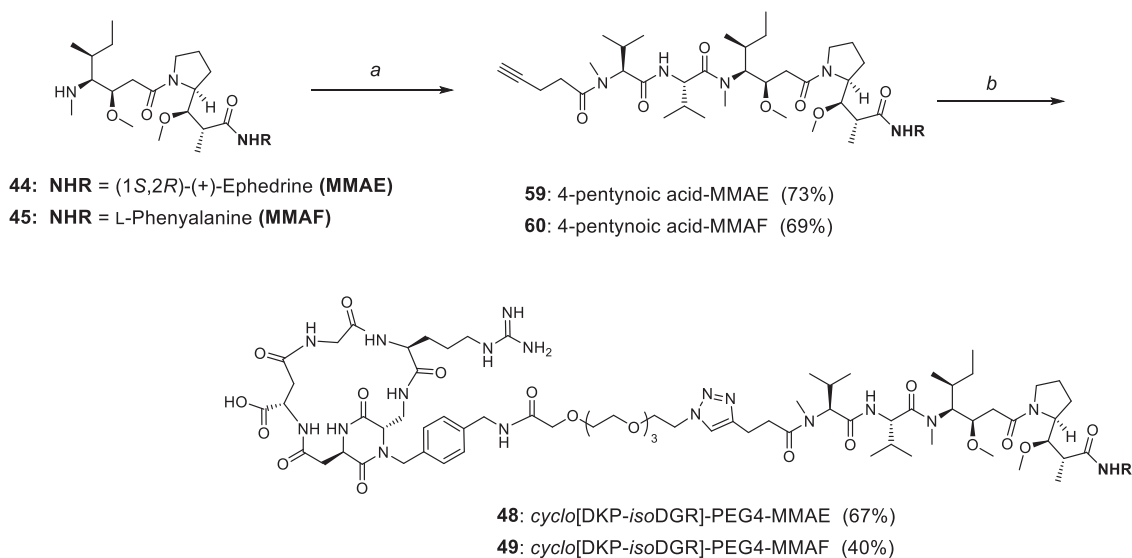
Scheme 9. Synthesis of "uncleavable" *cyclo*[DKP-*iso*DGR]-MMAE and *cyclo*[DKP-*iso*DGR]-MMAF conjugates. a) 4-pentynoic acid-NHS activated (39), DIPEA, DMF, rt., overnight; b) *cyclo*[DKP-*iso*DGR]-CH$_2$NH$_2$-PEG-4-N$_3$ (**41**), sodium ascorbate, CuSO$_4$·5H$_2$O, H$_2$O:DMF 1/1, rt., overnight.

During the synthesis of the conjugates, the formation of side products containing the drug connected to the linker and the PEG spacer but not containing the integrin ligand was detected. This was originated by the contamination of ligand **41** by hydrolyzed COOH-PEG-4-N$_3$ **51**, which reacted *via* CuAAC reaction with the intermediates containing the pentynoic moiety. This contamination could be avoided reducing the flow from 15 mL/min to 9 mL/min during the HPLC purification of *cyclo*[DKP-*iso*DGR]-CH$_2$NH$_2$-PEG-4-N$_3$ (**41**), improving in this way the separation from the hydrolysis product. The side products of the click reaction between **41** and the MMAE intermediates **57** and **59**, were isolated to be used as a control for the targeting activity in the cell viability assays (**61** and **62**, Figure 45).
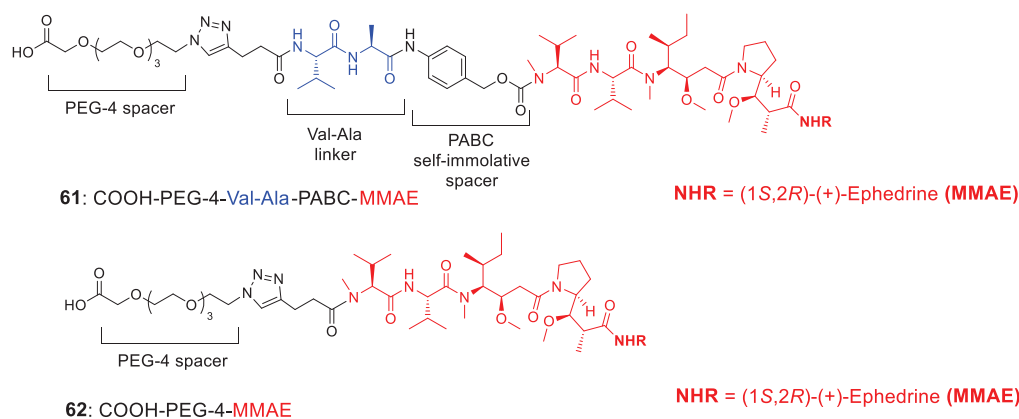

Figure 45. Side products from the click reaction of MMAE conjugates

3.2.3. *In vitro* studies and discussion

3.2.3.1. Binding affinity assays

The conjugates *iso*DGR-MMAE and *iso*DGR-MMAF **46-49** were evaluated for their ability to inhibit the binding of biotinylated vitronectin to the purified $\alpha_v\beta_3$ receptor in a competitive binding assay. The immobilized integrin receptor was incubated with solutions of the conjugates **46-49** at different concentrations in presence of biotinylated vitronectin (1 μg mL^{-1}), then the bound vitronectin was measured. The half-maximal inhibitory concentrations (IC$_{50}$) are presented in the Table 8.

Table 8. Inhibition of biotinylated vitronectin binding to $\alpha_v\beta_3$ receptor

Compound	Structure	IC$_{50}$ (nM) [a] $\alpha_v\beta_3$
46	c[DKP-*iso*DGR]-PEG-4-Val-Ala-PABC-MMAE	36.2 ± 0.2
47	c[DKP-*iso*DGR]-PEG-4-Val-Ala-PABC-MMAF	43.9 ± 2.1
48	c[DKP-*iso*DGR]-PEG-4-MMAE	14.5 ± 0.6
49	c[DKP-*iso*DGR]-PEG-4-MMAF	10.7 ± 2.8

[a] IC$_{50}$ values were calculated as the concentration of compound required for 50% inhibition of biotinylated vitronectin binding as estimated by GraphPad Prism software. All values are the arithmetic mean ± the standard deviation (SD) of duplicated determinations

The four conjugates **46-49** retained a good binding affinity for the $\alpha_v\beta_3$ receptor with IC$_{50}$ values in the nanomolar range. It was observed though, a slight increase of the IC$_{50}$ of the conjugates compared to the free ligand *cyclo*[DKP-3-*iso*DGR] **11** ($\alpha_v\beta_3$ IC$_{50}$ 9.2 nM, cf. Table 4), differently from what observed for the cleavable *iso*DGR-α-amanitin conjugates. These result suggest that the conformational modifications resulting from the conjugation to the linker and the drug might have a moderate effect on the binding affinity of the *iso*DGR ligand to the $\alpha_v\beta_3$ receptor.

3.2.3.2. Cell viability assays

The *iso*DGR conjugates **46-49**, together with their RGD analogs (Figure 45, compounds **63-66**) synthetized by André Dias (University of Milano), were evaluated for their ability to selectively target $\alpha_v\beta_3$-expressing tumor cells in cell viability assays on U87 human glioblastoma cell line, that is known to express the $\alpha_V\beta_3$ integrin receptor,[173,174] and in

HT29 (human colon cancer) cell line, which was selected as $\alpha_V\beta_3$ negative.[173] Compounds **61** and **62**, containing the PEG spacer, the linker and MMAE but not the integrin ligand, were tested as a negative control for the $\alpha_v\beta_3$ targeting.

Lysosomally cleavable linker system

63: c[DKP-RGD]-PEG-4-Val-Ala-PABC-MMAE
64: c[DKP-RGD]-PEG-4-Val-Ala-PABC-MMAF
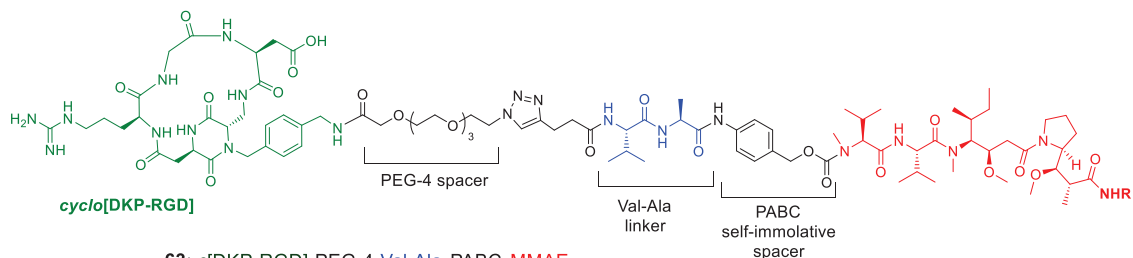
NHR = (1R,2S)-(-)-Norephedrine **(MMAE)**
NHR = L-Phenyalanine **(MMAF)**

Uncleavable linker system

65: c[DKP-RGD]-PEG-4-MMAE
66: c[DKP-RGD]-PEG-4-MMAF
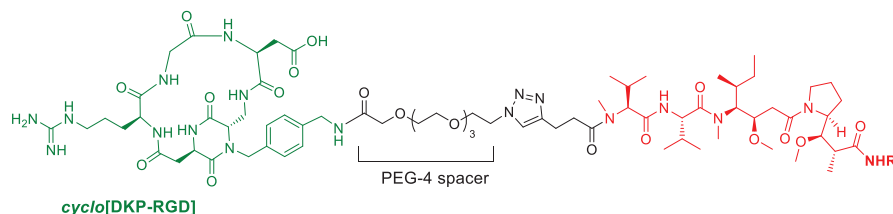
Figure 46. Structure of *cyclo*[DKP-RGD]-MMAE and *cyclo*[DKP-RGD]-MMAF conjugates

U87 and HT29 cells were treated with different concentrations of the free drug MMAE or MMAF and the conjugates for 72 hours with or without washout. For the washout experiments, the cells were washed after 6 hours of incubation, the media was replaced and then the cells were incubated for other 66 hours. This procedure has been previously used by our research group,[70] intending to simulate the *in vivo* conditions where the administered prodrug is rapidly cleared from the tumor extracellular environment. In this way the conjugates degraded or unbound to the integrin receptors are removed from the medium, minimizing the effect of metabolites produced by extracellular cleavage of the linker. The cell viability was quantified by MTT (3-(4,5-dimethylthiazol-2-yl)-2,5-diphenyltetrazolium bromide) assay. The IC_{50} values presented in Table 9 and Table 10 were calculated using GraphPad Prism 6.

Table 9. Antiproliferative activity of RGD-MMAE and *iso*DGR-MMAE conjugates in human glioblastoma U87-MG cell line after 72 h incubation with and without washout after 6h, and in human colon cancer HT29 after 72 h incubation without washout.

Entry	Structure	IC$_{50}$ (nM) U87-MG ($\alpha_v\beta_3$+) [a]		IC$_{50}$ (nM) HT29 ($\alpha_v\beta_3$ -, $\alpha_v\beta_5$+, $\alpha_v\beta_6$+) [a]
		WO 6h + 66h	72h no WO	72h no WO
1	MMAE (44)	0.144 ± 0.06	0.076 ± 0.08	0.030 ± 0.04
2	COOH-PEG-4-Val-Ala-PABC-MMAE (61)	128.6 ± 0.16	75.72 ± 0.07	298.5 ± 0.08
3	c[DKP-RGD]-PEG-4-Val-Ala-PABC-MMAE (63)	363.9 ± 0.04	38.99 ± 0.11	51.20 ± 0.08
4	c[DKP-*iso*DGR]-PEG-4-Val-Ala-PABC-MMAE (46)	83.54 ± 0.04	11.5 ± 0.13	27.71 ± 0.04
5	COOH-PEG-4-MMAE (62)	n.d.	n.d.	>10000
6	c[DKP-RGD]-PEG-4-MMAE (65)	738.8 ± 34.3	1228 ± 0.21	464.2 ± 0.08
7	c[DKP-*iso*DGR]-PEG-4-MMAE (48)	n.d. [b]	685.5	382 ± 0.08

[a]Cells were treated with different concentrations of free **MMAE,** conjugates **46, 48, 63, 65** and compounds **61** and **62** for 72 hours, with washout (WO) after 6h and without washout (no WO). IC$_{50}$ values were calculated as the concentration of compound required for 50% inhibition of cell viability. [b] IC$_{50}$ could not be determined.

As can be appreciated in Table 9, the MMAE conjugates **63** and **46** bearing the cleavable Val-Ala linker displayed nanomolar IC$_{50}$ values in the experiment at 72 hours incubation without washout in U87 cell line (IC$_{50}$ = 38.99 and 11.5 nM, entry 3 and 4 in Table 9), proving to be more cytotoxic than the "uncleavable" conjugates **65** and **48** and the non-targeting compound **61**, even if much less potent (150-500 times less) than free MMAE that displays picomolar activity. In particular, the conjugate *cyclo*[DKP-*iso*DGR]-PEG-4-Val-Ala-PABC-MMAE (**46**) resulted 60 fold-more toxic than uncleavable *cyclo*[DKP-*iso*DGR]-PEG-4-MMAE (**48**), 6.6-fold more toxic than the non-targeting COOH-PEG-4-Val-Ala-PABC-MMAE (**61**) and 3.4-times more potent than its RGD analog *cyclo*[DKP-RGD]-PEG-4-MMAE (**63**).

In the experiment with washout after 6 hours, both MMAE and the conjugates were, as expected, less cytotoxic, and also in this case, the MMAE conjugates displayed a

reduced cytotoxicity with respect to free MMAE, being the "uncleavable" conjugates **65** and **48** the least cytotoxic. In particular, the loss of activity of conjugates **63** and **46**, containing the cleavable linker, compared to free MMAE is increased by a factor of 4-5 in the experiment with washout, as can be calculated comparing the ratio **63**/MMAE and **46**/MMAE in both experiments (cf. entry 3 and 4 with entry 1 in Table 9). These results suggest that the activity observed for the MMAE conjugates is not completely consistent with an $\alpha_V\beta_3$ integrin-mediated internalization process. In fact, the differences observed in both experiments, notably in the cytotoxicity of the cleavable conjugates **63** and **46**, could be attributed to the early release and diffusion of MMAE after extracellular cleavage of the Val-Ala linker by serine proteases present in the cellular environment or by cathepsin B released upon cell dead and degradation after 72 hours.[42,197,198]

The antiproliferative activity of the MMAE conjugates in HT29 ($\alpha_V\beta_3$ negative) cell line, indicate a loss of potency respect to the unconjugated MMAE, similar to what observed in the experiment with U87 ($\alpha_V\beta_3$ positive) cell line, as well as an increase in the cytotoxicity of the conjugates compared to the non-targeting compounds (**61** and **62**), up to 10.7-fold times in the case of the cleavable MMAE conjugate *cyclo*[DKP-*iso*DGR]-PEG-4-Val-Ala-PABC-MMAE **46** (cf. entry 4 with entry 2 in Table 9). Interestingly, for the cleavable MMAE conjugates **46** and **63**, the loss in the cytotoxicity compared to free MMAE was more pronounced in HT29 than in U87 cell line: *cyclo*[DKP-RGD]-PEG-4-Val-Ala-PABC-MMAE (**63**) was 500 less toxic than MMAE in U87 ($\alpha_V\beta_3$+) and 1700 times less toxic than MMAE in HT29 ($\alpha_V\beta_3$-) cell line (cf. entry 3 with entry 1 in Table 9), whereas *cyclo*[DKP-*iso*DGR]-PEG-4-Val-Ala-PABC-MMAE (**46**) was 150 times less toxic than MMAE in U87 ($\alpha_V\beta_3$+) and 920 times less toxic than MMAE in HT29 ($\alpha_V\beta_3$-) (cf. entry 4 with entry 1 in Table 9). These results show a moderate targeting index, TI = 6.1 and 3.3 for MMAE cleavable conjugates **46** and **63** respectively (Table 10), suggesting that the activity of the conjugates is possibly associated to other integrins different from $\alpha_V\beta_3$ in both cell lines (i.e. $\alpha_V\beta_5$ in U87 and $\alpha_V\beta_5$, $\alpha_V\beta_6$ in HT29).

Table 10. Targeting index of cleavable MMAE conjugates **63** and **46**

| Entry | Structure | IC$_{50}$ (nM)[a] | | S[b] | TI[c] |
		U87-MG ($\alpha_v\beta_3$+)	HT29 ($\alpha_v\beta_3$-)		
1	MMAE (44)	0.076 ± 0.08	0.030 ± 0.04	0.39	1
2	*c*[DKP-RGD]-PEG-4-Val-Ala-PABC-MMAE (63)	38.99 ± 0.11	51.20 ± 0.08	1.31	3.3
3	*c*[DKP-*iso*DGR]-PEG-4-Val-Ala-PABC-MMAE (46)	11.5 ± 0.13	27.71 ± 0.04	2.4	6.1

[a]IC$_{50}$ values were calculated as the concentration of compound required for 50% inhibition of cell viability. [b] IC$_{50}$ could not be determined; [b] Selectivity (S): IC$_{50}$ ($\alpha_v\beta_3$-) / IC$_{50}$ ($\alpha_v\beta_3$+); [c] Targeting index (TI): S $_{conjugate}$ / S $_{free\ MMAE}$

The antiproliferative activity of the MMAF conjugates in U87 and HT29 cell line is shown in Table 11. In the experiment with U87 cell line at 72 hours incubation without washout, free MMAF was, as expected, less toxic than MMAE due to the charged carboxylic group that limits its capacity to diffuse through the cell membrane.[199,200] The conjugates **64** and **47**, bearing the cleavable Val-Ala linker, presented cytotoxic activity values in the sub-micromolar range, 1.7-3.4 times less potent than the activity registered for MMAF (cf. entry 2 and 3 with entry 1 in Table 11). Also, like in the previous experiments, the "uncleavable" conjugates proved the least cytotoxic, with IC$_{50}$ values > 10 µM in the case of *cyclo*[DKP-RGD]-PEG-4-MMAF (**66**). The experiment with washout after 6 hours was also run but, in this case, no cytotoxic activity was determined for free MMAF or the MMAF conjugates, with exception of *cyclo*[DKP-*iso*DGR]-PEG-4-Val-Ala-PABC-MMAF (**47**) that displayed micromolar cytotoxicity (IC$_{50}$ = 3358 nM, entry 3 in Table 11). These data indicate that the conjugation to *cyclo*[DKP-RGD] or *cyclo*[DKP-*iso*DGR] integrin ligands does not significantly improve the cellular uptake of MMAF, and the activity displayed by the cleavable MMAF conjugates is mainly due to a poor cell membrane diffusion rather than an integrin-mediated endocytosis.

Table 11. Antiproliferative activity of RGD-MMAF and *iso*DGR-MMAF conjugates in human glioblastoma U87-MG cell line after 72 h incubation with and without washout after 6h

Entry	Structure	IC$_{50}$ (nM) U87-MG ($\alpha_V\beta_3$+) [a]		IC$_{50}$ (nM) HT29 ($\alpha_V\beta_3$-, $\alpha_V\beta_5$+, $\alpha_V\beta_6$+) [a]
		WO 6h + 66h	72h no WO	72h no WO
1	MMAF (45)	n.d.[b]	94.4 ± 0.06	52.16 ± 0.06
2	*c*[DKP-RGD]-PEG-4-Val-Ala-PABC-MMAF (64)	n.d.[b]	331.9 ± 0.10	719.2 ± 0.07
3	*c*[DKP-*iso*DGR]-PEG-4-Val-Ala-PABC-MMAF (47)	3358	165.9 ± 0.06	511 ± 0.04
4	*c*[DKP-RGD]-PEG-4-MMAF (66)	n.d.[b]	> 10000	>10000
5	*c*[DKP-*iso*DGR]-PEG-4-MMAF (49)	n.d.	763.7 ± 0.08	1197 ± 0.07

[a]Cells were treated with different concentrations of free **MMAF,** conjugates **47, 49, 64, and 67** for 72 hours, with washout (WO) after 6h and without washout (no WO). IC$_{50}$ values were calculated as the concentration of compound required for 50% inhibition of cell viability. [b]Non-determined.

In the experiment with HT29 ($\alpha_V\beta_3$-) cell line, MMAF conjugates presented a loss of potency regarding the activity of free drug MMAF more pronounced that in the experiment with U87 ($\alpha_V\beta_3$-) cell line: *cyclo*[DKP-RGD]-PEG-4-Val-Ala-PABC-MMAF (**64**) was 3.5 less toxic than MMAF in U87 ($\alpha_V\beta_3$+) and 14 times less toxic than MMAF in HT29 ($\alpha_V\beta_3$-) (cf. entry 2 with entry 1 in Table 10), *cyclo*[DKP-*iso*DGR]-PEG-4-Val-Ala-PABC-MMAF (**47**) was 1.7 times less toxic than MMAF in U87 ($\alpha_V\beta_3$+) and 10 times less toxic than MMAF in HT29 ($\alpha_V\beta_3$-) (cf. entry 3 with entry 1 in Table 10), and *cyclo*[DKP-*iso*DGR]-PEG-4-MMAF (**49**) was 8 times less toxic than MMAF in U87 ($\alpha_V\beta_3$+) and 23 times less toxic than MMAF in HT29 ($\alpha_V\beta_3$-) (cf. entry 5 with entry 1 in Table 10). These results indicate once more, a moderate targeting index, TI = 5.6 and 3.9 for MMAF cleavable conjugates **47** and **64** respectively (Table 12). Apparently, the activity of the MMAF conjugates could be associated to other integrins different from $\alpha_V\beta_3$, present in both cell lines.

Table 12. Targeting index of cleavable MMAF conjugates **64** and **47**

| Entry | Structure | IC$_{50}$ (nM)[a] | | S[b] | TI[c] |
		U87-MG ($\alpha_v\beta_3$+)	HT29 ($\alpha_v\beta_3$-)		
1	MMAF (45)	94.4 ± 0.06	52.16 ± 0.06	0.55	1
2	c[DKP-RGD]-PEG-4-Val-Ala-PABC-MMAF (63)	331.9 ± 0.10	719.2 ± 0.07	2.2	3.9
3	c[DKP-isoDGR]-PEG-4-Val-Ala-PABC-MMAF (47)	165.9 ± 0.06	511 ± 0.04	3.1	5.6

[a]IC$_{50}$ values were calculated as the concentration of compound required for 50% inhibition of cell viability. [b] IC$_{50}$ could not be determined; [b] Selectivity (S): IC$_{50}$ ($\alpha_v\beta_3$-) / IC$_{50}$ ($\alpha_v\beta_3$+); [c] Targeting index (TI): S $_{conjugate}$ / S $_{free MMAF}$

3.2.4. Conclusions

A small library of four SMDC containing the functionalized integrin ligand *cyclo*[DKP-*iso*DGR]-CH$_2$NH$_2$ (**14**) and the dolastatin derivatives MMAE or MMAF as payloads has been synthetized. The conjugates were obtained *via* copper (I) catalyzed alkyne-azide cycloaddition (CuAAC) between the integrin ligand functionalized with a PEG$_4$-azide spacer and an alkyne moiety directly attached to MMAE or MMAF (conjugates **48** and **49** respectively) or to the dipeptide Val-Ala linker bearing the PABC self-immolative spacer connected to MMAE or MMAF (conjugates **46** and **47**).

The four *iso*DGR conjugates were tested in a competitive binding assay, retaining good binding affinity for the purified $\alpha_v\beta_3$ receptor in the nanomolar range, although a slight increase in the $\alpha_v\beta_3$ IC$_{50}$ was detected for the cleavable conjugates **46** and **47** in contrast to the free integrin ligand *cyclo*[DKP-3-*iso*DGR] **11**. This revealed a moderate effect of the conjugation in the binding affinity towards the $\alpha_v\beta_3$ receptor non-observed before for the *iso*DGR conjugates.

The antiproliferative activity of the *iso*DGR-MMAE and *iso*DGR-MMAF conjugates (**46-49**), and their RGD analogs (**63-66**) was evaluated in a first set of cell viability assays carried out in U87 ($\alpha_v\beta_3$ expressing) cell line at 72 hours incubation time with and without washout after 6 hours. The results obtained during these tests showed in

general, a drop of cytotoxicity for the conjugates compared to the free MMAE or MMAF, especially for the uncleavable conjugates. The conjugates bearing the Val-Ala cleavable linker displayed better cytotoxic activity values, particularly the cleavable *iso*DGR-MMAE conjugate **46** that resulted 6.6-fold more toxic than the non-targeting compound COOH-PEG-4-Val-Ala-PABC-MMAE **61** and 3.4-times more toxic than its RGD analog *cyclo*[DKP-RGD]-PEG-4-MMAE **63** in the experiment without washout. Nevertheless, the washout experiment involving the MMAF conjugates revealed that the conjugation to the integrin ligands has a poor contribution to the cellular uptake of MMAF.

The cell viability assays carried out in HT29 ($\alpha_V\beta_3$-, $\alpha_V\beta_5$+, $\alpha_V\beta_6$+) cell line with 72 hours incubation time, confirmed the loss of cytotoxicity of the conjugates compared to free MMAE and MMAF, nonetheless, this loss of potency was more pronounced in the $\alpha_V\beta_3$-negative cell line HT29. In fact, the targeting index obtained for the cleavable MMAE and MMAF conjugates (6.1-3.3 and 5.6-3.9 respectively) indicate a moderate selectivity towards the $\alpha_V\beta_3$ receptor, even though the activity of the conjugates might also be governed by other integrins different from $\alpha_V\beta_3$ (e.g. $\alpha_V\beta_5$ in U87 and $\alpha_V\beta_5$, $\alpha_V\beta_6$ in HT29).

Overall, the results from the *in vitro* tests demonstrate that despite the high binding affinity towards the $\alpha_V\beta_3$ receptor, the conjugates are not necessarily internalized by integrin-mediated endocytosis. This becomes clearer in the case of the MMAF conjugates, whose cytotoxic activity is similar to the free MMAF, which is known to poorly penetrate the cell membrane due to its charged phenylalanine residue. In the case of the MMAE conjugates, the cytotoxic activity is boosted by the picomolar potency of the drug and its ability to diffuse through the cell membrane once it is released upon extracellular cleavage, as reported in the literature.[42,197,198] In effect, the conjugates containing the protease cleavable linker Val-Ala display higher cytotoxicity than the uncleavable conjugates because they allow the effective release of the payload when cleaved by extracellular proteases. Importantly, the increased cytotoxicity registered for the cleavable MMAE conjugates **46** and **63** compared to the non-targeting compounds **61** and **62** in U87 ($\alpha_V\beta_3$+, $\alpha_V\beta_5$+, $\alpha_V\beta_6$-) and HT29 ($\alpha_V\beta_3$-, $\alpha_V\beta_5$+,

$\alpha_V\beta_6$+) cell lines suggests, if not an $\alpha_V\beta_3$ integrin-mediated internalization, a possible interaction with other integrins that facilitates the delivery of the payload to the cells.

Experimental section

Material and methods

All manipulations requiring anhydrous conditions were carried out in flame-dried glassware, with magnetic stirring and under a nitrogen atmosphere. All commercially available reagents were used as received. Anhydrous solvents were purchased from commercial sources and withdrawn from the container by syringe, under a slight positive pressure of nitrogen. The reactions were monitored by analytical thin-layer chromatography (TLC) using Macherey-Nagel 0.20 mm silica gel 60 with fluorescent indicator pre-coated polyester sheets (40 × 80 mm). Visualization was accomplished by irradiation with a UV lamp and/or staining with Cerium/Molibdate reagent, ninhydrin or cinnamaldehyde. Flash column chromatography was performed according to the method of Still and co-workers[201] using Chromagel 60 ACC (40-63 μm) silica gel. Proton NMR spectra were recorded on a spectrometer operating at 400.16 MHz. Proton chemical shifts are reported in ppm (δ) with the solvent reference relative to tetramethylsilane (TMS) employed as the internal standard (D_2O δ = 4.79 ppm). The following abbreviations are used to describe spin multiplicity: s = singlet, d = doublet, t = triplet, q = quartet, m = multiplet, bs = broad signal, dd = doublet of doublet, ddd = doublet of doublet of doublet, ddt = doublet of doublet of triplet, td= triplet of doublet. Carbon NMR spectra were recorded on a spectrometer operating at 100.63 MHz, with complete proton decoupling. Carbon chemical shifts are reported in ppm (δ) relative to TMS with the respective solvent resonance as the internal standard. ESI-MS spectra were recorded on the ion trap mass spectrometer Finnigan LCQ Advantage or Micro Waters Q-Tof (ESI source) and on Thermo Fisher linear ion trap LTQ XL mass spectrometer.

HPLC purifications and HPLC traces of final products were performed on Dionex Ultimate 3000 equipped with Dionex RS Variable Wavelenght Detector (column: Atlantis Prep T3 OBD™ 5 μm 19 × 100 mm; flow 15 mL/min unless stated otherwise). The crude reaction mixture was dissolved in H_2O, acetonitrile/water 1:1 or by adding a small

quantity of DMF to the aqueous solution if the compound was insoluble (an ultrasonic bath was used to assist the dissolution). The solution obtained was filtered (polypropylene, 0.45 μm, 13 mm ø, PK/100) and injected in the HPLC, affording purified products. Purity analyses were carried on a Dionex Ultimate 3000 instrument equipped with a Dionex RS Variable Wavelenght detector (column: Atlantis® Prep T3 OBDTM 5 μm 19 × 100 mm). 1 mg of analyte was dissolved in 1 mL of H_2O and was injected using the same gradient used in the purification step. The analysis of the integrals and the relative percentage of purity was performed with the software Cromeleon 6.80 SR11 Build 3161. Also, preparative HPLC LaPrep∑ equipped with autosampler AS3950 and a Phenomenex Luna C-18(2) column, 10 μm, 250 × 21.2 mm, with precolumn at 30 mL/min flow rate and analytical HPLC performed on Hitachi Chromaster (column oven Chromaster 5310, pump Chromaster 5110, autosampler Chromaster 5210, DAD Chromaster 5430) equipped with a Phenomenex Luna C-18(2) column, 10 μm, 250 × 4.6 mm, with precolumn at 1.4 mL/min flow rate were used.

Freeze-drying: The product was dissolved in water or water/ acetonitrile 1:1 and frozen with dry ice. The freeze-drying was carried out at least for 48 h at -50 °C using the instrument 5Pascal Lio5P DGT.

Biological assays

Solid Phase Receptor Binding Assays

Recombinant human integrin $\alpha_V\beta_3$ (R&D Systems, Minneapolis, MN, USA) was diluted to 0.5 μg/mL in coating buffer containing 20 mM Tris-HCl (pH 7.4), 150 mM NaCl, 1 mM $MnCl_2$, 2 mM $CaCl_2$, and 1 mM $MgCl_2$. 100 Microliters of the diluted receptor (100 μL/well) were added to 96-well microtiter plates (Nunc MaxiSorp) and incubated overnight at 4 °C. The plates were treated for additional 2 h at room temperature with blocking solution (coating buffer plus 1% bovine serum albumin) to block nonspecific binding, and washed 2 times with the same solution. Different concentrations (10^{-5}–10^{-12} M) of the test compounds in the presence of 1 μg/mL biotinylated vitronectin were added to the plates, which were shaken for 3 h at room temperature. Vitronectin, (Molecular Innovations, Novi, MI, USA) was biotinylated using an EZ-Link Sulfo-NHS-Biotinylation kit (Pierce, Rockford, IL, USA). The plates were washed 3 times, and

incubated with shaking for 1 h, at room temperature, with streptavidin-biotinylated peroxidase complex (Amersham Biosciences, Uppsala, Sweden). The plates were again washed 3 times with blocking solution, and 100 µL/well of Substrate Reagent Solution (R&D Systems, Minneapolis, MN, USA) were added before shaking in the dark for 30 min and stopping the reaction with the addition of 50 µL/well 2 N H_2SO_4. Absorbance at 415 nm was read in a SynergyTM HT Multi-Detection Microplate Reader (BioTek Instruments, Inc.). Each data point represents the average of triplicate wells; data analysis was carried out by nonlinear regression analysis with GraphPad Prism software. Each experiment was repeated in triplicate or duplicate.

Determination of integrin $\alpha_V\beta_3$ expression by flow cytometry

The expression of integrin $\alpha_V\beta_3$ in U87-MG, A549 and MDA-MB 468 cells was determined by flow cytometry on a FACSCalibur device (Becton Dickinson). Before staining, cells were fixed with fixation solution (0.5% PFA in PBS). 5×10^5 cells per sample were stained in staining medium (PBS, 25 mM HEPES, 3% FCS, 0.02% Na-Azide) with an anti-human integrin $\alpha_V\beta_3$ antibody conjugated to Alexa Fluor 488 (R&D Systems) or isotype control conjugated to Alexa Fluor 488 (Thermo Fischer) at a concentration of 4µg/mL for 45 min at room temperature. Cells were washed with PBS and the mean fluorescence intensity was measured for 10.000 gated events. Data were analyzed using flow cytometry and associated software (BD Biosciences)

Cell culture for cell viability assays of integrin ligand-α-amanitin conjugates

All cell culture reagents were purchased at PAN-Biotech GmbH unless otherwise stated. Cell lines were obtained from CLS (U87-MG, MDA-MB 468 and A549). Cell lines were authenticated using Multiplex Cell Authentication by Multiplexion (Heidelberg, Germany) as described in the literature.[202] The SNP profiles matched known profiles or were unique. The purity of cell lines was validated using the Multiplex cell Contamination Test by Multiplexion (Heidelberg, Germany) as described in the literature.[203] No Mycoplasma, SMRV or interspecies contamination was detected. U87-MG, MDA-MB 468 and A549 cells were cultivated continuously for not more than 3 months in MEM Eagle´s, DMEM or Ham´s F12 medium, respectively supplemented with

10% heat inactivated fetus calf serum, L-glutamine and antibiotics. Cell lines were maintained at 37°C and 5% CO_2 in a high humidity atmosphere.

### Cell therapy and viability assays of integrin ligand-α-amanitin conjugates

Cell viability assays were performed in U87-MG, A549 and MDA-MB 468 cell lines according to the following procedure: 2×10^3 cells/well were plated in 96-well black clear bottom plates (Perkin Elmer) and incubated overnight. 1:5 serial dilutions of compounds **31-33** and **42-43** were prepared in cell culture media. Compounds were added to cell culture and incubated for additional 96 h. Starting concentration of compounds **31-33** and **42-43** in the wells was 1×10^{-5} M and cell viability was determined with the CellTiterGlo 2.0 assay (Promega) in accordance to manufacturer's instructions. Cell viability was calculated in relation to the non-treated controls for each cell line. All samples were measured in triplicate. Data analysis was carried out using software Graph Pad Prism (Graph Pad Software Inc., La Jolla, CA, USA).

Competition experiment for conjugates **32** and **33**

The competition experiments were performed in U87-MG and MDA-MB 468 cell lines according to the following procedure: 2×10^3 cells/well were plated in 96-well black clear bottom plates (Perkin Elmer) and incubated overnight. A solution containing 1×10^{-4} M of the conjugate (**32** or **33**) and 5×10^{-3} M of Cilengitide (50-fold excess of ligand in comparison to the conjugate) was prepared in the growth medium and 1:5 serial dilutions were prepared in cell culture media. The compounds were added to cell culture and incubated for 96 h. Starting concentration of the compounds in the wells was 0.01 mM whereas that of Cilengitide was 0.5 mM. Cell viability was determined with the CellTiterGlo 2.0 assay (Promega) in accordance to manufacturer's instructions. Cell viability was calculated in relation to the non-treated controls for each cell line. All samples were measured in triplicate. Data analysis was carried out using software Graph Pad Prism (Graph Pad Software Inc., La Jolla, CA, USA).

Cell therapy and viability assays of integrin ligand-MMAE/MMAF conjugates

Cell viability assays were performed in U-87 MG glioblastoma and H29 colon adenocarcinoma cells obtained from American Type Culture Collection (ATCC, Bethesda, MD, USA) were used. Cell viability was quantified by MTT (3-(4,5-dimethylthiazol-2-yl)-2,5-diphenyltetrazolium bromide) assay. Briefly, cells in EMEM supplemented with 10% FBS, 1% L-glutamine and 1% penicillin/streptomycin, were seeded in 96-well culture plates (5×10^4 cells/well) and incubated in a humidified, 37°C, 5% CO_2 atmosphere overnight to allow adherence. The following day cells were treated with serial dilutions of each compound starting at 500 nM for MMAE and 5000 nM for each one of the conjugates, or 0.1% DMSO as a control, and incubated as described for 72h. For the washout experiment, cells were washed once, and media replaced after 6h of incubation. At the end of treatment, 5 μL of MTT (5 mg/mL in dH_2O, Sigma #M5655) was added to each well. The cells were incubated for another 2 hours, 100 μL of lysis buffer (10% SDS, 10 mM HCl) were added, and then the cells were placed in the incubator overnight for the formazan crystal solubilization. Absorbance at 540 nm was measured and the growth inhibition ratio was calculated. Blank controls detecting cell-free media absorbance were performed in parallel. Three experimental replicates were used. The half-maximal inhibitory concentration values (IC_{50}) were obtained from viability curves using GraphPad Prism 6. The cell viability was expressed as percentage relative to the respective control conditions (0.1% of DMSO).

Synthesis of the DKP-*f3* scaffold

4-((4-methoxy-2,3,6-trimethyl-phenyl-sulfonyl)aminomethyl)benzaldehyde 16
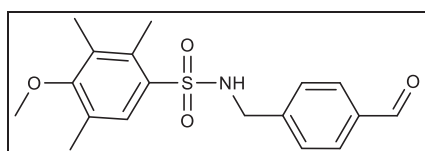
(4-aminomethyl-phenyl)methanol (2.6 g, 19 mmol, 1 eq.) was dissolved in 150 mL of dry THF under nitrogen atmosphere, DIPEA (6.5 mL, 38 mmol, 2 eq.) was added and the solution was cooled to 0 °C. A solution of 4-methoxy-2,3,6-trimethylbenzene-1-sulfonyl chloride (5.2 g, 21 mmol, 1.1 eq.) in 50 mL of dry THF was added dropwise and the

mixture was stirred at 0°C for 30 min, then at room temperature overnight. The white precipitate formed was separated by filtration over celite and the filtrate was concentrated under reduced pressure, re-dissolved in 5 mL of dry DCM (5 mL) and sonicated for few minutes until the formation of a white precipitate. The precipitate was collected by filtration, washed with cold DCM and cold Et2O and dried under vacuum to obtain the 4-((4-methoxy-2,3,6-trimethyl-phenyl-sulfonyl)aminomethyl) benzylic alcohol as a pale-yellow powder (4.98 g, 72% yield).

The protected alcohol (4.8 g, 13.7 mmol, 1 eq.) was dissolved in 150 mL of dry THF under nitrogen atmosphere, then activated MnO_2 (18 g, 0.2 mol, 15 eq.) was added, and the mixture was stirred overnight at room temperature. The suspension was filtered over celite and the filtrate was concentrated under reduced pressure to obtain **16** as a white solid. (4.76 g, 99% yield).

Rf=0.76 (Hexane/EtOAc 1:1); ^{1}H NMR (400 MHz, acetone-d_6) δ 9.96 (s, 1H), 7.75 (d, 2H, J = 8.2 Hz), 7.42 (d, 2H, J = 8.1 Hz), 6.92 (t, 1H, J = 6.3 Hz), 6.72 (s, 1H), 4.19 (d, 2H, J = 6.5 Hz), 3.83 (s, 3H), 2.62 (s, 3H), 2.53 (s, 3H).

(S)-methyl-3-hydroxy-2-((4-((4-methoxy-2,3,6-trimethyl-phenyl-sulfonamido)methyl) benzyl) amino)propanoate **17**
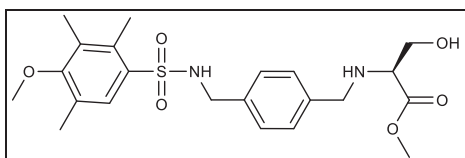
To a suspension of L-serine methyl ester hydrochloride (1.0 g, 6.5 mmol, 1.25 eq.) and aldehyde **16** (1.8 g, 5.1 mmol, 1 eq.) in 100 mL of dry THF, was added triethylamine (1.1 mL, 7.6 mmol, 1.5 eq.) under nitrogen atmosphere. Then, $NaBH(OAc)_3$ (3.1 g, 14.3 mmol, 2.8 eq.) was added in small portions and the mixture was stirred at room temperature for 4 h. A saturated solution of $NaHCO_3$ was added to the suspension till pH > 7 and it was extracted with EtOAc (3 × 60 mL). The combined organic phases were washed with brine (3 × 40 mL), dried over Na_2SO_4 and concentrated under reduced pressure. The crude product was purified by flash chromatography on silica gel (100 % EtOAc) affording the compound **17** as a white solid (1.5 g, 66%).

Rf=0.56 (EtOAc 100%); ^{1}H NMR (400 MHz, CD$_2$Cl$_2$) δ 7.21 (d, J = 7.9 Hz, 2H), 7.10 (d, J = 7.9 Hz, 2H), 6.62 (s, 1H), 4.90 (t, J = 6.1 Hz, 1H), 4.02 (d, J = 6.2 Hz, 2H), 3.85 (s, 3H), 3.82 (d, J = 12.8 Hz, 1H), 3.73 − 3.69 (m, 4H), 3.64 (d, J = 13.2 Hz, 1H), 3.59-3.55 (dd, J = 10.8, 6.2 Hz, 1H), 3.36 (m, 1H), 2.65 (s, 3H), 2.51 (s, 3H), 2.11 (s, 3H).

(R)-4-(allyloxy)-2-((tert-butoxycarbonyl)amino)-4-oxobutanoic acid **15**
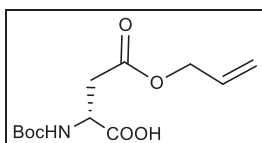
Acetyl chloride (10.7 mL, 15 mmol, 4 eq.) was added dropwise to 75 mL of ice-cold allyl alcohol. The solution was stirred at 0°C for 15 minutes and at room temperature for 1 hour, then D-aspartic acid (5 g, 37 mmol, 1 eq.) was added in single portion and the suspension was stirred overnight. The mixture was poured into 250 mL of ice-cold Et$_2$O and stirred for 1 hour, observing the formation of a white precipitate. The solid was collected by filtration and washed with cold Et$_2$O to give allyl aspartic acid hydrochloride (6.7 g, 82% yield).

D-allyl aspartic acid hydrochloride (6.7 g, 32 mmol, 1 eq.) was dissolved in dioxane/water 1:1 (80 mL) under nitrogen atmosphere, Boc$_2$O (8.3 g, 38 mmol, 1.2 eq.) was added and the mixture was cooled to 0 °C. Et$_3$N (13.3 mL, 95 mmol, 3 eq.) was added dropwise and the mixture was stirred at room temperature overnight. The solution was diluted in 150 mL of EtOAc, washed with KHSO$_4$ 1 M (3 × 50 mL) and brine (1 × 50 mL), the organic phase was dried over Na$_2$SO$_4$ and concentrated under reduced pressure affording the product **15** as a colorless oil (5.2 g, 79%).

(R)-4-allyl-1-((S)-3-methoxy-2-((4-((4-methoxy-2,3,6-trimethylphenylsulfonamido)
methyl)benzyl)amino)-3-oxopropyl) 2-((tert-butoxycarbonyl)amino)succinate **18**
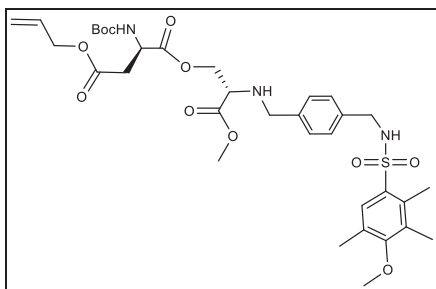
To a solution of **15** (1.2 g, 4.3 mmol, 1.3 eq.) in 15 mL of dry DMF at 0°C, HATU (1.6 g, 4.3 mmol, 1.3 eq.), HOAt (0.589 mg, 4.3 mmol, 1.3 eq.) and DIPEA (1.2 mL, 6.6 mmol, 2.0 eq.) were added, and the mixture was stirred for 30 minutes at 0 °C. A solution of **17** (1.5 g, 3.3 mmol) in DMF (10 mL) was added to the previous mixture and the reaction was stirred 1 h at 0°C and then at room temperature for 4 hours. The mixture was diluted with EtOAc (150 mL) and washed with KHSO$_4$ 1 M (3 × 30 mL), NaHCO$_3$ (2 × 30 mL) and brine (1 × 30 mL), the organic phase was dried over Na$_2$SO$_4$ and concentrated under reduced pressure to give the crude product as a pale-yellow oil (3 g) that was used in the next step without further purification. Rf=0.37 (Hexane/EtOAc 1:1)

OH-(3S-6R)-DKP-f3-COOAllyl **19**
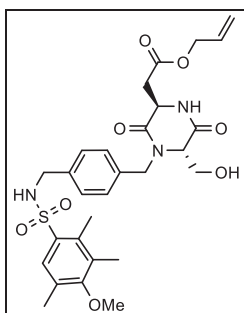
Boc-*iso*peptide **18** (2.3 g, 3.3 mmol, 1 eq.) was Boc-deprotected in a solution of CH$_2$Cl$_2$/TFA 2:1 (25 mL), stirring for 2 hours at room temperature. Volatiles were removed under reduced pressure by adding toluene (2 x 15 mL) and Et$_2$O (1 x 15 mL) to remove the excess of TFA. The corresponding trifluoroacetate salt was dried under vacuum and re-dissolved in *i*PrOH (54 mL). DIPEA (2.3 mL, 13.2 mmol, 4 eq.) was added, and the mixture was stirred at room temperature overnight. The solution was concentrated under reduced pressure and the residue was purified by flash chromatography on silica gel (Hexane/EtOAc, from 70% EtOAc to 100%) affording the product **19** as a white foam (1.7 g, 89%).

Rf=0.27 (EtOAc 100%); ^{1}H NMR (400 MHz, CDCl$_3$) δ 7.19 (m, 4H), 6.74 (s, 1H), 6.65 (s, 1H), 5.95 (m, 1H), 5.39-5.33 (m, 2H), 5.27, (dq, *J* = 10.4, 1.3 Hz, 1H), 5.15 (d, *J* = 15.2 Hz, 1H), 4.98 (t, *J* = 6.3 Hz, 1H), 4.64 (dt, *J* = 5.7, 1.3 Hz, 2H), 4.61 (dd, *J* = 8.7, 3.6 Hz, 1H), 4.13 (d, *J* = 15.5 Hz, 1H), 4.04 (d, *J* = 6.3, 2H), 3.99 (d, *J* = 11.8 Hz, 1H), 3.88 − 3.84 (m, 4H), 3.79 (t, *J* = 2.6 Hz, 1H), 3.23 (dd, *J* = 17.4, 3.7 Hz, 1H), 2.76 (dd, *J* = 17.6, 8.3 Hz, 1H), 2.67 (s, 3H), 2.56 (s, 3H), 2.16 (s, 3H).

N$_3$-(3S, 6R)-DKP-f3-COOAllyl **20**
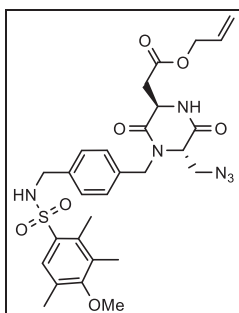
OH-(3S, 6R)-DKP-*f3*-COOAllyl **19** (1.68 g, 2.9 mmol, 1 eq.) was dissolved in 50 mL of a mixture of CH$_2$Cl$_2$/toluene 4:6 under nitrogen atmosphere. The mixture was cooled to -20°C and triphenylphosphine (1.0 g, 3.8 mmol, 1.3 eq.) was added. Once the dissolution was completed, hydrazoic acid (1 M in toluene, 19 mL, 19 mmol, 6.5 eq.) was added, followed by dropwise addition of DIAD (0.8 mL, 4.1 mmol, 1.4 eq.). The reaction was stirred at -20 °C for 5 hours, then the mixture was directly purified (without evaporating the solvent) by flash chromatography (EtOAc/Hexane from 1:1 to 70% EtOAc) affording the product **20** as a white foam (1.15 g, 66% yield).

Rf=0.6 (EtOAc/Hexane 8:2); ^{1}H NMR (400 MHz, CDCl$_3$) δ 7.18 (s, 4H), 6.76 (s, 1H), 6.59 (s, 1H), 5.91 (ddt, *J* = 16.4, 11.1, 5.8 Hz, 1H), 5.34 (d, *J* = 18.1, 1H), 5.27 (d, *J* = 10.4, 1H), 5.09 (d, *J* = 15.1 Hz, 1H), 4.64 (d, *J* = 5.8 Hz, 2H), 4.60 (dd, *J* = 9.1, 3.1 Hz, 1H), 4.19 (d, *J* = 15.1 Hz, 1H), 4.05 (s, 2H), 3.90 − 3.83 (m, 6H), 3.63 (dd, *J* = 12.4, 2.9 Hz, 1H), 3.28 (dd, *J* = 17.5, 3.3 Hz, 1H), 2.80 (dd, *J* = 17.5, 9.1 Hz, 1H), 2.68 (s, 3H), 2.57 (s, 3H), 2.14 (s, 3H).

Boc-(3S,6R)-DKP-f3-COOAllyl **21**
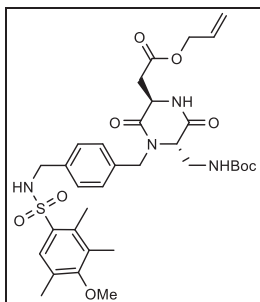
N$_3$-(3S, 6R)-DKP-*f3*-COOAllyl **20** (1.56 g, 2.6 mmol, 1 eq.) was dissolved in 64 mL of THF under nitrogen atmosphere and cooled down to -20 °C. Trimethylphosphine (1 M solution in THF, 6.5 mL, 6.5 mmol, 2.5 eq.) and Boc-ON (1.6 g, 6.5 mmol, 2.5 eq.) were sequentially added and the reaction was stirred at room temperature for 3h. The mixture was diluted in 300 mL of CH$_2$Cl$_2$ and the organic phase was washed with water (3×100 mL) and brine (1×100 mL), dried over Na$_2$SO$_4$ and concentrated under reduced pressure. The crude residue was purified by flash chromatography on silica gel (CH$_2$Cl$_2$/MeOH from 100% CH$_2$Cl$_2$ to 9:1) affording the product **21** as a white foam (1.55 g, 88% yield).

Rf=0.24 (CH$_2$Cl$_2$/MeOH 97:3); ^{1}H NMR (400 MHz, CDCl$_3$) δ 7.18 − 7.13 (m, 4H), 6.79 (s, 1H), 6.59 (s, 1H), 5.90 (ddt, J = 17.2, 10.6, 5.8 Hz, 1H), 5.42 (d, J = 15.2 Hz, 1H), 5.33 (d, J = 17.2 Hz, 1H), 5.26 (d, J = 10.3 Hz, 1H), 4.97 (bs, 1H), 4.63 (d, J = 5.5 Hz, 2H), 4.44 (dd, J = 9.0, 2.5 Hz, 1H), 4.03 (s, 3H), 3.86 (s, 3H), 3.74 − 3.68 (m, 2H), 3.50 (d, J = 15.3 Hz, 1H), 3.29 (d, J = 17.6 Hz, 1H), 2.76 (dd, J = 17.5, 9.2 Hz, 1H), 2.68 (s, 3H), 2.56 (s, 3H), 2.14 (s, 3H), 1.43 (s, 9H).

Synthesis of *cyclo*[DKP-*iso*DGR]-CH$_2$NH$_2$ integrin ligand

Mtr-Arg-(3S,6R)-DKP-f3-COOAllyl **22**
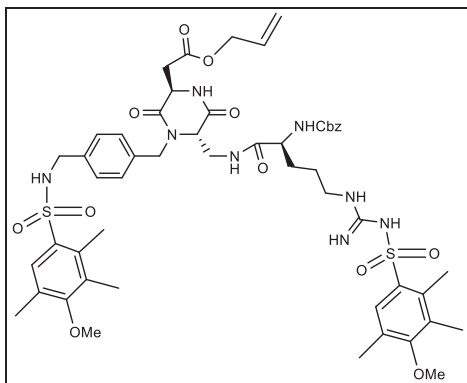
Cbz-Arg-Mtr-OH -CHA (cyclohexylamine salt) (0.595 g, 0.96 mmol, 1.2 eq.) was suspended in 40 mL of DCM. The organic phase was washed 3 times with KHSO$_4$, dried over Na$_2$SO$_4$ and concentrated under reduced pressure to give Cbz-Arg-Mtr-OH free as a white foam (quantitative). The foam was dissolved in 7 mL of DMF under nitrogen atmosphere and cooled to 0°C, then HATU (0.380 g, 0.96 mmol, 1.2 eq.), HOAt (0.130 g, 0.96 mmol, 1.2 eq.) and DIPEA (0.42 mL, 2.4 mmol, 3 eq.). The mixture was stirred at 0 °C for 30 minutes.

Boc-(3*S*,6*R*)-DKP-*f*3-COOAllyl **21** (0.523 g, 0,8 mmol, 1 eq.) was deprotected in a solution of 9 mL CH$_2$Cl$_2$/TFA 2:1 at room temperature. After 2 hours the solvent was evaporated, the excess of TFA was removed by adding toluene (2 × 5 mL) followed of evaporation. Diethyl ether (1 x 5) was also added and evaporated to afford the corresponding TFA salt, which was re-dissolved in DMF (9 mL) and DIPEA (0.13 mL, 0.8 mmol, 1 eq.) and incorporated to the reaction containing Cbz-Arg-Mtr-OH. The mixture was stirred for 1 hour at 0°C and the at room temperature overnight.

The mixture was then diluted in 150 mL of EtOAc. The organic phase was washed with KHSO$_4$ 1 M (3×45 mL), NaHCO$_3$ sat (3×45 mL) and brine (1×50 mL), then dried over Na$_2$SO$_4$ and concentrated under reduced pressure. The residue was purified by flash chromatography on silica gel (CH$_2$Cl$_2$/MeOH from 100% CH$_2$Cl$_2$ to 9:1) affording the product **22** as a white foam (0.730 g, 85% yield).

Rf=0.5 (CH$_2$Cl$_2$/MeOH 9:1); ^{1}H NMR (400 MHz, MeOD-d_4) δ 7.40 − 7.25 (m, 5H), 7.13 (dd, J = 34.5, 8.1 Hz, 4H), 6.67 (s, 1H), 6.64 (s, 1H), 5.95-5.85 (m, 1H), 5.35 − 5.28 (m, 2H), 5.20 (dd, J = 10.5, 1.3 Hz, 1H), 5.08 (q, J = 12.5 Hz, 2H), 4.64 − 4.50 (m, 3H), 4.09 (m, 1H), 4.05 − 3.98 (m, 3H), 3.90 − 3.83 (m, 4H), 3.81 (s, 3H), 3.77 − 3.74 (m, 1H), 3.59 (dd, J = 13.8, 2.4 Hz, 1H), 3.21 (bs, 1H), 3.15 − 3.11 (m, 1H), 3.07 (dd, J = 17.7, 4.6 Hz, 1H), 2.88 (dd, J = 17.6, 4.8 Hz, 1H), 2.66 (s, 3H), 2.60 (s, 6H), 2.48 (s, 3H), 2.11 (s, 3H), 2.07 (s, 3H), 1.79 − 1.67 (m, 1H), 1.62 − 1.44 (m, 3H); ^{13}C NMR (101 MHz, MeOD-d_4) δ 171.32, 168.73, 168.22, 160.68, 159.88, 158.44, 139.87, 139.52, 138.56, 137.89, 135.98, 134.77, 133.47, 130.99, 129.52, 129.35, 129.21, 129.07, 128.92, 126.06, 125.71, 118.56, 113.15, 112.79, 67.82, 66.50, 60.36, 56.16, 56.00, 51.94, 49.00, 47.70, 46.91, 40.11, 36.91, 30.16, 24.47, 24.35, 18.84, 18.20, 12.10.

Mtr-Arg-(3S,6R)-DKP-f3-COOH **23**
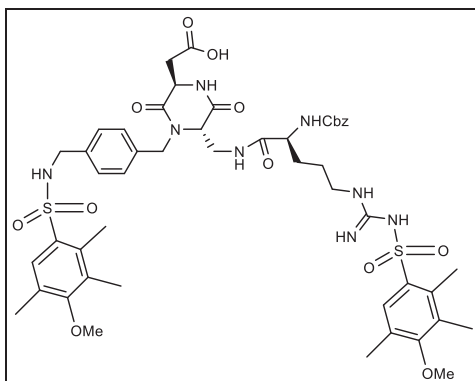
Mtr-Arg-(3S,6R)-DKP-*f3*-COOAllyl **22** (0.537 g, 0.5 mmol, 1 eq.) was dissolved in 20 mL of dry DCM under nitrogen atmosphere at 0 °C. [Pd(PPh$_3$)$_4$] (cat.) and *N*-methylaniline (0.23 mL, 2 mmol, 4 eq.) were added, the reaction mixture was stirred 5 min at 0 °C and then 2 hours at room temperature. The mixture was diluted in 70 mL of DCM and washed with KHSO$_4$ 1 M (3×20 mL). The organic phase was dried over Na$_2$SO$_4$, volatiles were removed under reduced pressure and the residue was purified by flash chromatography DCM/MeOH from 98/2 to 8/2 affording **23** as a pale-yellow foam (0.373 g, 72%).

Rf=0.2 (CH$_2$Cl$_2$/MeOH 95:5); ^{1}H NMR (400 MHz, MeOD-d_4) δ 7.36 − 7.20 (m, 5H), 7.13 − 7.08 (m, 4H), 6.66 (s, 1H), 6.61 s, 1H), 5.24 (d, *J* = 15.2 Hz, 1H), 5.06 (m, 2H), 4.51 − 4.45 (m, 3H), 4.10 (m, 1H), 4.04 − 3.98 (m, 3H), 3.91 − 3.82 (m, 4H), 3.81 − 3.73 (m, 4H), 3.53 (d, *J* = 13.5 Hz, 1H), 3.26 − 3.07 (m, 2H), 2.96 (d, *J* = 14.1.7 Hz, 1H), 2.66 (s, 3H), 2.60 (s, 6H), 2.47 (s, 3H), 2.09 (s, 3H), 2.07 (s, 3H), 1.77 − 1.67 (m, 1H), 1.62 − 1.40 (m, 3H); ^{13}C NMR (101 MHz, MeOD-d_4) δ 168.44, 160.37, 159.50, 157.95, 157.78, 139.68, 139.29, 138.22, 137.54, 135.83, 134.39, 130.18, 129.28, 129.19, 128.85, 128.67, 125.95, 125.59, 112.95, 112.58, 67.70, 56.08, 55.94, 54.16, 49.64, 49.43, 49.21, 49.00, 48.79, 48.57, 48.36, 46.63, 24.54, 24.39, 18.81, 18.20, 12.15.

(*S*)-*tert*-butyl 2-amino-4-((2-(benzyloxy)-2-oxo-ethyl)amino)-4-oxobutanoate **26**
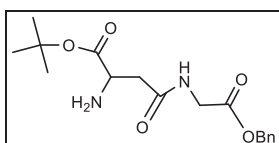
To a solution of Fmoc-L-Asp(OH)-OtBu (1.15 g, 2.80 mmol, 1.2 eq.) in DMF (15 mL), at 0 °C and under nitrogen atmosphere, HATU (1.06 g, 2.80 mmol, 1.2 eq.), HOAt (380 mg, 2.80 mmol, 1.2 eq.) and DIPEA (0.8 mL, 4.6 mmol, 2.0 eq.) were added, and the reaction

was stirred at 0 °C for 30 min. A solution of H$_2$N-Gly-OBn·HCl (465 mg, 2.3 mmol, 1 eq.) in 15 mL of DMF and DIPEA (1.2 mL, 6.9 mmol, 3 eq.) was added dropwise and the mixture was stirred at 0 °C for 1 h and at room temperature overnight. The mixture was diluted in500 mL of EtOAc and washed with KHSO$_4$ 1 M (3 × 100 mL), saturated aqueous NaHCO$_3$ (3 × 100 mL) and brine (1 × 100 mL). The organic phase was dried over Na$_2$SO$_4$, concentrated under reduced pressure, and the residue was purified by flash chromatography on silica gel (CH$_2$Cl$_2$/MeOH from CH$_2$Cl$_2$ 100% to 9:1, solid load) affording Fmoc-L.Asp-Gly-OBn as a white foam (0.985 g, 81%). The protected dipeptide (0.98 g, 1.8 mmol, 1 eq) in DMF (47 mL), at 0 °C under nitrogen atmosphere, piperidine (1.1.5 mL, 11.16 mmol, 5 eq) was added and the reaction mixture was stirred at 0 °C for 10 min and at room temperature for 3 h. The mixture was diluted with AcOEt (400 mL) and washed with H$_2$O (4×100 mL). The organic phase was dried over Na$_2$SO$_4$ and volatiles were removed under reduced pressure. The residue was purified by a Grace Reveleris system (column: Reveleris Silica 40 g; liquid load; flow rate: 33 mLmin-1; gradient: from DCM/MeOH 98/2 to 8/2 in 35 min) affording the desired product 41 as a white foam (600 mg, quant., 80% yield over 2 steps).

Rf=0.35 (CH$_2$Cl$_2$/MeOH 95:5); ^{1}H NMR (400 MHz, CDCl$_3$) δ 7.99 (bs, J = 5.2 Hz, 1H), 7.29 (m, 5H), 5.10 (s, 2H), 4.01 (m, J = 18.1, 5.2 Hz, 2H), 3.66 (m, J = 9.0, 3.2 Hz, 1H), 2.65 (dd, J = 15.4, 3.2 Hz, 1H), 2.44 (dd, J = 15.4, 9.0 Hz, 1H), 2.21 (bs, 2H), 1.40 (s, 9H).

Mtr-Arg-(3S,6R)-DKP-f3-COO-isoAsp-Gly-OBn **27**
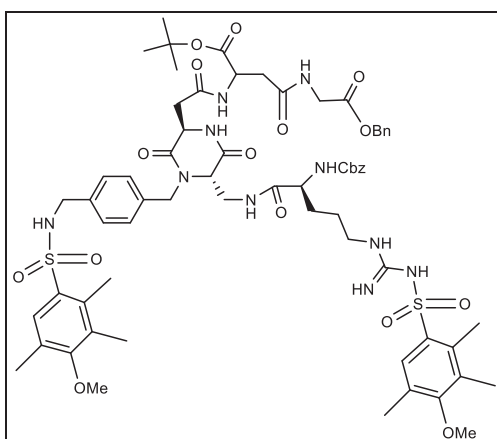
Mtr-Arg-(3S,6R)-DKP-*f3*-COOH **23** (0.509 g, 0.5 mmol, 1 eq.) was dissolved in 6 ml of DMF under nitrogen atmosphere and cooled to 0°C. HATU (0.228 g, 0.6 mmol, 1.2 eq.), HOAt (0.081 g, 0.6 mmol, 1.2 eq.) and DIPEA (0.3 mL, 1.5 mmol, 3 eq.) were added and

the reaction mixture was stirred at 0 °C for 30 min. The dipeptide isoAsp-Gly **26** (0.202 g, 0.6 mmol, 1.2 eq.), dissolved in 6 mL of DMF, was added and the mixture was stirred for 1 hour at 0 °C and then at room temperature overnight. The mixture was diluted in 100 mL of CH_2Cl_2 and washed with $KHSO_4$ 1 M (3×40 mL), $NaHCO_3$ (3×40 mL) and brine (1×25 mL). The organic phase was dried over Na_2SO_4, concentrated under reduced pressure and purified by flash chromatography DCM/MeOH from 100% DCM to 8/2 affording the product **27** as a pale-yellow foam (0.560 g, 83%).

Rf= 0.48 (CH_2Cl_2/MeOH 95:5); ^1H NMR (400 MHz, Acetone) δ 7.83 (m, 1H), 7.71 (m, 1H), 7.64 (d, J = 8.1 Hz, 1H), 7.51 (s, 1H), 7.38-7.29 (m, 10 H), 7.22-7.15 (dd, J = 18.4, 8.0 Hz, 4H), 6.76 (s, 1H), 6.72 (t, J = 6.3 Hz, 1H), 6.66 (s, 1H), 6.58 (bs, 1H), 6.53 (d, J = 8.0 Hz, 1H), 5.30 (d, J = 15.3 Hz, 1H), 5.14 (s, 2H), 5.11 − 5.02 (dd, J = 18.8, 12.8 Hz, 2H), 4.75-4.70 (m, 1H), 4.64 (s, 1H), 4.28-4.23 (m, 1H), 4.05 (dd, J = 16.6, 10.7 Hz, 5H), 3.95 (dd, J = 19.1, 5.7 Hz, 2H), 3.88 (s, 3H), 3.82 (s, 3H), 3.79 (m, 1H), 3.51-3.48 (d, J = 13.5 Hz, 1H), 3.30 (bs, 1H), 3.16-3.07 (m, 2H), 3.03-3.02 (m, 1H), 2.80-2.73 (m, 3H), 2.67 (s, 3H), 2.63 (s, 3H), 2.62 (s, 3H), 2.55 (s, 3H), 2.09 (m, 6H), 1.82 (m, 1H), 1.58 (m, 3H), 1.43 (s, 9H); ^{13}C NMR (101 MHz, Acetone) δ 174.10, 170.95, 170.89, 170.51, 167.33, 159.95, 158.90, 157.57, 139.44, 139.28, 139.16, 138.17, 138.09, 137.07, 136.96, 136.33, 129.34, 129.22, 129.02, 129.00, 128.76, 128.68, 128.65, 125.44, 124.83, 113.00, 112.47, 82.20, 67.20, 67.17, 66.92, 60.03, 56.08, 55.85, 55.70, 55.34, 52.34, 50.81, 47.27, 46.69, 41.78, 40.23, 39.75, 38.08, 30.42, 30.22, 30.03, 29.84, 29.65, 29.46, 29.26, 28.10, 27.92, 24.42, 24.31, 18.70, 18.15, 12.13, 12.11.

Mtr-Arg-(3S,6R)-DKP-f3-COO-isoAsp-Gly **28**
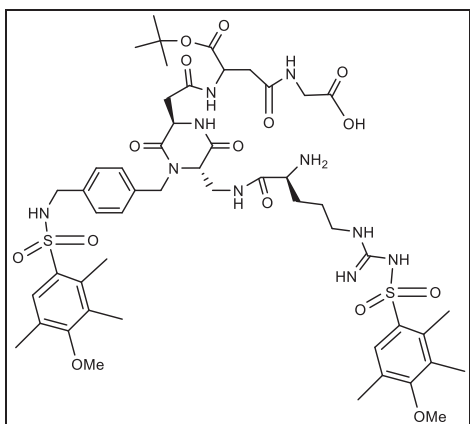
Mtr-Arg-(3S,6R)-DKP-*f3*-COO-isoAsp-Gly-OBn **27** (0.765 g, 0.56 mmol,1eq.) was dissolved in 50 mL of a solution THF/water 1:1. A catalytic amount of Pd/C 10 % was added, and the mixture was purged under stirring with 3 cycles of vacuum/H_2 atmosphere. The reaction was stirred overnight under H_2 atmosphere at room temperature. The mixture was filtered on a celite pad and rinsed with methanol. The filtrate was collected and concentrated under reduced pressure, affording the product **28** as a white solid (0.613 g, 90% yield).

Cyclo[(3S,6R)-DKP-f3-isoDGR]-Mtr **29**
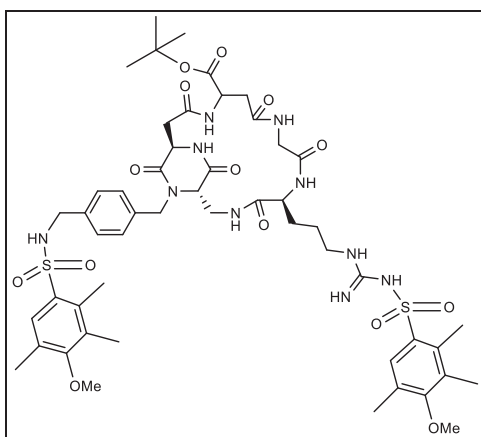
Mtr-Arg-(3S,6R)-DKP-*f3*-COO-*iso*Asp-Gly **28** (200 mg, 0.17 mmol, 1 eq.) was dissolved in 120 mL of DMF/CH_2Cl_2 1:1 (1.4 mM solution) under nitrogen atmosphere, the mixture was cooled to at 0 °C and HATU (266 mg, 0.7 mmol, 4 eq.), HOAt (95 mg, 0,7 mmol, 4 eq.) and DIPEA (0.2 mL, 1.0 mmol, 6 eq.) were added. the reaction was stirred at 0 °C for 1 hour and then at room temperature overnight. The mixture was concentrated under reduced pressure, the residue was diluted in 250 mL of EtOAc and washed with KHSO4 1 M (4 × 60 mL). The organic phase was dried over Na_2SO_4, concentrated under reduced pressure and the residue was purified by flash chromatography CH_2Cl_2/MeOH from 100% CH_2Cl_2 to 8/2 affording the product **29** as a pale-yellow solid (130 mg, 68%).

Rf=0.4 (CH_2Cl_2/MeOH 9:1); ^{1}H NMR (400 MHz, DMSO-d_6) δ 8.59 (d, J = 9.0 Hz, 1H), 8.29 (t, J = 6.2 Hz, 1H), 8.16 (d, J = 6.8 Hz, 1H), 7.87 (t, J = 6.0 Hz, 1H), 7.63 (dd, J = 6.8, 3.7 Hz, 1H), 7.50 (s, 1H), 7.16 − 7.08 (m, 4H), 6.75 (s, 1H), 6.68 (s, 1H), 6.43 (s, 1H), 5.19 (dd, J =

15.2, 7.1 Hz, 1H), 4.79 – 4.68 (m, 1H), 4.34 (d, *J* = 11.5 Hz, 1H), 4.16 (dd, *J* = 16.9, 7.3 Hz, 1H), 4.04 (dd, *J* = 13.2, 7.3 Hz, 1H), 3.92-3.87 (m, 3H), 3.82 (s, 3H), 3.79 (s, 3H), 3.63 – 3.57 (m, 2H), 3.49 (m, 3H), 3.03 (m, 3H), 2.60 – 2.51 (m, 11H), 2.44 (m, 3H), 2.12 (d, *J* = 12.9 Hz, 1H), 2.05 (m, 6H), 1.65-1.52 (m, 1H), 1.45-1.39 (m, 12H) ; ^{13}C NMR (101 MHz, DMSO) δ 172.75, 170.65, 169.75, 168.92, 168.66, 166.07, 165.86, 158.48, 157.47, 156.21, 147.59, 139.35, 138.21, 137.79, 137.65, 137.23, 135.63, 135.22, 134.47, 129.99, 127.89, 127.58, 124.03, 123.55, 119.11, 112.24, 111.73, 81.36, 55.66, 55.51, 48.62, 45.11, 41.27, 38.37, 37.72, 36.40, 27.58, 23.86, 23.66, 18.06, 17.68, 11.79, 11.77.

cyclo[(3S,6R)-DKP-f3-isoDGR] **14**
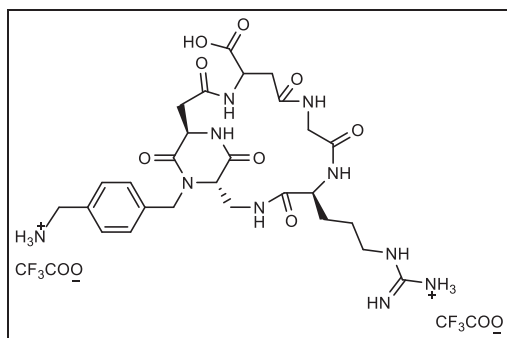
Cyclo[(3S,6R)-DKP-*f3-iso*DGR]-Mtr **29** (109 mg, 0.1 mmol) was treated with TFA (11 mL) in the presence of ion scavengers thioanisole (1.6 mL), ethanedithiol (0.8 mL) and phenol (175 mg). The mixture was cooled to 0 °C and flushed with N_2, then trimethylsilylbromide (2.2 mL) was added and the flask was opened. The mixture was allowed to reach room temperature and stirred for 2 h. Volatiles were removed under reduced pressure and the crude was dissolved in 30 mL of a mixture of water/diisopropyl ether 1:1. The aqueous phase was washed several times with diisopropyl ether and then concentrated under reduced pressure to give the crude compound, which was purified by semipreparative HPLC (gradient: 97% H_2O + 0.05% TFA/ 3% ACN + 0.05% TFA for 2 min, then to 80% H_2O + 0.05% TFA / 20% ACN + 0.05% TFA in 9 min, tR product = 7 min) to afford the product **14** (50 mg, 58% yield).

^{1}H NMR (500 MHz, D_2O) δ 7.49-7.39 (m, 4H), 5.30 (d, *J* = 15.7 Hz, 1H), 5.07 (dd, *J* = 11.5, 3.8 Hz, 1H), 4.48 (dd, *J* = 11.6, 2.2 Hz, 1H), 4.33 – 4.22 (m, 3H), 4.21 (s, 2H), 4.18 (d, *J* = 4.0 Hz, 1H), 4.05 (m, 1H), 3.84 (d, *J* = 17.2 Hz, 1H), 3.72 (d, *J* = 14.6 Hz, 1H), 3.24 (t, *J* =

6.7 Hz, 2H), 3.18 (dd, J = 13.7, 2.7 Hz, 1H), 3.11 (dd, J = 15.2, 3.9 Hz, 1H), 2.79 (dd, J = 15.1, 11.6 Hz, 1H), 2.46 − 2.38 (m, 1H), 1.93 − 1.82 (m, 1H), 1.77 − 1.63 (m, 2H); ^{13}C NMR (101 MHz, D$_2$O) δ 176.00, 174.05, 172.21, 172.10, 171.33, 167.85, 167.00, 156.78, 136.11, 132.34, 129.38, 128.31, 128.16, 59.63, 54.17, 51.16, 49.10, 47.43, 42.70, 41.50, 40.43, 39.26, 38.26, 37.38, 28.06, 24.49. MS (ESI) m/z calcd. for $[C_{27}H_{39}N_{10}O_8]^+$: 631.29 $[M + H]^+$; found: 631.33.

Synthesis of *cyclo*[DKP-*iso*DGR]-α-amanitin conjugates 31-33

14-Azido-3,6,9,12-tetraoxatetradecanoic acid -NHS ester **40**
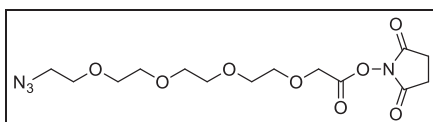
100 μL (0.05 mmol, 1 eq.) of a 0.5 M solution of 14-azido-3,6,9,12-tetraoxatetradecanoic acid (0.5 M in *tert*-butyl methyl ether) were diluted in 100 μL of dry DCM under argon and cooled to 0 °C. EDC.HCl (12,5 mg, 0.065 mmol, 1.3 eq.) and NHS (7.5 mg, 0.065 mmol, 1.3 eq.) were sequentially added to the solution and the reaction mixture was stirred overnight at room temperature. The mixture was diluted in 10 mL of DCM and the organic phase was washed with water (3 × 3 mL), dried over MgSO$_4$, filtrated and concentrated under reduced pressure to give the product as a transparent oil (18.2 mg, 97% yield). The crude product was used in next step without further modifications.

Rf= 0.35 (DCM/MeOH 95:5); ^{1}H NMR (400 MHz, CDCl$_3$): δ 4.52 (s, 2H), 3.81–3.79 (m, 2H), 3.68-3.65 (m, 12H), 3.39 (t, J = 5.0 Hz, 2H), 2.85 (s, 4H).

N$_3$-PEG-4-cyclo[DKP- isoDGR] **41**
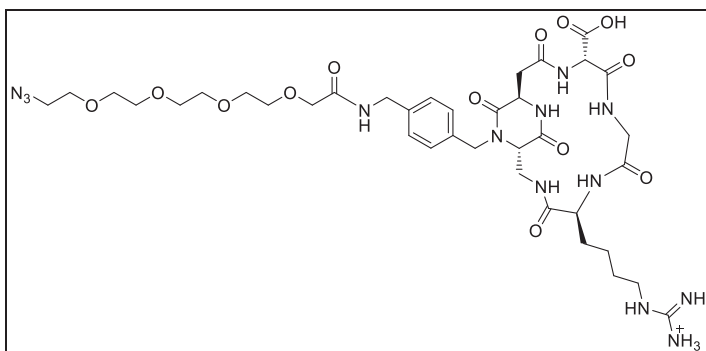
To a solution of compound **40** (9.2 mg, 24 µmol, 2 eq.) in 500 µL of ACN was added *cyclo*[DKP-*iso*DGR]-CH$_2$NH$_2$ **14** (10.5 mg, 12 µmol, 1 eq.) dissolved in 500 µL of PBS pH 7. The pH was adjusted to 7.4 with a solution of NaOH 0.2 M and the reaction was stirred overnight at room temperature. The mixture was filtered into a 3 mL vial, centrifuged and purified by preparative HPLC (gradient: from 95% (H$_2$O + 0.05 % CF$_3$COOH)/5% CH$_3$CN) to 60% (H$_2$O + 0.05 % CF$_3$COOH)/40% CH$_3$CN in 14.5 mins, t_R product = 8.3 min). The collected fraction was concentrated under reduced pressure and freeze-dried from 1:1 water/CH$_3$CN to afford the product as a white solid (5.5 mg, 46% yield).

^{1}H NMR (400 MHz, D$_2$O) δ 7.34 (dd, *J* = 15.6, 8.4 Hz, 4H), 5.27 (d, *J* = 15.5 Hz, 1H), 5.08 (dd, *J* = 11.5, 3.9 Hz, 1H), 4.50 − 4.43 (m, 3H), 4.32 − 4.17 (m, 3H), 4.15 (s, 2H), 4.12 (d, *J* = 4.1 Hz, 1H), 3.99 (dd, *J* = 14.8, 4.6 Hz, 1H), 3.83 (d, *J* = 17.2 Hz, 1H), 3.77 (m, 2H), 3.75 − 3.70 (m, 3H), 3.69 − 3.58 (m, 10H), 3.47 − 3.42 (m, 2H), 3.19 (m, 3H), 3.09 (dd, *J* = 15.1, 3.8 Hz, 1H), 2.78 (dd, *J* = 15.1, 11.6 Hz, 1H), 2.39 (dd, *J* = 13.4, 12.1 Hz, 1H), 1.89 − 1.75 (m, 1H), 1.72 − 1.59 (m, 2H); ^{13}C NMR (101 MHz, D$_2$O) δ 175.93, 173.99, 172.70, 172.19, 172.10, 171.27, 167.90, 166.91, 156.77, 137.64, 128.03, 127.79, 70.49, 70.12, 69.63, 69.56, 69.53, 69.19, 67.63, 59.39, 54.11, 51.12, 50.14, 49.09, 47.34, 42.15, 41.51, 40.42, 39.20, 38.14, 37.44, 28.04, 24.47. MS (ESI+): *m/z* calculated for [C$_{37}$H$_{56}$N$_{13}$O$_{13}$]$^+$= 890.41 [M + H]$^+$, found: 890.96.

*Glutarate NHS ester-aminohexyl-α-amanitin* <u>35</u>
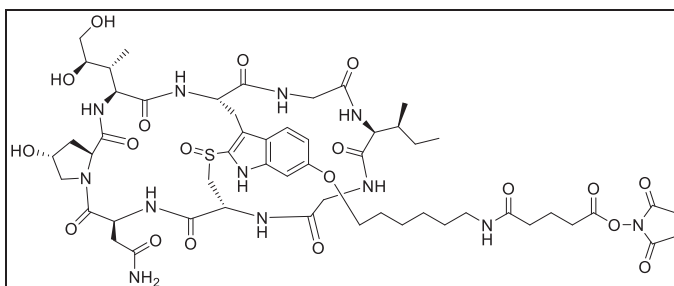
α-amanitin 6'-aminohexyl ether **34** (11 mg, 10.9 µmol, 1 eq.) was dissolved in 150 µL of dry DMF under nitrogen atmosphere. The solution was cooled to 0 °C, then commercial di-*N*-succinimidyl glutarate (4 mg, 12 µmol. 1.1 eq.) and DIPEA (2 µL, 12 µmol, 1.1 eq.) were added and the mixture was stirred at room temperature for 6 hours. The reaction was monitored by TLC (CHCl₃/MeOH/water 65/25/4, cinnamaldehyde staining). The crude was poured into 10 mL precooled MTBE placed in a 10 mL centrifugal tube (the reaction flask was rinsed with 3 × 50 µL of DMF and each rinsing solution was transferred to the MTBE tube). The tube was sealed, vortexed and placed in ice for 10 min. The tube was spun for 3 min at 4500 RPM in a pre-cooled centrifuge. The supernatant was transferred to a 50 mL flask. The pellet was suspended again into 10 mL of MTBE by vortexing and sonication. The tube was placed in ice for 10 mins and the centrifugation was repeated, then the pellet was dried *in vacuo*. The combined MTBE phases were concentrated under reduced pressure and checked for remaining product by TLC and HPLC. The dried pellet was used in next step without further purification (12 mg, 90% yield).

Cyclo[DKP-isoDGR]-uncleavable-α-amanitin **31**
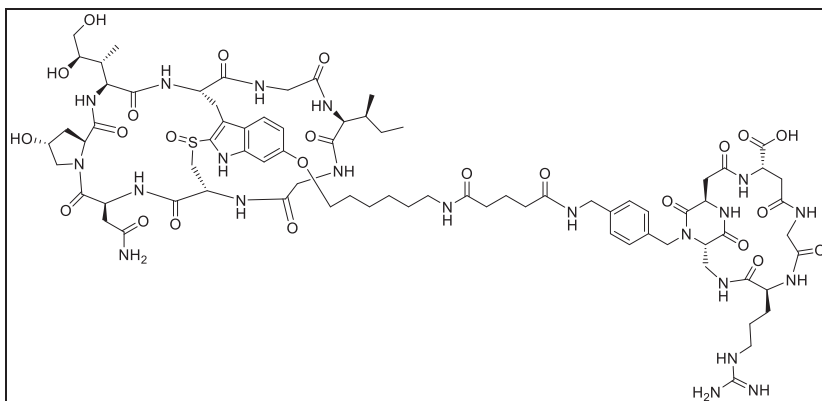
A solution of *cyclo*[DKP-*iso*DGR]-CH₂NH₂ **14** (5.0 mg, 5.8 µmol, 1 eq.) in 150 µL of PBS was added to a solution of **35** (12 mg, 10 µmol, 1.7 eq.) in 150 µL of DMF at 0 °C. The pH was adjusted to 7.3-7.6 by adding small aliquots of aqueous NaOH (0.2 M) during the first hours of reaction, until a stable value was observed, and then the reaction mixture was stirred overnight at room temperature.

The solution was directly filtered into a 3 mL vial and purified by preparative HPLC (gradient: from 95% (H₂O + 0.05 % CF₃COOH)/5% CH₃CN to 60% (H₂O + 0.05 %

CF$_3$COOH)/40% CH$_3$CN in 14.5 mins), t_R (product): 8.8 min. The purified product was freeze-dried to give the final product as a white solid (4.5 mg, 45% yield). MS (ESI+): *m/z* calcd. for [C$_{77}$H$_{110}$N$_{21}$O$_{24}$S]$^+$ = 1744.77 [M + H]$^+$, found: 1745,67.

Glutarate NHS ester-Val-Ala- α-amanitin **37**
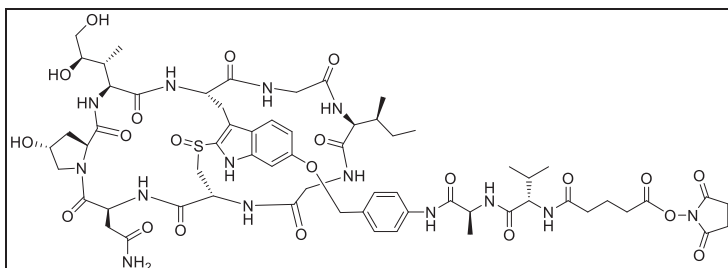
Val-Ala-PAB-α-amanitin **36** (10 mg, 8.3 µmol, 1 eq.) was dissolved in 150 µL of dry DMF under nitrogen atmosphere. The solution was cooled to 0 °C, then commercial di-*N*-succinimidyl glutarate (3.2 mg, 9.9 µmol, 1.2 eq.) and DIPEA (1.6 µL, 9.1 µmol, 1.1 eq.) were added and the mixture was stirred at room temperature for 6 hours. The reaction was monitored by TLC (CHCl$_3$/MeOH/water 65/25/4, cinnamaldehyde staining). The crude was poured into 10 mL pre-cooled MTBE placed in a 10 mL centrifugal tube (the reaction flask was rinsed with 3 × 50 µL of DMF and each rinsing solution was transferred to the MTBE tube). The tube was sealed, vortexed and placed in ice for 10 mins. The tube was spun for 3 mins at 4500 RPM in a precooled centrifuge. The supernatant was transferred to a 50 mL flask. The pellet was suspended again into 10 mL of MTBE by vortexing and sonication. The tube was placed on ice for 10 mins and the centrifugation was repeated. Then the pellet was dried *in vacuo*. The combined MTBE phases were concentrated under reduced pressure and checked for remaining product by TLC and HPLC. The dried pellet was used in next step without further purification (8.3 mg, 71% yield).

Cyclo[DKP-isoDGR]-Val-Ala-α-amanitin **32**
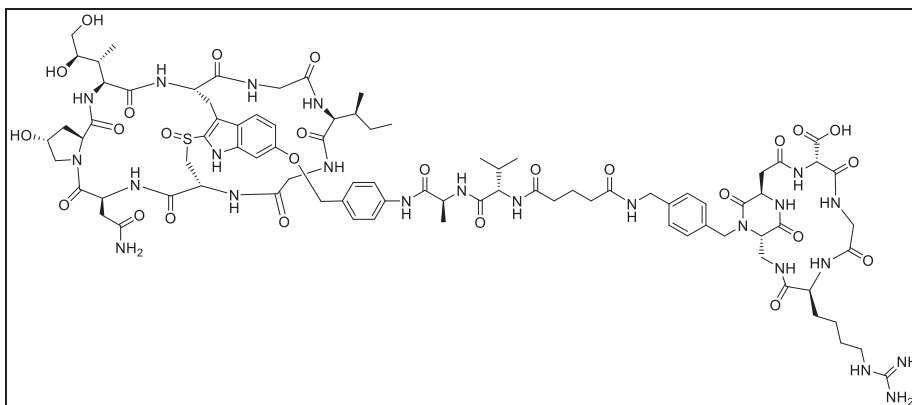
A solution of *cyclo*[DKP-*iso*DGR]-CH$_2$NH$_2$ **14** (3.4 mg, 3.9 µmol, 1 eq.) in 150 µL of PBS was added to a solution of **37** (8.3 mg, 5.9 µmol, 1.5 eq.) in 150 µL of DMF at 0 °C. The pH was adjusted to 7.3-7.6 by adding small aliquots of aqueous NaOH (0.2 M) during the first hours of reaction (until a stable value was observed), then the reaction mixture was stirred overnight at room temperature. The solution was directly filtered into a 3 mL vial and purified by preparative HPLC (gradient: from 95% (H$_2$O + 0.05 % CF$_3$COOH)/5% CH$_3$CN to 60% (H$_2$O + 0.05 % CF$_3$COOH)/40% CH$_3$CN in 14.5 mins), t_R (product): 9.2 min. The purified product was freeze-dried to give the final product as a white solid (4.8 mg, 62% yield). MS (ESI+): *m/z* calculated for [C$_{86}$H$_{118}$N$_{23}$O$_{26}$S]$^+$= 1921.05 [M + H]$^+$, found: 1921.75.

4-Pentynoic acid NHS ester **39**
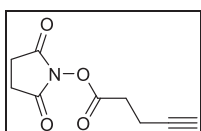
4-Pentynoic acid (10 mg, 0.100 mmol, 1 eq.) was dissolved in 2 mL of dry DCM under argon and cooled to 0 °C. EDC.HCl (23 mg, 0.120 mmol, 1.2 eq.) and NHS (14 mg, 0.120 mmol, 1.2 eq.) were sequentially added to the solution and the reaction mixture was stirred overnight at room temperature. The mixture was diluted in 20 mL of DCM and the organic phase was washed with water (3 × 7 mL), dried over MgSO$_4$, filtrated and concentrated under reduced pressure to give the product as a yellowish oil that was used in next step without further modifications.

4-Pentynoic acid-Val-Ala-α-amanitin **38**
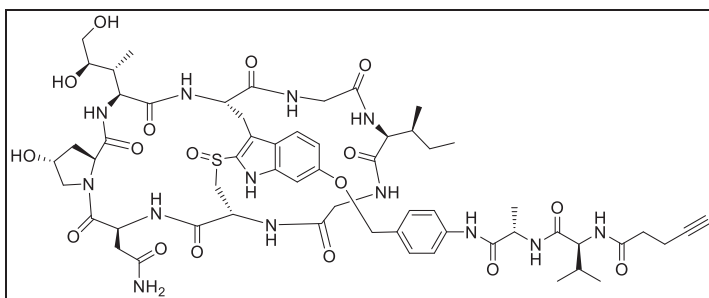
Under argon, DIPEA (1 µL, 6.3 µmol, 1.5 eq.) and compound **39** dissolved in DCM (200 µL) were added to a solution of compound **36** (5.0 mg, 4.2 µmol, 1 eq.) in 200 µL of DMF kept at 0 °C. The reaction mixture was stirred overnight at room temperature. Volatiles were evaporated under reduced pressure and the crude was dissolved in 500 µL of MeOH and then purified by preparative HPLC (gradient: from 95% (H_2O + 0.05% CF_3COOH) / 5% (CH_3CN) to 0% (H_2O + 0.05% CF_3COOH)/100% (CH_3CN) in 15 mins), t_R product = 7.97 min. The collected fraction was concentrated under reduced pressure and freeze-dried from water/ACN 1/1 to afford the product as a white solid (4.7 mg, 88% yield). MS (ESI+): *m/z* calculated for $[C_{59}H_{80}N_{13}O_{17}S]^+$ = 1273.54 [M + H]$^+$, found: 1274.55.

Cyclo[DKP-isoDGR]-PEG-4-Val-Ala- α-amanitin **33**
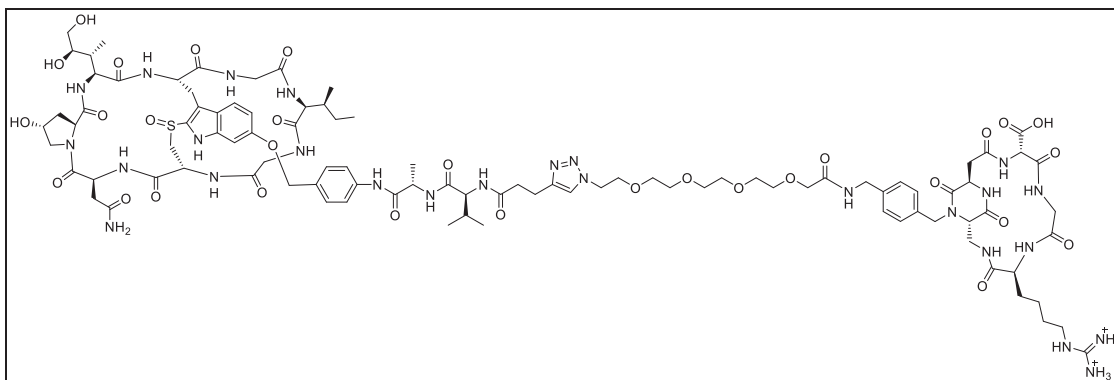
To a solution of **39** (2.9 mg, 2.3 µmol) in 1 mL of DMF at 0 °C, compound **41** (2.7 mg, 2,7 µmol) dissolved 1 mL of water, sodium ascorbate (0.2 mg, 0.88 µmol) and CuSO$_4$·5 H$_2$O (0.07 mg, 0.44 µmol) were sequentially added. The solution, which turned light yellow, was stirred overnight at room temperature until the color changed to light blue.

Volatiles were evaporated under reduced pressure and the crude was re-dissolved in 400 µL of MeOH, filtered and purified by preparative HPLC (gradient: from 95% (H_2O + 0.05% CF_3COOH) / 5% (CH_3CN + 0.05% CF_3COOH) to 0% (H_2O + 0.05% CF_3COOH)/100%

(CH$_3$CN + 0.05% CF$_3$COOH) in 15 min, t_R product = 7.2 min). The collected fraction was concentrated under reduced pressure and freeze-dried from 1:1 water/CH$_3$CN to afford the product as a white solid (3.33 mg, 62% yield). MS (ESI+): m/z calculated for [C$_{96}$H$_{136}$N$_{26}$O$_{30}$S$_2$]$^{2+}$= 1082.48 [M + 2H]$^{2+}$, found: 1082.92.

Synthesis of *cyclo*[DKP-*iso*DGR]-MMAE/MMAF conjugates 46-49

14-Hydroxy-3,6,9,12-tetraoxatetradecyl-4'-methylbenzolsulfonate **50-a**
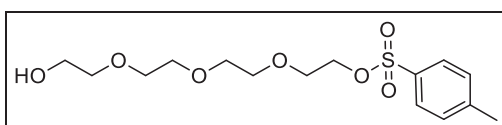
PEG-4 (8.7 mL, 50 mmol, 5 eq.) was dissolved in 2.5 mL of THF. Sodium hydroxide (640 mg, 16 mmol, 1.6 eq.) in 2.5 mL of H$_2$O was added and the mixture was cooled down to 0 °C. A solution of *p*-toluenesulfonyl chloride (1.9 g, 10 mmol, 1 eq.) in 7.5 mL of THF was slowly added and the mixture was stirred for 2 hours at 0 °C. The mixture was poured into water (40 mL), and the layers were separated. The aqueous phase was extracted with DCM (4 × 15 mL) and the combined organic phases were washed with water (3 × 15 mL), dried over Na$_2$SO$_4$ and concentrated under reduced pressure to yield the product as a colorless oil (3.33 g, 96% yield) which was used in the next step without further purification.

Rf= 0.7 (DCM/MeOH 95:5); ^{1}H NMR (400 MHz, CDCl$_3$): δ 7.79–7.77 (d, J = 8.0 Hz, 2H), 7.34-7.32 (d, J = 7.9, 1.0 Hz, 2H), 4.16–4.13 (m, 2H), 3.73–3.55 (m, 14H), 2.43 (s, 4H).

2-(2-(2-(2-Azidoethoxy) ethoxy) ethoxy) ethan-1-ol **50-b**
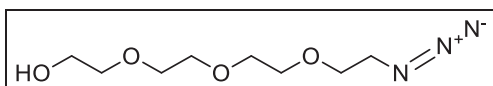
To a solution of **50-a** (3.18 g, 9.1mmol, 1 eq.) in 25 mL of ACN, was added sodium azide (0.975 g, 15 mmol, 1.6 eq.) and the mixture was heated to reflux with stirring for 8 h. The solution was allowed to cool down to room temperature then diluted in 25 mL of water and the aqueous phase was extracted with DCM (3 × 25 mL). The combined organic portions were dried over Na$_2$SO$_4$, filtered, and concentrated under reduced

pressure to give the product as a pale-yellow oil. The crude product was purified by flash chromatography on silica gel (CH$_2$Cl$_2$/MeOH from 100% CH$_2$Cl$_2$ to 95:5) affording the desired product **50-b** as a pale-yellow oil (1.46 g, 70% yield).

Rf= 0.6 (DCM/MeOH 95:5); ^{1}H NMR (400 MHz, CDCl$_3$): δ 3.73–3.60 (m, 14H), 3.40 (m, 2H), 2.18 (s, 1H).

14-Azido-3,6,9,12-tetraoxatetradecanoic acid **51**

A solution of **50-b** (100 mg, 0.4 mmol, 1 eq.) in 2.5 mL of dry THF was added dropwise to a stirred suspension of NaH (67 mg, 2.8 mmol, 7 eq.) in 2.5 mL of dry THF under N$_2$ at 0°C. The mixture was stirred for 1 h at room temperature. A solution of bromoacetic acid (111 mg, 0.8 mmol, 2 eq.) in 50 mL of dry THF was added dropwise and the mixture was stirred overnight at room temperature. Once the reaction was completed, the excess of NaH was quenched by carefully adding cold water and the solvent was evaporated under reduced pressure. The remaining aqueous solution was diluted in 5 mL of water, acidified with HCl 1 M solution until pH < 5 and extracted with DCM (3 x 10 mL). The organic extracts were combined, washed with water, dried over Na$_2$SO$_4$ and evaporated under reduced pressure, affording a dense oil. The crude residue was purified by flash chromatography on silica gel (CH$_2$Cl$_2$/MeOH from 100% CH$_2$Cl$_2$ to 8:2) to afford the product as a colorless oil (81 mg, 73%, yield).

Rf= 0.15 (DCM/MeOH 9:1); ^{1}H NMR (400 MHz, CDCl$_3$): δ 4.16 (s, 2H), 3.78–3.76 (m, 2H), 3.71-3.65 (m, 12H), 3.40 (t, *J* = 5.0 Hz, 2H).

Fmoc-Val-Ala-OH **52**

Fmoc-Val-OH (1.5 g, 4.4 mmol, 1 eq.) and NHS (0.560 g, 4.8 mmol, 1.1 eq.) were dissolved in 16 ml of dry THF under N$_2$. The solution was cooled to 0° C to add DCC (0.907 g, 4.4 mmol, 1 eq.) and then the mixture was stirred overnight at room

temperature. The suspension was filtered over cotton to separate the N,N'-dicyclohexylurea and the filtrate was concentrated under reduced pressure to afford the Fmoc-Val-O-succinimide as a white foam.

The activated amino acid was suspended in a mixture of THF/diethyl ether 1:1 and an aqueous solution of alanine (0.428 g, 4.8 mmol, 1.1 eq.) and $NaHCO_3$ (0.403 g, 4.8 mmol, 1.1 eq.) dissolved in 15 mL of water was added. The suspension was diluted with THF (5 mL approx..) till obtaining a clear solution that was stirred at room temperature for 4 days. The solvents were removed under reduced pressure, the residue was diluted in 30 mL of citric acid (15% w/v) and 50 mL ethyl acetate, and the mixture was stirred one hour at room temperature. The aqueous phase was extracted with EtOAc (3 x 30 mL), the combined organic phases were dried over Na_2SO_4 and concentrated under reduced pressure to give the crude product, that was purified by flash chromatography on silica gel (CH_2Cl_2/MeOH from 100% CH_2Cl_2 to 9:1 + 0.1% acetic acid) to afford the product as a white solid (1.3 g, 74%, yield).

Rf= 0.45 (DCM/MeOH 10:1); ^{1}H NMR (DMSO-d_6): δ 12.44 (bs., 1H), 8.20 (d, 1H, J = 6.7 Hz), 7.89 (d, 2H, J = 7.5 Hz), 7.75 (t, 2H, J = 6.5 Hz), 7.43-7.38 (m, 3H), 7.36-7.30 (m, 2H), 4.31-4.17 (m, 4H), 3.90 (t, 1H, J = 7.2 Hz), 2.0-1.95 (m, 1H), 1.27 (d, 3H, J = 7.3 Hz), 0.90 (d, 3H, J = 6.8 Hz), 0.87 (d, 3H, J = 6.8 Hz).

Fmoc-Val-Ala-PABOH **53**
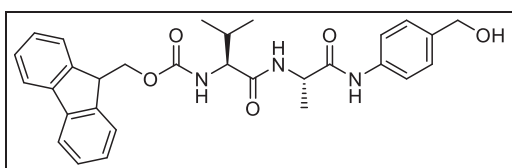
Fmoc-Val-Ala-OH **52** (180 mg, 0.43 mmol, 1 eq.), 4-aminobenzyl alcohol (65 mg, 0.52 mmol, 1.2 eq.) and EEDQ (165 mg, 0.64 mmol, 1.5 eq.) were suspended in 30 mL of dry DCM under nitrogen atmosphere. The mixture was treated with methanol (12 mL approx.) until a clear solution resulted and was stirred for 48 hours at room temperature. Once the reaction was completed, volatiles were evaporated at rotavapor, 10 mL of diethyl ether were added, and the mixture was sonicated for 15 mins. The precipitate formed after sonication was washed with cold diethyl ether and

filtered under reduce pressure. This operation was repeated twice, obtaining the Fmoc-Val-Ala-PABOH **53** as pale-yellow solid (129 mg, 58%).

^{1}H NMR (DMSO-d_6): δ 9.91 (bs., 1H), 8.16 (d, 1H, J = 6.8 Hz), 7.90 (d, 2H, J = 7.2 Hz), 7.74 (m, 2H), 7.54 (d, 2H, J = 8.1 Hz), 7.47-7.40 (m, 3H), 7.32 (m, 2H), 7.24 (d, 2H, J = 8.0 Hz), 5.08 (s, 1H), 4.43-4.40 (s, 3H), 4.30-4.22 (m, 3H) 3.91 (t, 1H, J = 7.6 Hz), 2.0-1.98 (m, 1H), 1.31 (d, 3H, J = 6.5 Hz), 0.90 (m, 6H).

Fmoc-Val-Ala-PAB-PNP **54**
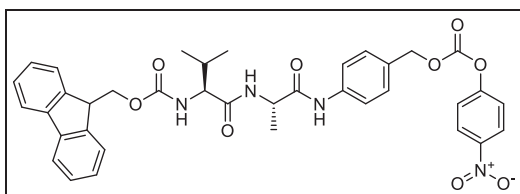
Fmoc-Val-Ala-PABOH **53** (166 mg, 0.32 mmol, 1eq.) was dissolved in 5 mL of dry THF under N_2, pyridine (64 μL, 0.8 mmol, 2.5 eq.) was added and the solution was cooled down to 0°C. 4-nitrophenyl chloroformate (97 mg, 0.48 mmol, 1.5 eq.) was added to the reaction and it was stirred at room temperature for 4 hours. The mixture was diluted in 35 mL of EtOAc and washed with $KHSO_4$ 1M (2 x 7 mL) and brine (2 x 7 mL), then the organic phase was dried over Na_2SO_4 and concentrated under reduced pressure. The crude residue was purified by flash chromatography on silica gel (Hexane/EtOAc from 5:5 to 20% hexane/80% EtOAc) affording the product as a white solid (135 mg, 62%, yield).

^{1}H NMR (DMSO-d_6): δ 10.07 (s, 1H), 8.32-8.30 (d, J = 9.0 Hz, 2H), 8.20-8.18 (d, J = 6.8 Hz, 1H), 7.90-7.88 (d, J = 7.5 Hz, 2H), 7.76-7.72 (t, J = 6.8 Hz, 2H), 7.65-7.62 (d, J = 8.3 Hz, 2H), 7.58-7.56 (d, J = 9.0 Hz, 2H), 7.42-7.40 (m, 5H), 7.34-7.30 (t, J = 7.2 Hz, 2H), 5.24 (s, 2H), 4.43 (m, 1H), 4.30-4.22 (m, 3H), 3.92 (t, 1H, J = 7.6 Hz), 2.0-1.97 (m, 1H), 1.32 (d, J = 7.0 Hz, 3H), 0.90-0.86 (m, 6H).

Val-Ala-PABC-MMAE **55**
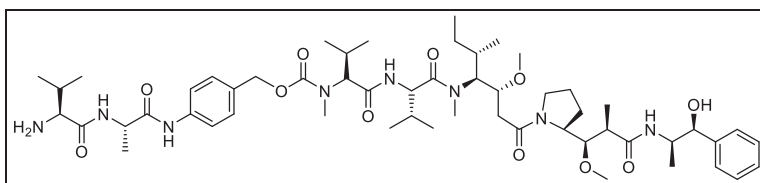
Monomethyl auristatin E (10 mg, 14 μmol, 1 eq.) was dissolved in dry DMF (300 μL) under nitrogen atmosphere. Fmoc-Val-Ala-PAB-PNP **54** (10 mg, 14 μmol, 1 eq.), HOAt (1 mg, 7 μmol, 0.5 eq.) and DIPEA (12 μL, 70 μmol, 5.0 eq.) were added subsequently and the mixture was stirred at room temperature overnight. Piperidine (8 μL, 70 μmol, 5 eq.) was added to the reaction and this was stirred for 2 additional hours at room temperature. The mixture was then diluted with 5mL of EtOAc, the organic phase was washed with NaHCO$_3$ $_{sat}$ (3 x 1 mL), dried and concentrated under reduced pressure. The crude product was purified by semipreparative HPLC (gradient: from 95% (H$_2$O + 0.1% CF$_3$COOH) / 5% (CH$_3$CN + 0.1% CF$_3$COOH) to 20% (H$_2$O + 0.1% CF$_3$COOH) / 80% (CH$_3$CN + 0.1% CF$_3$COOH) in 17 min, t_R product = 11 min). The collected fractions were concentrated under reduced pressure and freeze-dried from 1:1 water/CH$_3$CN to afford the product as a white solid (9.3 mg, 64% yield). MS (ESI+): *m/z* calculated for [C$_{55}$H$_{89}$N$_8$O$_{11}$]$^+$= 1038.66 [M + H]$^+$, found: 1038.65.

Val-Ala-PABC-MMAF **56**
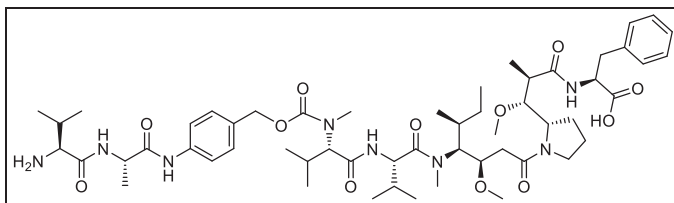
Monomethyl auristatin F (10 mg, 13.6 μmol, 1 eq.) was dissolved in dry DMF (100 μL) under nitrogen atmosphere. Fmoc-Val-Ala-PAB-PNP **54** (11 mg, 16.3 μmol, 1.2 eq.), HOAt (2 mg, 7 μmol, 0.5 eq.) and DIPEA (12 μL, 68 μmol, 5.0 eq.) were added subsequently and the mixture was stirred at room temperature overnight. Piperidine (7 μL, 68 μmol, 5 eq.) was added to the reaction and the mixture was stirred for 2 hours at room temperature. The solvent was removed reduced pressure and the crude product was purified by semipreparative HPLC (gradient: from 95% (H$_2$O + 0.1% CF$_3$COOH) / 5% (CH$_3$CN + 0.1% CF$_3$COOH) to 20% (H$_2$O + 0.1% CF$_3$COOH) / 80% (CH$_3$CN + 0.1% CF$_3$COOH) in 17 min, t_R product = 12 min). The collected fractions were concentrated under reduced pressure and freeze-dried from 1:1 water/CH$_3$CN to afford the product as a white solid (8.8 mg, 62% yield). MS (ESI+): *m/z* calculated for [C$_{55}$H$_{87}$N$_8$O$_{12}$]$^+$= 1052.65 [M + H]$^+$, found: 1052.38.

4-pentynoic acid-Val-Ala-PABC-MMAE **57**
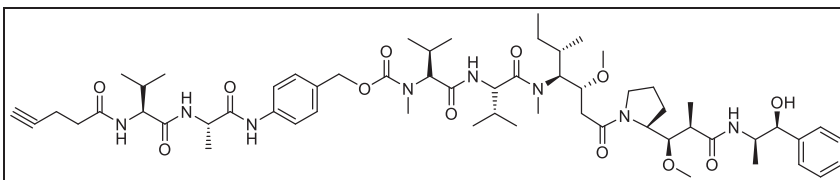
Val-Ala-PABC-MMAE **55** (9.3 mg, 9 µmol, 1 eq.) was dissolved in 100 µL of dry DMF under nitrogen atmosphere. 4-pentynoic acid-NHS ester **39** (4 mg, 18 µmol, 2 eq.) in 100 µL of dry DMF, and DIPEA (3 µL, 18 µmol, 2 eq.) were added and the mixture was stirred overnight at room temperature. The solvent was removed under reduced pressure and the crude residue was purified by semipreparative HPLC (gradient: from 95% (H_2O + 0.1% CF_3COOH) / 5% (CH_3CN + 0.1% CF_3COOH) to 20% (H_2O + 0.1% CF_3COOH) / 80% (CH_3CN + 0.1% CF_3COOH) in 17 min, t_R product = 14 min). The collected fractions were concentrated under reduced pressure and freeze-dried from 1:1 water/CH_3CN to afford the product as a white solid (7.5 mg, 75% yield). MS (ESI+): m/z calculated for $[C_{60}H_{93}N_8O_{12}]^+$= 1117.68 [M + H]$^+$, found: 1117.70.

4-pentynoic acid-Val-Ala-PABC-MMAF **58**
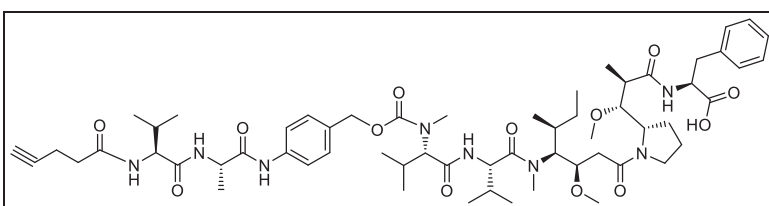
Val-Ala-PABC-MMAF **56** (8.8 mg, 8 µmol, 1 eq.) was dissolved in 100 µL of dry DMF under nitrogen atmosphere. 4-pentynoic acid-NHS ester **39** (3 mg, 16 µmol, 2 eq.) in 100 µL of dry DMF, and DIPEA (3 µL, 16 µmol, 2 eq.) were added and the mixture was stirred overnight at room temperature. The solvent was removed under reduced pressure and the crude residue was purified by semipreparative HPLC (gradient: from 95% (H_2O + 0.1% CF_3COOH) / 5% (CH_3CN + 0.1% CF_3COOH) to 20% (H_2O + 0.1% CF_3COOH) / 80% (CH_3CN + 0.1% CF_3COOH) in 17 min, t_R product = 14 min). The collected fractions were concentrated under reduced pressure and freeze-dried from

1:1 water/CH$_3$CN to afford the product as a white solid (5.6 mg, 62% yield). MS (ESI-): *m/z* calculated for [C$_{60}$H$_{89}$N$_8$O$_{13}$]$^-$= 1130.66 [M - H]$^-$, found: 1130.37.

Cyclo[DKP-isoDGR]-PEG-4-Val-Ala-PABC-MMAE **46**
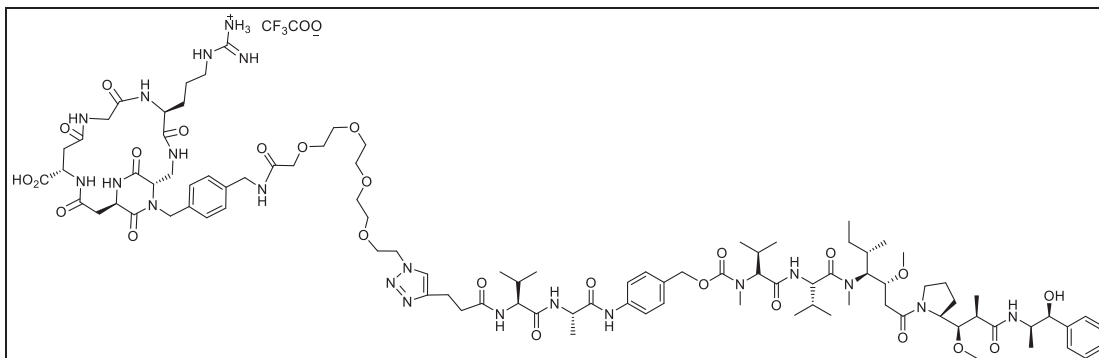
4-pentynoic acid-Val-Ala-PABC-MMAE **57** (3 mg, 2.7 µmol, 1 eq.) was dissolved in 500 µL of dry DMF and added to a solution of cyclo[DKP-*iso*DGR]-PEG-4 **41** (4 mg, 4 µmol, 1.5 eq.) in 500 µL of degassed water, under nitrogen atmosphere. Sodium ascorbate (0.3 mg, 1.4 µmol, 0.5 eq.) and CuSO$_4$.5H$_2$O (0.2 mg, 0.8 µmol, 0.3 eq.) were added to the solution and the mix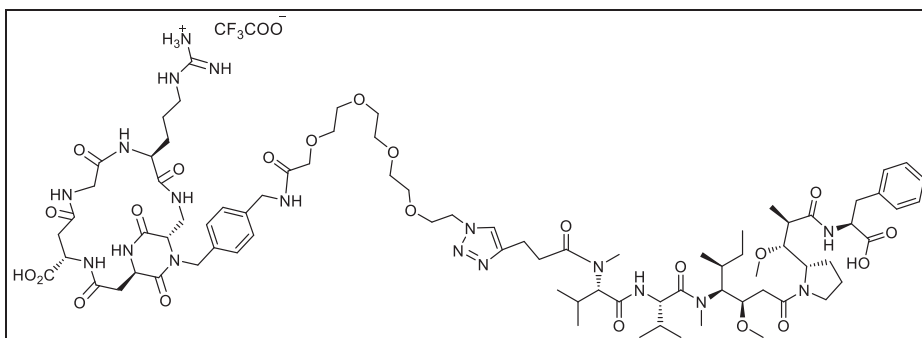ture was stirred overnight at room temperature. Volatiles were removed under reduced pressure and the residue was purified by semipreparative HPLC (gradient: from 95% (H$_2$O + 0.1% CF$_3$COOH) / 5% (CH$_3$CN + 0.1% CF$_3$COOH) to 20% (H$_2$O + 0.1% CF$_3$COOH) / 80% (CH$_3$CN + 0.1% CF$_3$COOH) in 17 min, *t*$_R$ product = 11.3 min). The collected fractions were concentrated under reduced pressure and freeze-dried from 1:1 water/CH$_3$CN to afford the product as a white solid (4.2 mg, 66% yield). MS (ESI+): *m/z* calculated for [C$_{97}$H$_{149}$N$_{21}$O$_{25}$]$^{2+}$ = 1005.17 [M + 2H]$^{2+}$, found: 1005.08.

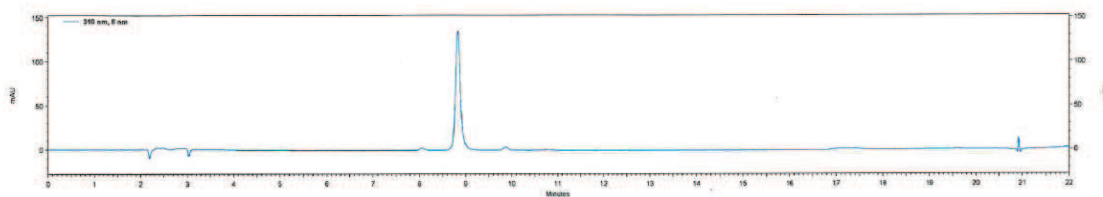*Cyclo[DKP-isoDGR]-PEG-4-Val-Ala-PABC-MMAF* **47**
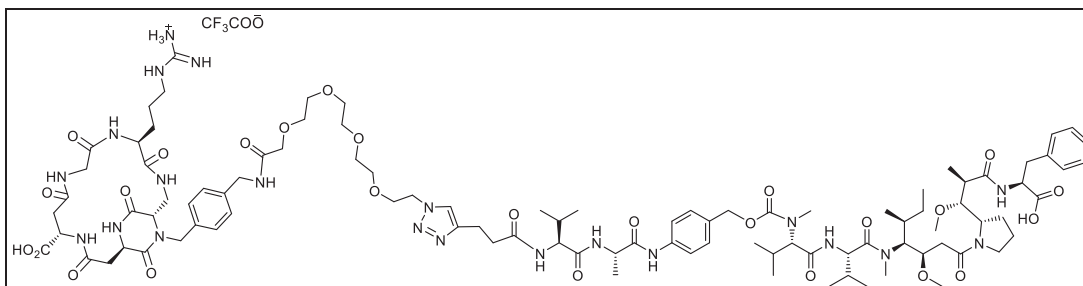
4-pentynoic acid-Val-Ala-PABC-MMAF **58** (3.5 mg, 3 µmol, 1 eq.) was dissolved in 500 µL of dry DMF and added to a solution of cyclo[DKP-*iso*DGR]-PEG-4 **41** (4.5 mg, 4.5 µmol, 1.5 eq.) in 500 µL of degassed water, under nitrogen atmosphere. Sodium ascorbate

(0.3 mg, 1.5 μmol, 0.5 eq.) and $CuSO_4.5H_2O$ (0.3 mg, 1 μmol, 0.3 eq.) were added to the solution and the mixture was stirred overnight at room temperature. Volatiles were removed under reduced pressure and the residue was purified by semipreparative HPLC (gradient: from 95% (H_2O + 0.1% CF_3COOH) / 5% (CH_3CN + 0.1% CF_3COOH) to 20% (H_2O + 0.1% CF_3COOH) / 80% (CH_3CN + 0.1% CF_3COOH) in 17 min, t_R product = 11.5 min). The collected fractions were concentrated under reduced pressure and freeze-dried from 1:1 water/CH_3CN to afford the product as a white solid (2.8 mg, 45% yield). MS (ESI+): m/z calculated for $[C_{97}H_{147}N_{21}O_{26}]^{2+}$ = 1011.54 $[M + 2H]^{2+}$, found: 1011.96

4-pentynoic acid-MMAE **59**

MMAE (7 mg, 9.7 μmol, 1 eq.) was dissolved in 100 μL of dry DMF. 4-pentynoic acid-NHS ester **39** (3 mg, 15 μmol, 1.5 eq.) in 100 μL of dry DMF, and DIPEA (3 μL, 15 μmol, 1.5 eq.) were added and the mixture was stirred overnight at room temperature. The solvent was removed under reduced pressure and the residue was purified by semipreparative HPLC (gradient: from 95% (H_2O + 0.1% CF_3COOH) / 5% (CH_3CN + 0.1% CF_3COOH) to 20% (H_2O + 0.1% CF_3COOH) / 80% (CH_3CN + 0.1% CF_3COOH) in 17 min, t_R product = 14 min). The collected fractions were concentrated under reduced pressure and freeze-dried from 1:1 water/CH_3CN to afford the product as a white solid (5.5 mg, 73% yield). MS (ESI+): m/z calculated for $[C_{44}H_{72}N_5O_8]^+$= 799.54 $[M + H]^+$, found: 799.23.

4-pentynoic acid-MMAF **60**
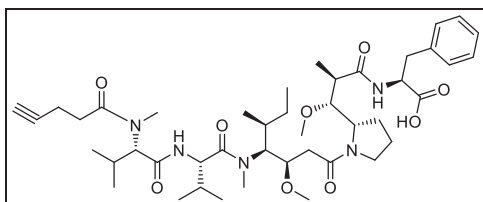
MMAF (6 mg, 8 μmol, 1 eq.) was dissolved in 100 μL of dry DMF. 4-pentynoic acid-NHS ester **39** (2.5 mg, 12 μmol, 1.5 eq.) in 100 μL of dry DMF, and DIPEA (3 μL, 12 μmol, 1.5 eq.) were added and the mixture was stirred overnight at room temperature. The

solvent was removed under reduced pressure and the residue was purified by semipreparative HPLC (gradient: from 95% (H_2O + 0.1% CF_3COOH) / 5% (CH_3CN + 0.1% CF_3COOH) to 20% (H_2O + 0.1% CF_3COOH) / 80% (CH_3CN + 0.1% CF_3COOH) in 17 min, t_R product = 13.8 min). The collected fractions were concentrated under reduced pressure and freeze-dried from 1:1 water/CH_3CN to afford the product as a white solid (5.5 mg, 73% yield). MS (ESI+): m/z calculated for $[C_{44}H_{70}N_5O_9]^+$= 813.52 $[M + H]^+$, found: 813.11.

Cyclo[DKP-isoDGR]-PEG-4-MMAE **48**
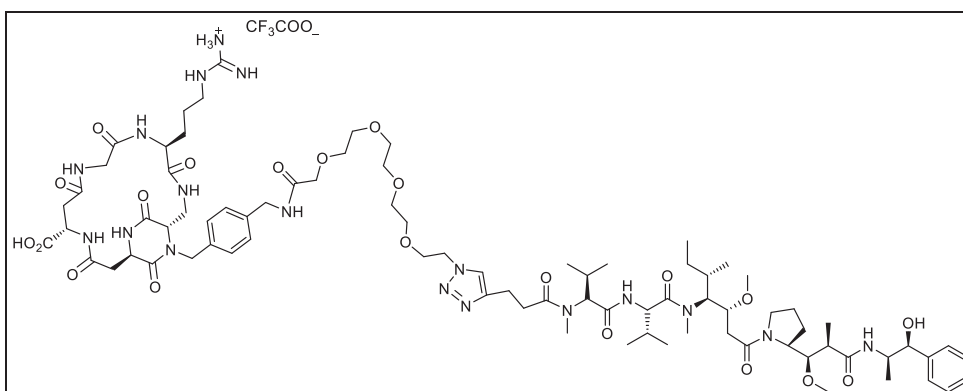
4-pentynoic acid-MMAE **59** (3 mg, 3.8 µmol, 1 eq.) was dissolved in 500 µL of dry DMF and added to a solution of cyclo[DKP-*iso*DGR]-PEG-4 **41** (6 mg, 6 µmol, 1.5 eq.) in 500 µL of degassed water, under nitrogen atmosphere. Sodium ascorbate (0.4 mg, 2 µmol, 0.5 eq.) and $CuSO_4.5H_2O$ (0.3 mg, 1.2 µmol, 0.3 eq.) were added to the solution and the mixture was stirred overnight at room temperature. Volatiles were removed under reduced pressure and the residue was purified by semipreparative HPLC (gradient: from 95% (H_2O + 0.1% CF_3COOH) / 5% (CH_3CN + 0.1% CF_3COOH) to 20% (H_2O + 0.1% CF_3COOH) / 80% (CH_3CN + 0.1% CF_3COOH) in 17 min, t_R product = 9.7 min). The collected fractions were concentrated under reduced pressure and freeze-dried from 1:1 water/CH_3CN to afford the product as a white solid (4.2 mg, 66% yield). MS (ESI+): m/z calculated for $[C_{81}H_{128}N_{18}O_{21}]^{2+}$ = 845.48 $[M + 2H]^{2+}$, found: 845.31.

Cyclo[DKP-isoDGR]-PEG-4-MMAF **49**

4-pentynoic acid-MMAF **60** (4.5 mg, 5.5 µmol, 1 eq.) was dissolved in 500 µL of dry DMF and added to a solution of cyclo[DKP-*iso*DGR]-PEG-4 **41** (8 mg, 8 µmol, 1.5 eq.) in 500 µL of degassed water, under nitrogen atmosphere. Sodium ascorbate (0.6 mg, 2.8 µmol, 0.5 eq.) and $CuSO_4.5H_2O$ (0.4 mg, 1.2 µmol, 0.3 eq.) were added to the solution and the mixture was stirred overnight at room temperature. Volatiles were removed under reduced pressure and the residue was purified by semipreparative HPLC (gradient: from 95% (H_2O + 0.1% CF_3COOH) / 5% (CH_3CN + 0.1% CF_3COOH) to 20% (H_2O + 0.1% CF_3COOH) / 80% (CH_3CN + 0.1% CF_3COOH) in 17 min, t_R product = 10.2 min). The collected fractions were concentrated under reduced pressure and freeze-dried from 1:1 water/CH_3CN to afford the product as a white solid (4.2 mg, 66% yield). MS (ESI+): *m/z* calculated for $[C_{81}H_{126}N_{18}O_{22}]^{2+}$ = 852.47 $[M + 2H]^{2+}$, found: 852.33.

HPLC traces of the final compounds

Cyclo[DKP-isoDGR]-uncleavable-α-amanitin **31**

Phenomenex Luna C-18(2) column 10 µm, 250 × 21.2 mm, with precolumn at 30 mL/min flow rate; gradient: 95% (H_2O + 0.05 % CF_3COOH)/5% CH_3CN to 60% (H_2O + 0.05 % CF_3COOH)/40% CH_3CN in 14.5 mins, t_R product: 8.8 min

Purity: 96.2%

Cyclo[DKP-isoDGR]-Val-Ala-α-amanitin **32**

Phenomenex Luna C-18(2) column 10 μm, 250 × 21.2 mm, with precolumn at 30 mL/min flow rate; gradient: 95% (H_2O + 0.05 % CF_3COOH)/5% CH_3CN to 60% (H_2O + 0.05 % CF_3COOH)/40% CH_3CN in 14.5 mins, t_R product: 9.2 min

Purity: 100%.
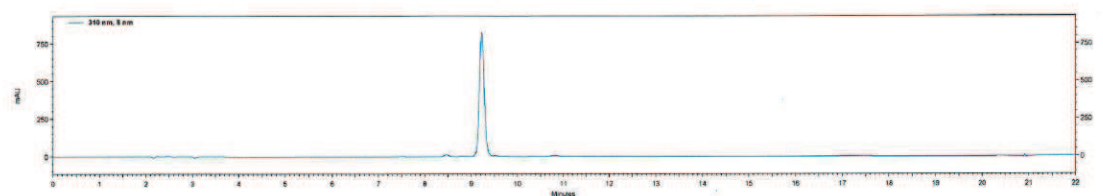
Cyclo[DKP-isoDGR]-PEG-4-Val-Ala- α-amanitin **33**

Phenomenex Luna C-18(2) column 10 μm, 250 × 21.2 mm, with precolumn at 30 mL/min flow rate; gradient: 95% (H_2O + 0.05 % CF_3COOH)/5% CH_3CN to 100% CH_3CN in 15 mins, t_R product: 7.2 min

Purity: 89.9%
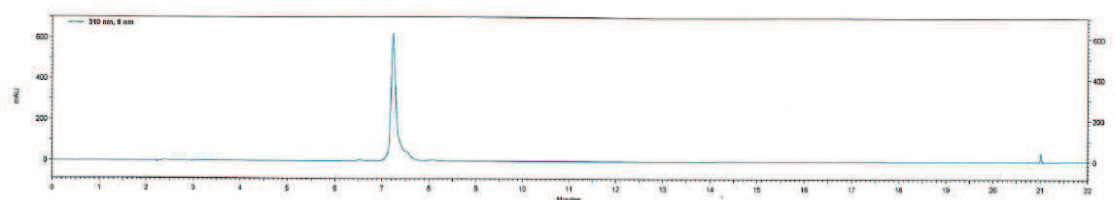
Cyclo[DKP-isoDGR]-PEG-4-Val-Ala-PABC-MMAE **46**

Waters Atlantis 21 mm × 10 cm column; flow: 15 mL/min, gradient: 95% (H_2O + 0.1% CF_3COOH) / 5% (CH_3CN + 0.1% CF_3COOH) to 20% (H_2O + 0.1% CF_3COOH) / 80% (CH_3CN + 0.1% CF_3COOH) in 17 min, t_R product: 11.3 min

Purity: 99.3%
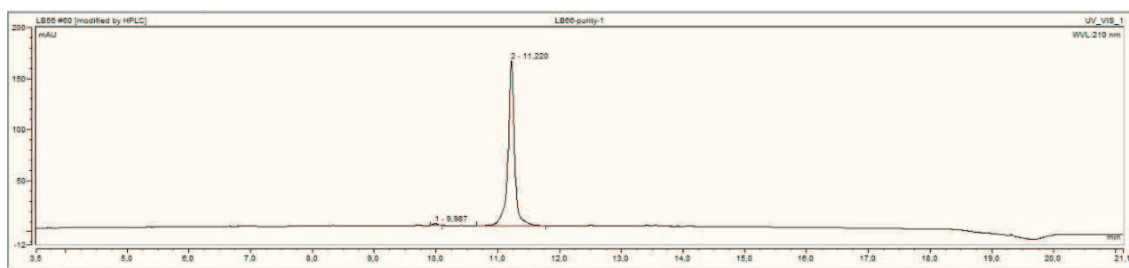
Cyclo[DKP-isoDGR]-PEG-4-Val-Ala-PABC-MMAF **47**

Waters Atlantis 21 mm × 10 cm column; flow: 15 mL/min, gradient: 95% (H_2O + 0.1% CF_3COOH) / 5% (CH_3CN + 0.1% CF_3COOH) to 20% (H_2O + 0.1% CF_3COOH) / 80% (CH_3CN + 0.1% CF_3COOH) in 17 min, t_R product: 11.5 min

Purity: 95.5%
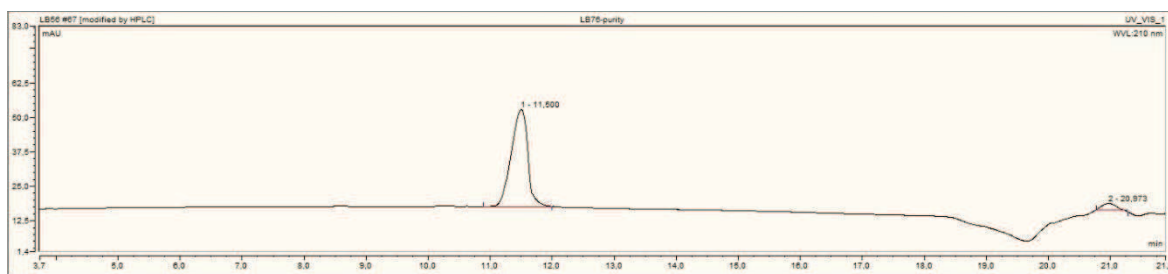
Cyclo[DKP-isoDGR]-PEG-4-MMAE **48**

Waters Atlantis 21 mm × 10 cm column; flow: 15 mL/min, gradient: 95% (H_2O + 0.1% CF_3COOH) / 5% (CH_3CN + 0.1% CF_3COOH) to 20% (H_2O + 0.1% CF_3COOH) / 80% (CH_3CN + 0.1% CF_3COOH) in 17 min, t_R product: 9.7 min

Purity: 98.6%
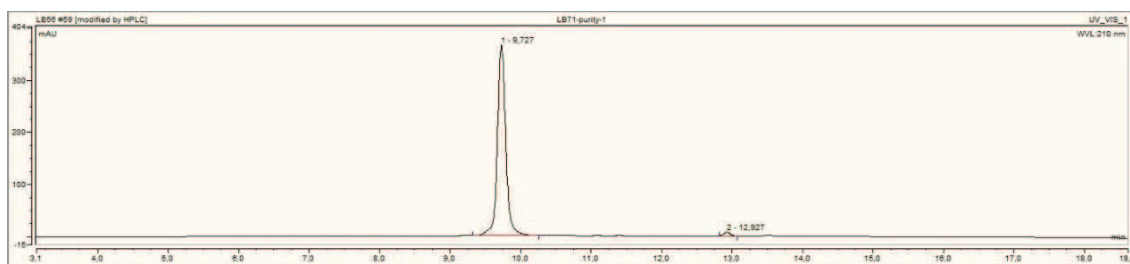
Cyclo[DKP-isoDGR]-PEG-4-MMAF **49**

Waters Atlantis 21 mm × 10 cm column; flow: 15 mL/min, gradient: 95% (H_2O + 0.1% CF_3COOH) / 5% (CH_3CN + 0.1% CF_3COOH) to 20% (H_2O + 0.1% CF_3COOH) / 80% (CH_3CN + 0.1% CF_3COOH) in 17 min, t_R product: 10.2 min

Purity: 94.4%
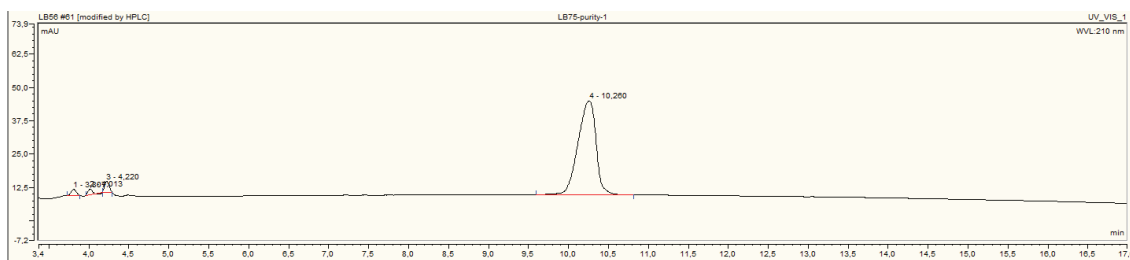
ESI-MS Spectra

Cyclo[(3S,6R)-DKP-f3-*iso*DGR] **14**
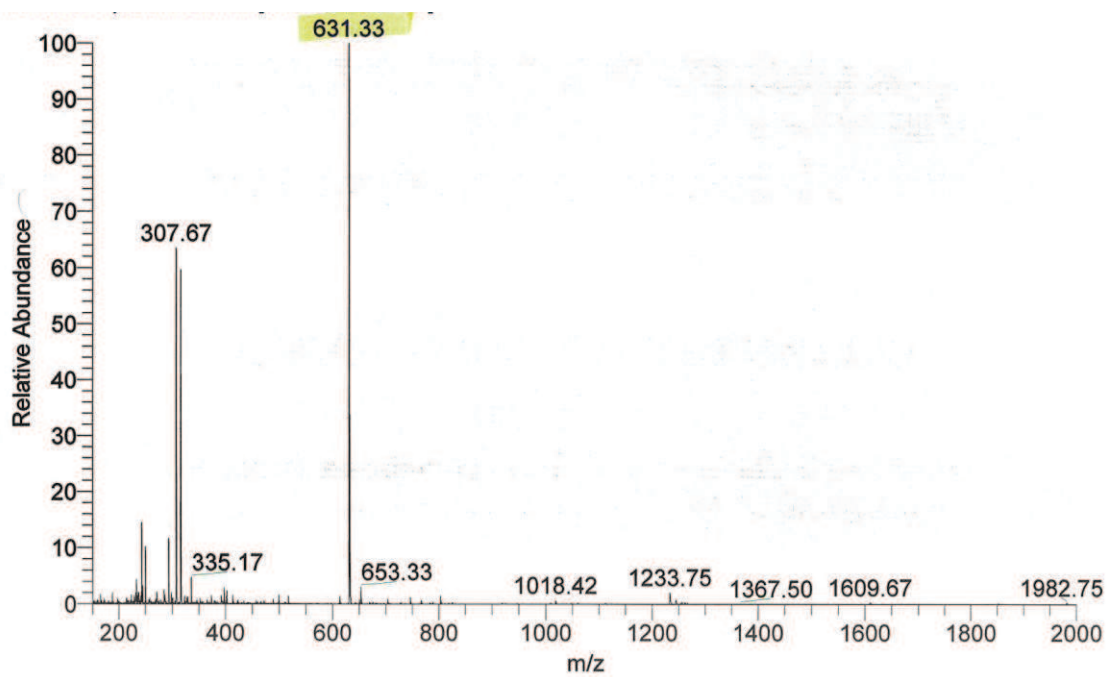
N₃-PEG-4-*cyclo*[DKP- *iso*DGR] **41**
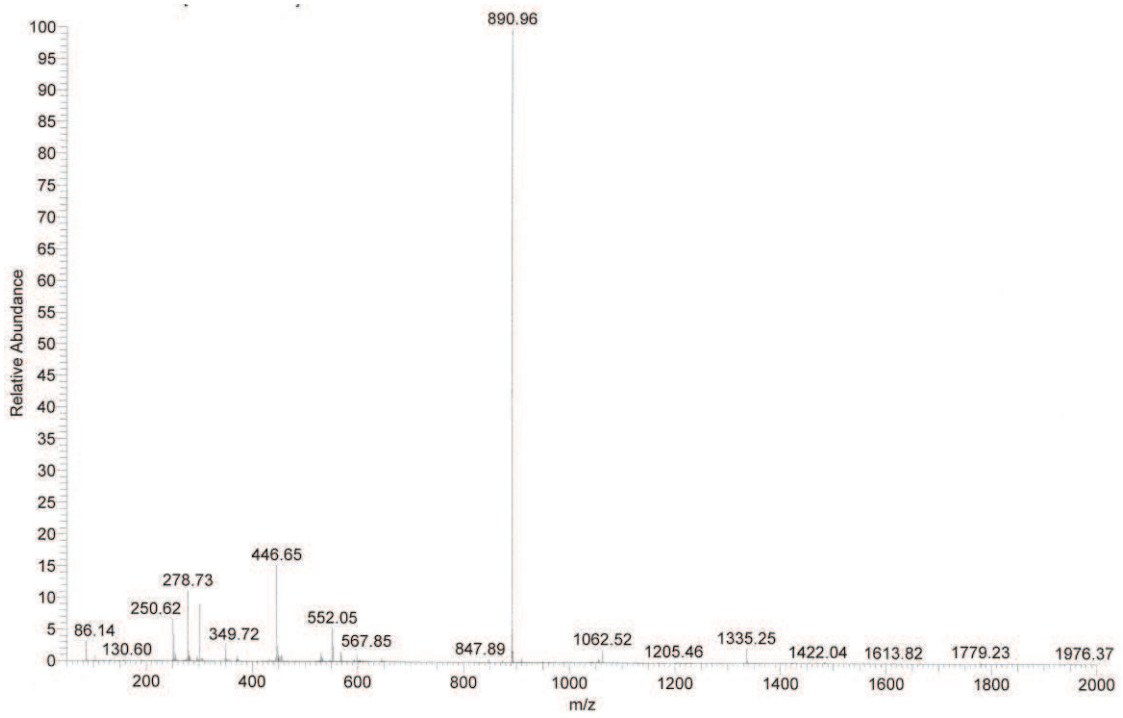
Cyclo[DKP-*iso*DGR]-uncleavable-α-amanitin **31**
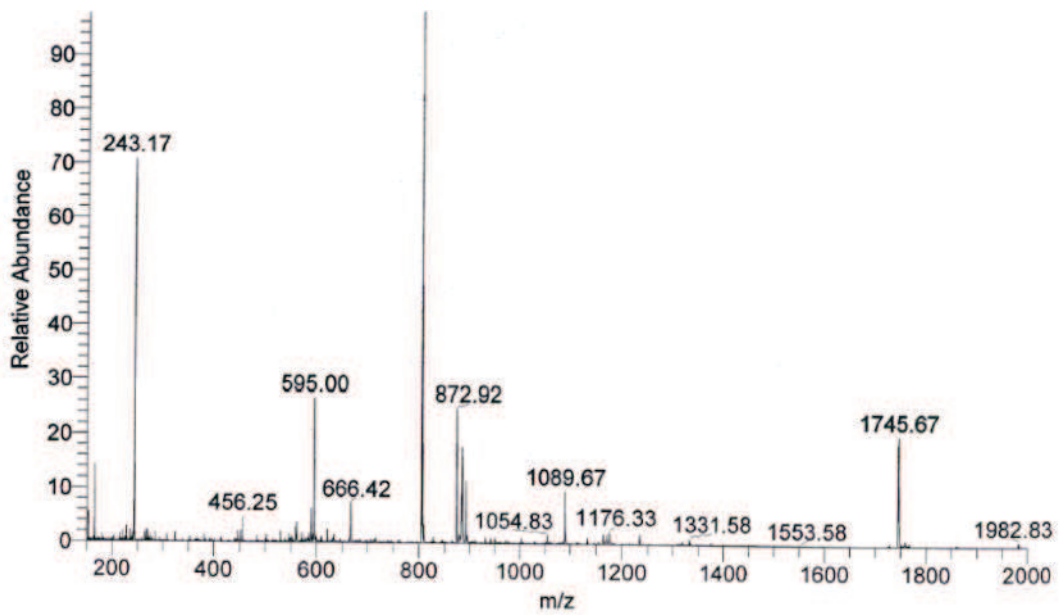
Cyclo[DKP-*iso*DGR]-Val-Ala-α-amanitin **32**
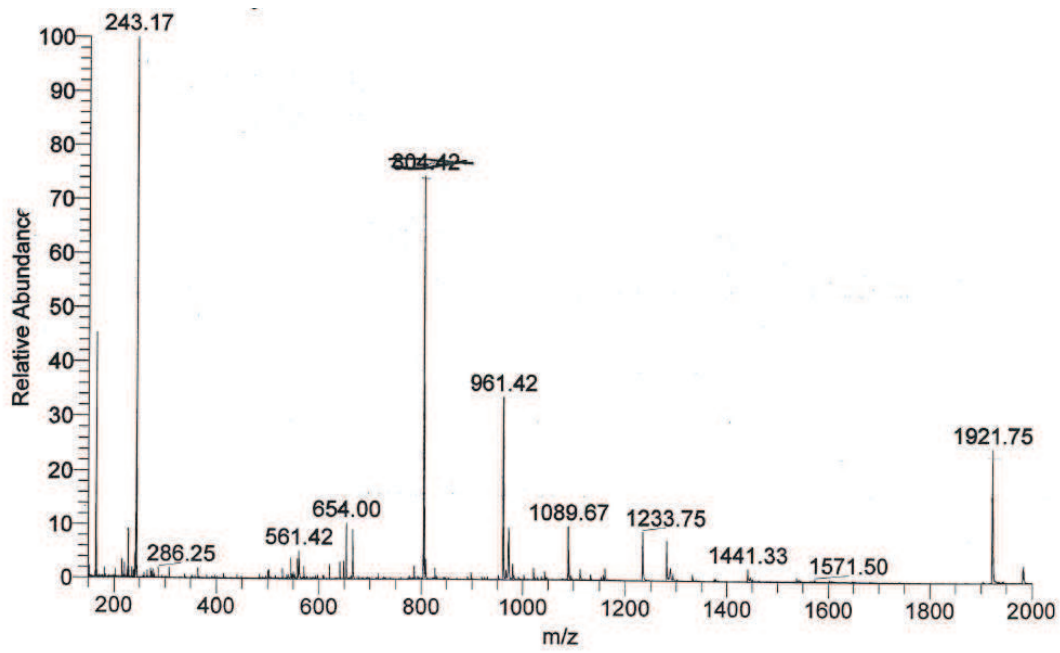
Cyclo[DKP-*iso*DGR]-PEG-4-Val-Ala- α-amanitin **33**

Val-Ala-PABC-MMAE **55**

F: ITMS + c ESI Full ms [50.00-2000.00]

Val-Ala-PABC-MMAF **56**

F: ITMS + c ESI Full ms [50.00-2000.00]
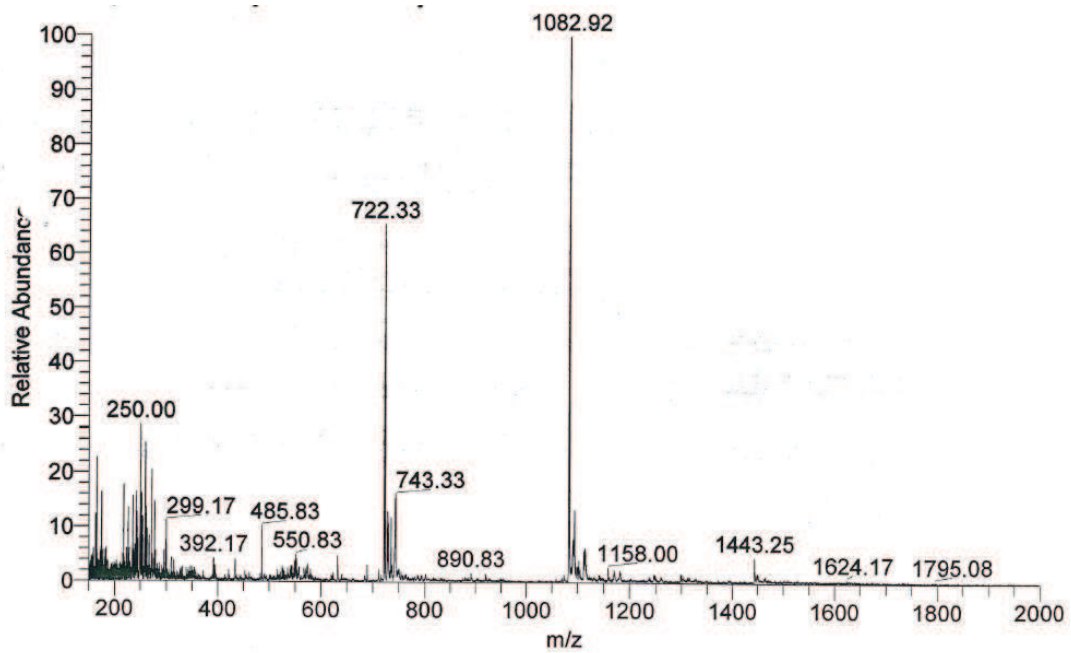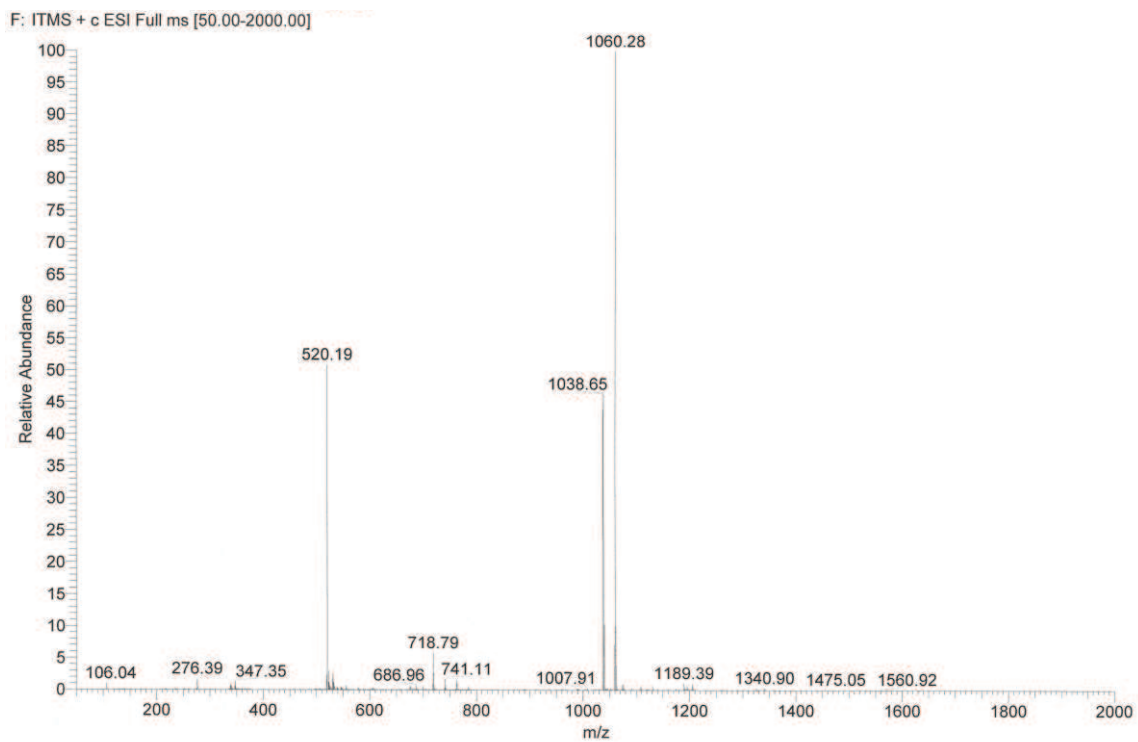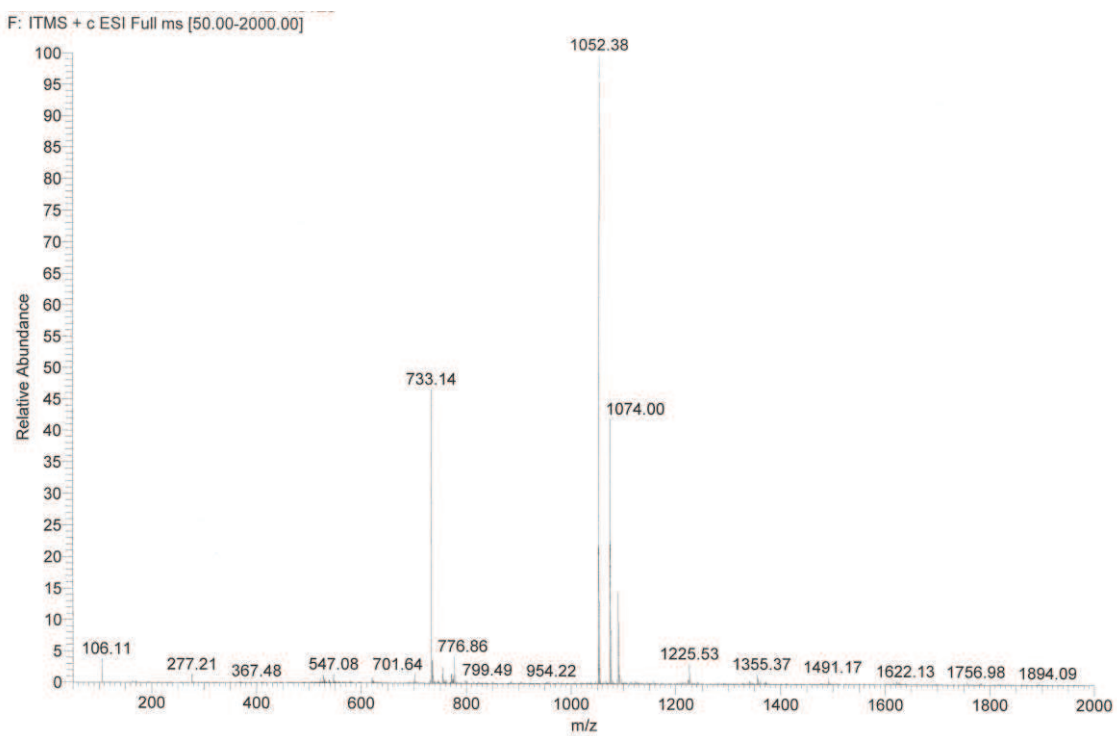
4-pentynoic acid-Val-Ala-PABC-MMAE **57**
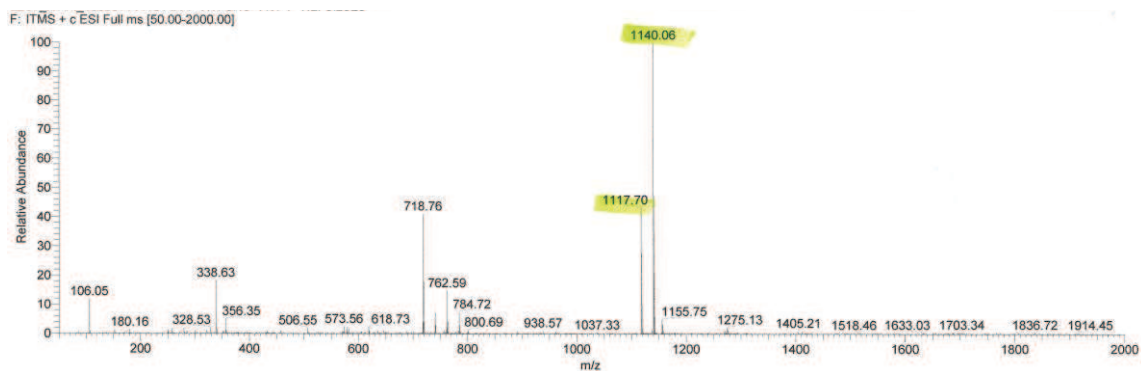
4-pentynoic acid-Val-Ala-PABC-MMAF **58**
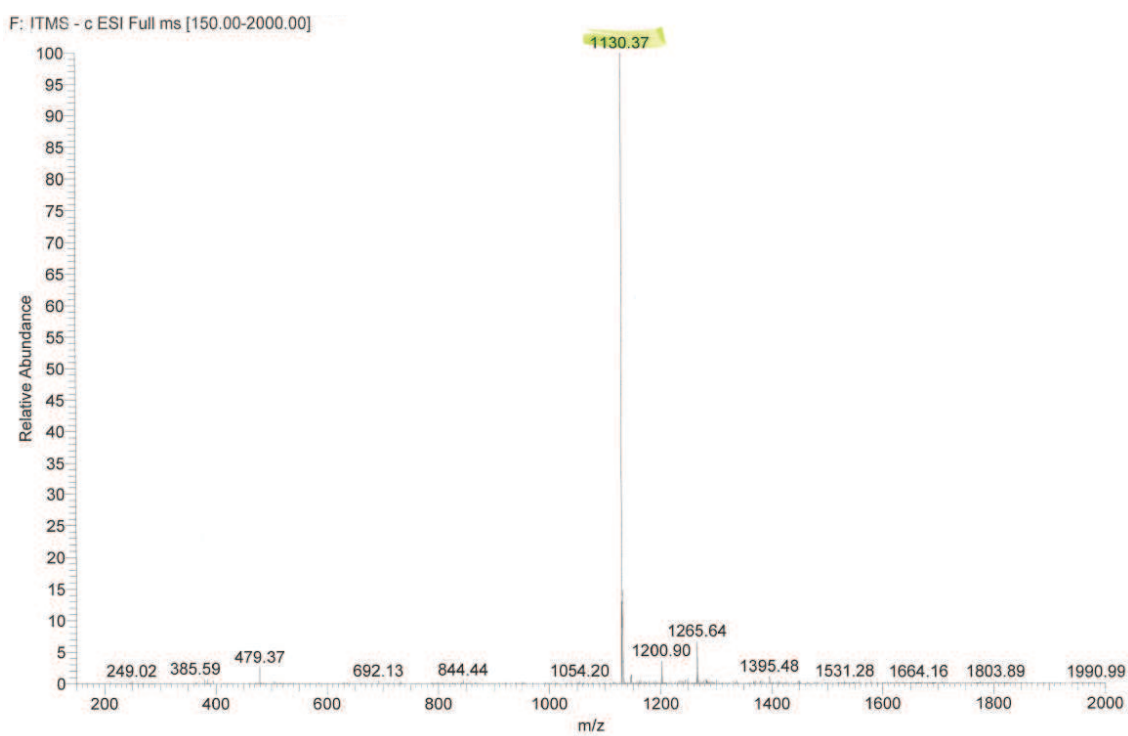
Cyclo[DKP-*iso*DGR]-PEG-4-Val-Ala-PABC-MMAE **46**
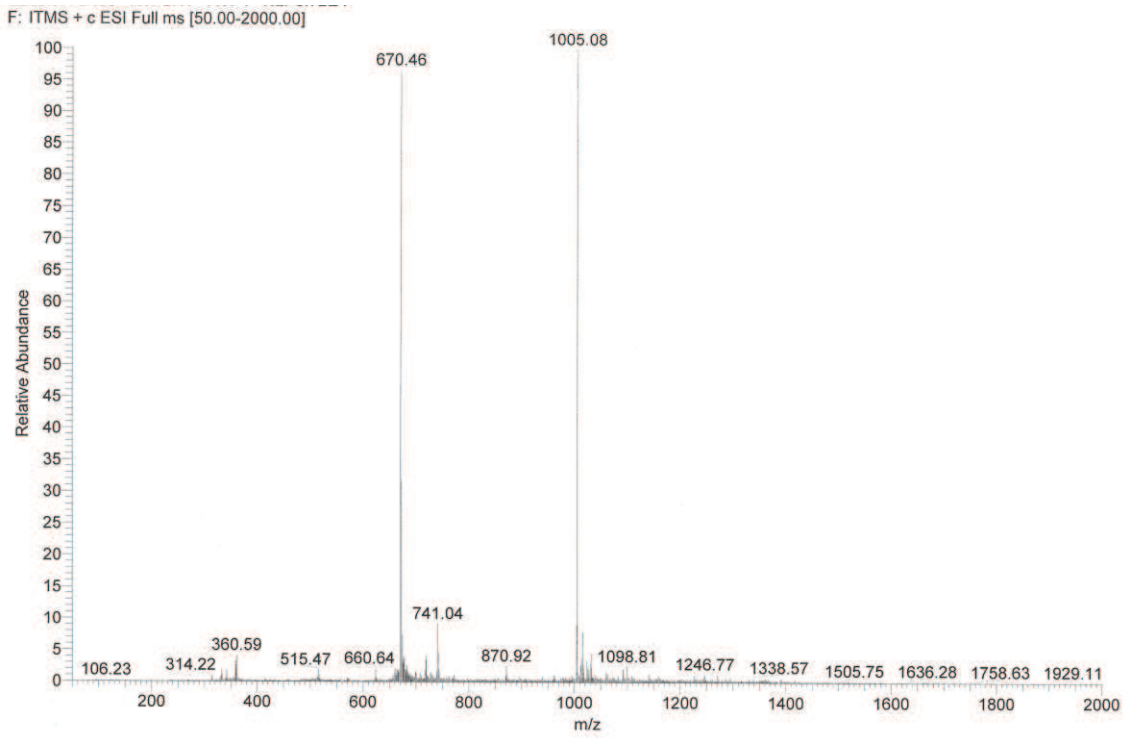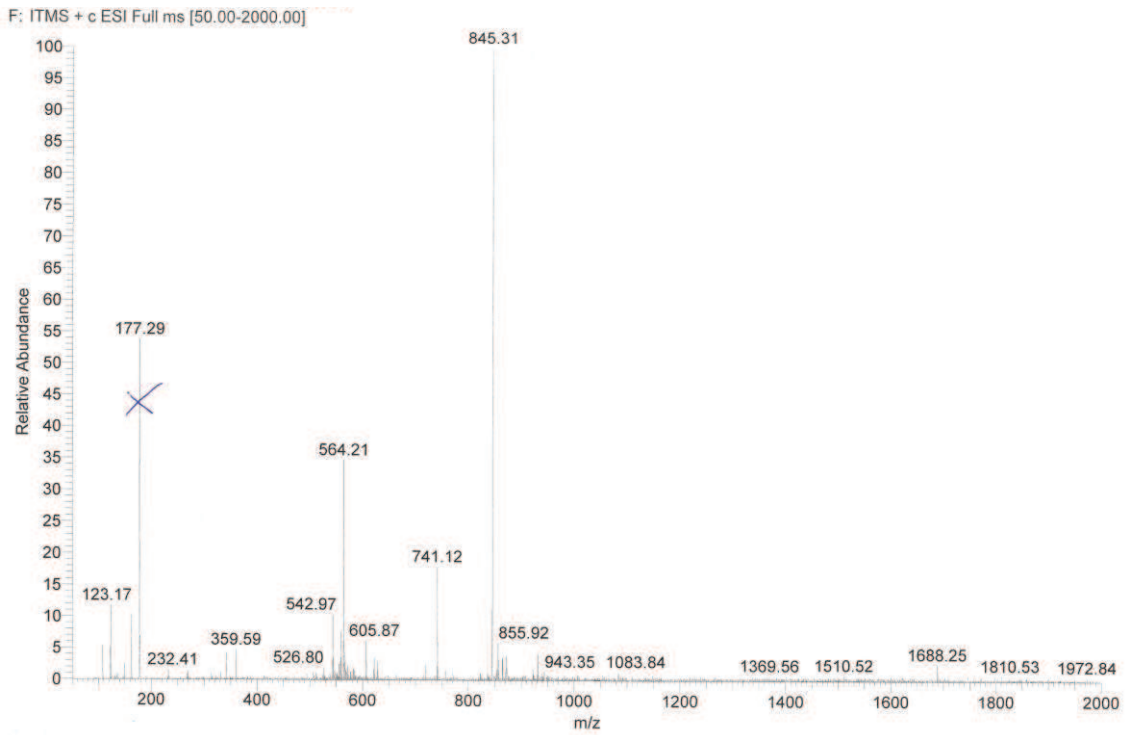

Cyclo[DKP-*iso*DGR]-PEG-4-Val-Ala-PABC-MMAF **47**
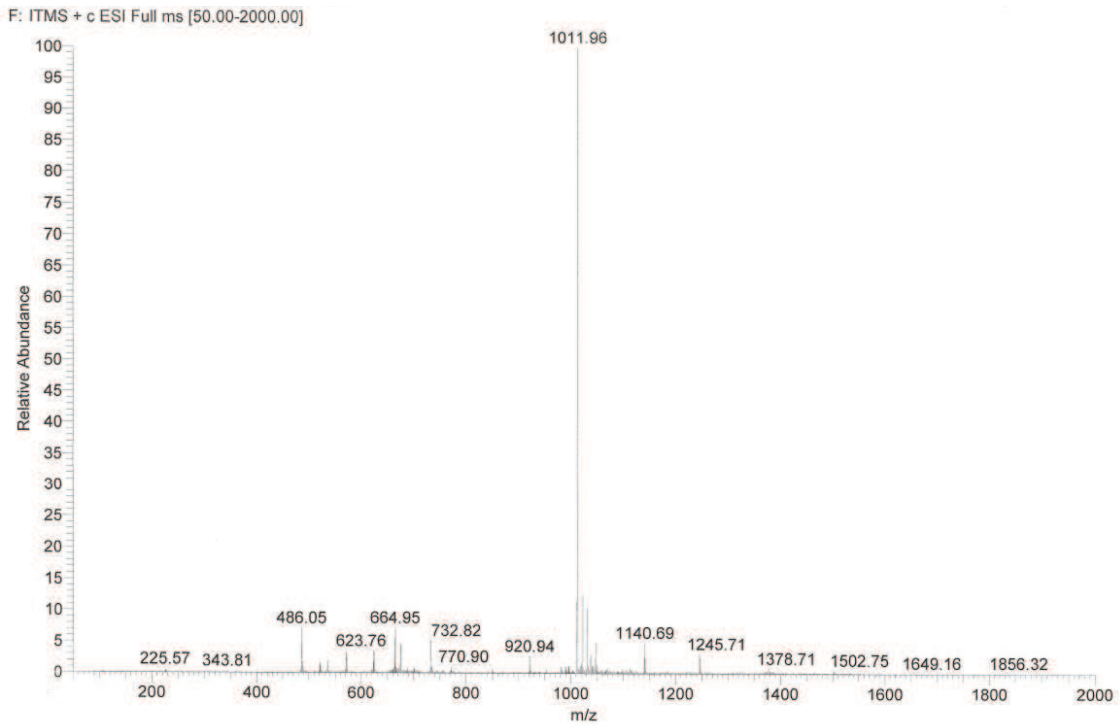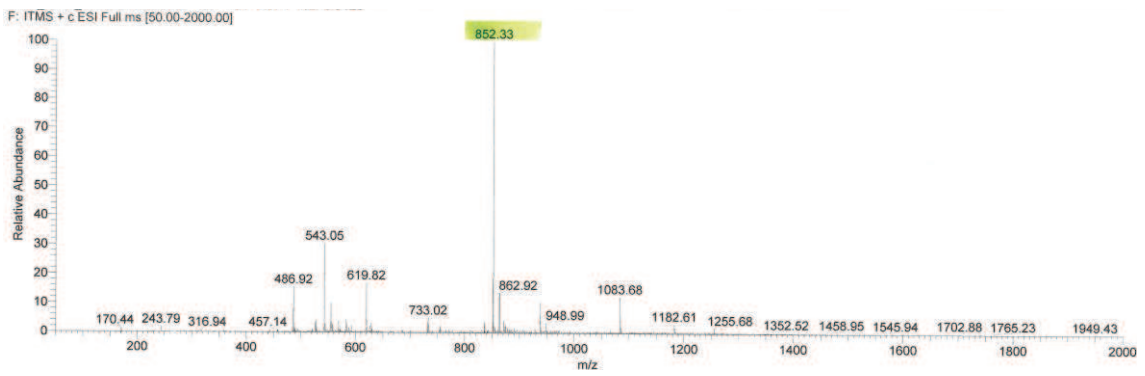
4-pentynoic acid-MMAE **59**
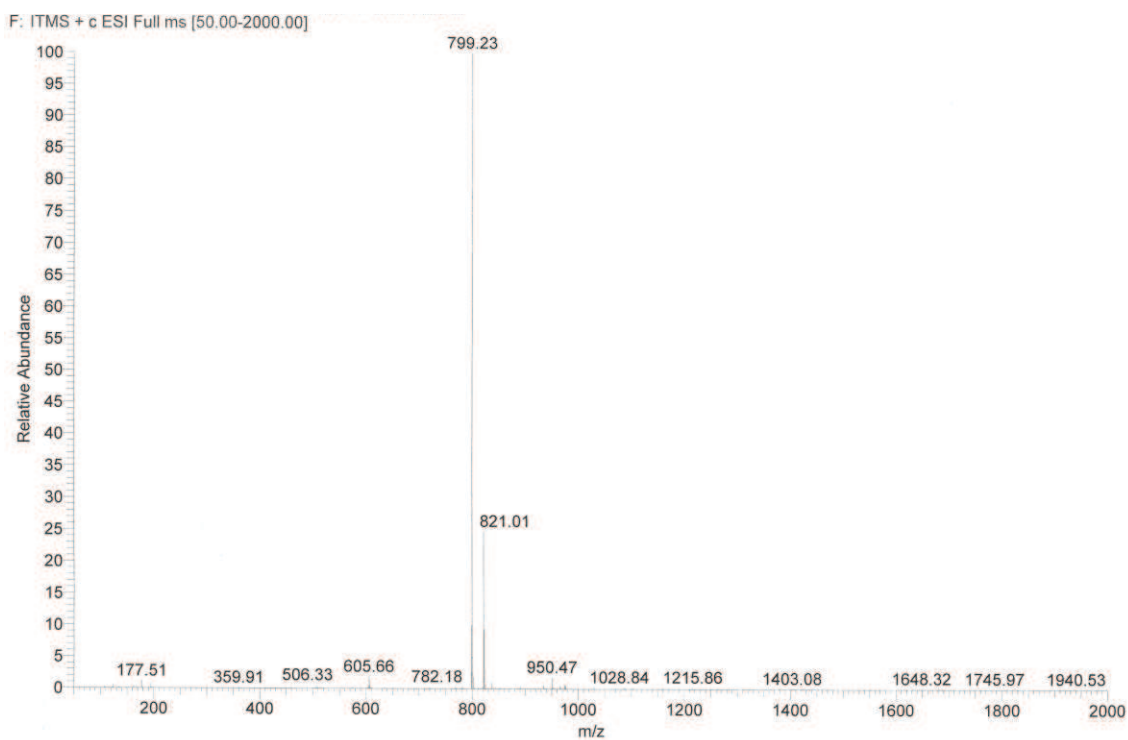
4-pentynoic acid-MMAF **60**
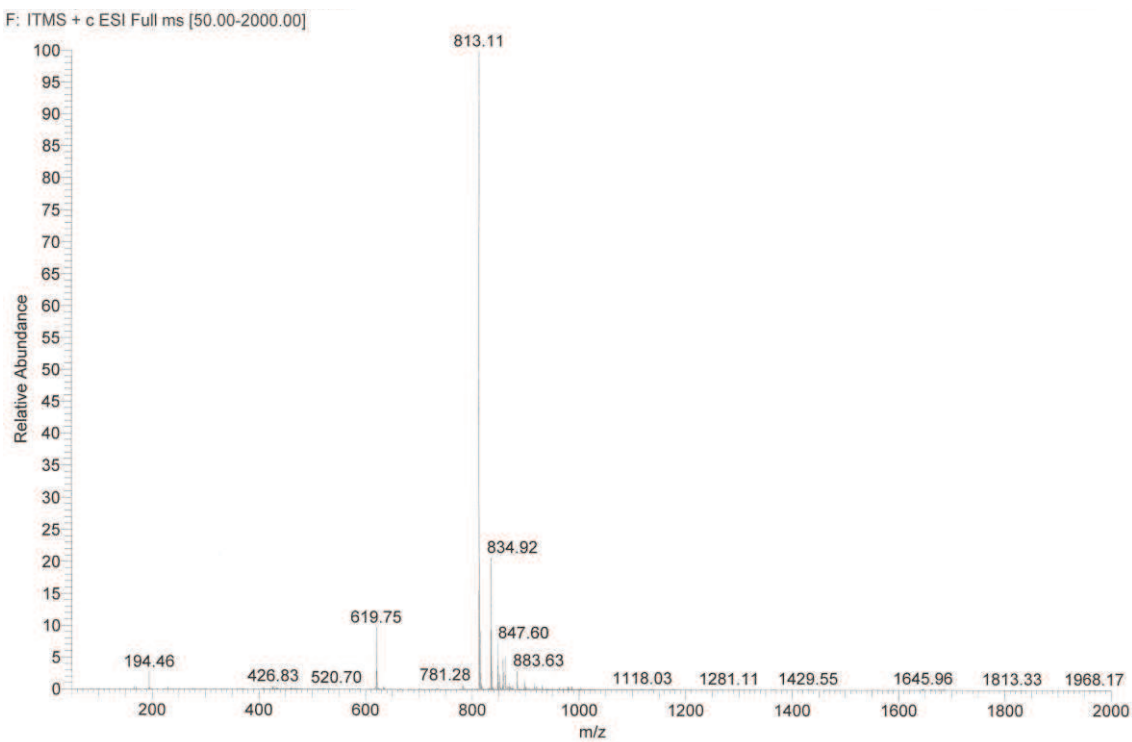
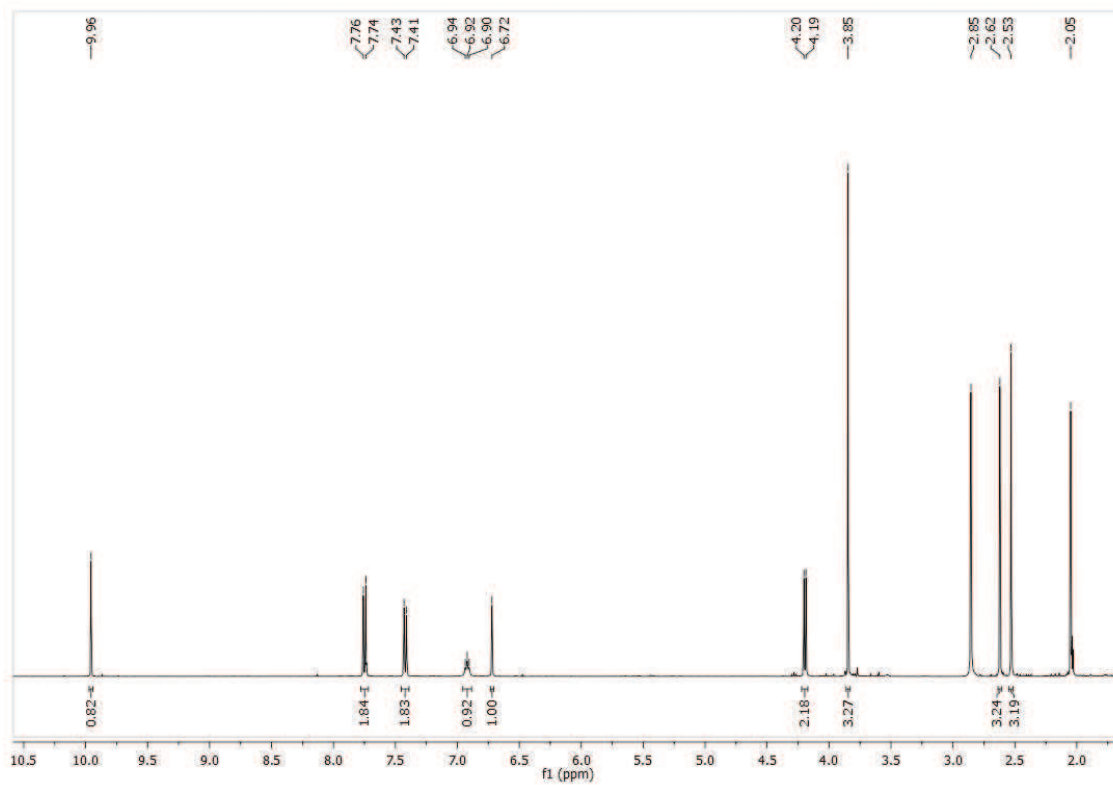Cyclo[DKP-*iso*DGR]-PEG-4-MMAE **48**

Cyclo[DKP-*iso*DGR]-PEG-4-MMAF **49**
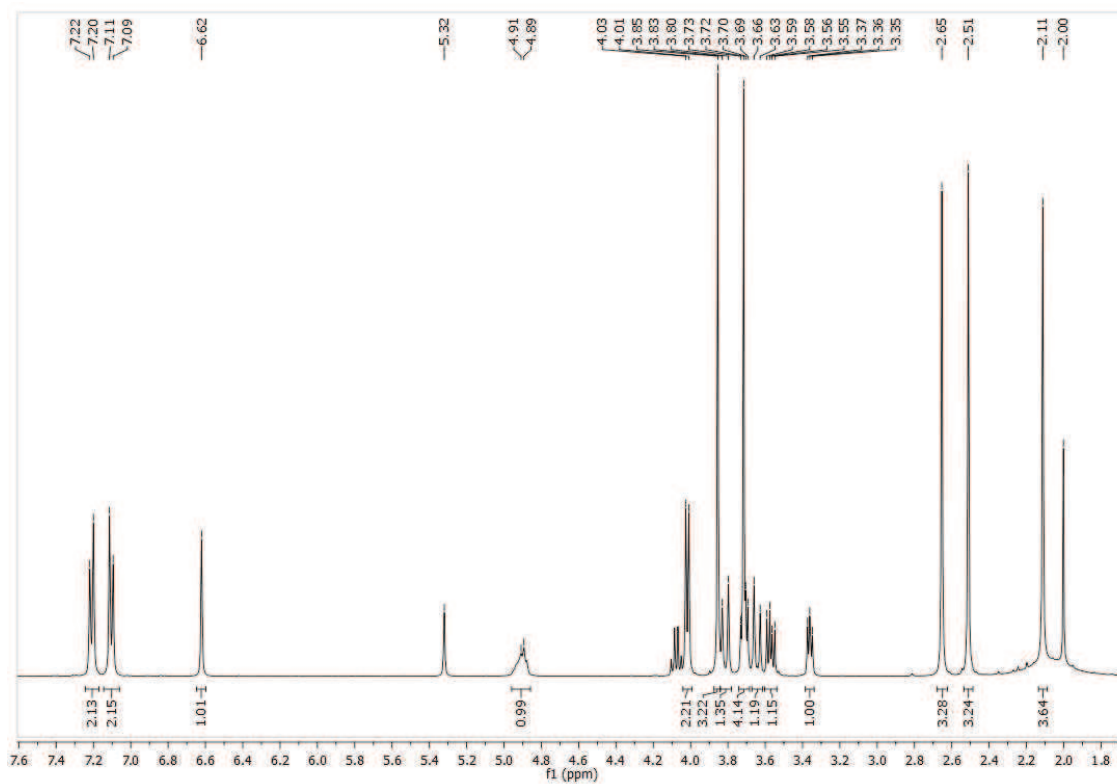
Appendix of NMR data

4-((4-methoxy-2,3,6-trimethylphenylsulfonyl)aminomethyl)benzaldehyde **16**
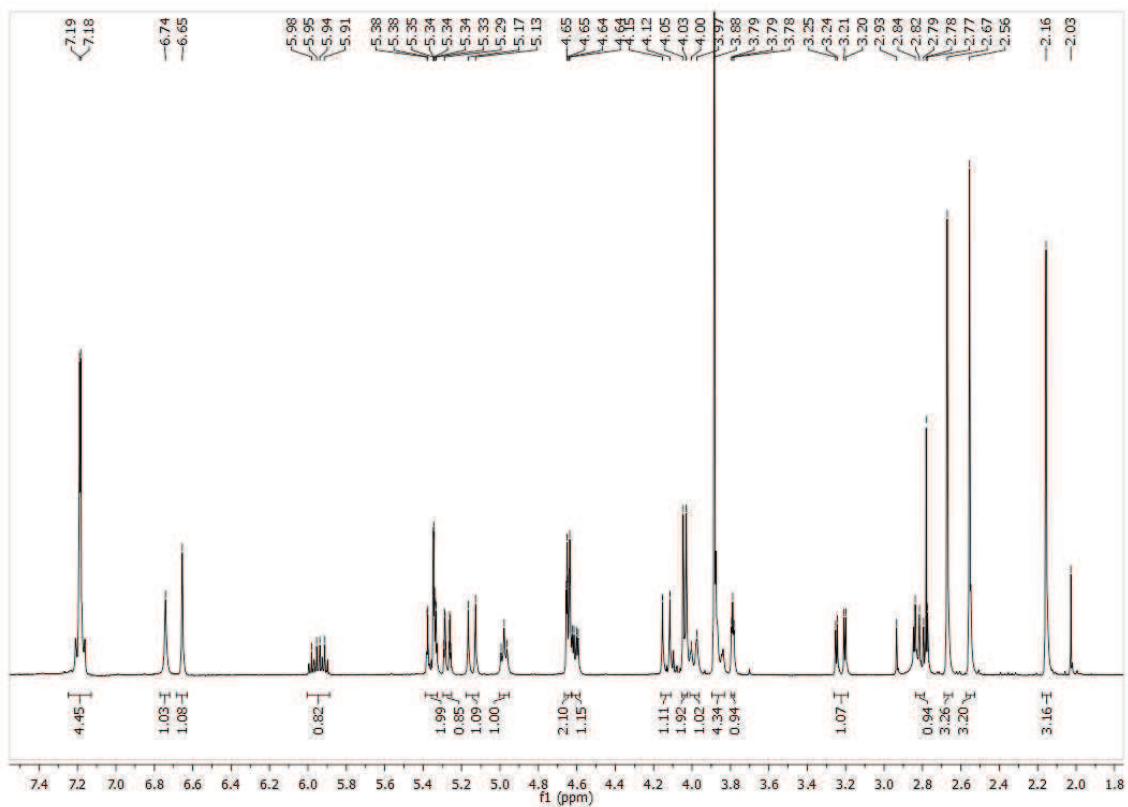
^{1}H NMR (400 MHz, acetone-d_6)

(S)-methyl-3-hydroxy-2-((4-((4-methoxy-2,3,6-trimethyl-phenylsulfonamido)methyl)

benzyl)amino)propanoate **17**
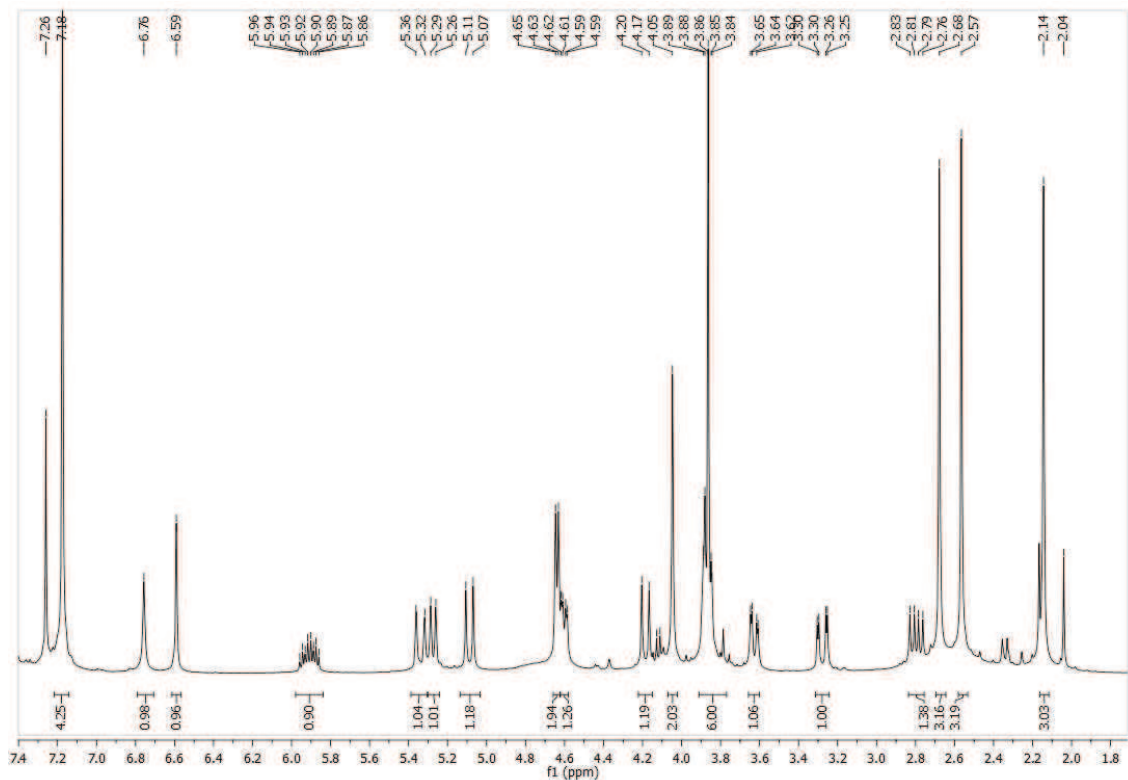
^{1}H NMR (400 MHz, CD$_2$Cl$_2$)

OH-(3S-6R)-DKP-*f3*-COOAllyl **19**

^{1}H NMR (400 MHz, CDCl$_3$)

N$_3$-(3S-6R)-DKP-*f3*-COOAllyl **20**

^{1}H NMR (400 MHz, CDCl$_3$)

Boc-(3S-6R)-DKP-*f3*-COOAllyl **21**

^{1}H NMR (400 MHz, CDCl$_3$)
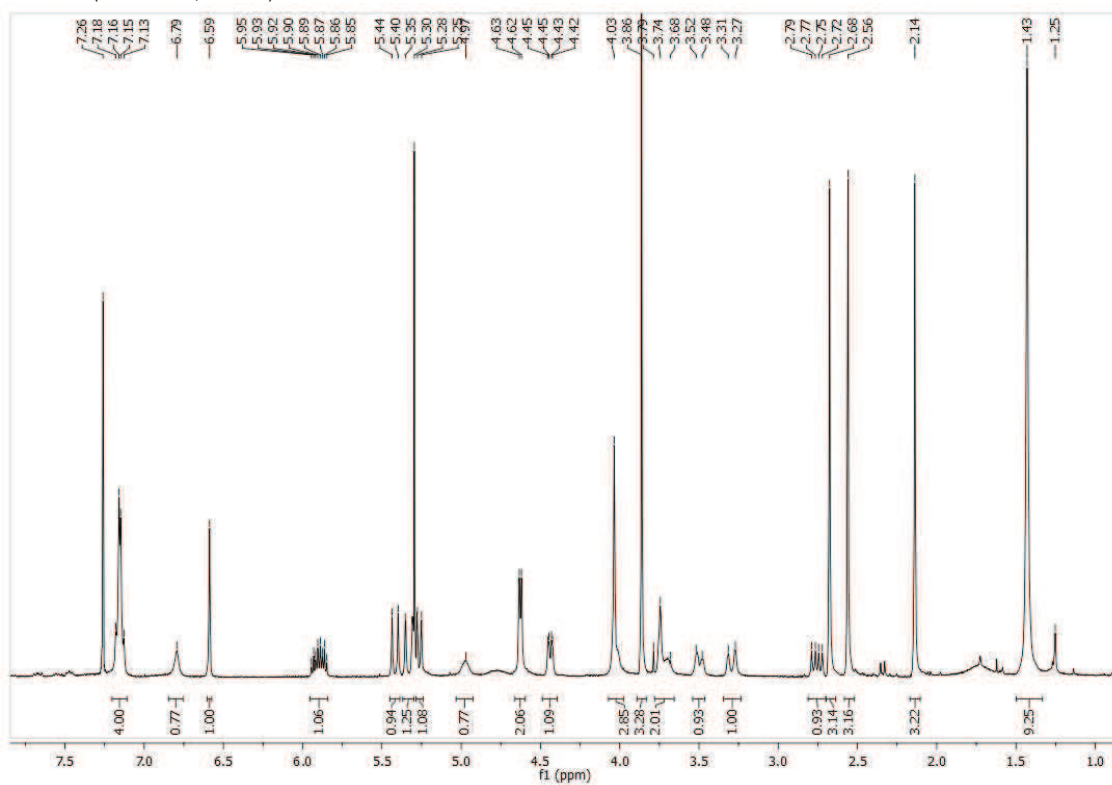
Mtr-Arg-(3S-6R)-DKP-*f3*-COOAllyl **22**

¹H NMR (400 MHz, MeOD-*d₄*)
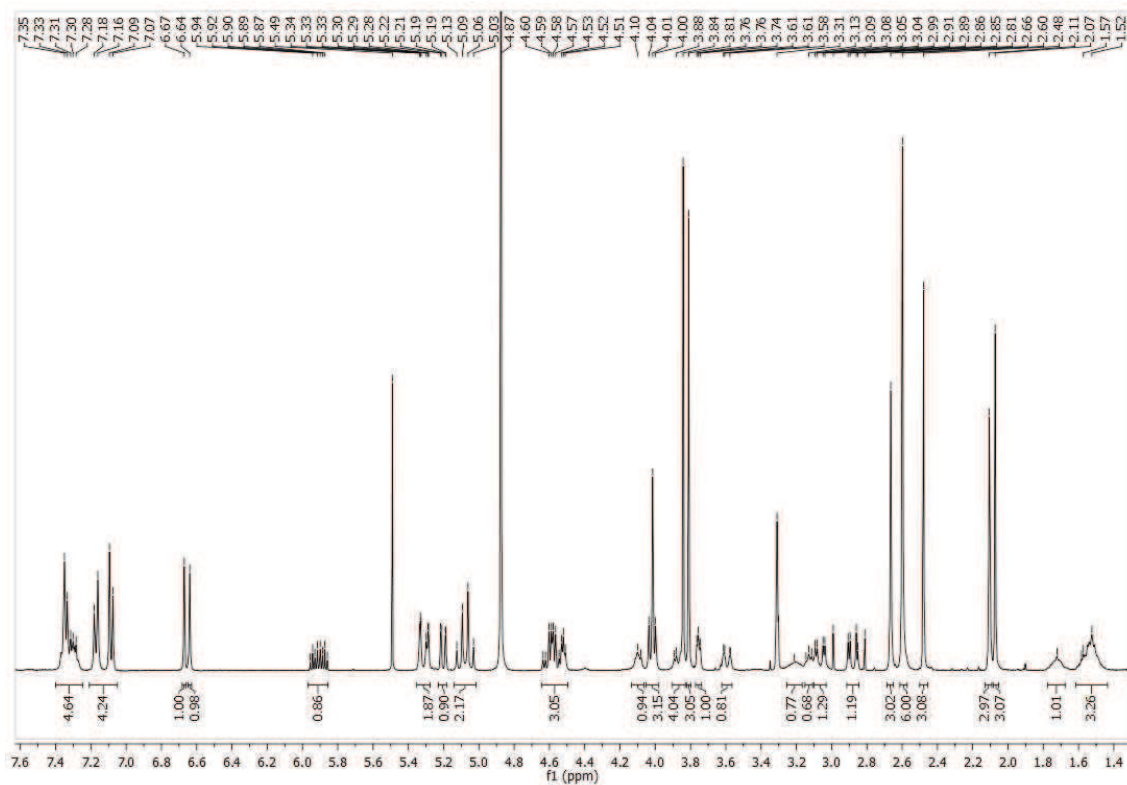
¹H NMR (101 MHz, MeOD-*d₄*)
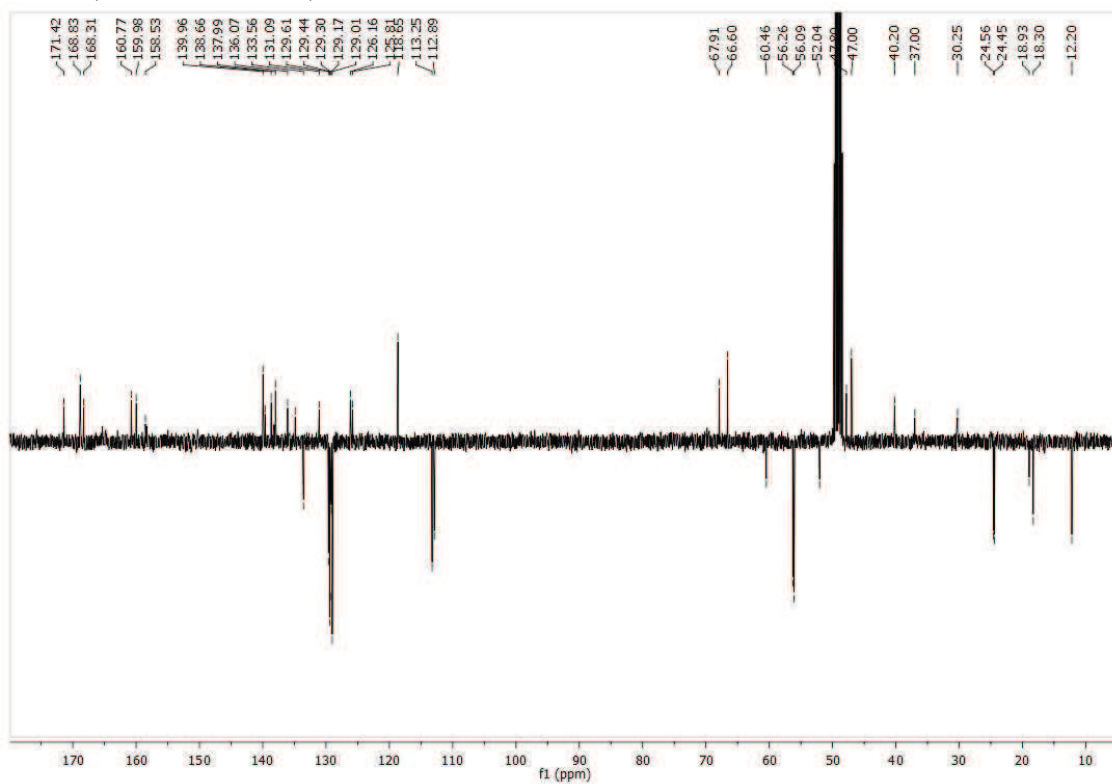
Mtr-Arg-(3S-6R)-DKP-*f3*-COOH 23

^{1}H NMR (400 MHz, MeOD-*d₄*)
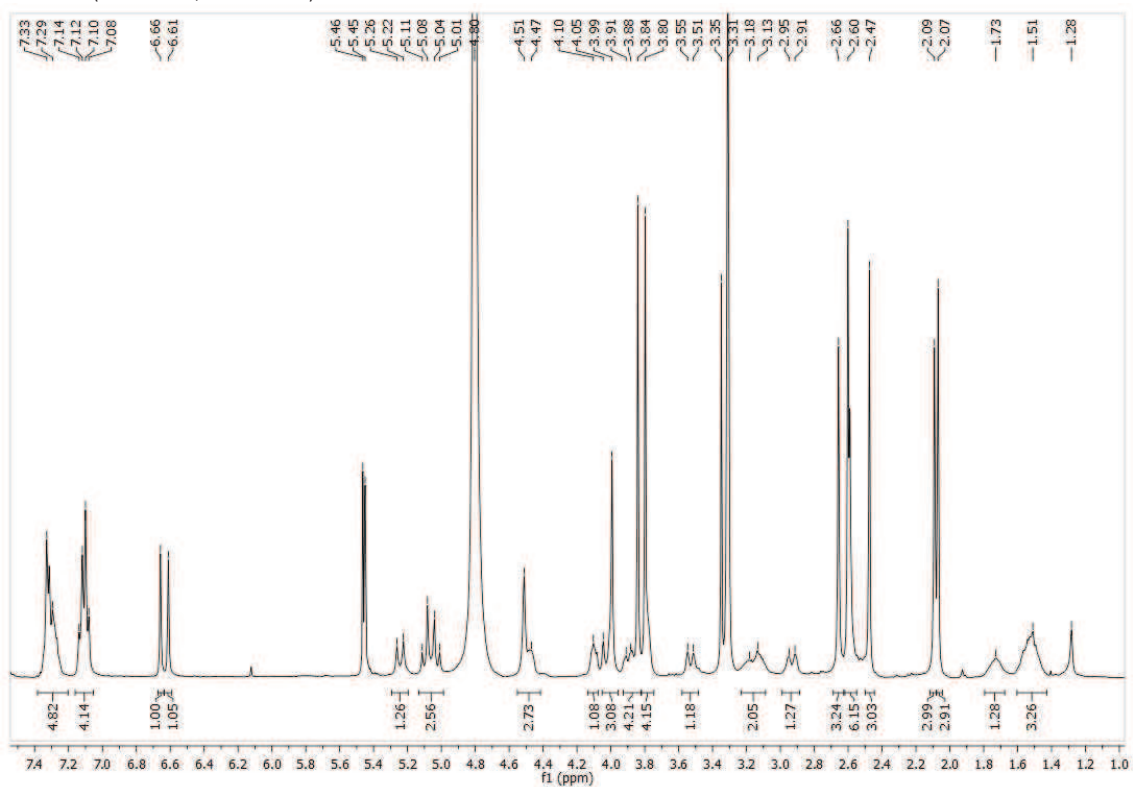
^{13}C NMR (101 MHz, MeOD-*d₄*)
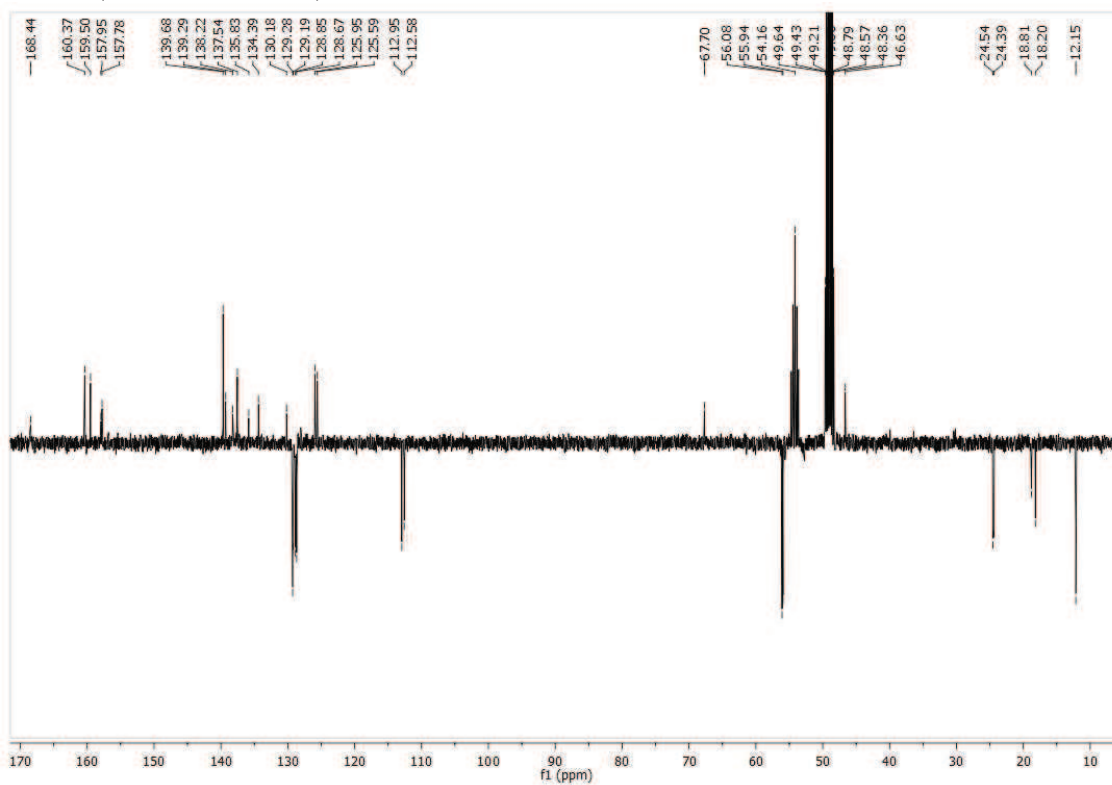
(*S*)-*tert*-butyl 2-amino-4-((2-(benzyloxy)-2-oxo-ethyl)amino)-4-oxobutanoate **26**

^{1}H NMR (400 MHz, CDCl$_3$)
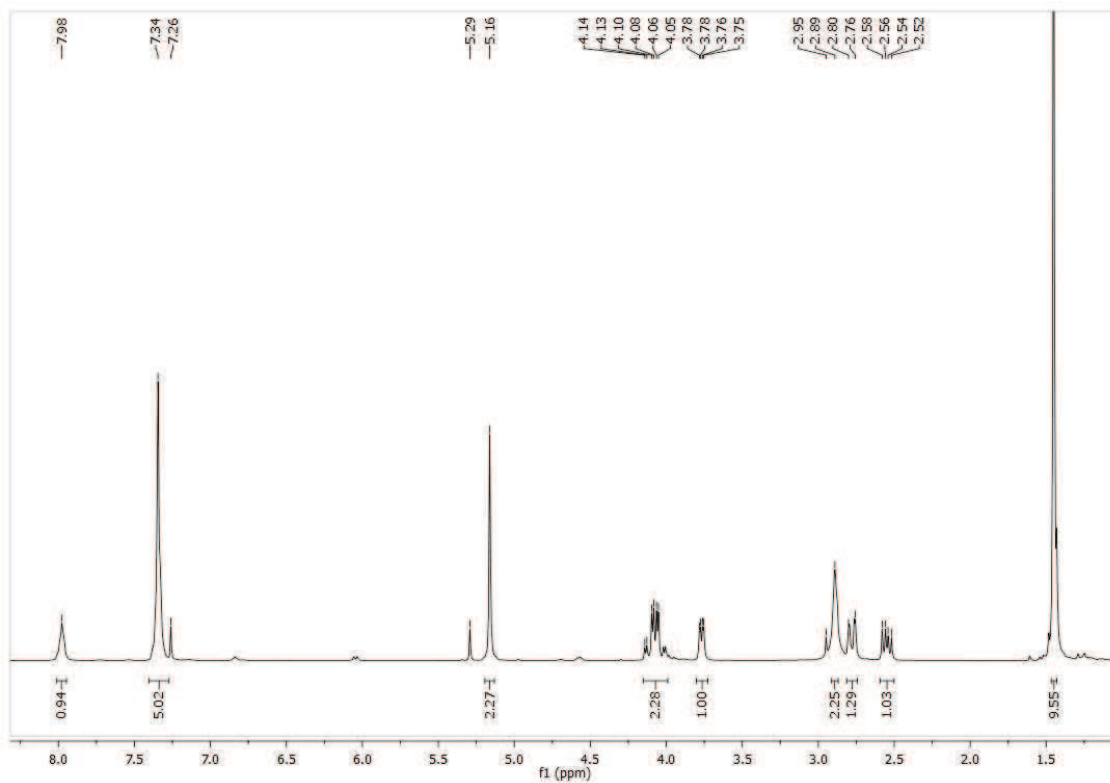
Mtr-Arg-(3S,6R)-DKP-*f3*-COO-*iso*Asp-Gly-OBn **27**

¹H NMR (400 MHz, acetone)
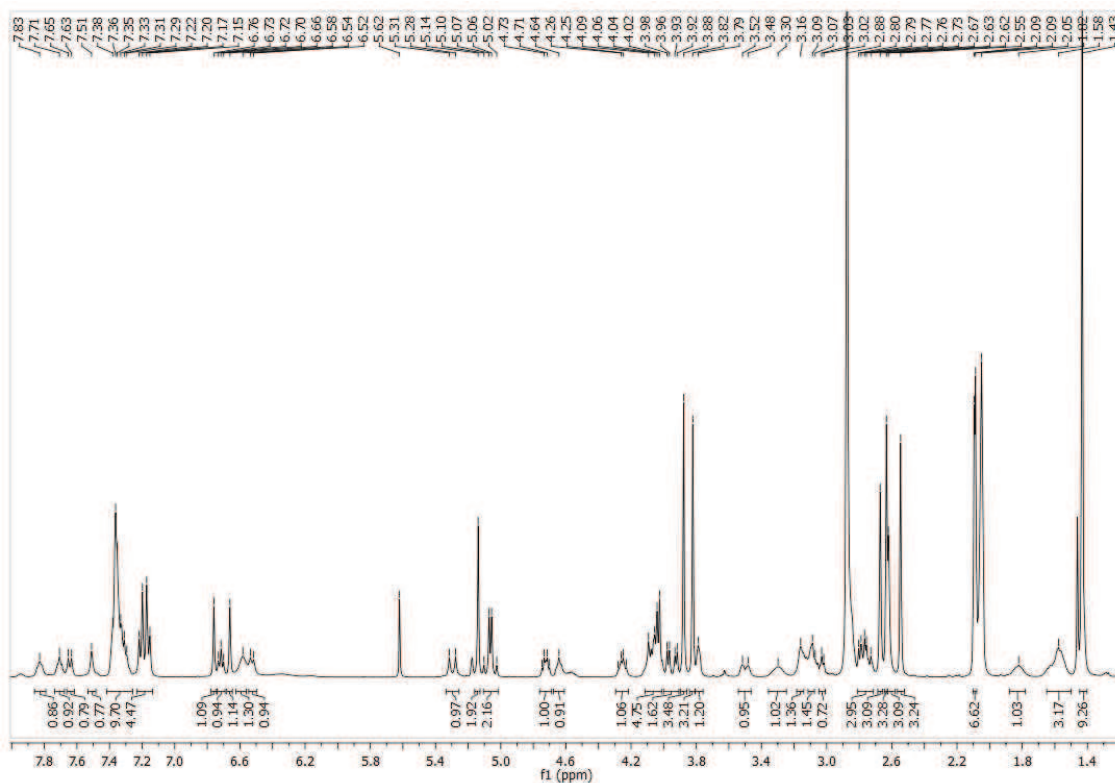
¹³C NMR (101 MHz, acetone)
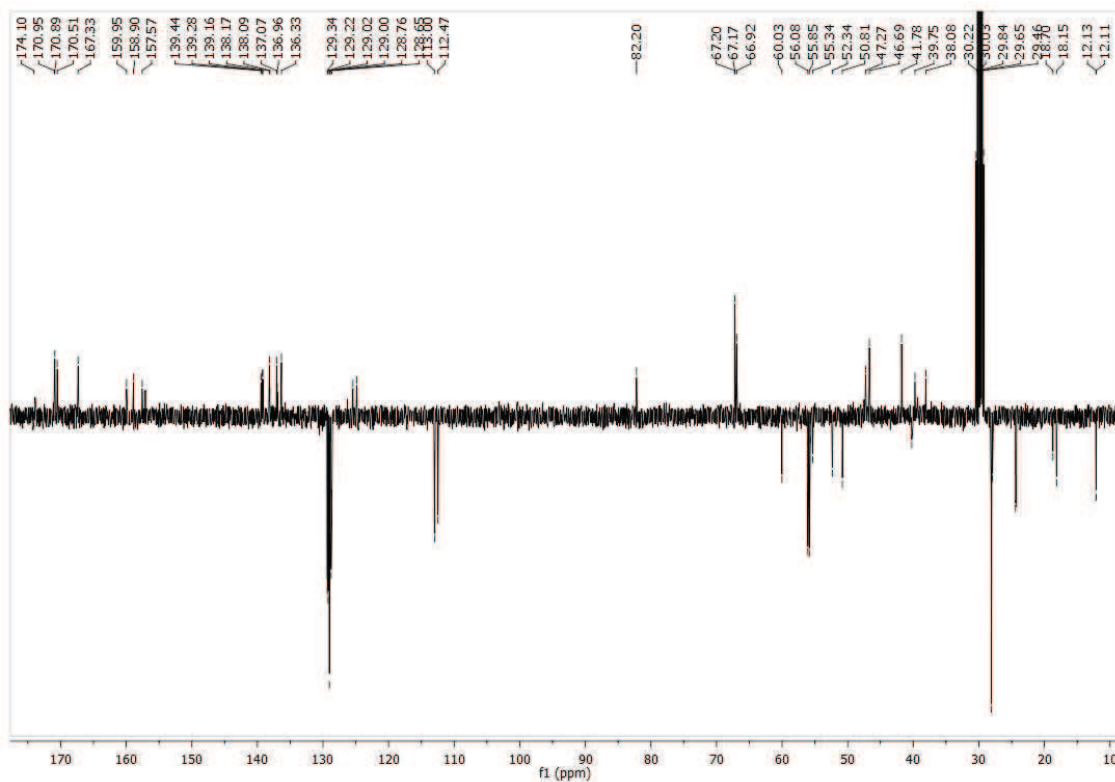
cyclo[(3S,6R)-DKP-*f3-iso*DGR]-Mtr **29**

¹³C NMR (400 MHz, DMSO-*d₆*)
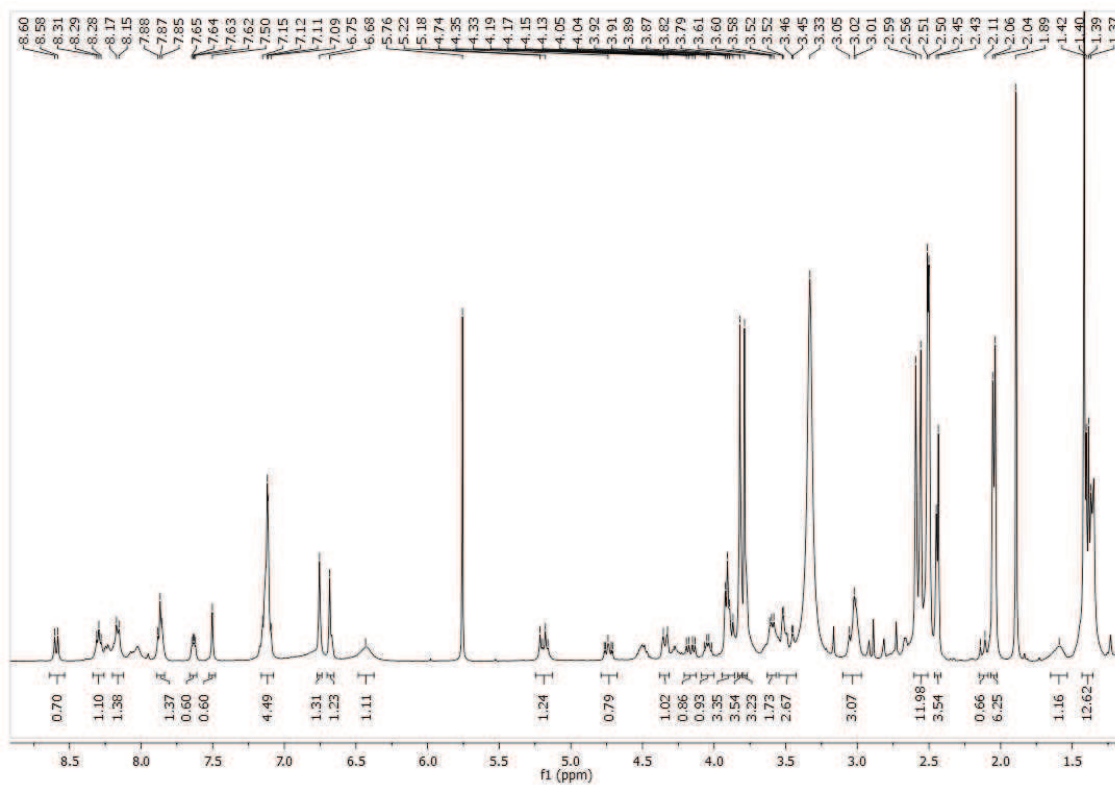
¹³C NMR (101 MHz, DMSO-*d₆*)
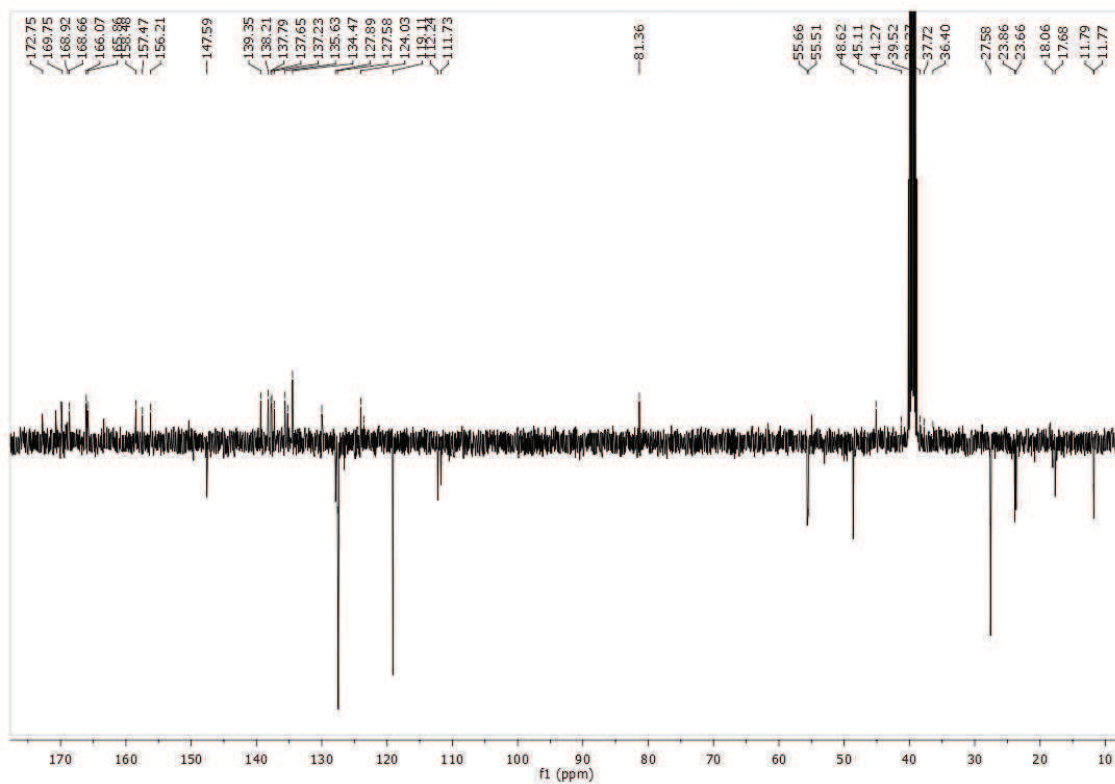
cyclo[(3S,6R)-DKP-f3-isoDGR] 14

^{1}H NMR (400 MHz, D$_2$O)
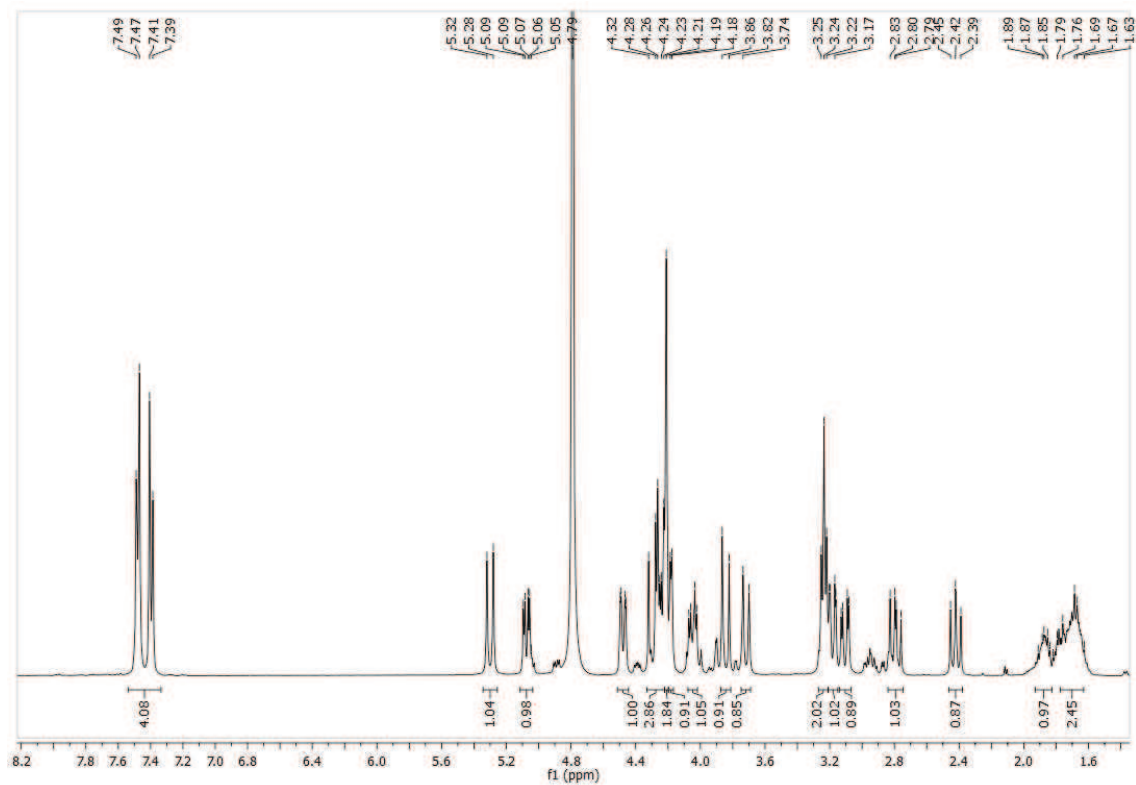
^{13}C NMR (101 MHz, D$_2$O)
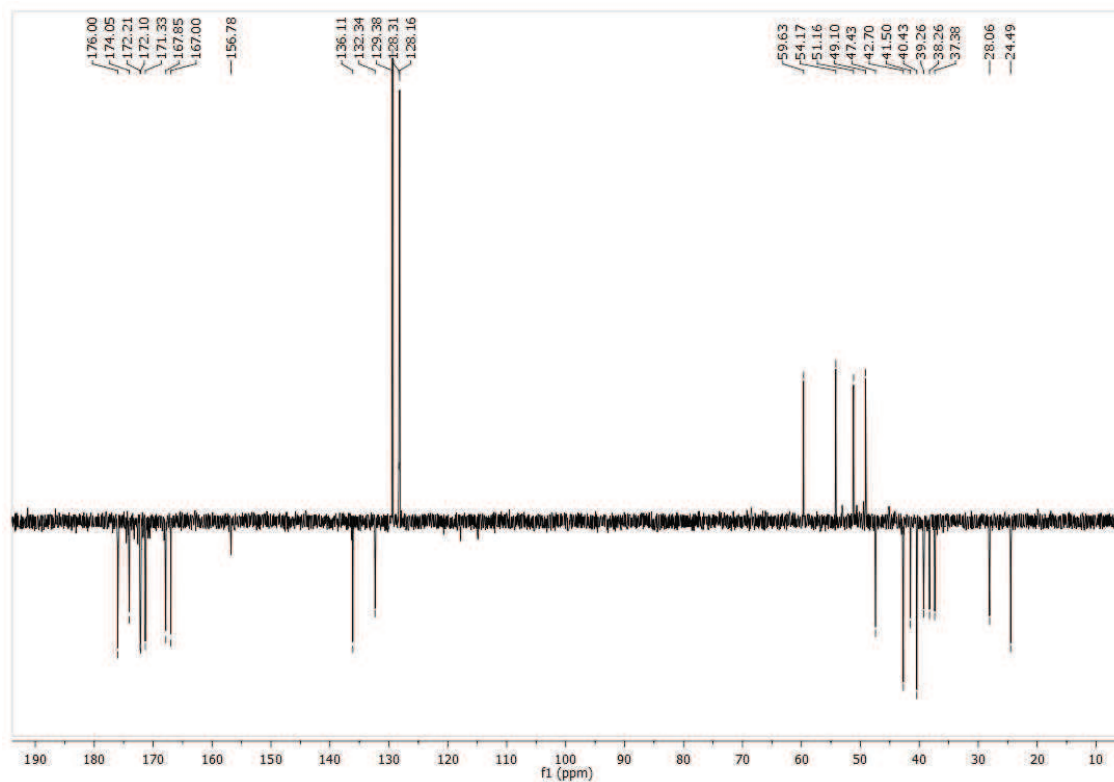
14-Hydroxy-3,6,9,12-tetraoxatetradecyl-4'-methylbenzolsulfonate **50-a**

^{1}H NMR (400 MHz, CDCl$_3$)
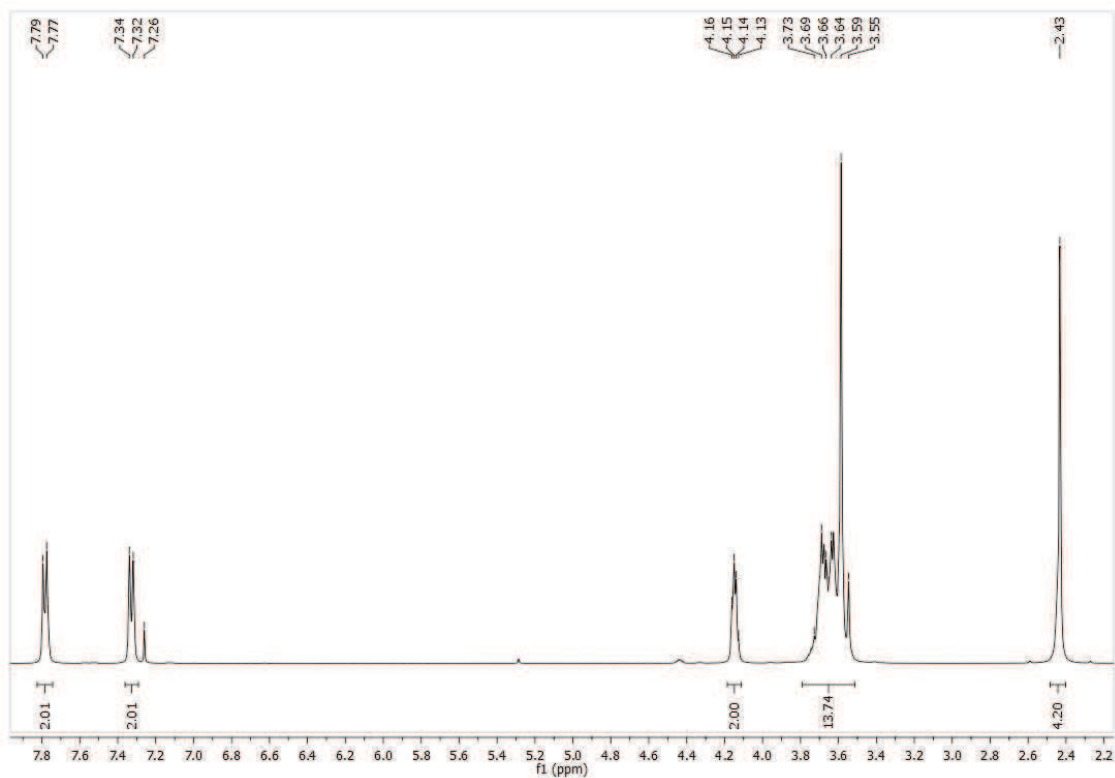
2-(2-(2-(2-Azidoethoxy) ethoxy) ethoxy) ethan-1-ol **50-b**

^{1}H NMR (400 MHz, CDCl$_3$)
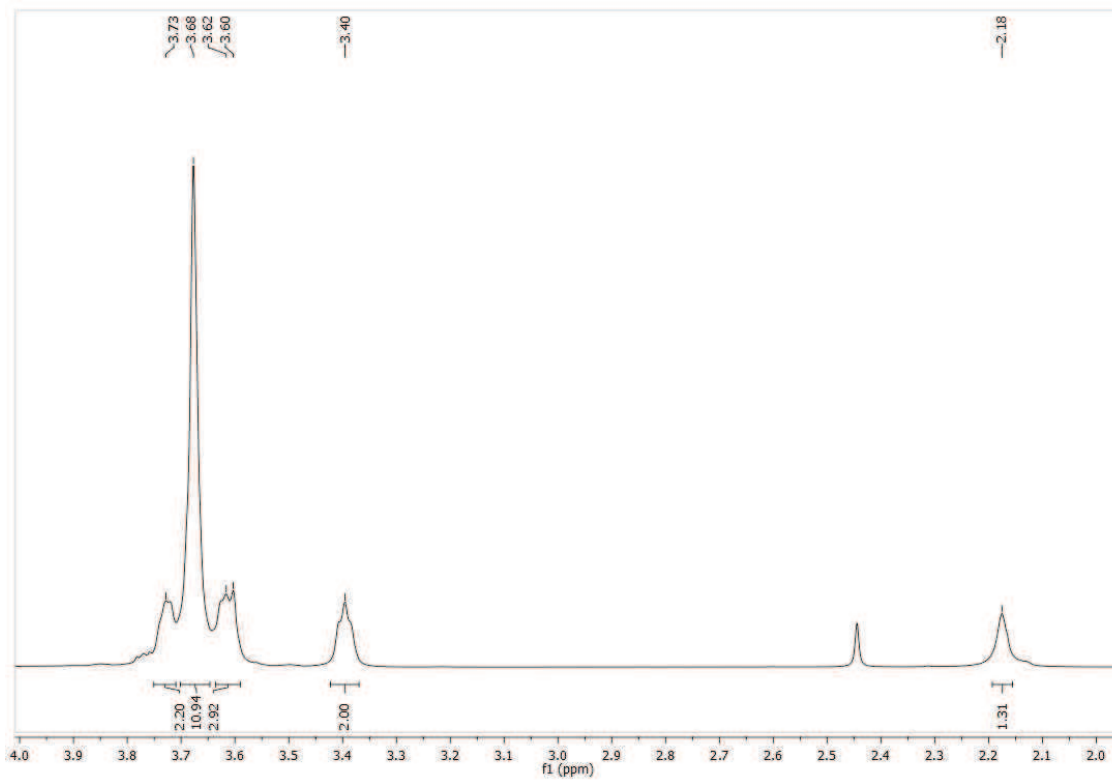
14-Azido-3,6,9,12-tetraoxatetradecanoic acid **51**
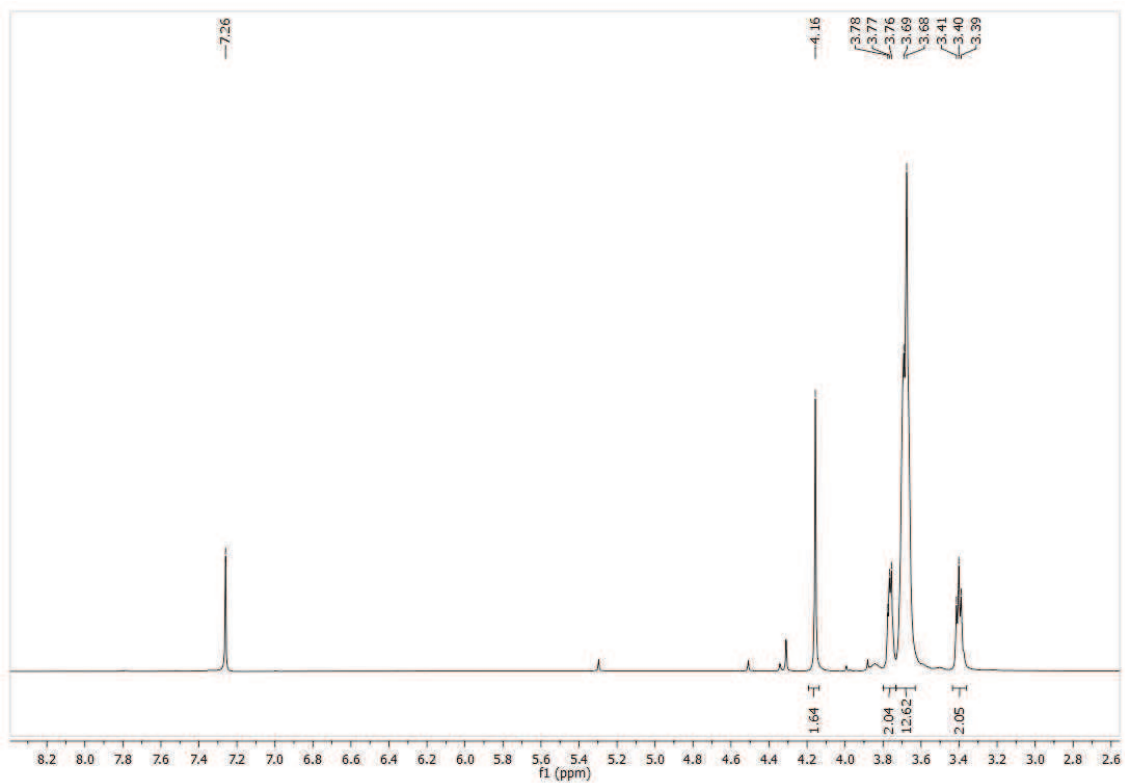
14-Azido-3,6,9,12-tetraoxatetradecanoic acid -NHS ester **40**

¹H NMR (400 MHz, D₂O)
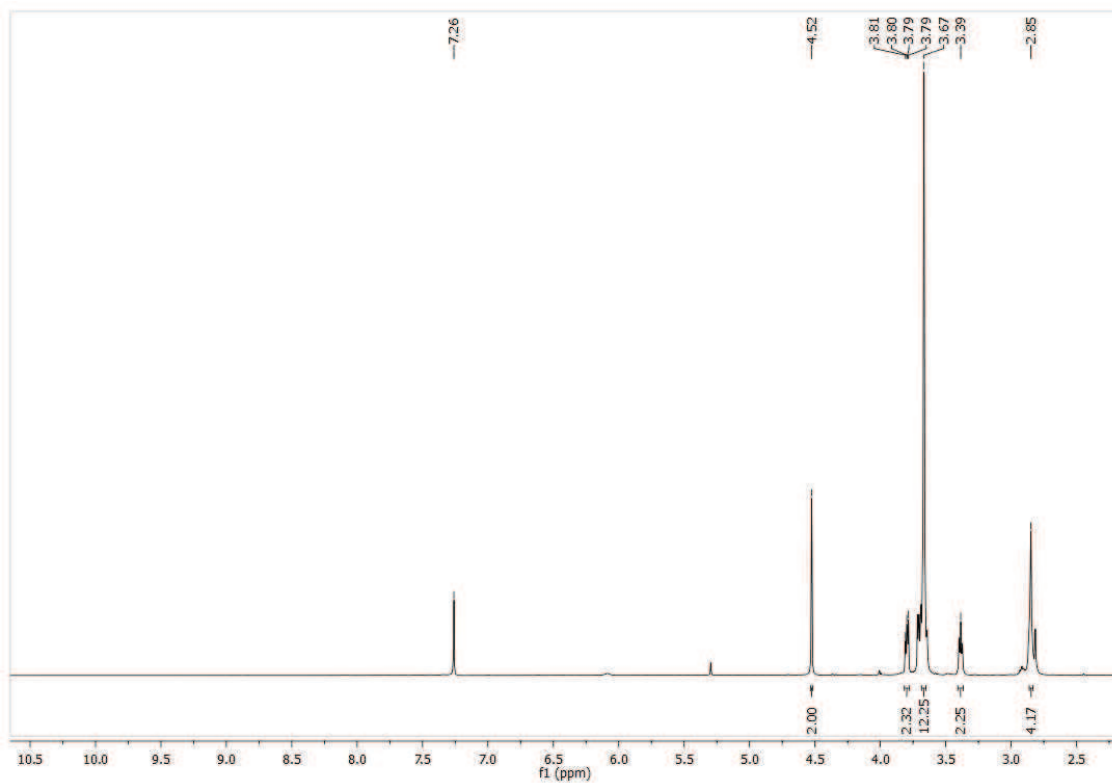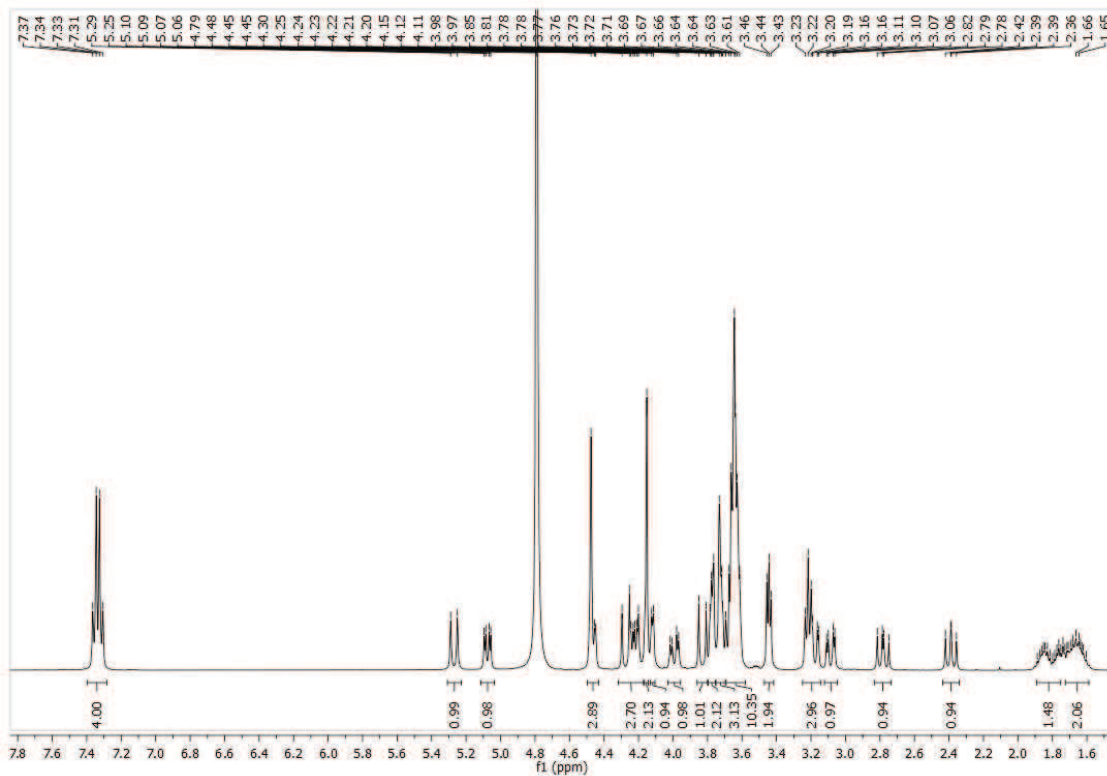
¹³C NMR (101 MHz, D₂O)
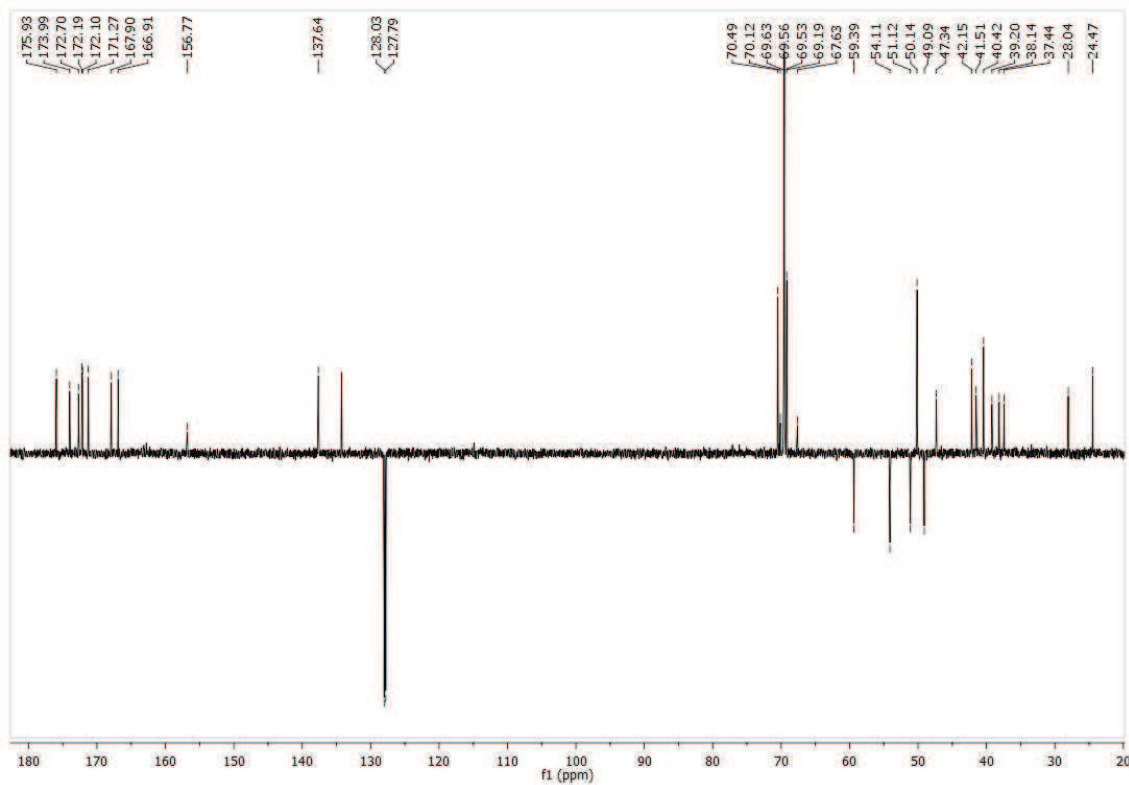
Fmoc-Val-Ala-OH **52**

^{1}H NMR (400 MHz, DMSO-d_6)
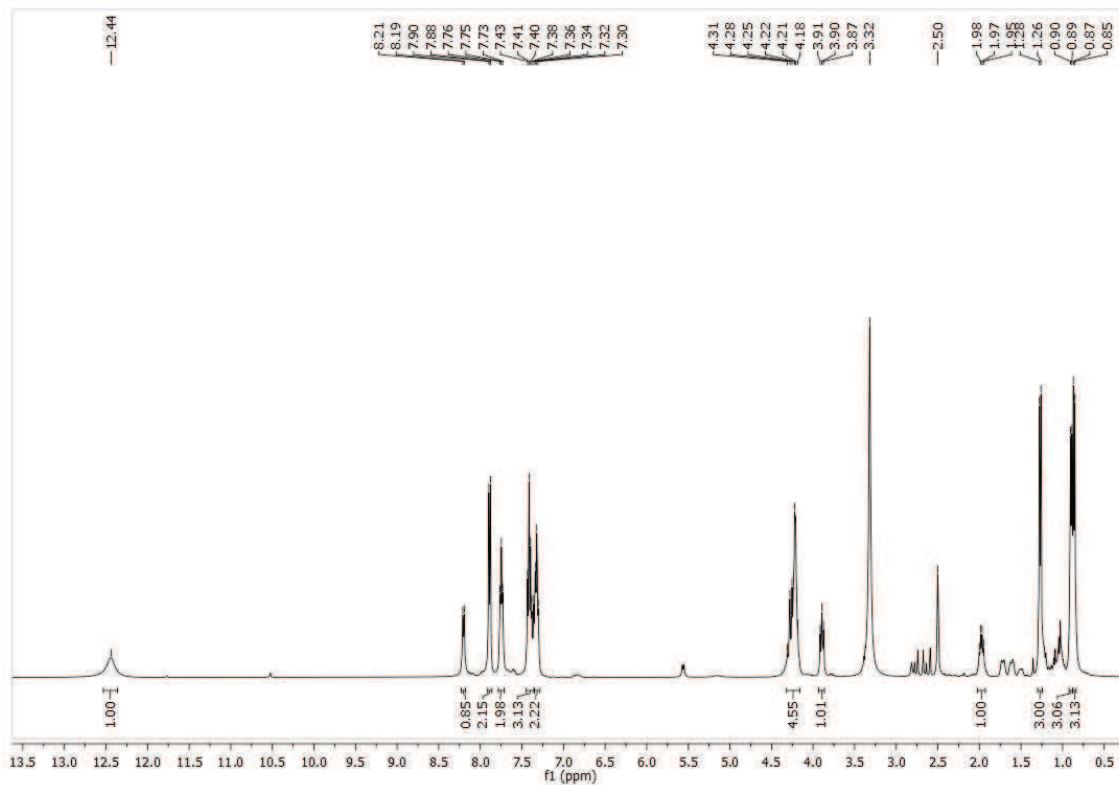
Fmoc-Val-Ala-PABOH **53**

^{1}H NMR (400 MHz, DMSO-d_6)
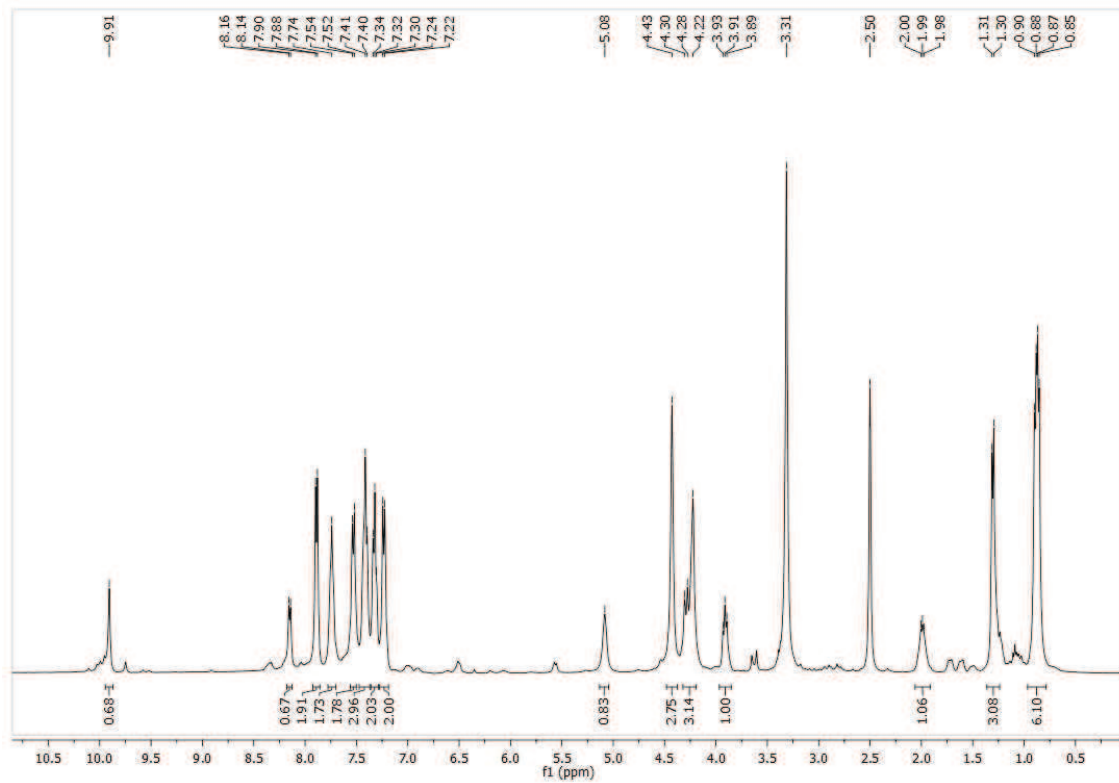
Fmoc-Val-Ala-PAB-PNP **54**
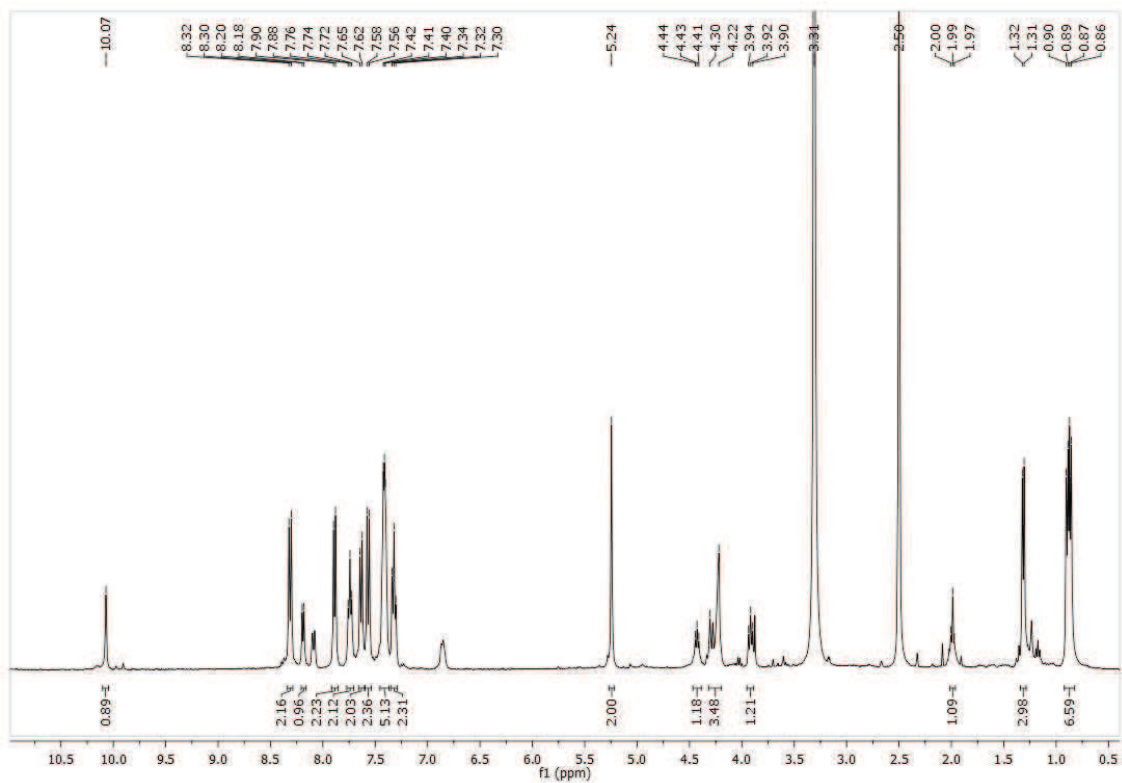
REFERENCES

(1)   WHO: World Health Organization - Cancer http://www.who.int/mediacentre/factsheets/ fs297/en/ (accessed May 28, 2018).

(2)   DeVita, V. T.; Chu, E. A History of Cancer Chemotherapy. *Cancer Res.* **2008**, *68* (21), 8643–8653.

(3)   Chari, R. V. J.; Miller, M. L.; Widdison, W. C. Antibody-Drug Conjugates: An Emerging Concept in Cancer Therapy. *Angew. Chemie Int. Ed.* **2014**, *53* (15), 3796–3827.

(4)   Nussbaumer, S.; Bonnabry, P.; Veuthey, J.-L.; Fleury-Souverain, S. Analysis of Anticancer Drugs: A Review. *Talanta* **2011**, *85* (5), 2265–2289.

(5)   Cheung-Ong, K.; Giaever, G.; Nislow, C. DNA-Damaging Agents in Cancer Chemotherapy: Serendipity and Chemical Biology. *Chem. Biol.* **2013**, *20* (5), 648–659.

(6)   Dezhenkova, L. G.; Tsvetkov, V. B.; Shtil, A. A. Topoisomerase I and II Inhibitors: Chemical Structure, Mechanisms of Action and Role in Cancer Chemotherapy. *Russ. Chem. Rev.* **2014**, *83* (1), 82–94.

(7)   Negi, A. S.; Gautam, Y.; Alam, S.; Chanda, D.; Luqman, S.; Sarkar, J.; Khan, F.; Konwar, R. Natural Antitubulin Agents: Importance of 3,4,5-Trimethoxyphenyl Fragment. *Bioorg. Med. Chem.* **2015**, *23* (3), 373–389.

(8)   Comprehensive Cancer Information - National Cancer Institute https://www.cancer.gov/ (accessed Jun 7, 2018).

(9)   Krall, N.; Scheuermann, J.; Neri, D. Small Targeted Cytotoxics: Current State and Promises from DNA-Encoded Chemical Libraries. *Angew. Chemie Int. Ed.* **2013**, *52* (5), 1384–1402.

(10)   Casi, G.; Neri, D. Antibody–Drug Conjugates and Small Molecule–Drug Conjugates: Opportunities and Challenges for the Development of Selective Anticancer Cytotoxic Agents. *J. Med. Chem.* **2015**, *58* (22), 8751–8761.

(11)   van der Veldt, A. A. M.; Hendrikse, N. H.; Smit, E. F.; Mooijer, M. P. J.; Rijnders, A. Y.; Gerritsen, W. R.; van der Hoeven, J. J. M.; Windhorst, A. D.; Lammertsma, A. A.; Lubberink, M. Biodistribution and Radiation Dosimetry of 11C-Labelled Docetaxel in Cancer Patients. *Eur. J. Nucl. Med. Mol. Imaging* **2010**, *37* (10), 1950–1958.

(12)   Strebhardt, K.; Ullrich, A. Paul Ehrlich's Magic Bullet Concept: 100 Years of Progress. *Nat. Rev. Cancer* **2008**, *8* (6), 473–480.

(13)   Cazzamalli, S.; Corso, A. D.; Neri, D. Targeted Delivery of Cytotoxic Drugs: Challenges, Opportunities and New Developments. *Chim. Int. J. Chem.* **2017**, *71* (10), 712–715.

(14)   Sun, G.-C.; Yang, X.; Yu, Y.; Zhao, D.-W. The Applications of Targeting Anti-Cancer Agents in Cancer Therapeutics. *Anticancer. Agents Med. Chem.* **2015**, *15* (7), 869–880.

(15)   Baudino, T. Targeted Cancer Therapy: The Next Generation of Cancer Treatment. *Curr. Drug Discov. Technol.* **2015**, *12* (1), 3–20.

(16)   Bhullar, K. S.; Lagarón, N. O.; McGowan, E. M.; Parmar, I.; Jha, A.; Hubbard, B. P.; Rupasinghe, H. P. V. Kinase-Targeted Cancer Therapies: Progress, Challenges and Future Directions. *Mol. Cancer* **2018**, *17* (1), 48.

(17)   Allen, T. M. Ligand-Targeted Therapeutics in Anticancer Therapy. *Nat. Rev. Cancer* **2002**, *2* (10), 750–763.

(18)   Srinivasarao, M.; Galliford, C. V.; Low, P. S. Principles in the Design of Ligand-Targeted Cancer Therapeutics and Imaging Agents. *Nat. Rev. Drug Discov.* **2015**, *14* (3), 203–219.

(19)   Wang, J.; Iyer, S.; Fielder, P. J.; Davis, J. D.; Deng, R. Projecting Human Pharmacokinetics of Monoclonal Antibodies from Nonclinical Data: Comparative Evaluation of Prediction Approaches in Early Drug Development. *Biopharmaceutics and Drug Disposition*. 2016, pp 51–65.

(20)   Köhler, G.; Milstein, C. Continuous Cultures of Fused Cells Secreting Antibody of Predefined Specificity. *Nature* **1975**, *256* (5517), 495–497.

(21)   Rodgers, K. R.; Chou, R. C. Therapeutic Monoclonal Antibodies and Derivatives: Historical Perspectives and Future Directions. *Biotechnology Advances*. Elsevier November 1, 2016, pp 1149–1158.

(22)   Kennedy, P. J.; Oliveira, C.; Granja, P. L.; Sarmento, B. Monoclonal Antibodies: Technologies for Early Discovery and Engineering. *Crit. Rev. Biotechnol.* **2018**, *38* (3), 394–408.

(23)   Scott, A. M.; Wolchok, J. D.; Old, L. J. Antibody Therapy of Cancer. *Nat. Rev. Cancer* **2012**, *12* (4), 278–287.

(24)   Baldo, B. A. Monoclonal Antibodies Approved for Cancer Therapy. In *Safety of Biologics Therapy*; Springer International Publishing: Cham, 2016; pp 57–140.

(25)   Leget, G. A.; Czuczman, M. S. Use of Rituximab, the New FDA-Approved Antibody. *Curr. Opin. Oncol.* **1998**, *10* (6), 548–551.

(26)   Marsh, R. A.; Lane, A.; Mehta, P. A.; Neumeier, L.; Jodele, S.; Davies, S. M.; Filipovich, A. H. Alemtuzumab Levels Impact Acute GVHD, Mixed Chimerism, and Lymphocyte Recovery Following Alemtuzumab, Fludarabine, and Melphalan RIC HCT. *Blood* **2016**, *127* (4), 503–512.

(27)   Arjaans, M.; Schröder, C. P.; Oosting, S. F.; Dafni, U.; Kleibeuker, J. E.; de Vries, E. G. E. VEGF Pathway Targeting Agents, Vessel Normalization and Tumor Drug Uptake: From Bench to Bedside. *Oncotarget* **2016**, *7* (16), 21247–21258.

(28)   Wu, M.; Rivkin, A.; Pham, T. Panitumumab: Human Monoclonal Antibody against Epidermal Growth Factor Receptors for the Treatment of Metastatic Colorectal Cancer. *Clin. Ther.* **2008**, *30* (1), 14–30.

(29)   Baselga, J.; Albanell, J. Mechanism of Action of Anti-HER2 Monoclonal Antibodies. *Ann. Oncol.* **2001**, *12* (suppl 1), S35–S41.

(30)   Privitera, G.; Luca, T.; Musso, N.; Vancheri, C.; Crimi, N.; Barresi, V.; Condorelli, D.; Castorina, S. In Vitro Antiproliferative Effect of Trastuzumab (Herceptin®) Combined with Cetuximab (Erbitux®) in a Model of Human Non-Small Cell Lung Cancer Expressing EGFR and HER2. *Clin. Exp. Med.* **2016**, *16* (2), 161–168.

(31)   Lin, J. H.; Guo, Y.; Wang, W. Challenges of Antibody Drug Conjugates in Cancer Therapy: Current Understanding of Mechanisms and Future Strategies. *Curr. Pharmacol. Reports* **2018**, *4* (1), 10–26.

(32)   Chari, R. V. J. Targeted Cancer Therapy: Conferring Specificity to Cytotoxic Drugs. **2007**.

(33)   Thomas, A.; Teicher, B. A.; Hassan, R. Antibody–drug Conjugates for Cancer Therapy. *Lancet Oncol.* **2016**, *17* (6), e254–e262.

(34)   Panowski, S.; Bhakta, S.; Raab, H.; Polakis, P.; Junutula, J. R. Site-Specific Antibody Drug Conjugates for Cancer Therapy. *MAbs* **2014**, *6* (1), 34–45.

(35)   Beck, A.; Goetsch, L.; Dumontet, C.; Corvaïa, N. Strategies and Challenges for the next Generation of Antibody–drug Conjugates. *Nat. Rev. Drug Discov.* **2017**, *16* (5), 315–337.

(36)   Tsuchikama, K.; An, Z. Antibody-Drug Conjugates: Recent Advances in Conjugation and Linker Chemistries. *Protein Cell* **2018**, *9* (1), 33–46.

(37)   Ritchie, M.; Tchistiakova, L.; Scott, N. Implications of Receptor-Mediated Endocytosis and Intracellular Trafficking Dynamics in the Development of Antibody Drug Conjugates. *MAbs* **2013**, *5* (1), 13–21.

(38)   Chalouni, C.; Doll, S. Fate of Antibody-Drug Conjugates in Cancer Cells. *J. Exp. Clin. Cancer Res.* **2018**, *37* (1), 20.

(39) Kovtun, Y. V; Goldmacher, V. S. Cell Killing by Antibody-Drug Conjugates. *Cancer Lett.* **2007**, *255* (2), 232–240.

(40) Li, F.; Emmerton, K. K.; Jonas, M.; Zhang, X.; Miyamoto, J. B.; Setter, J. R.; Nicholas, N. D.; Okeley, N. M.; Lyon, R. P.; Benjamin, D. R.; et al. Intracellular Released Payload Influences Potency and Bystander-Killing Effects of Antibody-Drug Conjugates in Preclinical Models. *Cancer Res.* **2016**, *76* (9), 2710–2719.

(41) Perrino, E.; Steiner, M.; Krall, N.; Bernardes, G. J. L.; Pretto, F.; Casi, G.; Neri, D. Curative Properties of Noninternalizing Antibody-Drug Conjugates Based on Maytansinoids. *Cancer Res.* **2014**, *74* (9), 2569–2578.

(42) Gébleux, R.; Stringhini, M.; Casanova, R.; Soltermann, A.; Neri, D. Non-Internalizing Antibody-Drug Conjugates Display Potent Anti-Cancer Activity upon Proteolytic Release of Monomethyl Auristatin E in the Subendothelial Extracellular Matrix. *Int. J. Cancer* **2017**, *140* (7), 1670–1679.

(43) Dal Corso, A.; Gébleux, R.; Murer, P.; Soltermann, A.; Neri, D. A Non-Internalizing Antibody-Drug Conjugate Based on an Anthracycline Payload Displays Potent Therapeutic Activity in Vivo. *J. Control. Release* **2017**, *264*, 211–218.

(44) Litvak-Greenfeld, D.; Benhar, I. Risks and Untoward Toxicities of Antibody-Based Immunoconjugates. *Adv. Drug Deliv. Rev.* **2012**, *64* (15), 1782–1799.

(45) Diamantis, N.; Banerji, U. Antibody-Drug Conjugates--an Emerging Class of Cancer Treatment. *Br. J. Cancer* **2016**, *114* (4), 362–367.

(46) Rossin, R.; Versteegen, R. M.; Wu, J.; Khasanov, A.; Wessels, H. J.; Steenbergen, E. J.; ten Hoeve, W.; Janssen, H. M.; van Onzen, A. H. A. M.; Hudson, P. J.; et al. Chemically Triggered Drug Release from an Antibody-Drug Conjugate Leads to Potent Antitumour Activity in Mice. *Nat. Commun.* **2018**, *9* (1), 1484.

(47) Deonarain, M.; Yahioglu, G.; Stamati, I.; Pomowski, A.; Clarke, J.; Edwards, B.; Diez-Posada, S.; Stewart, A. Small-Format Drug Conjugates: A Viable Alternative to ADCs for Solid Tumours? *Antibodies* **2018**, *7* (2), 16.

(48) Orcutt, K. D.; Adams, G. P.; Wu, A. M.; Silva, M. D.; Harwell, C.; Hoppin, J.; Matsumura, M.; Kotsuma, M.; Greenberg, J.; Scott, A. M.; et al. Molecular Simulation of Receptor Occupancy and Tumor Penetration of an Antibody and Smaller Scaffolds: Application to Molecular Imaging. *Mol. Imaging Biol.* **2017**, *19* (5), 656–664.

(49) Pollaro, L.; Raghunathan, S.; Morales-Sanfrutos, J.; Angelini, A.; Kontos, S.; Heinis, C. Bicyclic Peptides Conjugated to an Albumin-Binding Tag Diffuse Efficiently into Solid Tumors. *Mol. Cancer Ther.* **2015**, *14* (1), 151–161.

(50) Srinivasarao, M.; Low, P. S. Ligand-Targeted Drug Delivery. *Chem. Rev.* **2017**, *117* (19), 12133–12164.

(51) Nomura, N.; Pastorino, S.; Jiang, P.; Lambert, G.; Crawford, J. R.; Gymnopoulos, M.; Piccioni, D.; Juarez, T.; Pingle, S. C.; Makale, M.; et al. Prostate Specific Membrane Antigen (PSMA) Expression in Primary Gliomas and Breast Cancer Brain Metastases. *Cancer Cell Int.* **2014**, *14* (1), 26.

(52) Parker, N.; Turk, M. J.; Westrick, E.; Lewis, J. D.; Low, P. S.; Leamon, C. P. Folate Receptor Expression in Carcinomas and Normal Tissues Determined by a Quantitative Radioligand Binding Assay. *Anal. Biochem.* **2005**, *338* (2), 284–293.

(53) Crane, L. M. A.; Arts, H. J. G.; van Oosten, M.; Low, P. S.; van der Zee, A. G. J.; van Dam, G. M.; Bart, J. The Effect of Chemotherapy on Expression of Folate Receptor-Alpha in Ovarian Cancer. *Cell. Oncol.* **2012**, *35* (1), 9–18.

(54) Taylor, R. M.; Severns, V.; Brown, D. C.; Bisoffi, M.; Sillerud, L. O. Prostate Cancer Targeting Motifs: Expression of Av B3, Neurotensin Receptor 1, Prostate Specific Membrane Antigen, and Prostate Stem Cell Antigen in Human Prostate Cancer Cell Lines and Xenografts. *Prostate* **2012**, *72* (5), 523–532.

(55) Kularatne, S. A.; Wang, K.; Santhapuram, H.-K. R.; Low, P. S. Prostate-Specific Membrane Antigen

Targeted Imaging and Therapy of Prostate Cancer Using a PSMA Inhibitor as a Homing Ligand. *Mol. Pharm.* **2009**, *6* (3), 780–789.

(56)   Low, P. S.; Henne, W. A.; Doorneweerd, D. D. Discovery and Development of Folic-Acid-Based Receptor Targeting for Imaging and Therapy of Cancer and Inflammatory Diseases. *Acc. Chem. Res.* **2008**, *41* (1), 120–129.

(57)   Krall, N.; Pretto, F.; Decurtins, W.; Bernardes, G. J. L.; Supuran, C. T.; Neri, D. A Small-Molecule Drug Conjugate for the Treatment of Carbonic Anhydrase IX Expressing Tumors. *Angew. Chemie Int. Ed.* **2014**, *53* (16), 4231–4235.

(58)   Cazzamalli, S.; Dal Corso, A.; Widmayer, F.; Neri, D. Chemically Defined Antibody– and Small Molecule–Drug Conjugates for in Vivo Tumor Targeting Applications: A Comparative Analysis. *J. Am. Chem. Soc.* **2018**, *140* (5), 1617–1621.

(59)   Leamon, C. P.; Vlahov, I. R.; Reddy, J. A.; Vetzel, M.; Santhapuram, H. K. R.; You, F.; Bloomfield, A.; Dorton, R.; Nelson, M.; Kleindl, P.; et al. Folate–Vinca Alkaloid Conjugates for Cancer Therapy: A Structure–Activity Relationship. *Bioconjug. Chem.* **2014**, *25* (3), 560–568.

(60)   Kaminskas, L. M.; Kelly, B. D.; McLeod, V. M.; Sberna, G.; Owen, D. J.; Boyd, B. J.; Porter, C. J. H. Characterisation and Tumour Targeting of PEGylated Polylysine Dendrimers Bearing Doxorubicin via a PH Labile Linker. *J. Control. Release* **2011**, *152* (2), 241–248.

(61)   Chytil, P.; Etrych, T.; Koňák, Č.; Šírová, M.; Mrkvan, T.; Říhová, B.; Ulbrich, K. Properties of HPMA Copolymer–doxorubicin Conjugates with PH-Controlled Activation: Effect of Polymer Chain Modification. *J. Control. Release* **2006**, *115* (1), 26–36.

(62)   Hu, X.; Wang, R.; Yue, J.; Liu, S.; Xie, Z.; Jing, X. Targeting and Anti-Tumor Effect of Folic Acid-Labeled Polymer–Doxorubicin Conjugates with PH-Sensitive Hydrazone Linker. *J. Mater. Chem.* **2012**, *22* (26), 13303.

(63)   Rodrigues, P.; Scheuermann, K.; Stockmar, C.; Maier, G.; Fiebig, H.; Unger, C.; Mulhaupt, R.; Kratz, F. Synthesis and in Vitro Efficacy of Acid-Sensitive Poly(Ethylene Glycol) Paclitaxel Conjugates. *Bioorg. Med. Chem. Lett.* **2003**, *13* (3), 355–360.

(64)   Aryal, S.; Hu, C.-M. J.; Zhang, L. Polymer–Cisplatin Conjugate Nanoparticles for Acid-Responsive Drug Delivery. *ACS Nano* **2010**, *4* (1), 251–258.

(65)   Binauld, S.; Scarano, W.; Stenzel, M. H. PH-Triggered Release of Platinum Drugs Conjugated to Micelles via an Acid-Cleavable Linker. *Macromolecules* **2012**, *45* (17), 6989–6999.

(66)   Wong, P. T.; Choi, S. K. Mechanisms of Drug Release in Nanotherapeutic Delivery Systems. *Chem. Rev.* **2015**, *115* (9), 3388–3432.

(67)   Yang, J.; Chen, H.; Vlahov, I. R.; Cheng, J.-X.; Low, P. S. Evaluation of Disulfide Reduction during Receptor-Mediated Endocytosis by Using FRET Imaging. *Proc. Natl. Acad. Sci.* **2006**, *103* (37), 13872–13877.

(68)   Griffith, O. W. Biologic and Pharmacologic Regulation of Mammalian Glutathione Synthesis. *Free Radic. Biol. Med.* **1999**, *27* (9–10), 922–935.

(69)   Dubowchik, G. M.; Firestone, R. A. Cathepsin B-Sensitive Dipeptide Prodrugs. 1. A Model Study of Structural Requirements for Efficient Release of Doxorubicin. *Bioorg. Med. Chem. Lett.* **1998**, *8* (23), 3341–3346.

(70)   Dal Corso, A.; Caruso, M.; Belvisi, L.; Arosio, D.; Piarulli, U.; Albanese, C.; Gasparri, F.; Marsiglio, A.; Sola, F.; Troiani, S.; et al. Synthesis and Biological Evaluation of RGD Peptidomimetic-Paclitaxel Conjugates Bearing Lysosomally Cleavable Linkers. *Chem. - A Eur. J.* **2015**, *21* (18), 6921–6929.

(71)   Lewis Phillips, G. D.; Li, G.; Dugger, D. L.; Crocker, L. M.; Parsons, K. L.; Mai, E.; Blattler, W. A.; Lambert, J. M.; Chari, R. V. J.; Lutz, R. J.; et al. Targeting HER2-Positive Breast Cancer with Trastuzumab-DM1, an Antibody-Cytotoxic Drug Conjugate. *Cancer Res.* **2008**, *68* (22), 9280–9290.

(72)   Lambert, J. M.; Chari, R. V. J. Ado-Trastuzumab Emtansine (T-DM1): An Antibody–Drug Conjugate (ADC) for HER2-Positive Breast Cancer. *J. Med. Chem.* **2014**, *57* (16), 6949–6964.

(73) Cazzamalli, S.; Dal Corso, A.; Neri, D. Acetazolamide Serves as Selective Delivery Vehicle for Dipeptide-Linked Drugs to Renal Cell Carcinoma. *Mol. Cancer Ther.* **2016**, *15* (12), 2926–2935.

(74) Nahrwold, M.; Weiß, C.; Bogner, T.; Mertink, F.; Conradi, J.; Sammet, B.; Palmisano, R.; Royo Gracia, S.; Preuße, T.; Sewald, N. Conjugates of Modified Cryptophycins and RGD-Peptides Enter Target Cells by Endocytosis. *J. Med. Chem.* **2013**, *56* (5), 1853–1864.

(75) Krall, N.; Pretto, F.; Neri, D. A Bivalent Small Molecule-Drug Conjugate Directed against Carbonic Anhydrase IX Can Elicit Complete Tumour Regression in Mice. *Chem. Sci.* **2014**, *5* (9), 3640.

(76) Reddy, J. A.; Dorton, R.; Bloomfield, A.; Nelson, M.; Vetzel, M.; Guan, J.; Leamon, C. P. Rational Combination Therapy of Vintafolide (EC145) with Commonly Used Chemotherapeutic Drugs. *Clin. Cancer Res.* **2014**, *20* (8), 2104–2114.

(77) U.S. National Library of Medicine. ClinicalTrials.gov https://clinicaltrials.gov/ (accessed Jul 23, 2018).

(78) Leamon, C. P.; Lovejoy, C. D.; Nguyen, B. Pharmacogenomics and Personalized Medicine Patient Selection and Targeted Treatment in the Management of Platinum-Resistant Ovarian Cancer. *Pharmgenomics. Pers. Med.* **2013**, 6–113.

(79) Morris, M. J.; Vogelzang, N. J.; Sartor, O.; Armour, A.; Petrylak, D.; Tolcher, A.; Ejadi, S.; Babiker, H. M. Phase 1 Study of the PSMA-Targeted Tubulysin Small-Molecule Drug Conjugate EC1169 in Patients with Metastatic Castrate-Resistant Prostate Cancer (MCRPC): Study Update. *Ann. Oncol.* **2016**, *27* (suppl_6).

(80) Autio, K. A.; Dreicer, R.; Anderson, J.; Garcia, J. A.; Alva, A.; Hart, L. L.; Milowsky, M. I.; Posadas, E. M.; Ryan, C. J.; Graf, R. P.; et al. Safety and Efficacy of BIND-014, a Docetaxel Nanoparticle Targeting Prostate-Specific Membrane Antigen for Patients With Metastatic Castration-Resistant Prostate Cancer. *JAMA Oncol.* **2018**.

(81) Curnis, F.; Sacchi, A.; Borgna, L.; Magni, F.; Gasparri, A.; Corti, A. Enhancement of Tumor Necrosis Factor α Antitumor Immunotherapeutic Properties by Targeted Delivery to Aminopeptidase N (CD13). *Nat. Biotechnol.* **2000**, *18* (11), 1185–1190.

(82) Larrick, J. W.; Wright, S. C. Cytotoxic Mechanism of Tumor Necrosis Factor-Alpha. *FASEB J.* **1990**, *4* (14), 3215–3223.

(83) Kurzrock, R.; Gabrail, N.; Chandhasin, C.; Moulder, S.; Smith, C.; Brenner, A.; Sankhala, K.; Mita, A.; Elian, K.; Bouchard, D.; et al. Safety, Pharmacokinetics, and Activity of GRN1005, a Novel Conjugate of Angiopep-2, a Peptide Facilitating Brain Penetration, and Paclitaxel, in Patients with Advanced Solid Tumors. *Mol. Cancer Ther.* **2012**, *11* (2), 308–316.

(84) Humphries, M. J. Integrin Structure. *Biochem. Soc. Trans.* **2000**, *28* (4), 311–339.

(85) Hynes, R. O. Integrins: Bidirectional, Allosteric Signaling Machines. *Cell* **2002**, *110* (6), 673–687.

(86) Barczyk, M.; Carracedo, S.; Gullberg, D. Integrins. *Cell Tissue Res.* **2010**, *339* (1), 269–280.

(87) Danhier, F.; Le Breton, A.; Préat, V. RGD-Based Strategies To Target Alpha(v) Beta(3) Integrin in Cancer Therapy and Diagnosis. *Mol. Pharm.* **2012**, *9* (11), 2961–2973.

(88) Nieberler, M.; Reuning, U.; Reichart, F.; Notni, J.; Wester, H.-J.; Schwaiger, M.; Weinmüller, M.; Räder, A.; Steiger, K.; Kessler, H. Exploring the Role of RGD-Recognizing Integrins in Cancer. *Cancers (Basel).* **2017**, *9* (12), 116.

(89) Mas-Moruno, C.; Fraioli, R.; Rechenmacher, F.; Neubauer, S.; Kapp, T. G.; Kessler, H. Avβ3- or A5β1-Integrin-Selective Peptidomimetics for Surface Coating. *Angew. Chemie Int. Ed.* **2016**, *55* (25), 7048–7067.

(90) Cox, D.; Brennan, M.; Moran, N. Integrins as Therapeutic Targets: Lessons and Opportunities. *Nat. Rev. Drug Discov.* **2010**, *9* (10), 804–820.

(91) Guo, W.; Giancotti, F. G. Integrin Signalling during Tumour Progression. *Nat. Rev. Mol. Cell Biol.* **2004**, *5* (10), 816–826.

(92) Desgrosellier, J. S.; Cheresh, D. A. Integrins in Cancer: Biological Implications and Therapeutic

Opportunities. *Nat. Rev. Cancer* **2010**, *10* (1), 9–22.

(93) Seguin, L.; Desgrosellier, J. S.; Weis, S. M.; Cheresh, D. A. Integrins and Cancer: Regulators of Cancer Stemness, Metastasis, and Drug Resistance. *Trends Cell Biol.* **2015**, *25* (4), 234–240.

(94) Pytela, R.; Pierschbacher, M. D.; Ruoslahti, E. Identification and Isolation of a 140 Kd Cell Surface Glycoprotein with Properties Expected of a Fibronectin Receptor. *Cell* **1985**, *40* (1), 191–198.

(95) Arosio, D.; Casagrande, C. Advancement in Integrin Facilitated Drug Delivery. *Adv. Drug Deliv. Rev.* **2016**, *97*, 111–143.

(96) Alghisi, G. C.; Rüegg, C. Vascular Integrins in Tumor Angiogenesis: Mediators and Therapeutic Targets. *Endothelium* **2006**, *13* (2), 113–135.

(97) Avraamides, C. J.; Garmy-Susini, B.; Varner, J. A. Integrins in Angiogenesis and Lymphangiogenesis. *Nat. Rev. Cancer* **2008**, *8* (8), 604–617.

(98) Francavilla, C.; Maddaluno, L.; Cavallaro, U. The Functional Role of Cell Adhesion Molecules in Tumor Angiogenesis. *Semin. Cancer Biol.* **2009**, *19* (5), 298–309.

(99) Ruoslahti, E.; Pierschbacher, M. D. New Perspectives in Cell Adhesion: RGD and Integrins. *Science* **1987**, *238* (4826), 491–497.

(100) Xiong, J. P.; Stehle, T.; Zhang, R.; Joachimiak, A.; Frech, M.; Goodman, S. L.; Arnaout, M. A. Crystal Structure of the Extracellular Segment of Integrin AVβ3 in Complex with an Arg-Gly-Asp Ligand. *Science (80-.).* **2002**, *296* (5565), 151–155.

(101) Gottschalk, K.-E.; Kessler, H. The Structures of Integrins and Integrin–Ligand Complexes: Implications for Drug Design and Signal Transduction. *Angew. Chemie Int. Ed.* **2002**, *41* (20), 3767–3774.

(102) Katsamakas, S.; Chatzisideri, T.; Thysiadis, S.; Sarli, V. RGD-Mediated Delivery of Small-Molecule Drugs. *Future Med. Chem.* **2017**, *9* (6), 579–604.

(103) Kapp, T. G.; Rechenmacher, F.; Neubauer, S.; Maltsev, O. V.; Cavalcanti-Adam, E. A.; Zarka, R.; Reuning, U.; Notni, J.; Wester, H.-J.; Mas-Moruno, C.; et al. A Comprehensive Evaluation of the Activity and Selectivity Profile of Ligands for RGD-Binding Integrins. *Sci. Rep.* **2017**, *7*, 39805.

(104) Hautanen, A.; Gailit, J.; Mann, D. M.; Ruoslahti, E. Effects of Modifications of the RGD Sequence and Its Context on Recognition by the Fibronectin Receptor. *J. Biol. Chem.* **1989**, *264* (3), 1437–1442.

(105) Bogdanowich-Knipp, S. J.; Chakrabarti, S.; Williams, T. D.; Dillman, R. K.; Siahaan, T. J. Solution Stability of Linear vs. Cyclic RGD Peptides. *J. Pept. Res.* **1999**, *53* (5), 530–541.

(106) Meyer, A.; Auernheimer, J.; Modlinger, A.; Kessler, H. Targeting RGD Recognizing Integrins: Drug Development, Biomaterial Research, Tumor Imaging and Targeting. *Curr. Pharm. Des.* **2006**, *12* (22), 2723–2747.

(107) Chatterjee, J.; Gilon, C.; Hoffman, A.; Kessler, H. N-Methylation of Peptides: A New Perspective in Medicinal Chemistry. *Acc. Chem. Res.* **2008**, *41* (10), 1331–1342.

(108) Aumailley, M.; Gurrath, M.; Müller, G.; Calvete, J.; Timpl, R.; Kessler, H. Arg-Gly-Asp Constrained within Cyclic Pentapoptides Strong and Selective Inhibitors of Cell Adhesion to Vitronectin and Laminin Fragment P1. *FEBS Lett.* **1991**, *291* (1), 50–54.

(109) Pfaff, M.; Tangemann, K.; Muller, B.; Gurrath, M.; Muller, G.; Kessler, H.; Timpl, R.; Engel, J. Selective Recognition of Cyclic RGD Peptides of NMR Defined Conformation by AIIbβ3, AVβ3, and A5β1 Integrins. *J. Biol. Chem.* **1994**, *269* (32), 20233–20238.

(110) Haubner, R.; Gratias, R.; Diefenbach, B.; Goodman, S. L.; Jonczyk, A.; Kessler, H. Structural and Functional Aspects of RGD-Containing Cyclic Pentapeptides as Highly Potent and Selective Integrin α(v)B3 Antagonists. *J. Am. Chem. Soc.* **1996**, *118* (32), 7461–7472.

(111) Dechantsreiter, M. A.; Planker, E.; Mathä, B.; Lohof, E.; Hölzemann, G.; Jonczyk, A.; Goodman, S. L.; Kessler, H. N-Methylated Cyclic RGD Peptides as Highly Active and Selective AVβ3 Integrin Antagonists. *J. Med. Chem.* **1999**, *42* (16), 3033–3040.

(112) Mas-Moruno, C.; Rechenmacher, F.; Kessler, H. Cilengitide: The First Anti-Angiogenic Small Molecule Drug Candidate Design, Synthesis and Clinical Evaluation. *Anticancer. Agents Med. Chem.* **2010**, *10* (10), 753–768.

(113) Nabors, L. B.; Fink, K. L.; Mikkelsen, T.; Grujicic, D.; Tarnawski, R.; Nam, D. H.; Mazurkiewicz, M.; Salacz, M.; Ashby, L.; Zagonel, V.; et al. Two Cilengitide Regimens in Combination with Standard Treatment for Patients with Newly Diagnosed Glioblastoma and Unmethylated MGMT Gene Promoter: Results of the Open-Label, Controlled, Randomized Phase II CORE Study. *Neuro. Oncol.* **2015**, *17* (5), 708–717.

(114) Tucci, M.; Stucci, S.; Felici, C.; Cafforio, P.; Resta, L.; Rossi, R.; Silvestris, F. Cilengitide Restrains the Osteoclast-like Bone Resorbing Activity of Myeloma Plasma Cells. *Br. J. Haematol.* **2016**, *173* (1), 59–69.

(115) Alva, A.; Slovin, S.; Daignault, S.; Carducci, M.; Dipaola, R.; Pienta, K.; Agus, D.; Cooney, K.; Chen, A.; Smith, D. C.; et al. Phase II Study of Cilengitide (EMD 121974, NSC 707544) in Patients with Non-Metastatic Castration Resistant Prostate Cancer, NCI-6735. A Study by the DOD/PCF Prostate Cancer Clinical Trials Consortium. *Invest. New Drugs* **2012**, *30* (2), 749–757.

(116) Stupp, R.; Hegi, M. E.; Gorlia, T.; Erridge, S. C.; Perry, J.; Hong, Y. K.; Aldape, K. D.; Lhermitte, B.; Pietsch, T.; Grujicic, D.; et al. Cilengitide Combined with Standard Treatment for Patients with Newly Diagnosed Glioblastoma with Methylated MGMT Promoter (CENTRIC EORTC 26071-22072 Study): A Multicentre, Randomised, Open-Label, Phase 3 Trial. *Lancet. Oncol.* **2014**, *15* (10), 1100–1108.

(117) Marelli, U. K.; Rechenmacher, F.; Sobahi, T. R. A.; Mas-Moruno, C.; Kessler, H. Tumor Targeting via Integrin Ligands. *Front. Oncol.* **2013**, *3*, 222.

(118) Dal Corso, A.; Pignataro, L.; Belvisi, L.; Gennari, C. Avβ3 Integrin-Targeted Peptide/Peptidomimetic-Drug Conjugates: In-Depth Analysis of the Linker Technology. *Curr. Top. Med. Chem.* **2016**, *16* (3), 314–329.

(119) Kolvunen, E.; Wang, B.; Ruoslahti, E. Phage Libraries Displaying Cyclic Peptides with Different Ring Sizes: Ligand Specificities of the Rgd-Directed Integrine. *Bio/Technology* **1995**, *13* (3), 265–270.

(120) Arap, W.; Pasqualini, R.; Ruoslahti, E. Cancer Treatment by Targeted Drug Delivery to Tumor Vasculature in a Mouse Model. *Science* **1998**, *279* (5349), 377–380.

(121) de Groot, F. M. H.; Broxterman, H. J.; Adams, H. P. H. M.; van Vliet, A.; Tesser, G. I.; Elderkamp, Y. W.; Schraa, A. J.; Kok, R. J.; Molema, G.; Pinedo, H. M.; et al. Design, Synthesis, and Biological Evaluation of a Dual Tumor-Specific Motive Containing Integrin-Targeted Plasmin-Cleavable Doxorubicin Prodrug. *Mol. Cancer Ther.* **2002**, *1* (11), 901–911.

(122) Xiong, X.-B.; Mahmud, A.; Uludağ, H.; Lavasanifar, A. Multifunctional Polymeric Micelles for Enhanced Intracellular Delivery of Doxorubicin to Metastatic Cancer Cells. *Pharm. Res.* **2008**, *25* (11), 2555–2566.

(123) Xiong, X.-B.; Ma, Z.; Lai, R.; Lavasanifar, A. The Therapeutic Response to Multifunctional Polymeric Nano-Conjugates in the Targeted Cellular and Subcellular Delivery of Doxorubicin. *Biomaterials* **2010**, *31* (4), 757–768.

(124) Wang, H.; Chen, K.; Cai, W.; Li, Z.; He, L.; Kashefi, A.; Chen, X. Integrin-Targeted Imaging and Therapy with RGD4C-TNF Fusion Protein. *Mol. Cancer Ther.* **2008**, *7* (5), 1044–1053.

(125) Ressurreição, A. S. M.; Bordessa, A.; Civera, M.; Belvisi, L.; Gennari, C.; Piarulli, U. Synthesis and Conformational Studies of Peptidomimetics Containing a New Bifunctional Diketopiperazine Scaffold Acting as a β-Hairpin Inducer. *J. Org. Chem.* **2008**, *73* (2), 652–660.

(126) da Ressurreição, A. S. M.; Vidu, A.; Civera, M.; Belvisi, L.; Potenza, D.; Manzoni, L.; Ongeri, S.; Gennari, C.; Piarulli, U. Cyclic RGD-Peptidomimetics Containing Bifunctional Diketopiperazine Scaffolds as New Potent Integrin Ligands. *Chem. - A Eur. J.* **2009**, *15* (45), 12184–12188.

(127) Marchini, M.; Mingozzi, M.; Colombo, R.; Guzzetti, I.; Belvisi, L.; Vasile, F.; Potenza, D.; Piarulli, U.; Arosio, D.; Gennari, C. Cyclic RGD Peptidomimetics Containing Bifunctional Diketopiperazine

Scaffolds as New Potent Integrin Ligands. *Chem. - A Eur. J.* **2012**, *18* (20), 6195–6207.

(128) Guzzetti, I.; Civera, M.; Vasile, F.; Araldi, E. M.; Belvisi, L.; Gennari, C.; Potenza, D.; Fanelli, R.; Piarulli, U. Determination of the Binding Epitope of RGD-Peptidomimetics to Avβ3 and AIIbβ3 Integrin-Rich Intact Cells by NMR and Computational Studies. *Org. Biomol. Chem.* **2013**, *11* (23), 3886.

(129) Fanelli, R.; Schembri, L.; Piarulli, U.; Pinoli, M.; Rasini, E.; Paolillo, M.; Galiazzo, M. C.; Cosentino, M.; Marino, F. Effects of a Novel Cyclic RGD Peptidomimetic on Cell Proliferation, Migration and Angiogenic Activity in Human Endothelial Cells. *Vasc. Cell* **2014**, *6*, 11.

(130) Panzeri, S.; Zanella, S.; Arosio, D.; Vahdati, L.; Dal Corso, A.; Pignataro, L.; Paolillo, M.; Schinelli, S.; Belvisi, L.; Gennari, C.; et al. Cyclic *Iso* DGR and RGD Peptidomimetics Containing Bifunctional Diketopiperazine Scaffolds Are Integrin Antagonists. *Chem. - A Eur. J.* **2015**, *21* (16), 6265–6271.

(131) Colombo, R.; Mingozzi, M.; Belvisi, L.; Arosio, D.; Piarulli, U.; Carenini, N.; Perego, P.; Zaffaroni, N.; De Cesare, M.; Castiglioni, V.; et al. Synthesis and Biological Evaluation (in Vitro and in Vivo) of Cyclic Arginine–Glycine–Aspartate (RGD) Peptidomimetic–Paclitaxel Conjugates Targeting Integrin α ᵥ β ₃. *J. Med. Chem.* **2012**, *55* (23), 10460–10474.

(132) Pina, A.; Dal Corso, A.; Caruso, M.; Belvisi, L.; Arosio, D.; Zanella, S.; Gasparri, F.; Albanese, C.; Cucchi, U.; Fraietta, I.; et al. Targeting Integrin AVβ3with Theranostic RGD-Camptothecin Conjugates Bearing a Disulfide Linker: Biological Evaluation Reveals a Complex Scenario. *ChemistrySelect* **2017**, *2* (17), 4759–4766.

(133) López Rivas, P.; Ranđelović, I.; Raposo Moreira Dias, A.; Pina, A.; Arosio, D.; Tóvári, J.; Mező, G.; Dal Corso, A.; Pignataro, L.; Gennari, C. Synthesis and Biological Evaluation of Paclitaxel Conjugates Involving Lysosomally Cleavable Linkers and AVβ3-Integrin Ligands for Tumor Targeting. *European J. Org. Chem.* **2018**, *23* (71), 18066–18073.

(134) Bareford, L. M.; Swaan, P. W. Endocytic Mechanisms for Targeted Drug Delivery. *Advanced Drug Delivery Reviews*. August 10, 2007, pp 748–758.

(135) Temming, K.; Schiffelers, R. M.; Molema, G.; Kok, R. J. RGD-Based Strategies for Selective Delivery of Therapeutics and Imaging Agents to the Tumour Vasculature. *Drug Resistance Updates*. Churchill Livingstone December 1, 2005, pp 381–402.

(136) Chen, K.; Chen, X. Integrin Targeted Delivery of Chemotherapeutics. *Theranostics* **2011**, *1*, 189–200.

(137) Gaertner, F. C.; Kessler, H.; Wester, H.-J.; Schwaiger, M.; Beer, A. J. Radiolabelled RGD Peptides for Imaging and Therapy. *Eur. J. Nucl. Med. Mol. Imaging* **2012**, *39* (S1), 126–138.

(138) Burkhart, D. J.; Kalet, B. T.; Coleman, M. P.; Post, G. C.; Koch, T. H. Doxorubicin-Formaldehyde Conjugates Targeting Alphavbeta3 Integrin. *Mol. Cancer Ther.* **2004**, *3* (12), 1593–1604.

(139) Ryppa, C.; Mann-Steinberg, H.; Fichtner, I.; Weber, H.; Satchi-Fainaro, R.; Biniossek, M. L.; Kratz, F. In Vitro and in Vivo Evaluation of Doxorubicin Conjugates with the Divalent Peptide E-[c(RGDfK)2] That Targets Integrin α Vβ3. *Bioconjug. Chem.* **2008**, *19* (7), 1414–1422.

(140) Crisp, J. L.; Savariar, E. N.; Glasgow, H. L.; Ellies, L. G.; Whitney, M. A.; Tsien, R. Y. Dual Targeting of Integrin v 3 and Matrix Metalloproteinase-2 for Optical Imaging of Tumors and Chemotherapeutic Delivery. *Mol. Cancer Ther.* **2014**, *13* (6), 1514–1525.

(141) Dal Pozzo, A.; Ni, M.-H.; Esposito, E.; Dallavalle, S.; Musso, L.; Bargiotti, A.; Pisano, C.; Vesci, L.; Bucci, F.; Castorina, M.; et al. Novel Tumor-Targeted RGD Peptide–camptothecin Conjugates: Synthesis and Biological Evaluation. *Bioorg. Med. Chem.* **2010**, *18* (1), 64–72.

(142) Curnis, F.; Longhi, R.; Crippa, L.; Cattaneo, A.; Dondossola, E.; Bachi, A.; Corti, A. Spontaneous Formation of L-Isoaspartate and Gain of Function in Fibronectin. *J. Biol. Chem.* **2006**, *281* (47), 36466–36476.

(143) Corti, A.; Curnis, F. Isoaspartate-Dependent Molecular Switches for Integrin-Ligand Recognition. *J. Cell Sci.* **2011**, *124* (4), 515–522.

(144) Spitaleri, A.; Mari, S.; Curnis, F.; Traversari, C.; Longhi, R.; Bordignon, C.; Corti, A.; Rizzardi, G.-P.; Musco, G. Structural Basis for the Interaction of IsoDGR with the RGD-Binding Site of Alphavbeta3 Integrin. *J. Biol. Chem.* **2008**, *283* (28), 19757–19768.

(145) Curnis, F.; Sacchi, A.; Gasparri, A.; Longhi, R.; Bachi, A.; Doglioni, C.; Bordignon, C.; Traversari, C.; Rizzardi, G.-P.; Corti, A. Isoaspartate-Glycine-Arginine: A New Tumor Vasculature-Targeting Motif. *Cancer Res.* **2008**, *68* (17), 7073–7082.

(146) Curnis, F.; Cattaneo, A.; Longhi, R.; Sacchi, A.; Gasparri, A. M.; Pastorino, F.; Di Matteo, P.; Traversari, C.; Bachi, A.; Ponzoni, M.; et al. Critical Role of Flanking Residues in NGR-to-IsoDGR Transition and CD13/Integrin Receptor Switching. *J. Biol. Chem.* **2010**, *285* (12), 9114–9123.

(147) Ghitti, M.; Spitaleri, A.; Valentinis, B.; Mari, S.; Asperti, C.; Traversari, C.; Rizzardi, G. P.; Musco, G. Molecular Dynamics Reveal That IsoDGR-Containing Cyclopeptides Are True Avβ3 Antagonists Unable To Promote Integrin Allostery and Activation. *Angew. Chemie Int. Ed.* **2012**, *51* (31), 7702–7705.

(148) Curnis, F.; Sacchi, A.; Longhi, R.; Colombo, B.; Gasparri, A.; Corti, A. IsoDGR-Tagged Albumin: A New Avβ3 Selective Carrier for Nanodrug Delivery to Tumors. *Small* **2013**, *9* (5), 673–678.

(149) Nardelli, F.; Paissoni, C.; Quilici, G.; Gori, A.; Traversari, C.; Valentinis, B.; Sacchi, A.; Corti, A.; Curnis, F.; Ghitti, M.; et al. Succinimide-Based Conjugates Improve IsoDGR Cyclopeptide Affinity to Avβ3 without Promoting Integrin Allosteric Activation. *J. Med. Chem.* **2018**, acs.jmedchem.8b00745.

(150) Reynolds, A. R.; Hart, I. R.; Watson, A. R.; Welti, J. C.; Silva, R. G.; Robinson, S. D.; Da Violante, G.; Gourlaouen, M.; Salih, M.; Jones, M. C.; et al. Stimulation of Tumor Growth and Angiogenesis by Low Concentrations of RGD-Mimetic Integrin Inhibitors. *Nat. Med.* **2009**, *15* (4), 392–400.

(151) Mingozzi, M.; Dal Corso, A.; Marchini, M.; Guzzetti, I.; Civera, M.; Piarulli, U.; Arosio, D.; Belvisi, L.; Potenza, D.; Pignataro, L.; et al. Cyclic Iso DGR Peptidomimetics as Low-Nanomolar α v β 3 Integrin Ligands. *Chem. - A Eur. J.* **2013**, *19* (11), 3563–3567.

(152) Frank, A. O.; Otto, E.; Mas-Moruno, C.; Schiller, H. B.; Marinelli, L.; Cosconati, S.; Bochen, A.; Vossmeyer, D.; Zahn, G.; Stragies, R.; et al. Conformational Control of Integrin-Subtype Selectivity in IsoDGR Peptide Motifs: A Biological Switch. *Angew. Chemie Int. Ed.* **2010**, *49* (48), 9278–9281.

(153) Russo, M. A.; Paolillo, M.; Sanchez-Hernandez, Y.; Curti, D.; Ciusani, E.; Serra, M.; Colombo, L.; Schinelli, S. A Small-Molecule RGD-Integrin Antagonist Inhibits Cell Adhesion, Cell Migration and Induces Anoikis in Glioblastoma Cells. *Int. J. Oncol.* **2013**, *42* (1), 83–92.

(154) Sulzmaier, F. J.; Jean, C.; Schlaepfer, D. D. FAK in Cancer: Mechanistic Findings and Clinical Applications. *Nat. Rev. Cancer* **2014**, *14* (9), 598–610.

(155) Zanella, S.; Angerani, S.; Pina, A.; López Rivas, P.; Giannini, C.; Panzeri, S.; Arosio, D.; Caruso, M.; Gasparri, F.; Fraietta, I.; et al. Tumor Targeting with an *Iso* DGR-Drug Conjugate. *Chem. - A Eur. J.* **2017**, *23* (33), 7910–7914.

(156) Marchini, M.; Mingozzi, M.; Colombo, R.; Gennari, C.; Durini, M.; Piarulli, U. Selective O-Acylation of Unprotected N-Benzylserine Methyl Ester and O,N-Acyl Transfer in the Formation of Cyclo[Asp-Ser] Diketopiperazines. *Tetrahedron* **2010**, *66* (49), 9528–9531.

(157) Bodero, L.; López Rivas, P.; Korsak, B.; Hechler, T.; Pahl, A.; Müller, C.; Arosio, D.; Pignataro, L.; Gennari, C.; Piarulli, U. Synthesis and Biological Evaluation of RGD and IsoDGR Peptidomimetic-α-Amanitin Conjugates for Tumor-Targeting. *Beilstein J. Org. Chem.* **2018**, *14* (1), 407–415.

(158) Wienland, T.; Faulstich, H. Fifty Years of Amanitin. *Experientia* **1991**, *47* (11–12), 1186–1193.

(159) Wieland, T.; Faulstich, H.; Fiume, L. Amatoxins, Phallotoxins, Phallolysin, and Antamanide: The Biologically Active Components of Poisonous *Amanita* Mushroom. *CRC Crit. Rev. Biochem.* **1978**, *5* (3), 185–260.

(160) Vetter, J. Toxins of Amanita Phalloides. *Toxicon* **1998**, *36* (1), 13–24.

(161) Anderl, J.; Echner, H.; Faulstich, H. Chemical Modification Allows Phallotoxins and Amatoxins to

Be Used as Tools in Cell Biology. *Beilstein J. Org. Chem.* **2012**, *8* (1), 2072–2084.

(162)   Fiume, L.; Stirpe, F. Decreased RNA Content in Mouse Liver Nuclei after Intoxication with [Alpha]-Amanitin. *Biochim. Biophys. Acta - Nucleic Acids Protein Synth.* **1966**, *123* (3), 643–645.

(163)   Bushnell, D. A.; Cramer, P.; Kornberg, R. D. Structural Basis of Transcription: Alpha-Amanitin-RNA Polymerase II Cocrystal at 2.8 A Resolution. *Proc. Natl. Acad. Sci. U. S. A.* **2002**, *99* (3), 1218–1222.

(164)   Letschert, K.; Faulstich, H.; Keller, D.; Keppler, D. Molecular Characterization and Inhibition of Amanitin Uptake into Human Hepatocytes. *Toxicol. Sci.* **2006**, *91* (1), 140–149.

(165)   Garcia, J.; Costa, V. M.; Carvalho, A.; Baptista, P.; de Pinho, P. G.; de Lourdes Bastos, M.; Carvalho, F. Amanita Phalloides Poisoning: Mechanisms of Toxicity and Treatment. *Food Chem. Toxicol.* **2015**, *86*, 41–55.

(166)   Davis, M. T.; Preston, J. F. A Conjugate of Alpha-Amanitin and Monoclonal Immunoglobulin G to Thy 1.2 Antigen Is Selectively Toxic to T Lymphoma Cells. *Science* **1981**, *213* (4514), 1385–1388.

(167)   Moldenhauer, G.; Salnikov, A. V.; Lüttgau, S.; Herr, I.; Anderl, J.; Faulstich, H. Therapeutic Potential of Amanitin-Conjugated Anti-Epithelial Cell Adhesion Molecule Monoclonal Antibody Against Pancreatic Carcinoma. *JNCI J. Natl. Cancer Inst.* **2012**, *104* (8), 622–634.

(168)   Moshnikova, A.; Moshnikova, V.; Andreev, O. A.; Reshetnyak, Y. K. Antiproliferative Effect of PHLIP-Amanitin. *Biochemistry* **2013**, *52* (7), 1171–1178.

(169)   Zhao, L.; May, J. P.; Blanc, A.; Dietrich, D. J.; Loonchanta, A.; Matinkhoo, K.; Pryyma, A.; Perrin, D. M. Synthesis of a Cytotoxic Amanitin for Biorthogonal Conjugation. *ChemBioChem* **2015**, *16* (10), 1420–1425.

(170)   Anderl, J.; Mueller, C.; Simon, W. Amatoxin-Conjugates with Improved Linkers, WO2012041504, 2012.

(171)   Anderl, J.; Hechler, T.; Mueller, C.; Pahl, A. Amatoxin-Antibody Conjugates, WO 201614204, 2016.

(172)   Bauer, K.; Mierke, C.; Behrens, J. Expression Profiling Reveals Genes Associated with Transendothelial Migration of Tumor Cells: A Functional Role for Avβ3 Integrin. *Int. J. Cancer* **2007**, *121* (9), 1910–1918.

(173)   Goodman, S. L.; Grote, H. J.; Wilm, C. Matched Rabbit Monoclonal Antibodies against V-Series Integrins Reveal a Novel v3-LIBS Epitope, and Permit Routine Staining of Archival Paraffin Samples of Human Tumors. *Biol. Open* **2012**, *1* (4), 329–340.

(174)   Currier, N. V.; Ackerman, S. E.; Kintzing, J. R.; Chen, R.; Filsinger Interrante, M.; Steiner, A.; Sato, A. K.; Cochran, J. R. Targeted Drug Delivery with an Integrin-Binding Knottin–Fc–MMAF Conjugate Produced by Cell-Free Protein Synthesis. *Mol. Cancer Ther.* **2016**, *15* (6), 1291–1300.

(175)   Liu, Z.; Yan, Y.; Liu, S.; Wang, F.; Chen, X. [18]F, ^{64}Cu, and [68]Ga Labeled RGD-Bombesin Heterodimeric Peptides for PET Imaging of Breast Cancer. *Bioconjug. Chem.* **2009**, *20* (5), 1016–1025.

(176)   Lautenschlaeger, T.; Perry, J.; Peereboom, D.; Li, B.; Ibrahim, A.; Huebner, A.; Meng, W.; White, J.; Chakravarti, A. In Vitro Study of Combined Cilengitide and Radiation Treatment in Breast Cancer Cell Lines. *Radiat. Oncol.* **2013**, *8*, 246.

(177)   Kwon, K. C.; Ko, H. K.; Lee, J.; Lee, E. J.; Kim, K.; Lee, J. Enhanced In Vivo Tumor Detection by Active Tumor Cell Targeting Using Multiple Tumor Receptor-Binding Peptides Presented on Genetically Engineered Human Ferritin Nanoparticles. *Small* **2016**, *12* (31), 4241–4253.

(178)   Cox, N.; Kintzing, J. R.; Smith, M.; Grant, G. A.; Cochran, J. R. Integrin-Targeting Knottin Peptide–Drug Conjugates Are Potent Inhibitors of Tumor Cell Proliferation. *Angew. Chemie - Int. Ed.* **2016**, *55* (34), 9894–9897.

(179)   Civera, M.; Arosio, D.; Bonato, F.; Manzoni, L.; Pignataro, L.; Zanella, S.; Gennari, C.; Piarulli, U.; Belvisi, L. Investigating the Interaction of Cyclic RGD Peptidomimetics with AVβ6 Integrin by Biochemical and Molecular Docking Studies. *Cancers (Basel).* **2017**, *9* (12), 128.

(180)   Pettit, G. R.; Kamano, Y.; Herald, C. L.; Tuinman, A. A.; Boettner, F. E.; Kizu, H.; Schmidt, J. M.;

Baczynskyj, L.; Tomer, K. B.; Bontems, R. J. The Isolation and Structure of a Remarkable Marine Animal Antineoplastic Constituent: Dolastatin 10. *J. Am. Chem. Soc.* **1987**, *109* (22), 6883–6885.

(181) Bai, R.; Pettit, G. R.; Hamel, E. Structure-Activity Studies with Chiral Isomers and with Segments of the Antimitotic Marine Peptide Dolastatin 10. *Biochem. Pharmacol.* **1990**, *40* (8), 1859–1864.

(182) Amador, M. L.; Jimeno, J.; Paz-Ares, L.; Cortes-Funes, H.; Hidalgo, M. Progress in the Development and Acquisition of Anticancer Agents from Marine Sources. *Ann. Oncol.* **2003**, *14* (11), 1607–1615.

(183) Doronina, S. O.; Toki, B. E.; Torgov, M. Y.; Mendelsohn, B. A.; Cerveny, C. G.; Chace, D. F.; DeBlanc, R. L.; Gearing, R. P.; Bovee, T. D.; Siegall, C. B.; et al. Development of Potent Monoclonal Antibody Auristatin Conjugates for Cancer Therapy. *Nat. Biotechnol.* **2003**, *21* (7), 778–784.

(184) Doronina, S. O.; Mendelsohn, B. A.; Bovee, T. D.; Cerveny, C. G.; Alley, S. C.; Meyer, D. L.; Oflazoglu, E.; Toki, B. E.; Sanderson, R. J.; Zabinski, R. F.; et al. Enhanced Activity of Monomethylauristatin F through Monoclonal Antibody Delivery: Effects of Linker Technology on Efficacy and Toxicity. *Bioconjug. Chem.* **2006**, *17* (1), 114–124.

(185) Katz, J.; Janik, J. E.; Younes, A. Brentuximab Vedotin (SGN-35). *Clinical Cancer Research*. October 15, 2011, pp 6428–6436.

(186) Koga, Y.; Manabe, S.; Aihara, Y.; Sato, R.; Tsumura, R.; Iwafuji, H.; Furuya, F.; Fuchigami, H.; Fujiwara, Y.; Hisada, Y.; et al. Antitumor Effect of Antitissue Factor Antibody-MMAE Conjugate in Human Pancreatic Tumor Xenografts. *Int. J. cancer* **2015**, *137* (6), 1457–1466.

(187) Kratschmer, C.; Levy, M. Targeted Delivery of Auristatin-Modified Toxins to Pancreatic Cancer Using Aptamers. *Mol. Ther. - Nucleic Acids* **2018**, *10*, 227–236.

(188) Burns, K. E.; Robinson, M. K.; Thévenin, D. Inhibition of Cancer Cell Proliferation and Breast Tumor Targeting of PHLIP–Monomethyl Auristatin E Conjugates. *Mol. Pharm.* **2015**, *12* (4), 1250–1258.

(189) Cazzamalli, S.; Dal Corso, A.; Neri, D. Linker Stability Influences the Anti-Tumor Activity of Acetazolamide-Drug Conjugates for the Therapy of Renal Cell Carcinoma. *J. Control. Release* **2017**, *246*, 39–45.

(190) Temming, K.; Meyer, D. L.; Zabinski, R.; Dijkers, E. C. F.; Poelstra, K.; Molema, G.; Kok, R. J. Evaluation of RGD-Targeted Albumin Carriers for Specific Delivery of Auristatin E to Tumor Blood Vessels. *Bioconjug. Chem.* **2006**, *17* (6), 1385–1394.

(191) Sutherland, M. S. K.; Sanderson, R. J.; Gordon, K. A.; Andreyka, J.; Cerveny, C. G.; Yu, C.; Lewis, T. S.; Meyer, D. L.; Zabinski, R. F.; Doronina, S. O.; et al. Lysosomal Trafficking and Cysteine Protease Metabolism Confer Target-Specific Cytotoxicity by Peptide-Linked Anti-CD30-Auristatin Conjugates. *J. Biol. Chem.* **2006**, *281* (15), 10540–10547.

(192) Polson, A. G.; Yu, S.-F.; Elkins, K.; Zheng, B.; Clark, S.; Ingle, G. S.; Slaga, D. S.; Giere, L.; Du, C.; Tan, C.; et al. Antibody-Drug Conjugates Targeted to CD79 for the Treatment of Non-Hodgkin Lymphoma. *Blood* **2007**, *110* (2), 616–623.

(193) Temming, K.; Meyer, D. L.; Zabinski, R.; Senter, P. D.; Poelstra, K.; Molema, G.; Kok, R. J. Improved Efficacy of Avβ3-Targeted Albumin Conjugates by Conjugation of a Novel Auristatin Derivative. *Mol. Pharm.* **2007**, *4* (5), 686–694.

(194) Václavík, J.; Zschoche, R.; Klimánková, I.; Matoušek, V.; Beier, P.; Hilvert, D.; Togni, A. Irreversible Cysteine-Selective Protein Labeling Employing Modular Electrophilic Tetrafluoroethylation Reagents. *Chem. - A Eur. J.* **2017**, *23* (27), 6490–6494.

(195) Brunner, K.; Harder, J.; Halbach, T.; Willibald, J.; Spada, F.; Gnerlich, F.; Sparrer, K.; Beil, A.; Möckl, L.; Bräuchle, C.; et al. Cell-Penetrating and Neurotargeting Dendritic SiRNA Nanostructures. *Angew. Chemie - Int. Ed.* **2015**, *54* (6), 1946–1949.

(196) Hochdörffer, K.; Abu Ajaj, K.; Schäfer-Obodozie, C.; Kratz, F. Development of Novel Bisphosphonate Prodrugs of Doxorubicin for Targeting Bone Metastases That Are Cleaved PH Dependently or by Cathepsin B: Synthesis, Cleavage Properties, and Binding Properties to Hydroxyapatite As Well As Bone Matrix. *J. Med. Chem.* **2012**, *55* (17), 7502–7515.

(197) Dal Corso, A.; Cazzamalli, S.; Gébleux, R.; Mattarella, M.; Neri, D. Protease-Cleavable Linkers Modulate the Anticancer Activity of Noninternalizing Antibody–Drug Conjugates. *Bioconjug. Chem.* **2017**, *28* (7), 1826–1833.

(198) Dorywalska, M.; Dushin, R.; Moine, L.; Farias, S. E.; Zhou, D.; Navaratnam, T.; Lui, V.; Hasa-Moreno, A.; Casas, M. G.; Tran, T.-T.; et al. Molecular Basis of Valine-Citrulline-PABC Linker Instability in Site-Specific ADCs and Its Mitigation by Linker Design. *Mol. Cancer Ther.* **2016**, *15* (5), 958–970.

(199) Doronina, S. O.; Mendelsohn, B. A.; Bovee, T. D.; Cerveny, C. G.; Alley, S. C.; Meyer, D. L.; Oflazoglu, E.; Toki, B. E.; Sanderson, R. J.; Zabinski, R. F.; et al. Enhanced Activity of Monomethylauristatin F through Monoclonal Antibody Delivery: Effects of Linker Technology on Efficacy and Toxicity. *Bioconjug. Chem.* **2006**, *17* (1), 114–124.

(200) Sutherland, M. S. K.; Sanderson, R. J.; Gordon, K. A.; Andreyka, J.; Cerveny, C. G.; Yu, C.; Lewis, T. S.; Meyer, D. L.; Zabinski, R. F.; Doronina, S. O.; et al. Lysosomal Trafficking and Cysteine Protease Metabolism Confer Target-Specific Cytotoxicity by Peptide-Linked Anti-CD30-Auristatin Conjugates. *J. Biol. Chem.* **2006**, *281* (15), 10540–10547.

(201) Still, W. C.; Kahn, M.; Mitra, A. Rapid Chromatographic Technique for Preparative Separations with Moderate Resolution. *Journal of Organic Chemistry*. American Chemical Society July 1978, pp 2923–2925.

(202) Castro, F.; Dirks, W. G.; Fähnrich, S.; Hotz-Wagenblatt, A.; Pawlita, M.; Schmitt, M. High-Throughput SNP-Based Authentication of Human Cell Lines. *Int. J. Cancer* **2013**, *132* (2), 308–314.

(203) Schmitt, M.; Pawlita, M. High-Throughput Detection and Multiplex Identification of Cell Contaminations. *Nucleic Acids Res.* **2009**, *37* (18), e119.

Synthesis of novel conjugates based on a functionalized *cyclo*[DKP-*iso*DGR] integrin ligand and potent cytotoxic agents

Abstract: Targeted drug delivery is a growing-interest field in cancer therapy as a strategy for overcoming the systemic cytotoxicity associated to traditional chemotherapy. One important approach in this research area is represented by the small molecule-drug conjugates (SMDCs), where the drug-targeting is performed by a low molecular weight ligand (peptide, vitamin or peptidomimetic) connected to a potent warhead through a stable linker. This PhD thesis describes the synthesis and biological evaluation of novel SMDCs containing the functionalized cyclo[DKP-*iso*DGR] integrin ligand developed by our research group and potent cytotoxic drugs (α-amanitin, MMAE and MMAF) combined *via* different linkers and spacers. The conjugates were evaluated for their binding affinity to the isolated $\alpha_v\beta_3$ receptor and for their antiproliferative activity on cancer cell lines with different levels of $\alpha_v\beta_3$ expression in order to study the efficacy of the cyclo[DKP-*iso*DGR] integrin ligand as a vector for tumor drug-delivery.

Keywords: cancer, drug delivery, integrins, peptidomimetics, *iso*DGR, SMDC